AN INVESTIGATION OF THE STRUCTURE OF THE SOUTHERN HEMISPHERE RADIO-METEOR STREAMS

A thesis submitted to Rhodes University for the Degree of Master of Sceince

by

DAVID GERHARDUS ROUX

Depertment of Physics & Electronics,
Rhodes University,
Grahamstown.
25 February 1988.

CONTENTS

Abstract

Our current knowledge of the Solar System, with a particular emphasis on the systems of interplanetary objects, is reviewed, and the theory of meteors and the reflection of radio waves from meteoric ionization is then discussed. A description of the meteor radar is given and a method of calibrating the antenna beam is developed. The main project comprises two parts: (a) A general survey of the radar echo-rate for 20 major and minor meteor streams and the sporadic meteor background, conducted from Grahamstown over the period 1986 April to 1988 January, is described. Definite shower activity was observed for all of the major and some of the minor showers. (b) Based on a scheme proposed by previous workers (Morton & Jones), a method of recovering meteor radiant distributions from the distribution of echo directions is developed. We devise a technique of compensating for possible distortions of the resulting radiant maps, which may arise due to the anisotropic antenna beam. This involves a system of echo-weighting. Radiant maps which showed considerably less distortion than those of the above workers were obtained without the weighting procedure. It is concluded that, although the method in its present form introduces spurious features into the maps, the principle is sound and should eventually be refined to produce the desired compensation.

Acknowledgements

I wish to thank the members of the Rhodes University Physics Department for their general cooperation, without which this thesis could not easily have been completed. I also wish to thank Prof. P. van der Watt for devoting considerable time and thought to the problem of echo-weighting. Above all I am grateful to Dr. L.M.G. Poole, my supervisor, who was constantly willing to help, give suggestions and generously share his insights.

I am indebted to the South African Council for Sceintific and Industrial Research for a bursary in 1986 and 1987.

Chapter 1: Introduction

1-1: The Solar System

1-1-1: Description

The Solar System forms a regular, well-structured unit. It is dominated by a central selfluminous body, the Sun (mass = 2 x 10^{30} kg). Nine large near spherical objects, the planets, spanning the range of masses from 10^{22} kg to 10^{27} kg, are gravitationally bound by the Sun, and co-orbit it in the same sense. Their almost circular, concentric orbits are approximately confined to a single plane, the **ecliptic** (see section 2-2), with the notable exception of the innermost and outermost planets whose orbital planes are inclined at 7 and 17 degrees to the ecliptic, respectively. The distribution of the orbital radii about the Sun follows fairly closely a regular geometrical progression. With the exception of the two innermost planets, all are accompanied by smaller orbiting objects (satellites). The masses of these secondary objects are roughly four to eleven orders of magnitude less than those of their primaries. Their orbits are circular and synchronous (that is, the orbital periods equal the sidereal rotational periods), and with only one exception the orbital poles are closely aligned with the rotational axes of their primaries. Forty-four such objects are known.

The Solar System also contains a host of smaller bodies. These span a broad mass range, from 10^{21} kg (diameter = 1000 km) down to submicron particles of 10^{-20} kg (dust), and exhibit a steep increase in abundance with decreasing mass. Included in this group are objects of icy composition (the comets) that move in disparately oriented, highly elongated orbits. The comets extend into a three-dimensional cloud (the **Oort cloud**) which stretches some 20% of the distance to the nearest star. Several thousand rocky objects (the **asteroids**) orbit the Sun in a roughly circular belt situated between two of the planets. These become collisionally eroded with time, producing progressively smaller fragments. It is generally agreed that some kind of 'genetic relationship' exists between the comets and the asteroids, since these groups of objects are both believed to be 'primitive' in the sense that their constituents are thought to have undergone negligible metamorphosis since their formation with the birth of the Solar System.

Each of the distinct groups mentioned above are discussed in sections 1-2 to 1-5 .

1-1-2: Some ideas concerning the evolution of the Solar System

The original Kant-Laplace hypothesis of a primordial nebula remains today a tenable theory of the origin of the Solar System. It appears that about 4.6 billion years ago a fragment of an interstellar cloud contracted under its own gravity to form the disc-like 'protosolar nebula'. This process was preceded by a supernova event, from which most of the elements presently contained in the Sun and the Planets were ejected. This vertical

contraction was accompanied by the formation of the Protosun, which co-rotated with the disc.

As the gas in the nebula cooled, different substances formed granular condensates in accordance with the radial temperature gradient of the nebula. Grains large enough to detach themselves from the gas were formed, settling on the midplane of the disc. It has been suggested (Safronov, 1969) that gravitational instabilities in the particle disc had given rise to 'dust condensations', whose subsequent coalescence and contraction formed kilometre-sized bodies ('planetesimals').

This rapid initial phase of planetary formation (1000 years) was then followed by a slower phase lasting several hundred million years, during which planetesimals with low relative collisional velocities fused on encounter, forming embryo planets (with sizes of the order of 1000 km). Through a process of gravitational accretion these bodies finally grew to full-sized planets.

Some planetesimals must have been left over after the formation of the larger bodies. These would probably have been stony in the terrestrial planet zone (asteroids) and icy in the giant planet zone (comets). They should also bear the signatures of their regions of formation, and if identified they could hold important clues concerning the origin of the Solar System and its early history.

1-2: The System of Planets

The planets occupy the region of the ecliptic (see section 2-2) between 0.4 and 40 astronomical units from the Sun (the astronomical unit (AU) being the mean Sun-Earth distance). 99.87% of the mass of the Solar System is contained within the Sun. The nine planets, whose masses span about five orders of magnitude from Pluto to Jupiter, contain nearly all the remaining mass. On the basis of differences in mass, bulk density, size, and composition, the planets fall into two distinct groups: (a) The terrestrial planets - Mercury, Venus, Earth and Mars - are essentially rocky, composed of heavy elements (silicates, magnesium, iron) and are relatively dense and small. (b) The giant planets - Jupiter, Saturn, Uranus and Neptune - consist mainly of ices and gases (H, He, NH_3, CH_4) plus some rock, have roughly the density of water, and are relatively large. The outermost, smallest planet, Pluto, fits into neither group.

1-3: The System of Asteroids

The search for a 'missing planet' began in the late 1790's, after Herschel's 1781 discovery of Uranus had lent credibility to the Titius-Bode planetary spacing relationship, according to which the existence of a planet with an orbit between those of Mars and Jupiter is predicted. In 1801 this search bore fruit with Piazzi's discovery of the largest asteriod, Ceres (d = 1000 km), with an orbital radius in accordance with the predictions of the law. Today, orbital data are available on more than 7300 such objects (Kresak, 1985a), which are referred to collectively as the **asteroids**.

Whereas in the past it was generally held that the asteroids originated in the cataclysmic disintegration (either collisional or spontaneous) of a parent planet, current thinking is that they are remnant planetesimals (Chapman, 1985). Jupiter (and its proto form) appears to have presided over the formation of the asteroidal belt preventing the planetesimals (proto Asteroids) in that region from forming a full-sized planet. However, it remains uncertain whether the asteroidal region contains remnants of material condensed in that portion of the Solar System, rather than matter implanted there from elsewhere.

Asteroidal orbits are apt to stray further from the plane of the ecliptic and be more elongated than those of the larger planets, and the bulk of these cluster within a toroid (the **main belt**) between the orbits of Mars and Jupiter. The asteroids span sizes ranging from that of Ceres down to large boulders; many are very irregular in shape and are generally supposed to be of rocky (more unusually of carbonaceous chondrite) composition. Their mineralogical compositions vary widely, and on this basis they fall into taxonomic types. The orderly progression of types with heliocentric distance mirrors variations in the compositions of nebular condensates due to the temperature decrease with increasing solar distance during formation. Because the asteroids have not suffered chemical metamorphosis during the solar lifetime as have the planets, their mineral contents hold clues to poorly understood primordial processes in the solar nebula and during the early stages of planetary accretion.

The outstanding feature of the belt is the Kirkwood gaps in the distribution of semi-major axes (see section 2-2), which are due to the perturbation, over the solar lifetime, of bodies out of orbits which resonate with that of Jupiter. In addition to such gravitational effects, their mutual collisional interaction has been a dominant process affecting both their physical and their dynamical evolution. It now seems that the largest asteroids are not easily fragmented and dispersed by collisions. Those larger than 50 km have probably retained an identity from primordial times, whereas those smaller than 25 km are most likely the fragments of larger bodies (Chapman, 1985).

The main belt does not, however, contain all the asteroids. Many cross the orbits of the terrestrial planets. The group of Earth-crossing asteroids is of particular interest. Not only are they the most likely source of meteorites (see section 2-1), but their abundance and their short lifetimes (10^5 - 10^7 years) relative to the age of the Solar System suggest constant replenishment from some as yet undetermined source. Main belt collisions near orbital resonance lanes could result in fragments being ejected into Earth-crossing orbits. Alternatively, some may be the defunct nuclei of 'extinct' short-period comets (Helin, 1985). The Earth-crossers present attractive targets for space missions as a consequence of their low velocities relative to the Earth. A joint US/European mission, which may even include a rendezvous, is envisaged within the next decade (Brahic, 1985).

1-4: The System of Comets

The comets are, by definition, objects which exhibit certain distinctive characteristics (the development of a gaseous coma, the formation of a tail and the release of dust) when sufficiently near the Sun. The current view of their composition is that they are loose conglomerates of dust particles trapped inside a matrix of frozen gases and water-ice (Whipple's 'dirty snowball'). Diameters range between roughly 1 and 10 km.

By June 1985 the orbits of 739 were known (Kresak, 1985a), and these are classifiable into groups according to whether the orbital periods are long (greater than 200 years), intermediate (20 - 200 years - the 'Halley family' with aphelia between Saturn and Pluto), or short (less than 20 years - the 'Jupiter family' whose aphelia cluster around the orbit of Jupiter).

Comets spend most of their lives in an inactive state far from the Sun, where none of their characteristic properties are evident. As the body approaches the Sun, first the coma forms and then the tail. Spectral work shows that finally, at distances of 2 AU, the tail becomes ionized.

The two main rival hypotheses concerning cometary origin are: (a) they originated within and are members of the Solar System, and (b) they are interstellar bodies captured by the Solar System. At present (a) is the more widely accepted. Current thinking is that they were formed from planetesimals in the icy giant planet region during the process of planetary accretion, and that subsequent perturbations by these planets caused their ejection into the space beyond the planets to form the vast cloud first proposed by Oort in 1950. The modern view of the structure of this cloud is that it consists of an outer, spherical component, the 'classical' Oort cloud, extending some 10^5 AU from the Sun and containing 10^{12} comets with a total mass of 2 Earth masses, and a much denser inner component, a transplutonian disc extending in the plane of the ecliptic to 10^4 AU. It is possible that this inner component formed directly from planetesimals beyond Pluto's orbit. Oort's original view is that close encounters of the Sun and another star (there have been an estimated 10^3 encounters within one parsec during the solar lifetime) randomize the cometary orbits in the outer cloud and inject comets into the planetary region. According to another more modern view, encounters with Giant Molecular Clouds (GMC's), unsuspected in Oort's time, have similar perturbing effects, which cause the outer Oort cloud to be depleted, but also replenished by the transport of comets from the outer part of the inner belt, during the same encounter. The idea that the comets actually originated in the GMC's has been dismissed for the lack of a viable mechanism for this process (Safronov, 1985).

An attractive coherent view of cometary behaviour is that of a dynamic equilibrium in which two evolutionary stages can be identified: (a) the regular injection of dynamically new comets from the Oort cloud into the

planetary region, and (b) the capture of all these objects, and the progressive decrease in the periods of their orbits. These stages are explained further below: (a) External disturbances by stars and/or GMC's denude the periphery of the outer cloud creating long-period comets, while internal perturbations by planets thin out the inner part of the the cloud and generate intermediate-period comets. (b) After capture the comets rapidly devolatilize and disintegrate, or change at the end of their lifetimes into 'extinct' Earth-crossing objects of asteroidal appearance and short collisional lifetimes (Kresak, 1985b). The final heritage is dust, in either case. Eventually this spirals into the Sun or is lost from the Solar System. The dust is dealt with in the following section.

1-5: The System of Interplanetary Dust (Meteoroids)

It is now generally accepted that the dust cloud which occupies interplanetary space represents the collisional progeny of larger parent bodies, or results from the disintegration of comets. The subsequent dynamical evolution of the bodies in this size-range (smaller than pebble-size) is the result of the complex collective action of gravitational forces, and effects arising from the interaction with the solar radiation. Both radiation pressure and the corpuscular solar wind sweep particles having sizes from 0.1 μm to a few centimetres clear of the Solar System, depending on their composition (Burns, 1985). In addition, the velocity-dependent Poynting-Robertson drag, due to the anisotropic re-emission of radiation in an inertial frame fixed to the Sun, modifies the orbits of such particles. The Yarkovsky drag is similar, except that it arises from asymmetries (due to particle rotation) in re-radiated thermal energy, and may affect the movement of particles ranging from centimetres to metres in size (Burns, 1985). For those particles which are able to withstand the effects of radiation pressure and the solar wind, these drag forces result firstly in the reduction of the orbital eccentricities and then the transformation of the orbit into a slender spiral which eventually carries the particle into the Sun.

Most of our knowledge about this dust cloud is observationally restricted to the near - Earth particle flux. One of the most successful means of obtaining information is from observations of 'meteors' (see section 2-1), which occur in the height range 80 -140 km and can be observed visually, photographically, or by means of radar. From these techniques the velocity, direction of travel, and hence the orbit, of a meteoroid (see section 2-1) may be deduced. The interest in meteoric orbital motion derives from questions concerning their origin and the dynamical evolution of the Solar System. Although the optical methods are more precise, radar has the advantage that more numerous smaller meteors can be detected, throughout the day, in all weather. In addition, it is well suited to the continuous monitoring of daily and seasonal variations in meteoric influx. The interpretation of such variations is complicated by the fact that the observed influx is a function of geophysical conditions and, indirectly, the solar cycle.

Most dust orbits lie near the ecliptic, exhibiting a prevailing prograde motion and with broadly dispersed streaming patterns. Superimposed on this distribution (the 'sporadic' background) are the streams - well-defined toroids of co-orbiting particles which are generally thought to be cometary in origin (see section 2-1). Several streams have been identified with particular comets, while in other cases the original comet seems to have completely disintegrated. Whenever the orbits of the Earth and a stream intersect we have the phenomenon of a meteor shower. These showers are annual events at particular solar longitudes (see section 2-2).Although the spatial density of such meteoroids is often no greater than that of the sporadic distribution, a shower event appears distinct

due to the high encounter velocity of its particles. If the stream is sufficiently broad and both orbital nodes are favourably placed, the same stream may give rise to annual showers at two intersections. The conspicuous showers associated with comet Halley are an example of this: the Eta-Aquarids (May) and the Orionids (October). Similarly, comet Encke is associated with the ß-Taurids (June) and the Taurids (November). Currently about a dozen meteor streams are known to produce significant annual shower events, although some authors list hundreds of minor showers. It is now accepted that the constituents of the streams are fragile dustballs, a structure consistent with a cometary origin. These invariably disintegrate completely high up in the atmosphere and hence there is no chance of a collision with the Earth's surface. The decrease in eccentricity and inclination of the orbits as the stream ages is accompanied by a lateral dispersion of the particles, until the stream loses its identity and merges with the sporadic background.

The Geminids (December) are unusual in that they appear to be associated with an Earth-crossing asteroid, 3200 Phaeton, thought to be an 'extinct' cometary nucleus. An asteroidal origin is generally accepted for the meteorites and some of the sporadic meteors.

Chapter 2: Definitions of Terms

This section contains the formal definitions of (a) specialized terms peculiar to meteor science (section 2-1) and (b) those which are common in the broader field of astronomy (section 2-2). Some the reader will already have encountered in Chapter 1; others will appear later in the text.

2-1: Definitions specific to meteor sceince

The definitions in this subsection are based on the decisions of a subcomission of the IAU at a convention held at Berkeley, California in 1961 under the chairmanship of P.M. Millman.

(1) Meteor - the (sometimes visual) phenomenon which results from the entry into the earth's atmosphere of a solid particle. The term is also generally applied as a noun or an adjective to any physical object or phenomenon associated with such an event.

(2) Meteoroid - an object, moving in interplanetary space, which may give rise to a meteor.

(3) Meteorite - a meteoroid which has struck the earth's surface without evaporating completely.

(4) Micrometeorite - a meteorite with a diameter in general less than a millimetre.

(5) Trajectory - the line of motion of a meteor relative to the earth, considered in three dimensions.

(6) Train - anything (such as light or ionization) which remains along the trajectory of the meteor after the meteoric body has passed.

(7) Persistent - an adjective used with 'train' indicating durations of appreciable length.

(8) Radiant - the point where the backward extension of the meteor trajectory intersects the celestial sphere (see section 2-2)

(9) Stream - a group of meteoroids travelling in nearly identical orbits.

(10) Shower - the (sometimes visual) phenomenon which arises when the earth passes through a recognisable stream.

(11) Zenith attraction - the effect of the earth's gravity on a meteoric body, increasing the velocity and moving the radiant

towards the zenith.

(12) **Zenith angle** - the angle between the train axis (and hence the radiant) and the zenith.

2-2: General astronomical definitions

(1) **Celestial sphere** - an imaginary sphere of infinite radius with the earth at its centre, and cut in two points by extensions of the earth's axis, the North and South Celestial Poles (see Fig.2-1). The plane of the Earth's equator cuts the celestial sphere along the Celestial Equator. By definition, the most distant stars are fixed on the celestial sphere.

(2) **Apex of the earth's way** - the point on the celestial sphere toward which the Earth is moving, at any moment.

(3) **Ecliptic** - the circle described on the celestial sphere by the motion of the Sun during one year. The term also refers to the plane of the earth's orbit.

(4) **Hour Circle** - as applied to an object or point on the celestial sphere the hour circle is a great circle on the celestial sphere, passing through the celestial poles and the object or point.

(5) **Meridian** - on the earth, any great circle through the poles; on the celestial sphere, the great circle through the zenith and the north and south points of the horizon.

(6) **Vernal equinox** - one of the two intersections of the celestial equator and the ecliptic. On or near March 21, the Sun passes through the 'vernal' equinox as it moves northwards across the celestial equator. This is also known as the 'First Point of Aries' (see Fig 2-1) and has, by definition, equatorial coordinates (see (7) and (8) below) RA = Ø, δ = Ø. This point moves slowly relative to the celestial sphere (fixed stars), but for many purposes can be considered fixed. Thw term 'vernal' (spring) is only really appropriate in the Northern Hemisphere.

The two common spherical coordinate systems with which we will be mainly concerned are: the equatorial system, which involves right ascension and declination (RA and δ), and the horizontal system which involves the coordinates of azimuth and altitude (Az and α).

(7) **Right ascension** (Ø° ≤ RA ≤ 36Ø°) - the right ascension of a point on the celestial sphere is measured in either hours or degrees eastward along the celestial equator, from the vernal equinox to the hour circle passing through the point in question (see Fig 2-1). Whereas the right ascension of an

observer's zenith increases by 15° every hour, the right ascension of any point on the celestial sphere is constant in time.

(8) **Declination** ($-90° \leq \delta \leq +90°$) - the declination of a point on the celestial sphere is the angular distance between the equatorial plane and the point, measured along the hour circle through the point in question and the poles. It is equivalent to terrestrial latitude (see Fig 2-1). The sign is taken as positive if the point is north of the celestial equator and negative if it is south.

(9) **Hour angle (HA)** - the hour angle of a point on the celestial sphere is the angle measured along the celestial equator, between the hour circle passing through the point and the meridian. It is positive if the point is west of the meridian.

(10) **Altitude** ($0° \leq \alpha \leq 90°$) - the altitude of a point is the angle measured perpendicularly from the observer's horizon to the point.

(11) **Azimuth** ($-180° \leq Az \leq +180°$) - the azimuth of a point is the angular distance, measured in the observer's horizontal plane, between the point and due north. Points to the east, that is, measured in the clockwise direction as viewed from the zenith, are positive.

(12) **Sidereal time** - time calculated with reference to the apparent rotation of the celestial sphere. The local sidereal time (LST) is defined as the hour angle (HA) of the vernal equinox. For any celestial oblect 'x',

$$LST = HA(x) + RA(x).$$

Since the hour angle of any object is zero when it transits the observers meridian, the object's right ascension at that time is the local sidereal time.

(13) **Universal time (UT) and South African Standard Time (SAST)** - universal time is the mean solar time at the Greenwich meridian, and is reckoned on a 24 hour basis commencing at midnight (i.e. 0 h UT occurs when the Greenwich hour angle of the mean sun is ±12 hours). South African Standard Time is 2 hours ahead of universal time.

(14) **Solar longitude** - angular distance from the First Point of Aries to the position of the Sun, measured eastward along the ecliptic. The 'ecliptic longitude' of any other object is measured in a similar way.

(15) **Orbital elements** - these uniquely describe the size, shape, and orientation of an orbit and relative to the Sun. It is first necessary to consider some of the geometrical elements of an ellipse, shown in Fig. 2-2.

a = semi-major axis
b = semi-minor axis
e = eccentricity = CS/CP
p = semi-altus rectum = $a(1 - e^2)$
q = perhelion distance = $a(1 - e)$
q'= aphelion distance = $a(1 + e)$
P = perhelion point
A = aphelion point
S,S' = two principle focii

The two focii coincide for a circular orbit (e = Ø). As e approaches unity the ellipse becomes progressively more elongated. When e = 1 the aphelion point recedes to infinity and the ellipse becomes a parabola. Finally, when e > 1, the semi-major axis becomes negative and the orbit becomes hyperbolic.

In Fig. 2-3, U (ascending node) defines the point at which the orbital path passes from south to north of the ecliptic. Conversely, D is the descending node. The Earth may encounter a meteoric body at either U or D, should the two orbits intersect. The vector SV points towards the vernal equinox and may be considered as fixed in space.

Three additional elements are needed to define the orientation of an orbit relative to the celestial sphere (see Fig. 2-3). These are: i = **inclination** ($Ø° \leq i \leq 180°$), the angle between the body's orbital plane and the ecliptic. If the body orbits in the same sense as the earth, the motion is termed direct and $i < 90°$. Conversely, for retrograde motion, $i > 90°$. w = **argument of the perhelion** ($Ø° \leq w \leq 360°$), USP in Fig 2-3. This describes the orientation of the orbit within the orbital plane. Ω = **longitude of the ascending node** ($Ø° \leq \Omega \leq 360°$), VSU in Fig 2-3. This measures the amount by which the orbital plane is pivoted about the Sun in the ecliptic.

The quantities a, e, i, Ω and w will define a meteor orbit completely. Elements a and e define the trajectory, i and Ω the orientation of the orbital plane with respect to the ecliptic, and w the orientation of the orbit within this plane.

Chapter 3: Physical Theory of Meteors

3.1: Theory of Meteor Ionization

A meteoroid strikes the rarified upper atmosphere with a speed of between 11 and 72 km/sec. It collides with air molecules and traps a portion of these on its surface. This process liberates heat which vapourizes the meteor atoms. These carry the meteoroid velocity relative to the surrounding atmosphere, and their subsequent collisions with air molecules are responsible for exciting and ionizing the meteoroid atoms. The ionization, together with the excited atoms, form a column in the wake of the meteor. This column is rapidly dispersed by various physical and chemical processes, which are discussed in section 3-2. In the process of returning to their ground state, the excited atoms emit light quanta. These, if sufficiently plentiful, may render the whole process visible.

Quantitative theories of meteor ionization developed by Whipple (1943, 1952) and Herlofson (1948) have been summarized by Kaiser (1953). Three assumptions underly these models:

(1) The atmosphere is homogeneous and isothermal at meteoric heights. Under these circumstances, the air density at some height h relative to some reference height is expressed as

$$\rho = \rho_{\oslash} \exp(-h/H) \qquad (3.1)$$

where $\rho_{\oslash}$ is the density at the reference height and H is the **atmospheric scale height** given by

$$H = \frac{kT}{m_a g} \qquad (3.2)$$

where k = Boltzmann's constant, T = absolute temperature, m_a = mean mass of an air molecule, and g = acceleration due to gravity. Although the assumption (1) holds well over small height differences it is certainly in error for a great range of heights. In fact T (and to a lesser extent m_a and g) varies with height. However these effects on H are negligible over the range of meteoric heights.

(2) The meteoroid collides with air molecules individually. This requires that its dimensions are small compared with the molecular mean free path in the atmosphere. Under such circumstances the atoms leave the meteoroid without serious mutual interference. Lower down where the atmosphere is denser, a shielding effect may arise owing to

a layer of vapourized atoms about the meteoroid. Lower still, an aircap may develop ahead of the meteoroid - particularly for larger bodies.

(3) There is negligible energy loss due to direct radiation from the meteoroid. Particles smaller than about 1 μm will dissipate most of their heat energy in this way (Whipple, 1952) and will therefore not cause ionization. However, this size is well below the threshold detectable by either visual or radar techniques.

The 'classical' ablation theory developed by these authors, on the assumption that these conditions are satisfied, may be summarized in the following two expressions:

$$n = (\mu H)^{-1}\, m\, v\, \cos X\, \left(\frac{\rho}{\rho_1}\right)\, \left(1 - \frac{\rho}{3\rho_1}\right)^2 \qquad (3.3)$$

where n = number of meteor atoms evaporated per unit time at a height where the atmospheric density is ρ,
μ = mass of a meteor atom,
H = atmospheric scale height,
m = initial mass of the meteoroid,
v = geocentric meteoroid velocity,
X = zenith angle of the meteor train,
ρ_1 = atmospheric density at the point of maximum evaporation rate,

$$= \left[\frac{2\Lambda}{\Omega v^2 A H}\right] m^{1/3} \cos X \qquad (3.4)$$

where Λ = latent heat of evaporation of the meteor,
Ω = 'heat transfer coefficient', defined as the ratio: (heat energy liberated)/(kinetic energy of the air mass intercepted by the meteoroid), and
A = 'shape factor'.

A is defined by: $A = a m^{-2/3}$ where a is the cross-sectional area normal to the line of flight and ρ_m the density of the meteoroid (Kaiser, 1953). The expression may be rewritten $A = A' \rho_m$. For a sphere, a simple calculation shows that $A' = (9\pi/16)^{1/3} = 1.2$. For a cube, $1.0 \leq A' \leq 1.7$, depending on its orientation. Long narrow bodies have $A' < 1$ for the streamlined aspect and $A' > 1$ for the broadside-on aspect. Irregularly shaped objects may have a mean A' of the same order as that for the sphere, owing to rotation. In any case, A' is often assumed to be close to unity (McKinley, 1961).

The heat-transfer coefficient is a measure of the efficiency of the collision process in converting kinetic energy into heat. Values in the range $0.1 \leq \Omega \leq 0.6$ have been proposed (op.cit.) although Herlofson (1948) takes $\Omega = 1$ (i.e. he assumes that all the impinging air molecules are trapped on the meteoroid's surface).

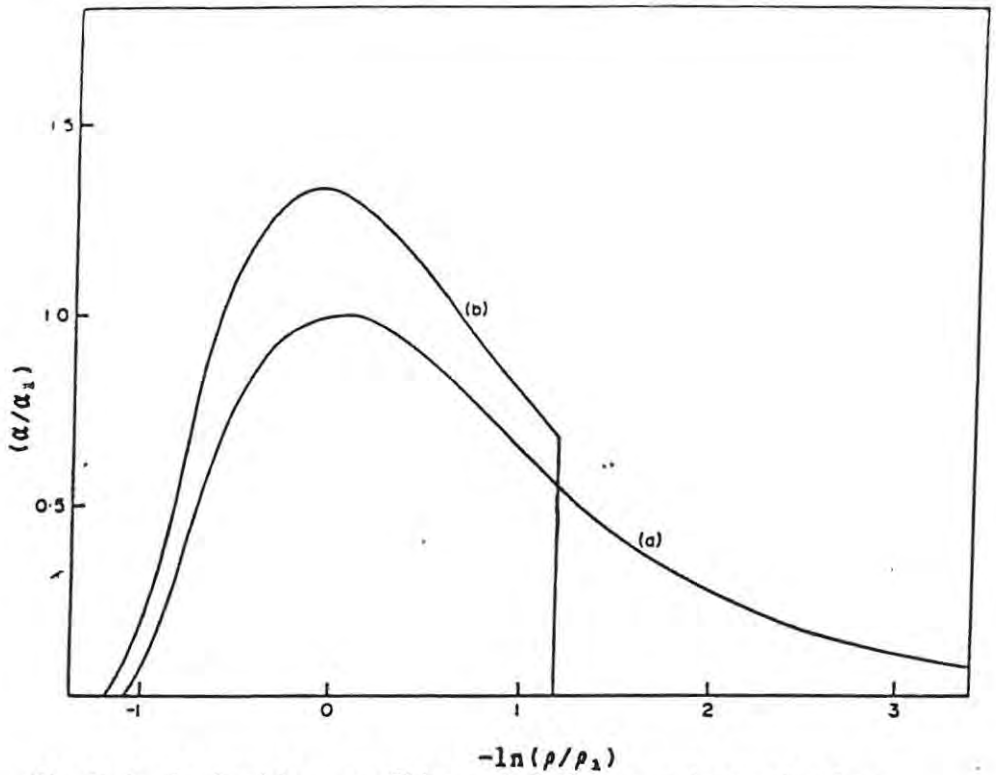

Fig 3-1: Ionization profiles: (a) for a meteor obeying equation (3-5), or equation (3.32) with τ = Ø; (b) for the same meteor obeying equation (3.32) with τ = Ø.3 (Poole, 1973).

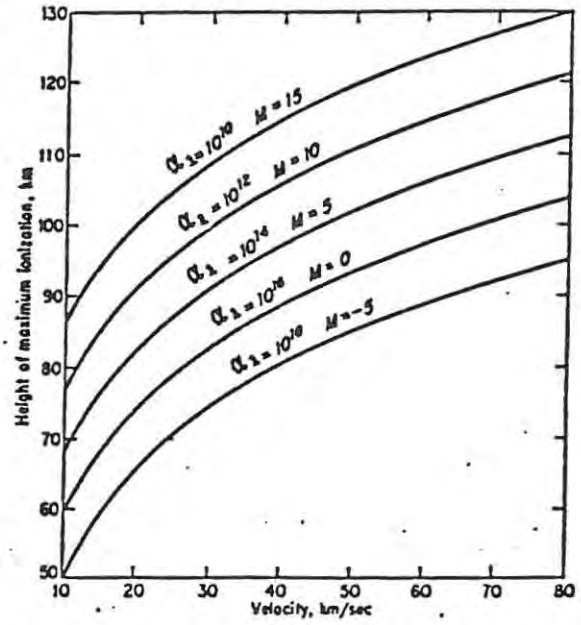

Fig 3-2: Height of point of maximum ionization as a function of velocity, for selected values of α_1, or for the equivalent radio magnitudes (McKinley, 1961).

Approximations made in the derivation of equations (3.3) and (3.4) require that $v^2 >> 121$, and in addition, the meteoroid deceleration is assumed to be small.

Equations (3.3) and (3.4) lead directly to the normalized ionization equation:

$$\alpha/\alpha_1 = 9/4\ (\rho/\rho_1)\ (1 - 1/3\ \rho/\rho_1)^2 \qquad ...(3.5)$$

where α_1 = the value of α which occurs at the level where $\rho = \rho_1$, and is given by:

$$\alpha_1 = 4/9\ \beta\ (\mu H)^{-1}\ m \cos X \qquad ...(3.6)$$

where β = the probability that a single evaporated meteor atom will produce a free electron. Equation (3.4) may now be expressed as:

$$\rho_1 = \frac{2Q}{v^2} \left(\frac{9}{4} \alpha_1 \frac{\cos^2 X}{H^2}\right)^{1/3} \qquad ...(3.7)$$

where

$$Q = \frac{1}{\Omega A} \left(\frac{\mu}{\beta}\right)^{1/3} .$$

The variation of line-density with height in the atmosmphere may be depicted by plotting α/α_1 against $-\ln(\rho/\rho_1) = (h - h_1)/H)$, where h and h_1 are heights corresponding to ρ and ρ_1, respectively. Such a normalized ionization profile is shown in Fig 3-1.

The maximum ionization produced is proportional to the initial mass and may depend on velocity through the ionization probability, β. However, the normalized ionization profile is independent of these parameters, as well as any other properties of the meteoroid. The theoretical dependence of h_1 on v has been plotted for several values of α_1 in Fig. 3-2.

The mass of the body at any point on its trajectory is given by:

$$m = m_\infty (1 - \rho/3\rho_1)^3 .$$

Here m_∞ is the initial mass. From this equation it is evident that at the point of maximum ionization, $m = 8/27\ m_\infty$.

3-2: Dissipation of Meteor Ionization

Once the meteoroid has finished its course, three processes are significant in reducing the volume density of free electrons in the train: ambipolar diffusion, ionic effects and wind-induced effects.

At heights greater than 85 km, ambipolar diffusion is the dominant process governing the rate of decay of ionization (Jones, 1975) , and reduces the volume density without affecting the total electron line density, α. It was once thought that the diffusion of trains across the geomagnetic field lines would be strongly reduced above 95 km (Huxley 1952, Kaiser 1953), but more recent work has shown that this is unlikely below 130 km except for trains which are closely aligned with the field (Kaiser, Pickering & Watkins 1969, Pickering 1973). Frictional heating of the train by kinetic energy transfer from the high velocity meteoric atoms would enhance the diffusion process.

Below 85 km, the atmosphere is sufficiently dense for the chemical processes to dominate over diffusion. This would apply to the so-called 'overdense' trains (see section 3-3) whose points of maximum ionization occur at these heights. Jones (1975) has listed six ionic or molecular processes which decrease the electron volume density within the train:

(1) radiative attachment to neutral species:

$$e^- + O_2 = O_2^- + h\nu$$

(2) dissociative attachment:

$$e^- + O_3 = O^- + O_2$$

(3) three-body attachment:

$$e^- + O_2 + N_2 = O_2^- + N_2$$

(4) radiative recombination of electrons and ions:

$$M^+ + e^- = M + h\nu$$

where M^+ is a meteoric ion,

(5) $N_2^+ + e^- = N^* + N^*$

(6) oxidation-dissociation: $M^+ + O_3 = MO^+ + O_2$

$$MO^+ + e^- = M + O.$$

An associative detachment reaction with atomic oxygen rapidly replaces any electrons which have been removed in reactions (2) and (3):

(7) $O_2^- + O = O_3 + e^-$

(8) $O^- + O = O_2 + e^-$ (Baggaley & Cummack, 1974).

The oxidation-dissociation mechanism is the most successful yet suggested for night time electron loss in overdense trains (Jones, 1975; Poole and Nicholson, 1975). It is now generally agreed that attachment processes play a minor role in determining echo duration.

In addition to the above processes, atmospheric turbulence will, in general, stir up the train and redistribute the ionization.

If it is assumed that the initial train radius is negligible and that only diffusion is active, then it may be shown that after a time the radial electron density distribution is gaussian. This is done by setting up and solving the diffusion equations for both the electrons and the ions in the absence of a magnetic field. Then the electron volume density at radius r from the train axis is given by

$$n_e = \left(\frac{\alpha}{4\pi Dt}\right) \exp\left[\frac{-r^2}{4Dt}\right] \qquad \ldots(3.8)$$

where D = ambipolar diffusion coefficient.

The quantity $(4Dt)^{\frac{1}{2}}$ is a measure of the column radius at time t. Thus, owing to diffusion, the shape of the column of ionization will be that of a paraboloid of revolution leading back from the meteoroid. The effect of the oxidation-dissociation and other deionization processes is to alter both the coefficient and the exponent in equation (3.8).

3-3: Radio Echoes from Meteor Trains

Two distinct types of radio-wave reflection from meteoric ionization are recognized: (1) If the train is rare enough, it will be freely penetrated by the incident wave and the individual free electrons will scatter the radiation coherently and independently; such a train is designated **underdense**; (2) If the volume density of free electrons is large enough, the incident radiation cannot penetrate the train, which behaves like a conducting cylinder, and total reflection of the wave occurs; a train exhibiting these properties is referred to as **overdense**.

The critical line density, which marks the transition between these two types, is

$$\alpha_c = 2.4 \times 10^{14} \text{ electrons/metre.}$$

This threshold is to some extent arbitrary.

3-3-1: The Underdense Train

An expression for the underdense echo power delivered by the antenna to the receiver terminals has been developed by Kaiser & Closs (1952). Taking the classical electron radius as

$$r_e = \frac{e^2}{4\pi\epsilon_0 mc^2}$$

in S.I. Units, the expression is (for a specular echo)

$$P_R = \frac{P_T G^2 \lambda^3 \alpha^2}{32\pi^2 R^3} r_e^2 \left(\frac{C^2 + S^2}{2}\right) \text{ watts} \qquad \ldots(3.9)$$

where P_R = received power,
P_T = transmitted power,
G = power gain of the antenna in the direction of the reflection point (defined as the point at which a vector from the observing station cuts the train perpendicularly),
λ = radio wavelength,
e = electronic charge,
m = electronic mass,
c = velocity of light,
R = range to the reflection point,
and C and S are the conventional Fresnel integrals used in optical diffraction theory.

In equation (3.9), the behaviour of the bracketed term is important.

This quantity varies with time during the formation of the train, and in the absence of diffusion, would give rise to the variation of P_R as shown in Fig 3-3 (curve a). The frequency of these fluctuations depends upon, amongst other things, the meteor velocity and forms the basis of a method of measuring meteoroid velocities (Davies & Ellyett, 1949). Most of the received echo power is returned from the first Fresnel zone on either side of the reflection point and becomes vanishingly small if the train does not make a right angle with the antenna beam. The train thus glints like a mirror and gives a specular reflection. Consequently, trains which are not normal to the beam are not observed.

In plotting Fig 3-3(curve a) no account has been taken of the effect on the returned echo power of both the initial train radius (discussed further in section (3-6)) or of diffusion. If the diameter of the column of ionization is comparable with the wavelength, components of the radiation scattered by the electrons across any given cross-section will interfere destructively. This reduces the echo power relative to the case of perfectly coherent scatterers concentrated along the train axis by the factor

$$\exp\left(\frac{-32\pi^2 Dt}{\lambda^2}\right) \exp\left(\frac{-8\pi^2 r_\phi^2}{\lambda^2}\right) \qquad \ldots(3.10)$$

where r_ϕ is the initial radius of the train (Baggaley, 1970). Hence the effect of the initial radius is to immediately reduce the echo power by the factor containing r_ϕ even before the onset of diffusion. The latter process results in an exponential decay of P_R with time as indicated in Fig 3-3 (curve b).

For many purposes it is more convenient to work with echo amplitude, which is proportional to the square root of the echo power. For the common case where diffraction effects are not important, equation (3.10) leads to the expression

$$A_t = A_\phi \exp(-t/T_{un}) \qquad \ldots(3.11)$$

where A_t = echo amplitude after a time t,
A_ϕ = initial amplitude, including the initial radius effect,

and

$$T_{un} = \frac{\lambda^2}{16\pi^2 D} \quad \text{seconds} \qquad \ldots(3.12)$$

is the time constant of the exponential decay, often referred to as the amplitude 'decay time' for underdense echoes (see Fig 3-4, curve a).

3-3-2: The Overdense Train

The overdense train is characterized by an effective critical train radius r_c, within which the electron volume density exceeds a minimum critical value, N_c, above which the dielectric constant of the plasma is negative and its refractive index imaginary. It is from this boundary that the incident wave is reflected, although the wave will penetrate inside r_c before the reflection is complete. As the train diffuses, r_c slowly expands until it reaches a maximum, after which it rapidly contracts. Once r_c has fallen to zero, the dielectric constant becomes positive throughout the train, which is now subcritical. This occurs, by definition, at a time T_{ov} - the **overdense echo duration** - given by Kaiser & Closs (1952) as

$$T_{ov} = \frac{\lambda^2 \alpha}{4\pi^2 D} \; r_E^2 \quad \text{seconds} \qquad \ldots(3.13).$$

The time variation of the overdense echo power is proportional to r_c, and the same authors (1952) have shown its maximum value to be

$$P_R = \frac{P_T G^2 \lambda^3 \alpha^{1/2}}{105\pi^3 R^3} \; r_E^{1/2} \quad \text{watts} \qquad \ldots(3.14).$$

It should be noted that, whereas the underdense echo decay time is independent of the line density, the overdense echo duration is proportional to the line density. Furthermore, the underdense echo amplitude is proportional to the line density, while the overdense echo amplitude varies according to the fourth root of the line density. However, both T_{un} and T_{ov} are proportional to the square of the wavelength and are inversely proportional to the diffusion coefficient.

The theoretical amplitude-time profile of an overdense echo is shown in Fig 3-4 (curve b), although real echo profiles are never like this due to wind-induced effects which distort the train, and the various ionic processes already discussed in section (3-2) which reduce the electron line density.

Finally, it is worth mentioning that although an overdense-type echo might be expected from a train with $\alpha > \alpha_c$, this is not necessarily the case: echo observations begin only after the train has already expanded to its 'initial' radius r_0, so that the axial electron volume density may already have dropped below the critical value, and total reflection will not occur. It may be shown that a decay-type echo will be received from a formally overdense train unless α exceeds the limiting value

$$\alpha = \pi^2 \left(\frac{r_0}{\lambda}\right)^2 \alpha_c \quad \text{(McKinley, 1961).}$$

3-3-3: The Radio Magnitude Relation

The absolute visual magnitude of a meteor has been defined as

$$M_v = -2.5 \log I + 6.8 \quad \ldots(3.15)$$

(Opik, 1955), where I = power in watts radiated over the visible spectrum. Formally, equation (3.15) gives the brightness that a meteor would have if it were placed in the zenith at a height of 100 km.

The ionization and the luminosity produced by a meteoroid are proportional, since both the ionization, and the excitation which causes the luminosity, are produced by collisions between evaporated meteor atoms and air molecules. It is therefore possible to use an expression analagous to (3.15) for the brightness of radio meteors, derived empirically from a comparison of the durations of overdense echoes with the absolute visual magnitudes of visual meteors observed simultaneously (Millman & McKinley, 1956). The expression varies according to meteoroid velocity, but for a velocity of 40 km sec^{-1}, a workable average, it becomes

$$M_r = -2.5 \log \alpha_1 + 40 \quad \ldots(3.16)$$

where α_1 = maximum electron line density in electrons per metre. Although (3.16) was derived from observations of overdense echoes, it is useful down to faint decay-type echoes ($M_r = +12$). The threshold line density marking the transition from decay to persistent-type echoes produces an echo of radio magnitude $M_r = +5$, corresponding to the faintest meteor visible to the unaided eye.

By substituting $\alpha_n = \alpha_1/\cos X$ for α_1 in (3.16), we have an expression for the **absolute zenithal magnitude** of radio meteors. X is the zenith angle of the train axis. Thus α_n is the value that α_1 would assume if the meteoroid were incident vertically.

3-4: Theory of the Radio Echo Rate

The absolute incident flux of radio meteors does not bear a straightforward relationship to the observed echo rate. The observed rate has been found to depend on factors such as:

(i) the incident flux and distribution in magnitude of the meteors,
(ii) the variation in ionization along a meteor train,
(iii) the radiant coordinates,
(iv) the nature of the reflection process, and
(v) the parameters of the meteor radar.

Kaiser (1960) has derived simple formulae which enable the incident flux to be deduced from the observed echo rate, for the case of shower meteors. This section summarizes part of Kaiser's paper. For the case of sporadic meteors, see a later publication (Kaiser, 1961).

It is first necessary to consider the geometry of the reflection process (Fig. 3-5). For a shower with a point radiant at R, all reflection points lie in the echo plane ABCD, which is, by definition, normal to the radiant direction OR, and passes through the observing station at O. On account of the aspect sensitivity (or specularity) of the reflection process, all possible reflection points for a particular radiant lie in this plane. At short wavelengths ($\lambda < 15$ m), the reflection points should be confined to a narrow height interval centred on a mean height of about 100 km. The **echo surface** is an imaginary surface at this height. Its curved intersection with the echo plane is denoted SS', the **echo line**. This moves through the antenna beam because of the diurnal motion of the radiant, and will be a band of finite width rather than a discrete curve, owing to the diffuseness of any real shower radiant.

The **minimum detectable line density** at a point P on the echo surface, α_p, is the threshold value which the line density must exceed if the meteor is to be detected at point P. Expressions which relate this quantity to the system parameters are arrived at by rearranging the expressions (3.9) and (3.14), respectively. They are:

$$\alpha_p = \left(\frac{32\pi^2 R^3 P_R}{P_T G^2 \lambda^3}\right)^{1/2} \frac{1}{r_E} \quad m^{-1} \qquad \ldots(3.20)$$

for decay-type (underdense) echoes, and

$$\alpha_p = \left(\frac{105\pi^3 R^3 P_R}{P_T G^2 \lambda^3}\right)^{2} \frac{1}{r_E} \quad m^{-1} \qquad \ldots(3.21)$$

for persistent (overdense) echoes, where P_R is the minimum detectable echo power. The normalized sensitivity parameter is given by $\rho = \alpha_{po}/\alpha_p$ where α_{po} is the minimum value of α_p, i.e. the value of α_p at the most sensitive point in the beam. In Chapter 4 the range-dependence of the system sensitivity is discussed; the values of ρ need to be corrected by an appropriate weighting factor to arrive

at ρ_w, the normalized range-weighted sensitivity parameter. Contours of constant ρ_w, for the half-wave dipole antenna system described in Chapter 4, are mapped onto the echo surface in Fig. 4-4.

If the position of the echo line relative to the sensitivity contours is known for a particular altitude and azimuth of the shower radiant, then the echo rate per unit length of the echo line may be expressed as a function of the position of P and the absolute incident flux, and finally, the total echo rate over part or the whole of the echo line may be established by numerical integration; that is, by summing all the contributions from infinitesimal segments of the echo line.

The incident meteoroid flux producing zenithal line densities between α_m and $\alpha_m + d\alpha_m$ is approximated by a simple power law:

$$\Phi(\alpha_m) = c\alpha_m^{-s} \qquad ...(3.22)$$

where c and s are constants (generally, $s > 2$ for sporadic and $s < 2$ for shower meteors). Upon integrating equation (3.22), the flux producing zenithal line densities greater than α_m is found to be:

$$\theta(\alpha_m) = \frac{c}{(s-1)\alpha_m^{s-1}} \qquad ...(3.23).$$

It is convenient to rewrite equation (3.5) in the form

$$\frac{\alpha}{\alpha_1} = \frac{27}{4} u(1 - u)^2 \qquad ...(3.24)$$

where $u = \rho/\rho_o = \exp(-x/H)$, $x = h - h_o$. $\rho_o = 3\rho_1$ is the atmospheric density at burn-out and h_o is the corresponding height. The parameter u varies along a given train, from $u = 0$ far above h_o where ionization is negligible, through the ionization maximum where $u = 1/3$, to a value of unity at h_o (burn-out).

The flux of meteoroids incident on a strip of the echo plane at P (Fig. 3-5) which is normal to SS' and of width dl, and passing through the interval of the strip between heights x and x + dx above h_o and with maximum line densities in excess of α_1 is given by

$$dN = \theta\left(\frac{\alpha_1}{\cos X}\right) \frac{dl\, dx}{\sin X} \qquad ...(3.25).$$

Fig. 3-6 illustrates the situation described above. Of these meteors, only those having line densities on the echo line in excess of α_p will be detected. Thus, a necessary condition for detection is that

$$\alpha_1 \geq \frac{4}{27} \alpha_p u^{-1} (1 - u)^{-2} \qquad ...(3.26)$$

where u is evaluated at the echo line. Then the total echo rate from meteors intersecting the strip is

$$N_1 dl = \frac{H\,dl}{\sin X} \int_0^1 \theta(\alpha_{mx})\ \frac{du}{u} \qquad \ldots(3.27)$$

where

$$\alpha_{mx} = \frac{\alpha_1}{\cos X} = \frac{4}{27}\ \frac{\alpha_p}{\cos X}\ u^{-1}\ (1-u)^{-2} \quad ,$$

and is the maximum zenithal line density of the faintest detectable meteor at height $h_o + x$; N_1 is the observed echo rate per unit length of the echo line. By substituting for $\theta(\alpha_{mx})$ from (3.23), equation (3.27) may be expressed as

$$N_1 = \frac{HI}{\sin X}\ \theta\left(\frac{\alpha_p}{\cos X}\right) \qquad \ldots(3.28)$$

where

$$I = \left(\frac{27}{4}\right)^{s-1} \int_0^1 u^{s-2}(1-u)^{2(s-1)}\,du$$

$$= \left(\frac{27}{4}\right)^{s-1} \frac{\Gamma(s-1)\ \Gamma(2s-1)}{\Gamma(3s-2)} \qquad \ldots(3.29).$$

A plot of I versus s will be found in Fig. 3-7.

In equation (3.28), the value of X at the point P differs slightly from X_o at the observer, but by making the approximations

$$\cos X \sim \cos X_o \quad \text{and}$$
$$\sin^2 X \sim \sin^2 X_o + 2\langle h\rangle / R_E$$

where R_E is the Earth radius and $\langle h\rangle$ the adopted height of the echo surface, it is possible to express equation (3.28) in the form

$$N_1 = H f_1(X_o, s)\,\theta(\alpha_p) \qquad \ldots(3.30)$$

where

$$f_1(X_o, s) = I\ (\cos X_o)^{s-1}\ \ (\sin^2 X_o + 2\langle h\rangle / R_E)^{-1/2},$$

which is plotted in Fig. 3-8 as a function of X_o for various values of s.

Finally, the total echo rate over part or the whole of the echo line is found to be, on integrating equation (3.30),

$$N = H\ f_1(X_o, s)\ \theta(\alpha_{po}) \int \rho^{s-1} dl \qquad \ldots(3.31).$$

This equation has been derived on the assumption that meteors ablate classically, but in fact this is not the case. Refinements to (3.31) are discussed later, in section (3-6).

3-5: A Note on Meteoroid Structure

Contrasting views on the structure and composition of meteoroids have been put forward by different investigators. For years it was believed that meteors were compact chunks of stone or iron; however, studies carried out on visual meteors by Jacchia (1955), McMrosky (1955) and Opik (1955) revealed that, in general, the light curves were non-classical, and fragmentation of the ablating bodies was therefore inferred. Jacchia (1955) and Opik (1955) suggested that meteors were fragile, porous structures, as might be expected on the basis of Whipple's icy comet model. Later, Jones & Kaiser (1966) assumed a solid structure for meteoroids, and suggested that fragmentation was due to internal thermal stresses. In a review of meteoroid structure, Verniani (1969) concluded firmly that meteoroids are fragile, loose conglomerates of spongy material, in accordance with Jacchia's (1955) idea.

The dustball model of Hawkes & Jones (1975) is a development of this view. It assumes a meteoroid to be a conglomerate of stony (or iron) grains held in a matrix of lower melting-point 'glue'. Upon entry into the atmosphere, two distinct stages may be identified in the ablation process: (i) the 'glue' heats up and melts; and (ii) the body fragments, releasing the dust grains (of typical mass 10^{-6} g) which then ablate according to the classical theory. Only during stage (ii) is ionization produced. Both the delay in the onset of ablation due to the finite heat capacity of the 'glue', and the injection of the grains into a region of finite air density, result in shorter ionization curves and enhanced maximum line densities, as Fig. 3-1 (curve b) illustrates. In the next section we shall consider how these effects influence meteor detectability.

To the author's knowledge, no advance on the Hawkes-Jones model has been proposed, although it has been suggested by Beech (1984) that meteoroids are more fragile than this model has assumed. This is also the finding of Hapgood et al. (1982), for Perseid meteor material.

3-6: Deviations from the Classical Ablation Theory

Equation (3.31), which was derived on the assumption that meteors obey the classical ablation theory, has been used to calculate absolute incident meteoroid fluxes from the observed echo rate (Kaiser et al., 1966; Poole et al.,1972; Webster et al.,1966). In several respects, however, the classical theory fails to give an adequate description of real meteoric behaviour. Various factors, which, for a given meteoric flux, mass and velocity distribution, affect the observed echo rate, will now be considered.

(1) **Reduced train lengths:** Factors which relate to meteoroid structure, and which result in shorter trains than classically predicted, have been mentioned in section (3-5). Poole (1973) has generalized the echo rate theory of Kaiser (1960) to take these effects into account. If a meteor does not begin to ablate until it has reached some finite height in the atmosphere specified by $\tau = \rho/\rho_1$, then the resulting expression for α is (c.f. equ. 3.5):

$$\alpha = 0 \qquad \frac{\rho}{\rho_1} < \tau$$
$$\alpha = \frac{\alpha_1}{4}\frac{\rho}{\rho_1}(3 + \tau - \frac{\rho}{\rho_1})^2 \qquad \frac{\rho}{\rho_1} \geq \tau \qquad \ldots(3.32)$$

Fig. 3-1 (curve b) illustrates such an ionization profile for the case $\tau = 0.3$, an effective mean value for radio meteors (Jones & Kaiser, 1966; Poole, 1967), and clearly shows the enhanced line density of the shorter train.

Associated with shorter ionization curves are two effects which work in opposition. (i) Shorter train lengths cause the factor $I(s,\tau)$ to be less than the factor $I(s,0)$ of equation (3.28), and a reduction in the observed echo rate below that expected for the case $\tau = 0$. This effect becomes more pronounced as τ increases. On the other hand, (ii) an enhancement of maximum line densities (when $\tau > 0$) will have the effect of reducing the minimum detectable meteor mass, increasing the observed rate.

If we retain the definition of θ in equation (3.31) as the flux of meteors that would produce zenithal line densities in excess of $\alpha_{p\theta}$ **if they were to behave classically**, then that equation, modified to take both the effects (i) and (ii) into account, still applies provided the previous expression for I is replaced by

$$I' = A(s,\tau)\left(\frac{27}{4}\right)^{s-1} \int_{\tau/(3+\tau)}^{1} u^{s-2}(1-u)^{2(s-1)}\,du \qquad \ldots(3.33)$$

where

$$A(s,\tau) = \left(\frac{3+\tau}{3}\right)^{3(s-1)} \qquad \text{(after Poole, 1973).}$$

$A(s,\tau)$ is the factor by which the actual flux of detectable meteors will be larger than $\theta(\alpha_{p\theta})$. The observed echo rate N is proportional to I'. Curves of I' as functions of τ for various s have been reproduced in Fig. 3-9. It should be noted that for $s = 2$, I' is a constant, indicating that the opposing effects (i) and (ii) compensate each other for all τ. For $s < 2$, the curves for I' show that the observed echo rate for a given $\theta(\alpha_{p\theta})$ decreases with increasing τ, while for $s > 2$ it actually increases. Similar results have been obtained in an approximate derivation by Jones & Hawkes (1975). Indeed, observations of sporadic meteors (for which $s > 2$, see section 3-4) have revealed anomalously high rates near solar minimum. Lindblad (1976) has suggested that this may be due to an inverse variation of the atmospheric density gradient at meteoric heights with sunspot activity. Near the solar minimum, the density gradient would be at its peak and so meteors would ionize over smaller height intervals. In this way the ionization column of any particular meteoroid would be compressed. Lindblad's suggestion has been supported by the work of Ellyett et al. (1980).

(2) <u>The radio echo ceiling.</u> Effects due to the width of the meteor train will now be considered. Two effects couple to produce an echo ceiling above which no radio meteors can be detected: one due to the initial train radius, and the other due to the finite meteoroid velocity.

Manning (1958) has identified two distinct stages in the diffusion of the ionization trail: (a) a rapid diffusion lasting about one third of a millisecond, after which the train has reached its 'initial radius' of the order of 14 ionic mean free paths, and (b) a slower diffusion, determined by the air temperature. It has already been mentioned in section (3-3-1) that, even before the onset of the second stage of diffusion, the initial train radius reduces the returned signal amplitude by the factor

$$\exp\left[-\frac{2\pi r_{\theta}}{\lambda}\right]^2$$

where r_{θ} is the initial radius. The latter increases with height and approximately doubles for an increase in velocity from 40 to 65 km s^{-1} (Baggaley, 1970). Hawkes & Jones (1978) have suggested that the observed initial radius may be due to the high spin rate of the meteors, which causes lateral spreading of the grains prior to the onset of ablation. In view of this effect alone, the chances of detecting any meteor which forms above 105 km with a 10 m radar are remote.

The second factor to be considered is that due to the finite meteor velocity. In section (3-3-1) it has been mentioned that the echo signal strength is dominated by the contributions from the first Fresnel zone on either side of the reflection point. Unless the meteor

reaches the end of the first Fresnel zone before the train at the beginning of the zone has diffused to a radius of about $\lambda/2\pi$, the echo amplitude is severely reduced. The attenuation factor is

$$\left[\frac{1 - \exp(-\Delta)}{\Delta}\right] \qquad \ldots(3.34)$$

where

$$\Delta = \frac{8\pi^2 D (2R)^{1/2}}{v\lambda^{3/2}} \quad ,$$

and D = diffusion coefficient,
R = range,
v = meteoroid velocity,
λ = radio wavelength (Baggaley, 1970).

The effects due to finite velocity and initial train radius are similar in that they both become more pronounced at higher frequencies. However, the former is more severe for slower meteors at any particular altitude, and in this respect they differ.

Because the height of maximum ionization increases as meteors get fainter (although the ionization heights of meteors fainter than M_r = +5 are mass-independent), echoes from meteors in the mass range 10^{-2}-10^{-6} g are likely to fall below the detection threshold of conventional meteor radars (λ < 15 m). Consequently, only by using a long wavelength radar for which the echo ceiling is inconsequential, can realistic flux values and height distributions be deduced. Such work has been carried out by Ollson-Steel and Elford (1987) at λ = 150 metres. This group has established that the true height distribution of radio meteors extends right up to 140 km, with echo heights clustering around 104 km. This peak is some 10 km higher than that deduced from observations at conventional wavelengths. A fourfold increase in the calculated mass influx of meteoroids results when this high velocity component is taken into account (Thomas et al., 1986).

Chapter 4: The Equipment

In section 4-1 we discuss the meteor radar and its operation. Much of the information on the system has been derived from a paper by L.M.G.Poole (1988): 'The Grahamstown all-sky meteor radar' (to be published shortly). In section 4-2, work done by the author to establish an empirical antenna pattern is discussed.

4-1: The Grahamstown meteor radar

The Grahamstown meteor radar, which is a coherent-wave system of the monostatic type, became fully operational during April 1986. For the most part the equipment is housed in the Rhodes University research 'hut' situated on the western outskirts of Grahamstown (33 19'S,26 30'E), and consists essentially of the following:

Transmitting subsystem:	transmitter
	transmitting antenna
Receiving subsystem:	4 receiving antennas
	2 receivers
	switching box
	filters
	data logging system.

Fig. 4-1 shows a simplified block diagram of the system.

The transmitter has a mean output power of approximately 30 watts and is operated at a fixed frequency of 27.99 MHz, less 40 Hz, square-wave modulated at 500 Hz. This facilitates transmit-receive switching, a necessity for all backscatter radars.

The two available receivers are shared between four receiving antennas. Each receiver input is switched at 250 Hz between two antennas, synchronized with the switching of each output between two low-pass filters. Fig. 4-1 illustrates this process schematically. The receivers are tuned to exactly 27.99 MHz; that is, an input signal at this frequency produces a DC output. The low-pass filters cut off near 100 Hz, and remove the 500 Hz switching frequency and its higher harmonics. After this the signal appears as a pure audio tone. If the target (meteor train) is stationary, then the frequency of this signal is the difference between the

transmitted and receiver-tuned frequencies: 40 Hz. In general, the train drifts with winds in the meteor region. Consequently the frequency is usually doppler-shifted from this value by an amount proportional to the component of the drift velocity along the observer's line of sight.

All five antennas are simple half-wave dipoles mounted one third of a wavelength above a flat ground plane. Their axes are aligned along the north-south meridian, so that the two broad lobes of the beam are directed east and west. The ground surface beneath the antennas has been made conducting by laying down a coarse galvanized wire grid ($1m^2$). About two-hundred metres separate the single transmitting antenna from the array of four used for receiving. The receiving array is arranged as illustrated in Fig. 4-1. The direction of arrival of an echo can be deduced, in principle, by comparing the phase of the reflected signal at each antenna. Initially only three receiving antennas were used (A, B and C). However, a phase comparison yielded a multiplicity of possible directions for any echo. Therefore it was necessary to introduce a fourth antenna (D) to discriminate between these options. This has been sited for maximum resolution of the ambiguity.

The most important property of an antenna system is its radiation pattern, or polar diagram. In general, the power radiated is concentrated in a particular direction. This directivity is usually expressed in terms of the antenna power gain G, which in the case of a transmitting antenna is defined as

$$G = \frac{P_\theta}{P_i}$$

where P_θ = radiated power flux in a given direction by the antenna, and P_i = radiated power flux in any direction from an isotropic radiator; in this definition it is assumed that equal power is fed into the antenna and the isotropic radiator. According to the principle of reciprocity, the identical polar diagram applies irrespective of whether the antenna is transmitting or receiving.

The antenna power gain, in the direction of any point P, of the system of antennas at Grahamstown is given by

$$G = 4\left[\frac{\cos(\tfrac{1}{2}\pi\cos\theta)}{\sin\theta}\sin\left(\frac{2\pi H}{\lambda}\sin a\right)\right]^2 \quad \ldots(4\text{-}1)$$

where H = height of the antennas above the ground (= $\lambda/3$),
a = altitude of P,
$\cos\theta$ = cosa cosA,
A = azimuth of P.

In equation (4-1) it is assumed that the ground is perfectly conducting. The beam maxima, where G = 4, are elevated at 48.5 degrees due east and west.

The normalized sensitivity parameter ρ is related to the directive antenna gain through the following expression:

$$\left(\frac{G}{R^{3/2}}\right) ,$$

normalized to a maximum value of unity (Baldwin & Kaiser, 1965). When normalized, this quantity is identical with $\alpha_{r\theta}/\alpha_r$ of section 3-4.

The 500 Hz modulation imposes a range-dependence on the system sensitivity. This may be understood with reference to Fig. 4-2. Power is transmitted for 1 ms when the transmitter (TX) switches on. In general only part of the delayed echo pulse will be 'seen' on any channel (CH). This is indicated by 'ECHO' where the dashed part of the pulse arrives while the channel is inactive. The full echo pulse is observed only for a delay of 1 ms, corresponding to a range of 150 km. It can be shown that once the pulse has been filtered as described above, the amplitude of this sinusoidal signal is proportional to the width τ of the 'seen' echo pulses (even though the received power is also proportional to τ). This quantity varies with the range of the reflecting point R as shown in Fig. 4-3. Once this function has been normalized, it defines a factor W by which the values of ρ defined in section 3-4 should be multiplied to take account of the fact that only a fraction of the echo power is 'seen'.

The range-weighted normalized sensitivity parameter is given by

$$\rho_W = \frac{(WGR^{-3/2})}{(WGR^{-3/2})_{max}} \qquad \ldots(4\text{-}2)$$

Normalized, range-weighted sensitivity contours, deduced from equation (4-2), are mapped onto an echo surface at a constant height of 95 km in Fig. 4-4. The altitude of maximum ρ_W (57°) is somewhat higher than that for G due to the factor $WR^{-3/2}$.

As a consequence of the antenna beam pattern and the diurnal motion of the echo line, the echo rate associated with a particular radiant is expected to vary symmetrically about the time of radiant transit. Fig. 4-5 shows how the diurnal rate of underdense echoes is expected to vary according to the declination of the radiant. For the Delta-Aquarid radiant, which has a southern declination ($\delta = -17^{\circ}$), the echo line intersects the beam close to either of the maxima three hours before and after transit (see Fig. 4-4). The echo rate is therefore expected to peak at these times, and should be zero at transit, when the echo line does not cross any beam contours of appreciable sensitivity. In fact the echo line passes well below the lower border of Fig. 4-4. Following similar reasoning, the rate would be expected to have an intermediate value at 1½ hours before and after transit. The corresponding echo lines are indicated in Fig. 4-4. Plot (a) of Fig. 4-5 illustrates the expected rate curve for the Delta-Aquarid radiant. The two distinct peaks of plot (a) become progressively merged the more northerly the radiant declination, as shown in plots (b) (Eta-Aquarids, $\delta = 0^{\circ}$) and (c) (Geminids, $\delta = +32^{\circ}$). This effect may be understood for these radiants by again considering the motion of the echo line across the beam. For a radiant which does not rise far above the northern horizon (eg. the Geminid radiant: altitude at transit time = 25°), the integral in equation (3.31) (and consequently also the rate) will have a maximum only near transit, when the echo line passes close to the beam centres. Comparisons between these theoretical rate curves and the observed shower echo rate appear in Chapter 5.

An Apple-type (FK-727) microcomputer controls the data logging system. Any signal whose amplitude exceeds a predetermined threshold activates the system, after which a multichannel A/D converter samples each channel at 256 Hz for one second. The data are then transferred to the computer memory where they are temporarily stored. Every few hours the memory contents are dumped onto a floppy disc for subsequent processing at a university computing facility (VAX-11/730 minicomputer). This processing involves transforming each time-varying signal to give its spectrum. A genuine meteor echo is recognized by comparing the frequency of the received signal on all four channels. If the frequency difference between any two channels exceeds a predetermined limit, the signal is regarded as a spurious echo. Finally, data for each positively identified echo are stored as 'O-files' on hard disc in the VAX-11/730, where it is accessible to the computer programs described in the following two

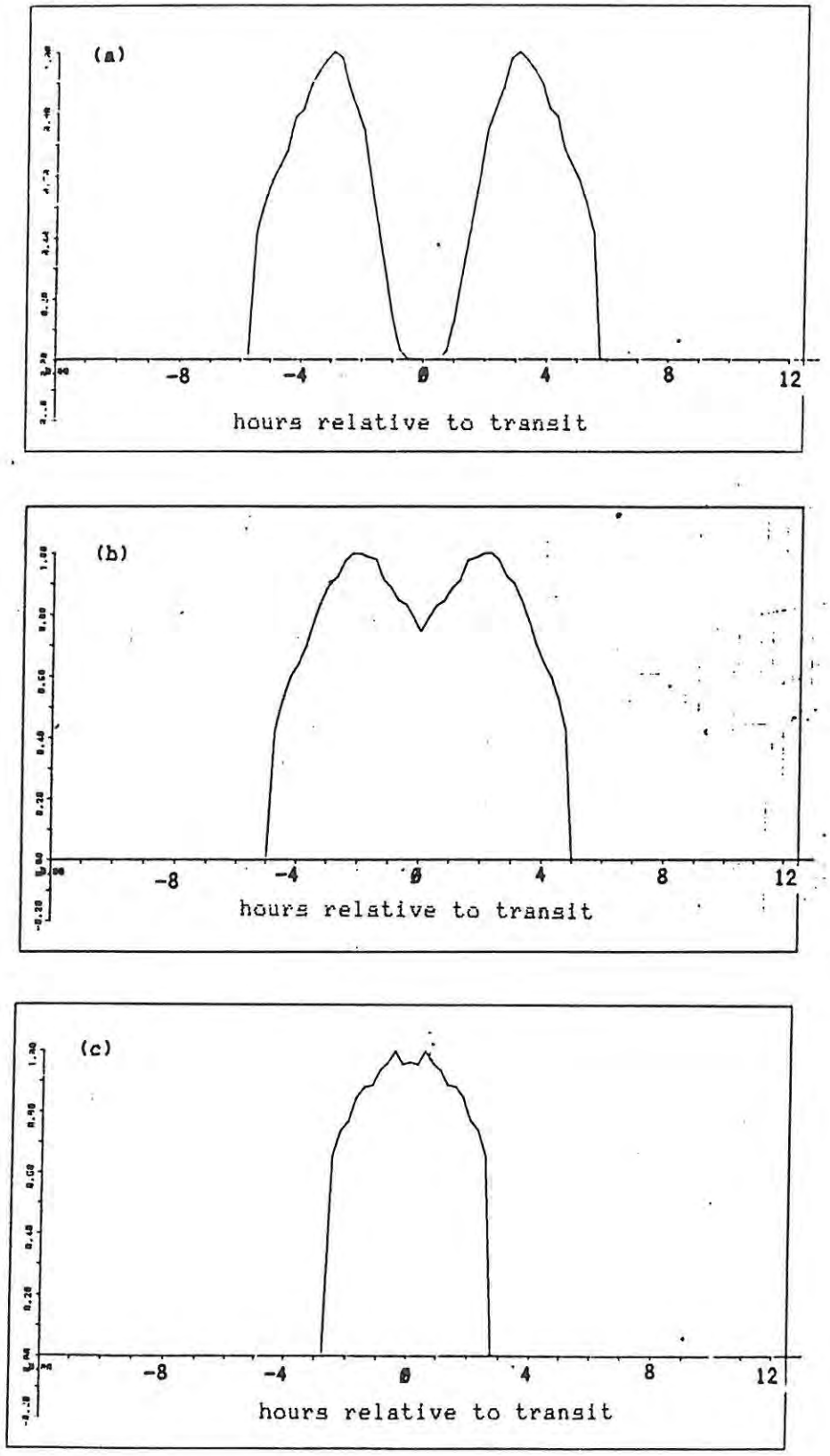

Fig 4-5: Normalised theoretical underdense echo rate associated with 3 different shower radiants: (a) southern δ-Aquarids (δ = -17°), (b) Eta-Aquarids (δ = 0°), and (c) Geminids (δ = +32°).

chapters. The data include, for each echo: Date and time of occurrence, amplitude, duration above the predetermined amplitude threshold, azimuth, and altitude. Information on the drift velocity of the train is also included, but is not utilized in this thesis. Echo directions which could not be resolved with certainty have been termed 'ambiguous'.

4-2: Empirical verification of the antenna pattern

One of the aims of the work described in this thesis is to improve upon the method of Morton & Jones (1982) for plotting meteor radiant maps, by eliminating the astigmatism present there. The results are presented in Chapter 6. Briefly, each meteor echo needs to be correctly weighted in accordance with the beam sensitivity in the echo direction. It is obvious that first the beam pattern must be known before the appropriate weighting can be deduced. We therefore decided to check the predictions of equations (4.1) and (4.2) empirically.

The sky was first divided into 432 direction bins in which ρ_w was assumed to be constant, 15° in azimuth by 5° in altitude. A curve of the distribution of echo amplitudes was then plotted for each bin, and compared with that for the most sensitive bin. The Fortran program AMPBIN was written for this purpose, and is listed in Appendix 1. The procedure for determining ρ_w from these curves may be understood with reference to the schematic amplitude distribution profiles shown in Fig. 4-6. The dashed curves show, on logarithmic scales, the form of the dependence of N, the total number of echoes observed in a bin as a function of A, the echo amplitude for (a) the bin at the most sensitive part of the beam ($\rho_w = 1$) and (b) a less sensitive bin ($\rho_w < 1$).

N for any bin is proportional to the meteoroid flux producing echoes in that bin, $\theta(\alpha_m)$. Starting from equation (3.23) with $\alpha_m = \alpha/\langle\cos X\rangle$, where $\langle\cos X\rangle$ is an average value of cosX for meteors observed in any bin, we obtain

$$N = K \frac{\langle\cos X\rangle^{s-1}}{\alpha^{s-1}} \qquad \ldots(4.3)$$

where K is a positive constant. For the case of underdense echoes, α in the denominator of (4.3) is proportional to A. For overdense echoes it is proportional to A^4. Substitution leads to two expressions:

underdense echoes: $$N = K' \frac{1}{A^{s-1}} \qquad \ldots(4.4)$$

and

overdense echoes: $$N = K'' \frac{1}{A^{4(s-1)}} \qquad \ldots(4.5).$$

Once these have been written in the straight line form, we have the following equations for the amplitude distribution

of specular meteor echoes in the under- and overdense regimes, respectively:

$$\log N = \log K' - (s-1)\log A \qquad \ldots(4.6)$$

$$\log N = \log K'' - 4(s-1)\log A \qquad \ldots(4.7).$$

The shallow and steep asymptotes in Fig. 4-6 are given by equations (4.6) and (4.7) respectively. The 'knees' of curves (a) and (b) in this diagram occur at the threshold amplitudes A_T and A_T' respectively, which correspond to the transition line density (α_T) marking the boundary between the under- and overdense echo types.

Due to the fact that echoes in the transition region between the under- and overdense regimes are hybrids of both echo types, the change from echoes whose character is predominantly underdense to echoes which are primarily overdense is a gradual one, giving rise to real amplitude distribution profiles of the form shown by the broken curves in Fig. 4-6. Consequently the 'knees' of the broken curves are not sharp discontinuities in the slope.

It has been mentioned in the above that the curves (a) and (b) are associated with the most sensitive, and a less sensitive bin, respectively. The differences between them may be understood from the foregoing considerations. If we move from the most sensitive to the less sensitive bin, the minimum detectable line density increases ($\alpha_P > \alpha_{P\phi}$), and the small meteors which are just above the detection threshold in the most sensitive bin can no longer be detected. If the meteoroid fluxes associated with the echoes detected in each of the bins are identical, then fewer meteors will be detected in this bin. This has the effect of shifting curve (b) downwards with respect to (a). A meteor of a given size (of line density α_T, say) will give rise to a smaller amplitude echo (A_T') in this bin, displacing curve (b) to the left of (a).

For the purpose of establishing the antenna pattern, the vertical shift of the profile is of no consequence since $\theta(\alpha_m)$, and $\langle\cos X\rangle$, may be different for different bins. The horizontal shift, however, is important. In both the over- and underdense regimes, the echo amplitude for a given α is proportional to ρ_w as given by equation (4.2). The amplitude is also proportional to α^n (n = 1 for under- and n = ¼ for overdense echoes). Hence we can write the general expression

$$A = c\rho_W\alpha^n \qquad \ldots(4.8)$$

where c is a positive constant. At the transition line density (α_T), equation (4.8) becomes

$$A_T = c\alpha_T^n \qquad \ldots(4.9)$$

for the beam centre (where $\rho_W = 1$). For a less sensitive sensitive bin, expression (4.8) becomes

$$A_T' = c\rho_W\alpha_T^n \qquad \ldots(4.10).$$

where A_T' is the echo amplitude associated with α_T in that bin. Dividing (4.9) by (4.10) gives

$$\frac{A_T}{A_T'} = \frac{1}{\rho_W} \qquad \ldots(4.11),$$

from which the following expression is easily derived:

$$\log \rho_W = -\Delta \log A_T \qquad \ldots(4.12)$$

where $\Delta \log A_T$ is the horizontal shift of the 'knee' of an amplitude distribution profile for a bin of a given sensitivity relative to the 'knee' of the profile corresponding to the most sensitive bin.

In Fig. 4-8 actual profiles, using data aquired over several months, for (a) the most sensitive bin (central (Az,Alt) coordinates (97.5°,57.5°)) and (b) a less sensitive bin have been reproduced. Although the exact positions of the 'knees' are not sharply defined, it was nevertheless possible to correctly dispose any of the curves relative to that for the most sensitive bin, by superimposing the plots on a light table and shifting the upper curve until it matched the lower one. Errors in the horizontal shift were estimated by considering the best and the worst match between the two curves. The magnitude of this shift was taken as the relative lateral displacement of the origins of the two graphs.

Once these measurements had been made for all the bins, and equation (4.12) invoked to compute ρ_W for each bin, a graph of ρ_W as a function of altitude was plotted for each of the 24 azimuth bins shown in Fig 4-7. On the assumption that the antenna pattern is symmetric with respect to inversion through the origin, these graphs were grouped into six sets

containing four equivalent azimuth bins each. For example, set 1 contained graphs for the azimuth bins 1, 12, 13, 24; set 2 graphs of bins 2, 11, 14, 23; etc.. The four individual curves of each set were then superimposed and the best average of the plots was estimated and drawn in by hand. The final result of this process was six curves, each representing four equivalent azimuth bins, of ρ_w as a function of altitude.

Such curves (solid lines) are compared with their theoretical counterparts (dashed lines) after equation (4.2), in Fig. 4-9. The solid curves have been plotted over the altitude range 20° to 70° only. Echo directions lying outside of this range were either spurious, or largely the result of non-specular reflection. The amplitude distribution of such echoes does not follow the profile described by the relations (4.6) and (4.7), and is therefore not suitable for the determination of ρ_w. For bins where the total echo count was lowest, the profiles are of poor quality. The quality improves progressively from due north (and south) where the bins of lowest sensitivity are located, through to due east (and west) where the bins of highest sensitivity are situated. The trend is reflected by the degree of similarity between the solid and dashed curves (Fig. 4-9) of ρ_w versus altitude. Curve (a) shows this for the azimuth bins due north and south (bins 1, 12, 13, 24, data of poor quality); curve (b) for bins located midway between the north-south meridian and the east-west line (bins 3, 10, 15, 22, data of intermediate quality); and curve (c) for bins located due east and west (bins 6, 7, 18, 19, data of highest quality).

The solid curves of plots (d) and (e) are averages over two bins instead of four. They represent the two most sensitive easterley azimuth bins (6 and 7) and the two most sensitive westerley bins (18 and 19), respectively. From these two plots, the east beam appears to be less sensitive than its westerley counterpart below approximately $\alpha = 50^\circ$, but slightly more sensitive above this altitude. In relation to the error bars this difference is not considered significant, and the combined data of four equivalent bins have been adopted for use. In Chapter 5 it is confirmed that the east and west beams are of similar sensitivity; Fig. 5-13 (a) and (b) show that, for the strong Delta-Aquarid radiant, shower rates were symmetrical with respect to transit.

For the azimuth bins where sufficiently good data for the amplitude distribution plots could be obtained, the agreement

between the solid and dashed curves (Fig. 4-9) was good. Plots (b) - (e) illustrate this. Although this was not the case for the bins of low sensitivity (plot (a)), it was assumed that, if data of suitably high quality were available for such bins, the agreement would be observed for all azimuths. The theoretical antenna pattern as given by equation (4.2) and plotted in Fig. 4-4, was therefore assumed to be valid over all azimuths and altitudes and was adopted for use in the calculation of the detection probability of echoes in different parts of the beam.

What is meant by the 'detection probability' may be understood with reference to Fig. 4-10. This shows the analytical function which was fitted to the amplitude distribution profile for the most sensitive bin (Fig. 4-8 (a)). The ordinate represents, on a logarithmic scale, the total number of echoes in this bin normalized to a maximum value of unity. We have called this quantity p, the 'detection probability'. On the abscissa, log ρ_w (related to Δ log A_T by equation (4.12)) has been plotted. The equation describing the curve is given by

$$\log p = \frac{-5.70 + [32.49 - 57.76\ (\log \rho_w)^2]^{1/2}}{2} \quad ; \quad \ldots(4.13)$$

$$|\log \rho_w| \leq 0.750$$

$$0 \leq p \leq 1$$

Now, consider a meteor of a given size, and larger than or equal to the faintest meteor detectable in the most sensitive bin (i.e. $\alpha_p > \alpha_{p0}$). Such a meteor would of necessity be observed if it fell in the most sensitive bin (i.e. p = 1), but the probability of detecting the meteor would be less than unity if it were to fall in a less sensitive bin. In this sense p is a measure of the detection probability, on the assumption that plots such as Fig 4-8 (b) for the other bins all have a similar shape. Clearly, p must vary according to the bin sensitivity ρ_w. The form of this dependence is given by equation (4.13). The radical in this expression becomes negative for values of log ρ_w < 0.750 and hence (4.13) is only valid for the parts of the beam where 1.000 > ρ_w > 0.178. It is safe to assume that negligibly few echoes will be detected in the remainder of the beam, as is indeed supported by Fig. 4-8 (a) where no meteors were observed above log A = 2.11 (this corresponds to Δ log A = 0.72 and ρ_w = 0.19). The use of p in devising a method of weighting to compensate for the anisotropy of the antenna pattern, is discussed in Chapter 6.

Chapter 5: A general survey of the Southern Hemisphere radar meteor rates.

5-1: Introduction

This subsection contains information of a general nature on the scope of the survey, and descriptions of the computer rate programs. The methods that were used to detect shower activity are discussed. All periods specified by initial and terminal dates are inclusive of those dates, unless otherwise stated. This holds for the present and the remaining chapters of the thesis.

Over the period 1986 April 25 to 1988 January a survey of radio meteors was conducted with the Grahamstown meteor radar (discussed in Chapter 4). During 1986 the survey was intermittent, and spanned the following dates: April 25 - May 15; July 20 - August 9; August 15 - September 3; September 13 - October 4; and October 20 - December 20. These periods of observation were chosen to include three major showers: the Eta-Aquarids (May), the Delta-Aquarids (July) and the Orionids (October). From 1986 December 22 the radar was operated continuously.

In general meteor activity was monitored for 24 hours per day. In each hour observation was generally limited to 40 minutes in order to eliminate interference from ionospheric chirp-sounding equipment located at the radar site, which was active during the remaining 20 minutes. This period of 'out-time' is valid for all the observations unless the contrary is indicated.

Occasionally data capture was temporarily suspended for two reasons: (1) unforseen power failures, and (2) for the sake of calibration procedures which were necessary to ensure that the system parameters remained constant. These periods seldom exceeded two or three hours. Occasionally data were lost due to malfunctioning floppy discs in the data capture system or human failings.

The graphs which are presented in this chapter were produced by a total of nine Fortran computer programs, written by the author for the VAX-11/730 digital minicomputer. A full listing of these programs appears in Appendix 1 at the end of this thesis. They will now be briefly described.

(1) RATE: Two options may be selected. This program either (a) computes the all-sky hourly rate of echoes (i) above each of 10 selected amplitude thresholds and (ii) whose amplitudes persist above a predetermined threshold for longer than 1.8 seconds ('long' echoes); or (b) calculates the hourly rate of (i) 'long' echoes and (ii) echoes

above the 10 amplitude levels in each of 432 direction bins, 5° in altitude by 15° in azimuth.

The 'long' echo criterion is not rigorous. Owing to fading effects (discussed in Chapter 3) and the appearance of multiple reflecting points, the amplitudes of persistent echoes may drop below the detection threshold, and rise above it again only after 1.8 seconds has elapsed. In this way some persistent echoes may escape detection as 'long' echoes.

To arrive at an hourly rate, the echo count for a particular hour is multiplied by a factor F which takes the total 'out-time' during the hour into account:

$$F = \frac{n \times 60}{(n \times 60) - OT}$$

where OT is the out-time in minutes, and n (the number of hours) serves to generalize the expression for time-windows involving more than a single hour. These are introduced in later programs. Included in OT is any time for which the system was inactive; in addition to the 20 minutes mentioned above, there were several seconds of out-time during the transfer of data by the computer from buffer to memory after every echo registration. This amounted to roughly two minutes every hour.

Program RATE writes data to a 'R-file'. This serves as input for later programs.

(2a) AVRATE1 computes the average echo rate for each hour of the day, averaged over several days, for echoes above each of the 10 amplitude thresholds and for long echoes. AVRATE1 is used in conjunction with option (a) of RATE. The program reads from a R-file and writes to an 'A-file', which serves as input for later programs.

(2b) AVRATE2 is a slightly different version of AVRATE1 and is used in conjunction with option (b) of RATE. It calculates the average hourly rate of echoes above the 10 amplitude thresholds, and of long echoes, in each of the 432 azimuth-altitude bins. It also computes the average hourly rate of echoes received from the west, and from the east. As for the previous program, AVRATE2 reads from a R-file and writes to an A-file.

(3) AVPLOT: This program is identical with (2a), except that instead of writing the data to a file, it passes the data to a graph plotter.

(4) DIFPLOT: This program subtracts an A-file containing non-shower average hourly rates (an assumed sporadic meteor background) from an A-

file containing data taken over the day/days of maximum activity of a particular shower. This difference is the shower-only average hourly rate as a function of SAST. Data are passed to a plotter.

(5) EASTWEST: Two options may be selected. This program either (a) plots a graph of the difference between the average hourly west and east rates, or (b) superimposes curves of the average hourly west rate and the average hourly east rate on the same set of axes. Only option (b) has been used in this chapter. EASTWEST reads from an R-file.

(6) OWL arrives at a shower-only average hourly rate in the same way as program (4). It then superimposes on this rate curve a theoretical shower rate curve normalized to a maximum value of unity, which is computed according to the theory described in section (3-4). This facilitates a comparison between the observed and predicted diurnal variation of the shower rate.

(7) ECHOPLOT: The idea behind this program was to detect any clustering of the reflection points along the imaginary echo line during strong shower activity. ECHOPLOT maps the distribution of reflecting points onto an echo surface at an assumed height of 95 km. The reflection points are those associated with unambiguous echoes (see section (4-1)) which have occurred within two time-windows of variable length, usually chosen to lie symmetrically about the transit time of a particular shower radiant. The time-windows are shifted earlier by 4 minutes every day, since this corresponds to the daily shift in the transit time of any radiant. Pollution from non-shower meteors may be reduced, optionally, by eliminating positive-azimuth echoes which occur during the time-window prior to transit (when the echo line intersects the west beam) and negative-azimuth echoes which occur after transit. ECHOPLOT reads data from O-files (see Chapter 4).

(8) NEWPEAK1 plots a graph of the shower-only average hourly rate as a function of day number. Data are taken over two time-windows of variable length, which are shifted 4 minutes earlier each day. These are usually chosen to lie symmetrically about radiant transit. An assumed sporadic background is subtracted out.

For the showers of southern declination where the diurnal activity manifests as two peaks, data for one of the pair were occasionally lost due to power failures. However a realistic hourly rate could still be obtained by averaging over the time-window for which full data were collected. Thus the operator may optionally choose a 'rejection parameter', R: if the echo count in one time-window is less than that in the remaining window by the factor R, the program ignores the data of the first window. As in program (1), the number of echo registrations is multiplied by a factor F in order to arrive at an hourly rate. NEWPEAK1

reads data from O-files.

(9) NEWPEAK2 was written with the weaker showers in mind. It is similar to NEWPEAK1 but with two important differences: (a) no assumed background is subtracted out, and (b) echoes are discriminated against on the basis of their directions of arrival. The program plots a graph of the normalized daily average hourly rate of 'shower' echoes which are associated with radiants contained within a variable sky-window. In this definition 'shower' echoes are those which satisfy the specular reflection condition to within 1.25°. The size of this square of sky may be varied between 1 and 20°, and the window is usually placed so as to cover the area of known shower radiant activity. This program has the advantage over (8) that no assumptions are made about background rates. Data are read from O-files.

These nine programs were used to obtain rate profiles for the sporadic background, and twenty annually recurrent minor and major streams which are accessible from the Grahamstown radar. Streams with radiants south of δ = +37° fall into this category. Searches for showers which are not regular annual events, but whose appearance during 1987 was predicted, were conducted, one during April and the other during October. The corresponding streams are the Puppids and Epsilon Geminids, respectively.

It would have been a worthwhile exercise to evaluate the variation of the mass distribution index s with solar longitude, from the shallow and the steep asymptotes of amplitude distribution profiles as shown in Fig. 4-6. The corresponding slopes are $-(s-1)$ and $-4(s-1)$, respectively (see equations (4.6) and (4.7)). However, the data on which the profiles illustrated in Fig. 4-8 are based were accumulated over several months, and the amount of data for a single day of observation would not give an amplitude distribution profile sufficiently well defined for meaningful determination of asymptotes. For this reason an evaluation of the mass distribution index was not attempted.

In the remainder of this chapter we present and discuss the results of our rate survey. Broken lines generally indicate missing data, unless the contrary is stated. All error bars are standard deviations based on the number of echoes represented by each data point, and represent 70% confidence limits.

5-2: The sporadic meteor background.

Fig. 5-1 (A) to (S) shows the diurnal variation in the observed hourly echo rates averaged over a week, for each month of the survey. Dates near the 20th of each month were chosen, in order that average rates for the weeks at the two equinoxes could be obtained. The graphs have been grouped in two complimentary sets, (a) and (b). Set (a) shows the all-sky average hourly rate for every month, and (b) curves of the average west (solid lines) and east rates (broken lines) for the same dates. The following features are evident from Fig. 5-1.

(1) The overall level of activity dropped from 1986 to 1987. The diurnal maxima during 1987 were consistently between 15 and 30% down on the maximum rates for the corresponding months of the previous year (see also Fig 5-3). In spite of this decrease in the overall echo rate, there is a striking similarity between the shapes of the rate curves of corresponding months over the two years. This similarity is greater than that between the curves of adjacent months. This was also the finding of Keay & Ellyett (1969), in a survey conducted from Christchurch New Zealand (43° S), over the periods 1960-61 and 1963-65. From this one can infer that the distribution of meteoroids along the earth's orbit does not undergo large fluctuations from year to year. It is more likely that the lower rates during 1987 were the result of the variation of the atmospheric density gradient at meteor ablation heights over the solar cycle. The way in which fluctuations in the atmospheric scale height affect the observed rate has been discussed in section (3-6).

(2) The times of day when meteor rates reached their extreme values varied from month to month. This information is displayed in a different way in Fig. 5-2, from which it is evident that the time of diurnal minimum varied by as much as 4 hours, from 16h30 (May 1987) to 20h30 (November 1986). The observed evening minimum is to be expected; the orbital velocities of the earth and the intercepted meteoroids add vectorially, with the result that the radar site is effectively shielded from the bulk of the meteoroids being swept up by the earth, when the antapex is in transit at roughly 18h daily. Only (a) those meteoroids travelling in the direction of the apex and which are able to overtake the earth, and (b) those with high orbital inclinations, will be observed. The low geocentric velocities of group (a) means that their ionizing efficiency is low, and hence so is their detectability. Although most meteoroid orbits are concentrated within 15° of the ecliptic, it has been established that a proportion of meteoroids with highly inclined orbits (i = 60°) does exist (Davies & Gill, 1960; Baldwin & Kaiser, 1965).

Diurnal maxima were observed as early as 02h30 (October 1987) and as late as 08h30 (January 1987, September 1986). Several of the curves display double maxima (April,September, October 1986; February, April,May, September, October 1987), and most show a secondary peak before midnight. In general the rate rose gently before midnight, and somewhat more sharply afterwards to a broad maximum lasting several hours. Activity would start to decline rapidly, before noon. The dawn maximum is explained by remembering that the dawn side of the earth is most exposed to the influx of meteoroids. These have high encounter velocities and readily create trains of high electron density. The exact time of the diurnal peak is governed by fine structure in the sporadic radiant distribution. This may be expected to fluctuate throughout the year.

(3) The magnitudes of the diurnal maxima (Fig. 5-3) were subject to large changes from month to month. Fig. 5-3 shows that the form of the variation was roughly sinusoidal, peaking during the autumn months (April, May) and reaching a minimum in spring (September). The maximum is displaced by a month relative to the March ('vernal') equinox while the minimum coincides with the September equinox. This supports the findings of Keay & Ellyett (1969).

The origin of this sinusoidal variation lies in two factors: (a) the tilt of the earth's polar axis in relation to the direction of its orbital motion, and (b) the fluctuation in the spatial density of meteoroids in the vicinity of the earth throughout the year. Factor (a) results in the sinusoidal variation, with an annual periodicity, of the declination of the apex, which attains its lowest value each year (δ = -23.4°) at the 'vernal' equinox (roughly March 21), and its highest value (δ = +23.4°) on roughly September 22. All apparent sporadic radiants (i.e. radiants observed from the earth) are attracted towards the apex, and there is a strong observational selection in favour of meteors incident from near the apex, as we have already indicated. One would thus expect, in the absence of factor (b), to observe the highest rates during March. Conversely, the lowest rates are expected during September, when the observing location is most effectively shielded from the incident flux. From Fig. 5-1(Ja) and Fig. 5-1(Pa) it is evident that the average diurnal maximum in March was greater than that in September by some 70%, during 1987. In the Northern Hemisphere the situation is the reverse. Factor (b) distorts the sinusoid. The distribution of meteoroids about the earth's orbit varies, and it has been shown that the spatial density in the vicinity of the earth is at its maximum during the second half of the year (Keay, 1963).

(4) From the curves of Fig. 5-1 set (b) it is evident that there was a regular diurnal variation in the preponderance of observed echo

directions. In general, the rate of west echoes climbed steeply after 18h from almost zero to a broad daily maximum between 02h and 08h, after which it declined rapidly to form a broad minimum which lasted from early afternoon until roughly 18h. Occasionally the maximum was a sharp peak, and in most cases a secondary maximum was observed shortly before midnight.

From the symmetry of the east and west antenna beams and the geometry of reflection, one would expect that, for a given distribution of sporadic radiants, any graphical feature due to the west beam would be reproduced in reverse several hours later due to the east beam. The curves of the east rate generally did mimick those of the west rate, being shifted 8 to 10 hours relative to the latter. In general the east rate had a broad maximum consisting of several peaks and lasting from roughly 02h to 16h. As a rule virtually no meteors were observed in the east between 16h and 02h, after which the numbers increased abruptly. The fact that minor irregularities in the west rate were not rigorously reproduced in the east rate, is probably attributable atmospheric effects, and possibly also fine structure in the sporadic radiant distribution.

The general shape of these curves can be explained by considering the motion of the apex on any particular day. For the sake of simple illustration we choose March 22, when the apex coordinates are (270°,-23°), and at apex transit (06h00) the intersection of the ecliptic with the celestial sphere is symmetrical with respect to the north-south meridian. Because apparent radiants tend to cluster around the apex, most sporadic meteors appear to radiate from an elongated, diffuse radiant with the apex at its centre. It is reasonable to assume that the breadth of this radiant is some 30° in declination, and for the purposes of this explanation we shall guess that its length is some 45° in ecliptic longitude. Let R1 and R2 be two hypothetical point radiants, located on the ecliptic and at either extreme of this region of sky, with coordinates R1:(247°) and R2:(293°). The echo rate from any radiant in the vicinity of the ecliptic, near dawn during the first half of the year, varies approximately as shown in Fig 4-6(a); echoes are received from the west beam between 6 and 1 hours before transit, and from the east beam between 1 and 6 hours after transit. The extrema of our broad radiant, marked by R1 and R2, transit at 04h30 and 07h30, respectively. In the west beam, echoes due to R1 will be observed from 22h30 to 03h30, and and echoes due to R2 from 01h30 to 06h30. R1 will produce echoes in the east beam from 05h30 to 10h30, and R2 from 08h30 to 13h30. Thus for a linear ecliptic radiant 45° in right ascension and centred on the apex, echoes from the west are expected from roughly 22h30 to 06h30, and from the east between 05h30 and 13h30. This is a plausible explanation for the shapes of the solid and broken curves for March 1987, as shown in Fig. 5-1(J-b). In view of the diffuseness of the radiant in the apex, which was ignored in our linear 'model', the high

west rate after 06h30 is not a significant departure from prediction. The above explanation applies equally to any of the curves of Fig. 5-1 set (b), although one should bear in mind that the declination of the apex varies seasonally.

(5) A further difference between the east and west rates is that the west rate frequently attained a higher diurnal maximum than the east rate. This phenomenon was observed consistently, so that it is not likely to be associated with rapid fluctuations in sporadic meteor activity. Since the sensitivities of the east and west lobes of the beam are similar (see section 4-2), we attribute the phenomenon to a change in D-region absorption. In many of the graphs the west rate peaks during the hours of darkness, while the east rate maximizes after sunrise at the echo surface (eg. Fig. 5-1 (Bb), (Db), (Eb), (Fb), (Kb), (Nb), (Pb), (Qb)). Studies have shown that D-region effects may significantly reduce the radio echo rate during the daylight hours (Baldwin & Kaiser, 1965).

Fig 5-1: The diagrams have been arranged in two complimentary sets: set (a) and set (b). Graphs (Aa) to (Sa) (i.e. set (a)) show the diurnal variation of the hourly echo rates for each month of the survey. Each data point represents the mean for that hour, taken over approximately a week. Graphs (Ab) to (Sb) show the diurnal variation of the west and the east rates, averaged over the corresponding dates. The average rate of echoes from the west is indicated by solid lines, while that from the east is shown by broken lines.

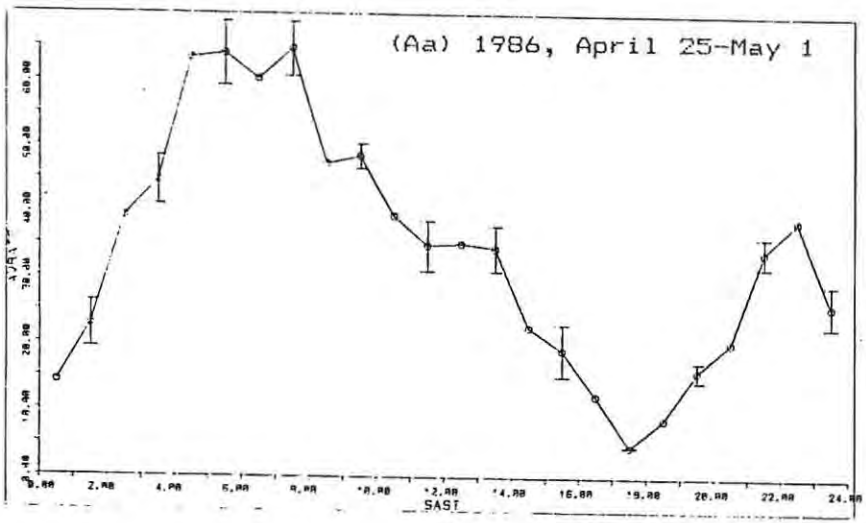
(Aa) 1986, April 25-May 1
SAST

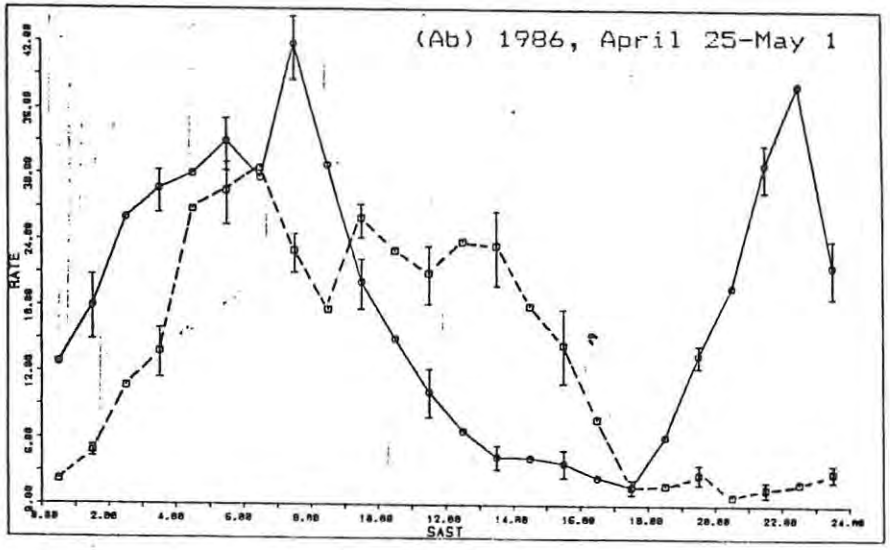
(Ab) 1986, April 25-May 1
RATE
SAST

Fig. 5-1

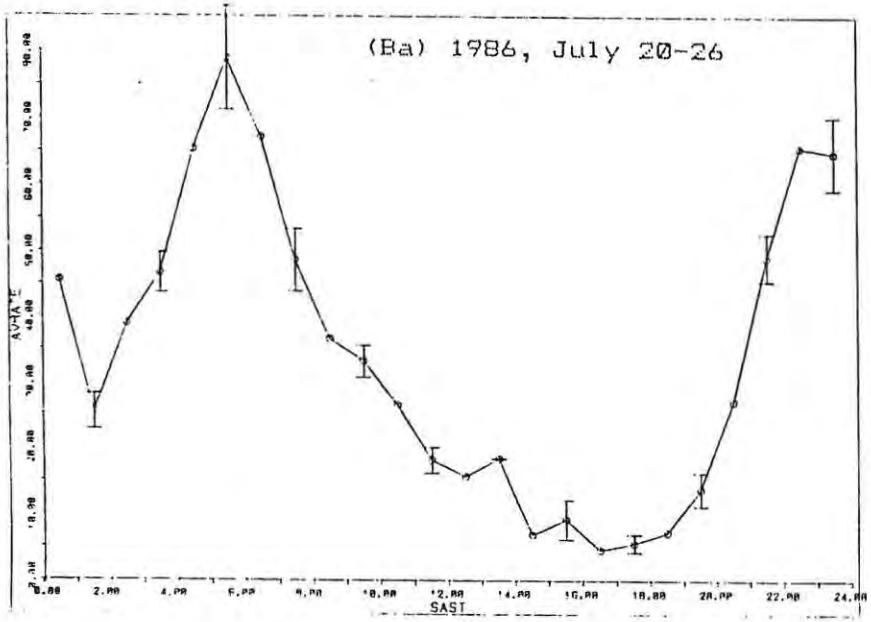
(Ba) 1986, July 20-26
SAST

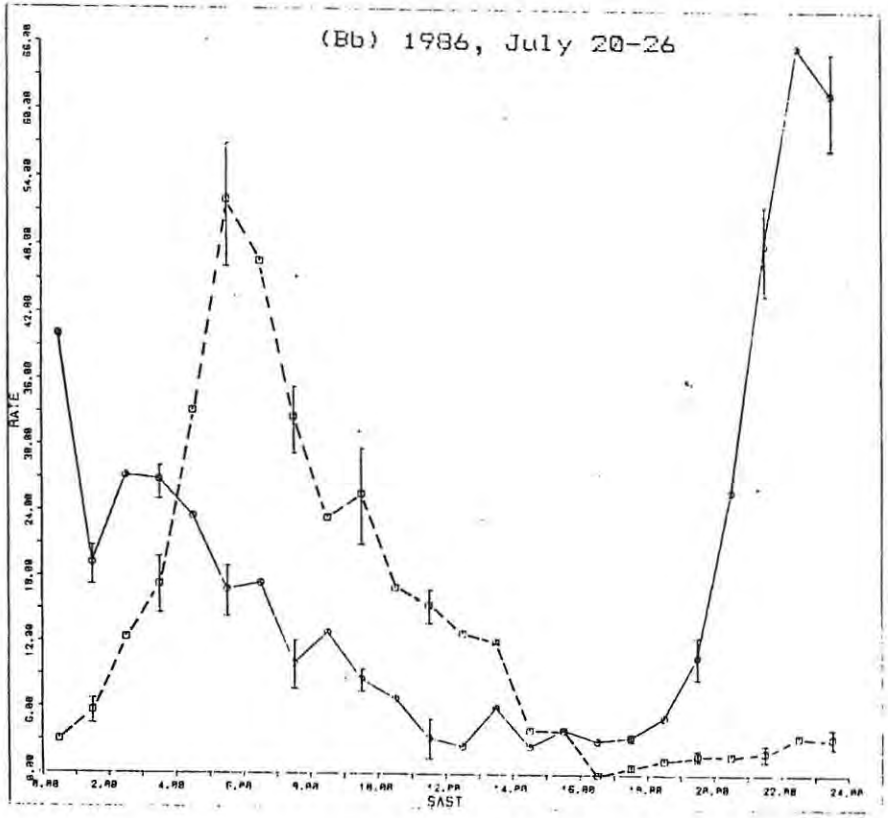
(Bb) 1986, July 20-26
RATE
SAST

Fig. 5-1 cont.

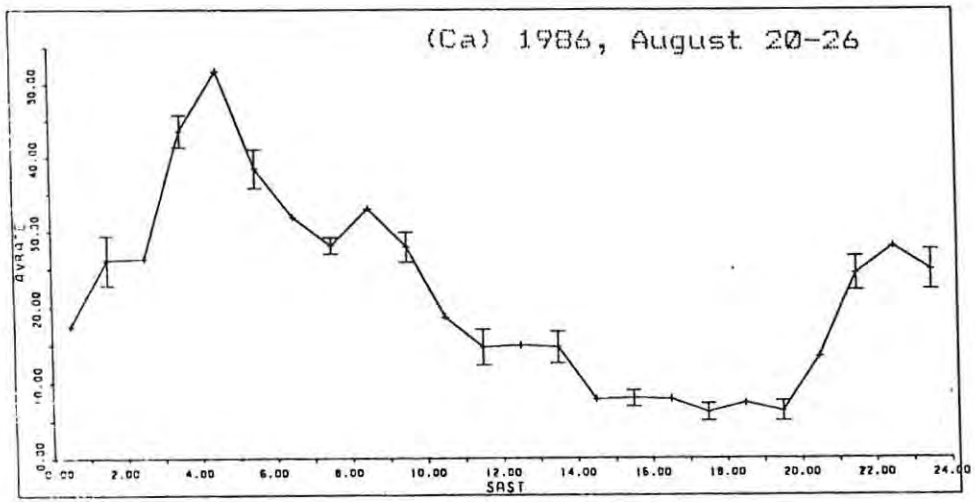
(Ca) 1986, August 20-26
AVRATE
SAST

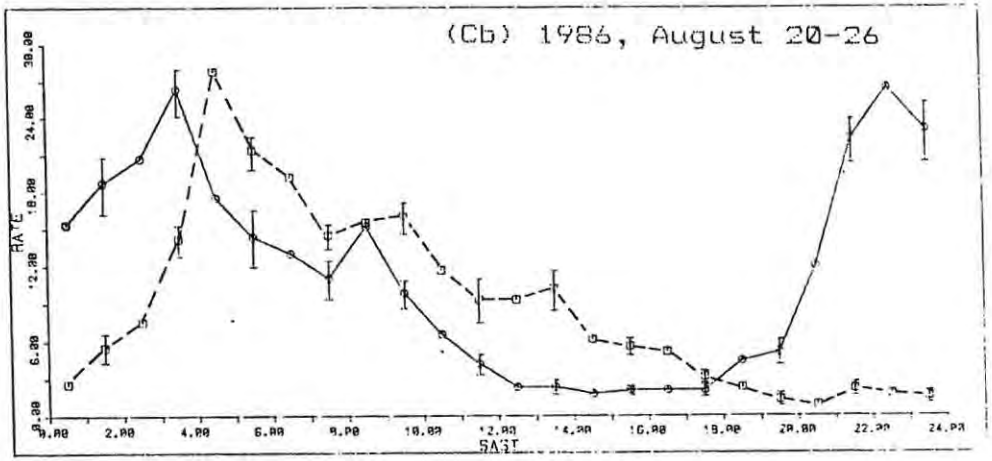
(Cb) 1986, August 20-26
RATE
SAST

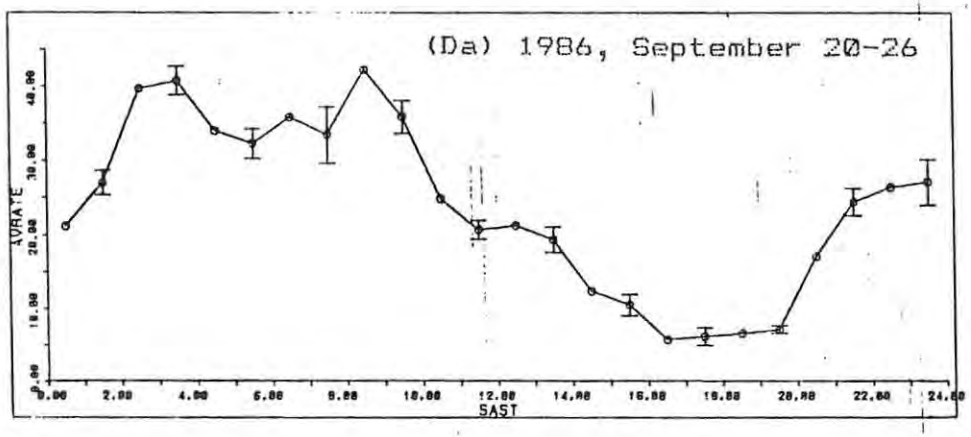
(Da) 1986, September 20-26
AVRATE
SAST

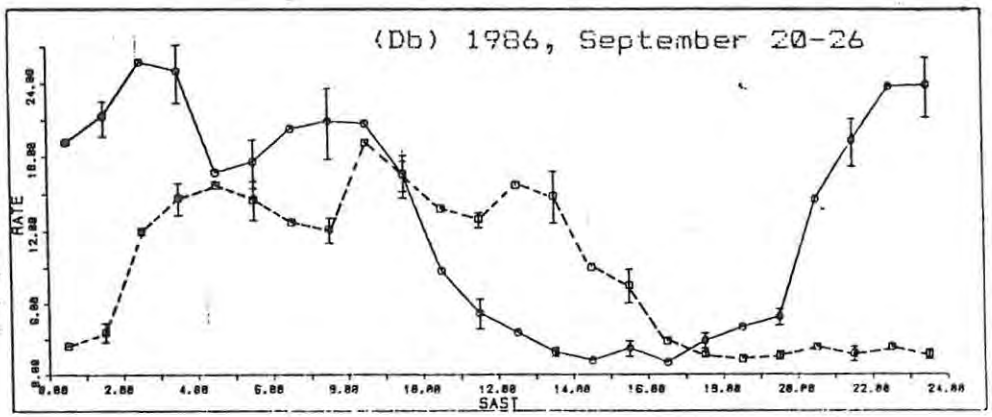
(Db) 1986, September 20-26
RATE
SAST

Fig. 5-1 cont.

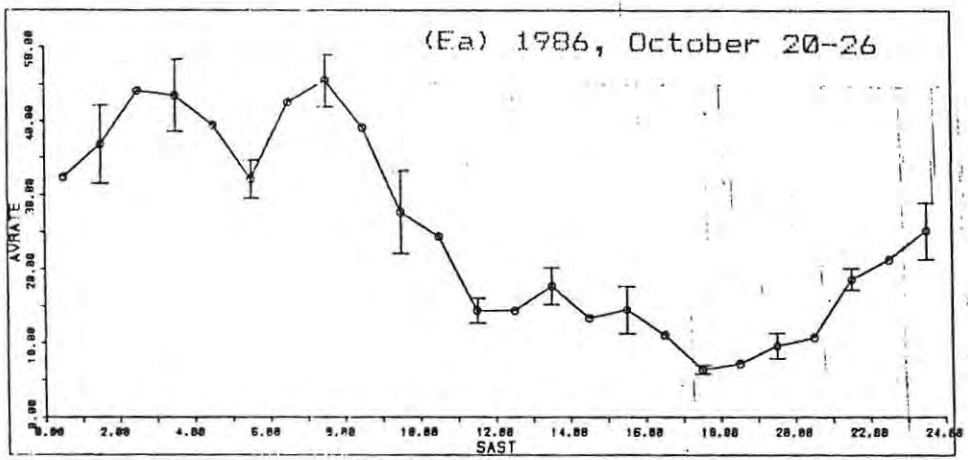
(Ea) 1986, October 20-26
AVRATE
SAST

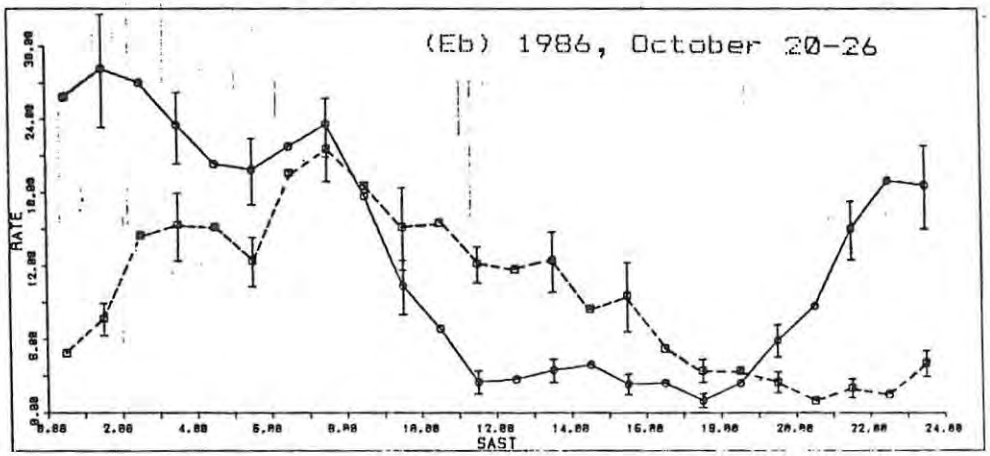
(Eb) 1986, October 20-26
RATE
SAST

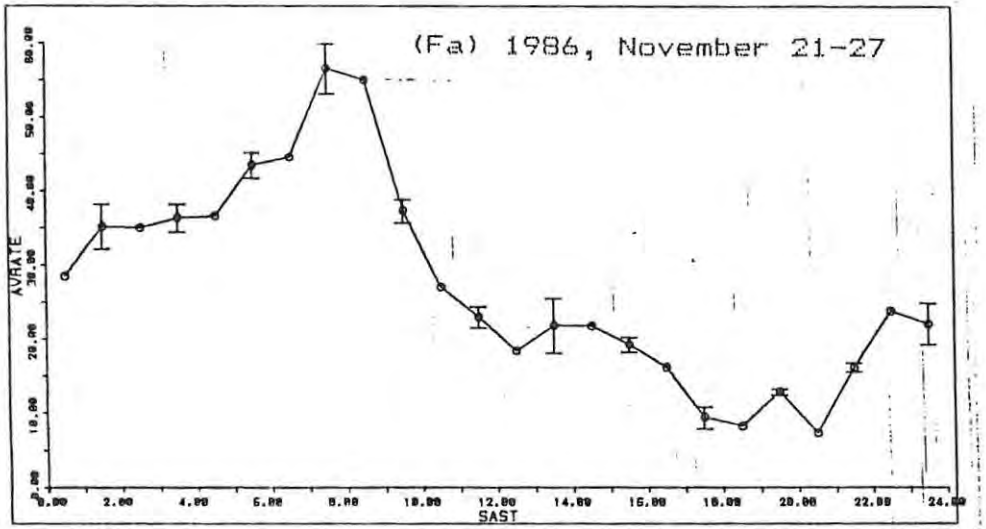
(Fa) 1986, November 21-27
AVRATE
SAST

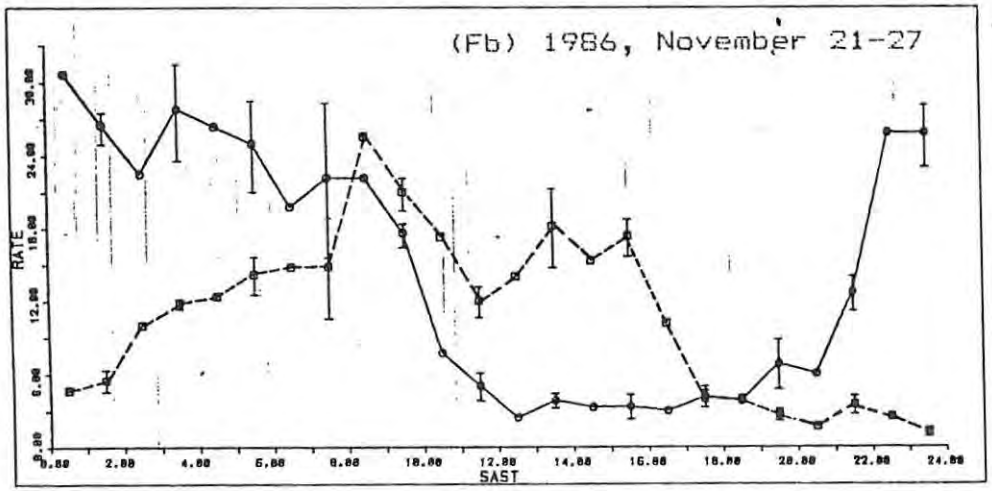
(Fb) 1986, November 21-27
RATE
SAST

Fig. 5-1 cont.

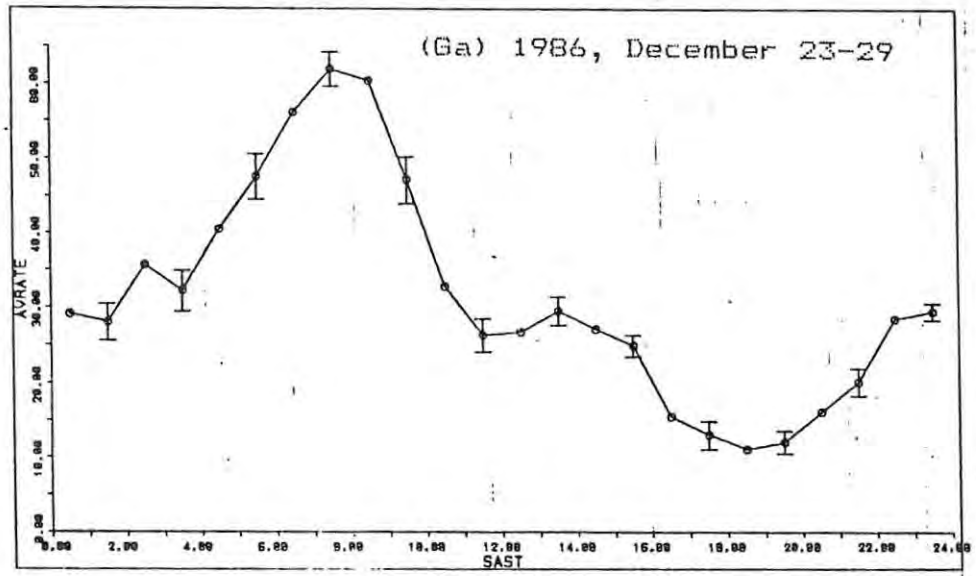
(Ga) 1986, December 23-29
AVRATE
SAST

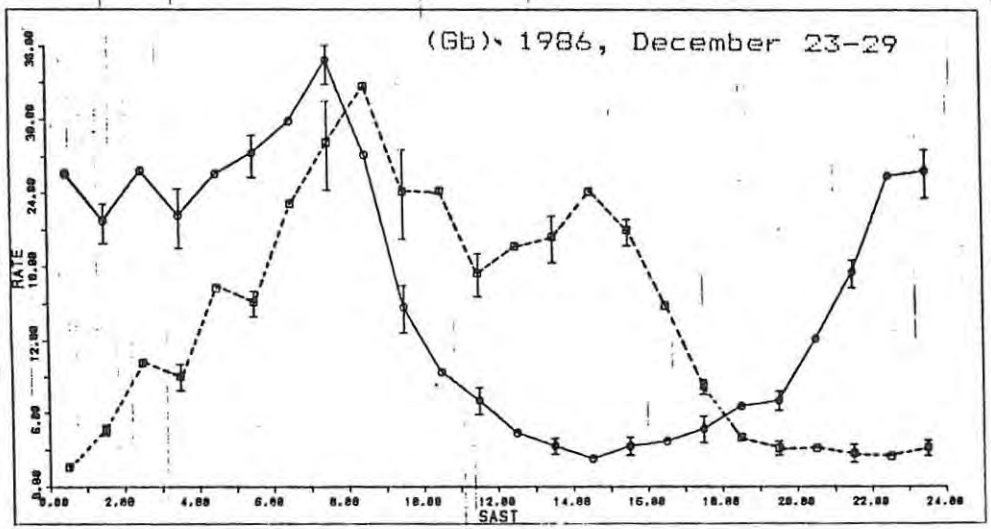
(Gb) 1986, December 23-29
RATE
SAST

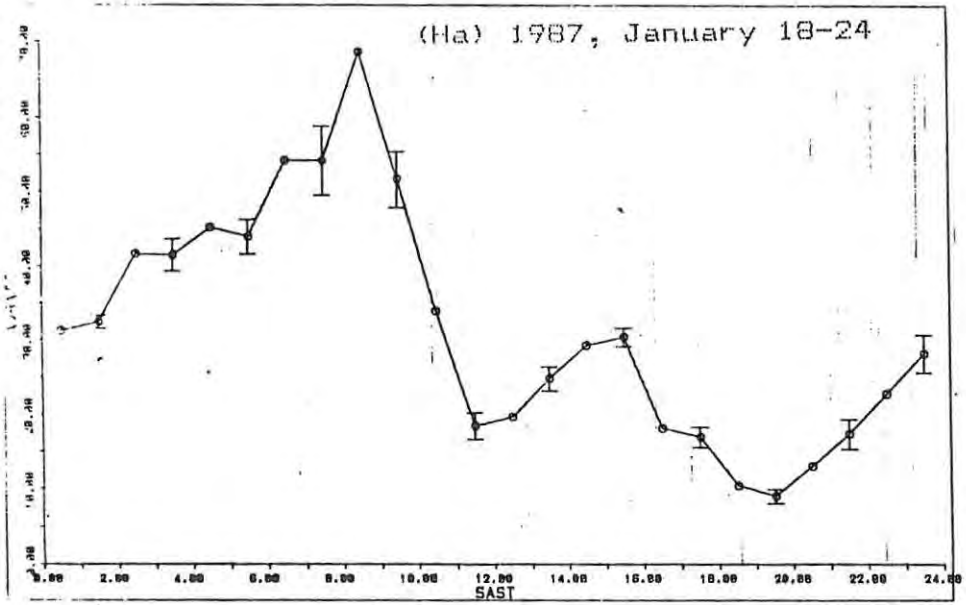
(Ha) 1987, January 18-24
SAST

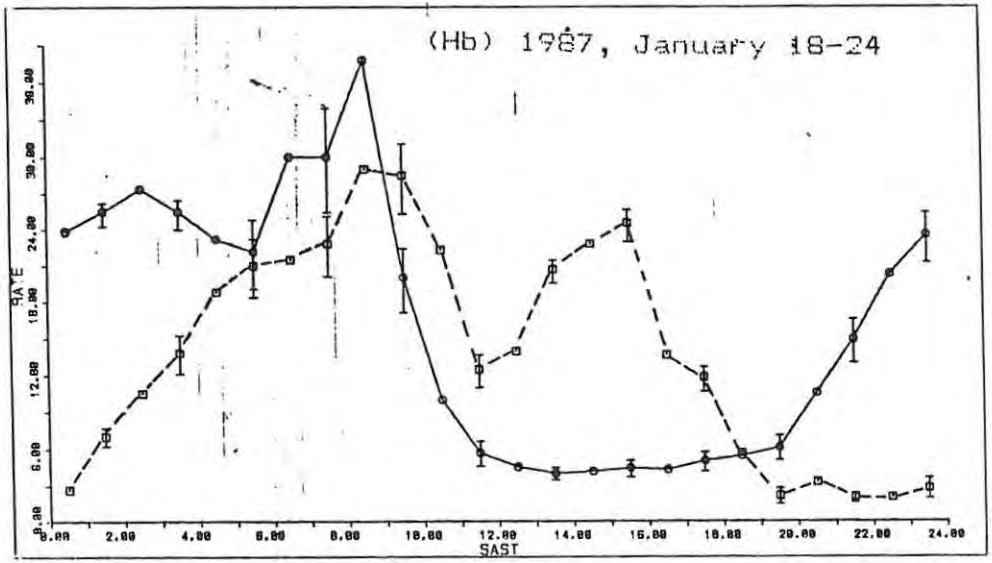
(Hb) 1987, January 18-24
RATE
SAST

Fig. 5-1 cont.

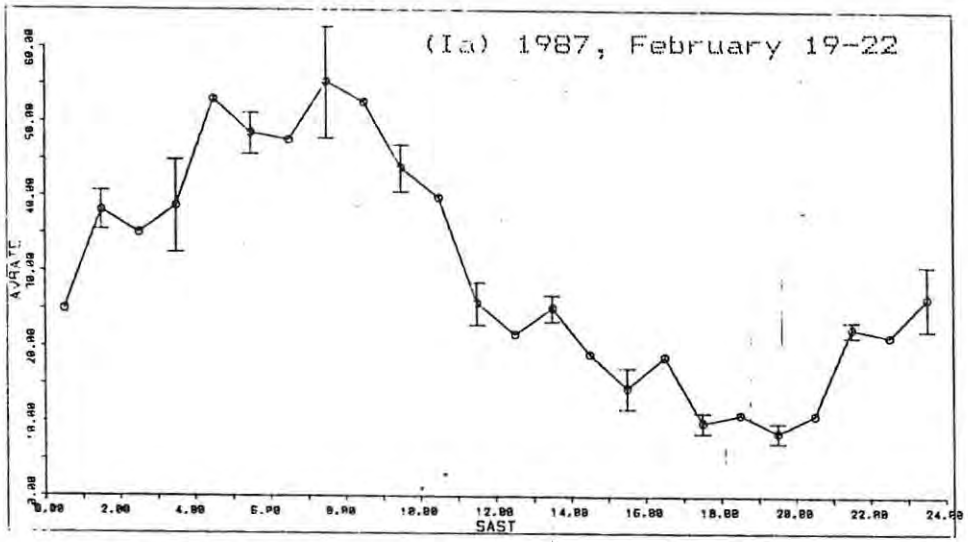
(Ia) 1987, February 19-22
AVRATE
SAST

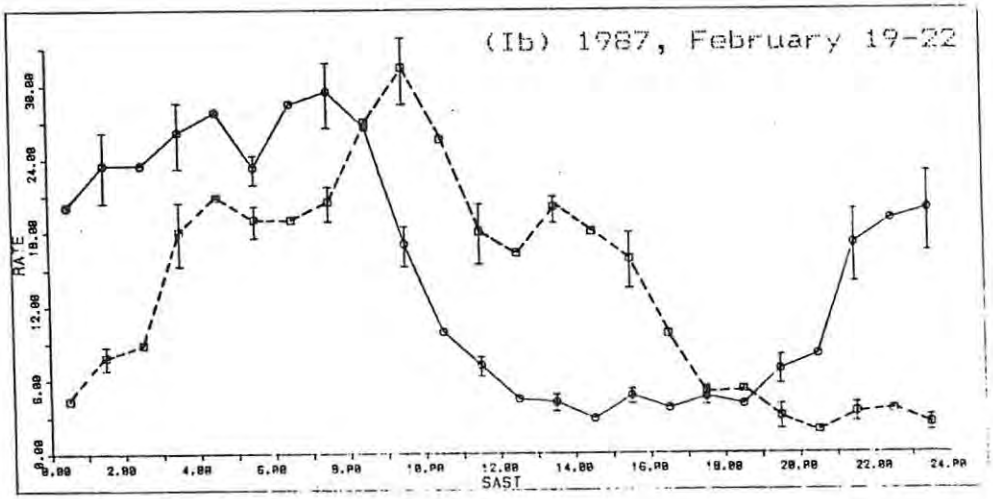
(Ib) 1987, February 19-22
RATE
SAST

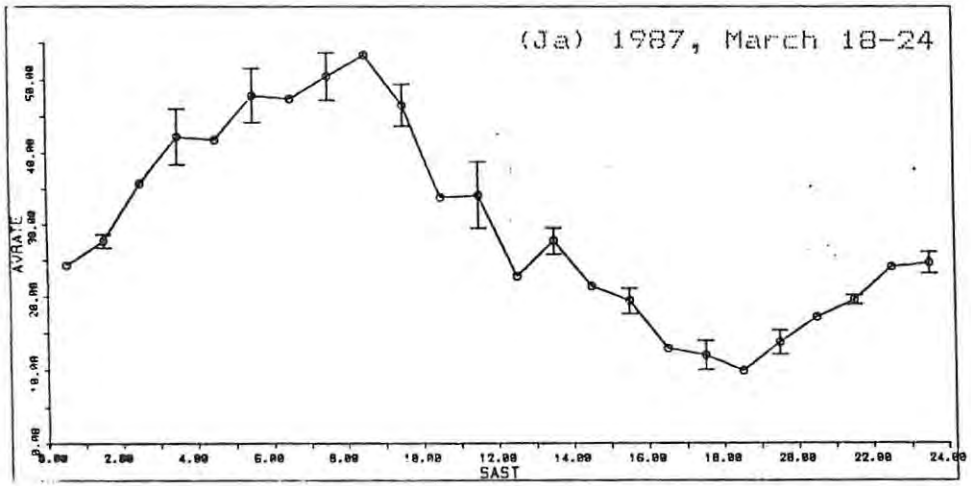
(Ja) 1987, March 18-24
AVRATE
SAST

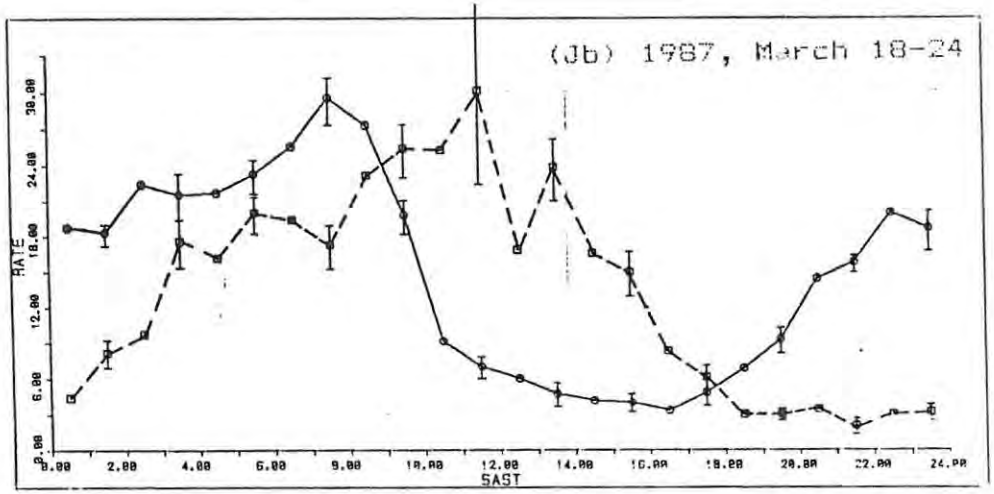
(Jb) 1987, March 18-24
RATE
SAST

Fig. 5-1 cont.

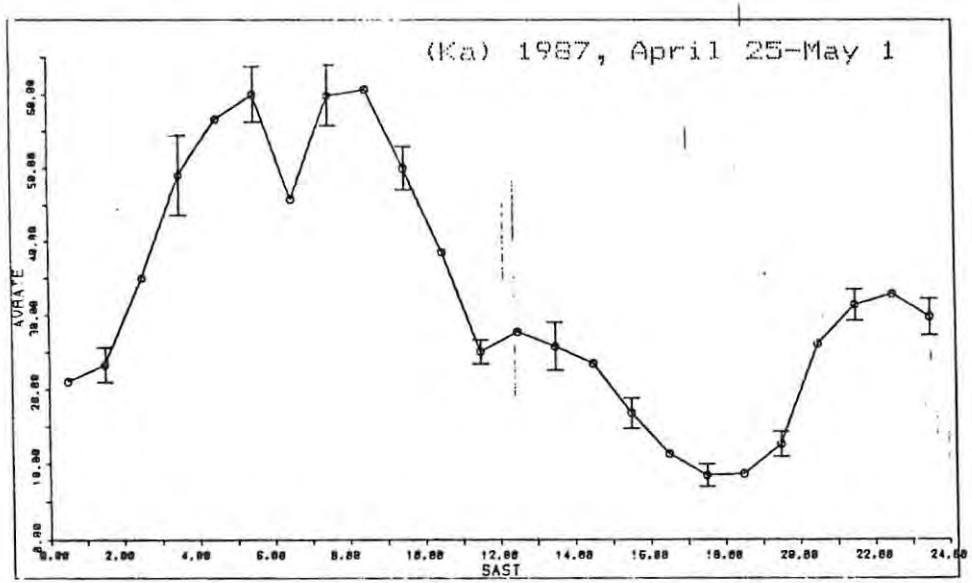
(Ka) 1987, April 25-May 1
AVRAYE
SAST

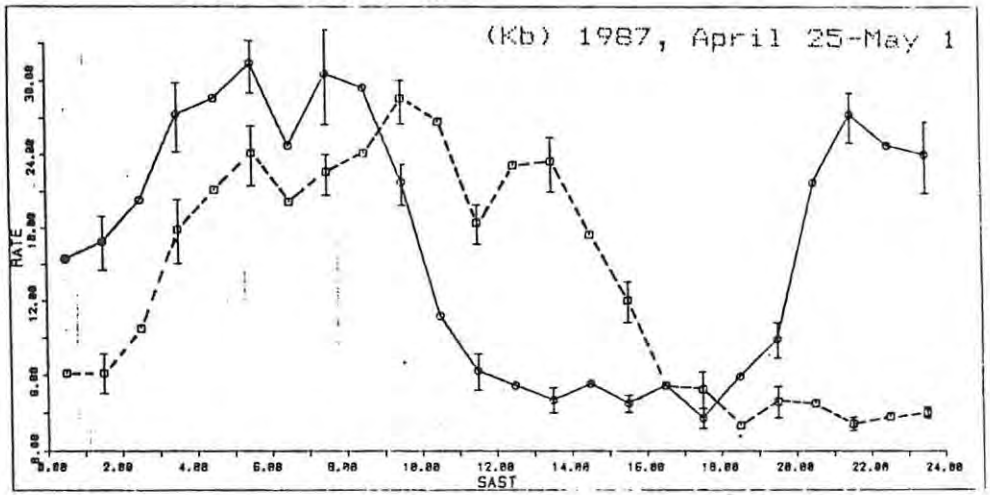
(Kb) 1987, April 25-May 1
RATE
SAST

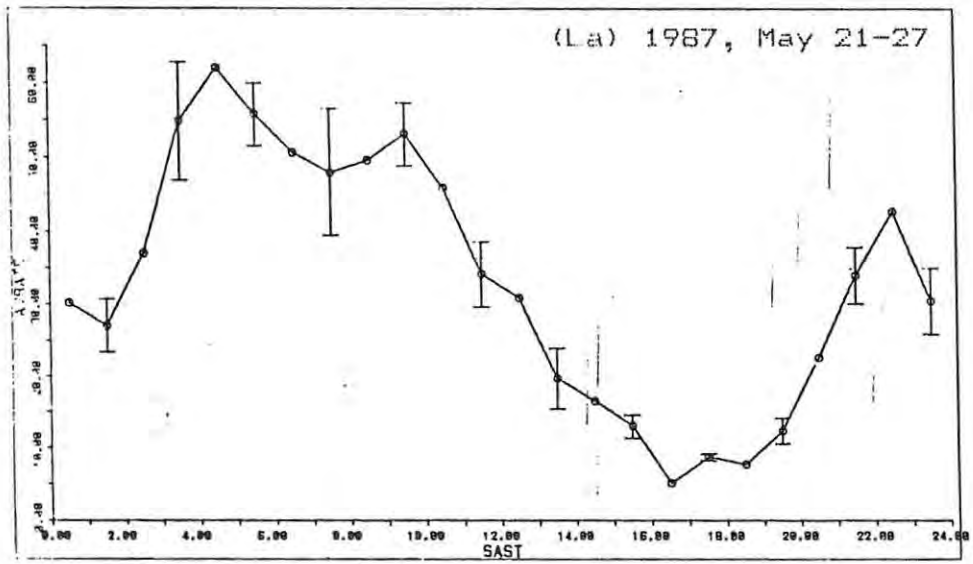
(La) 1987, May 21-27
SAST

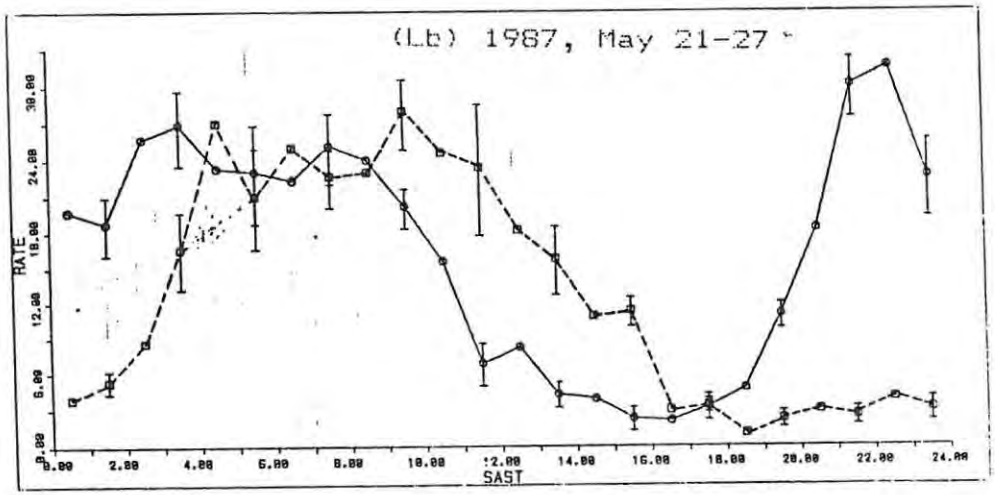
(Lb) 1987, May 21-27
RATE
SAST

Fig. 5-1 cont.

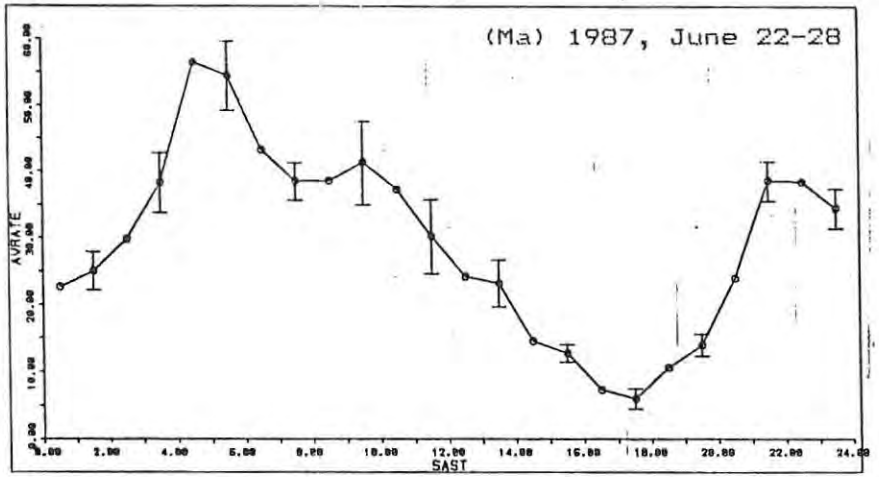
(Ma) 1987, June 22-28
AVRATE
SAST

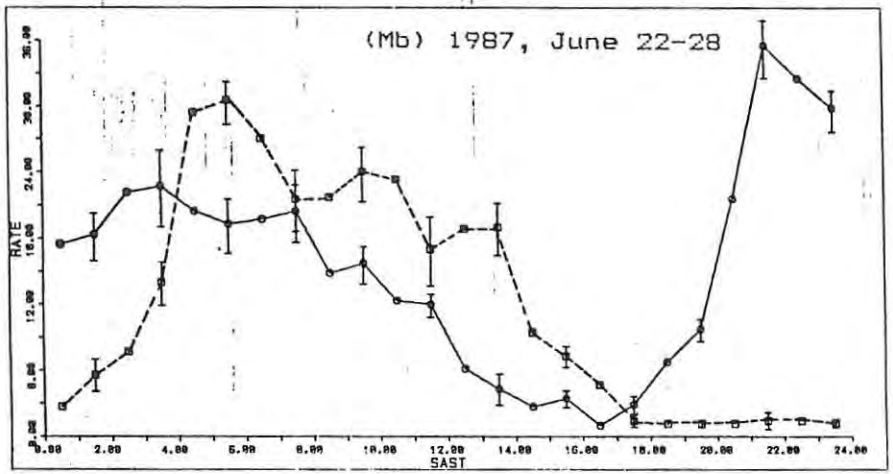
(Mb) 1987, June 22-28
RATE
SAST

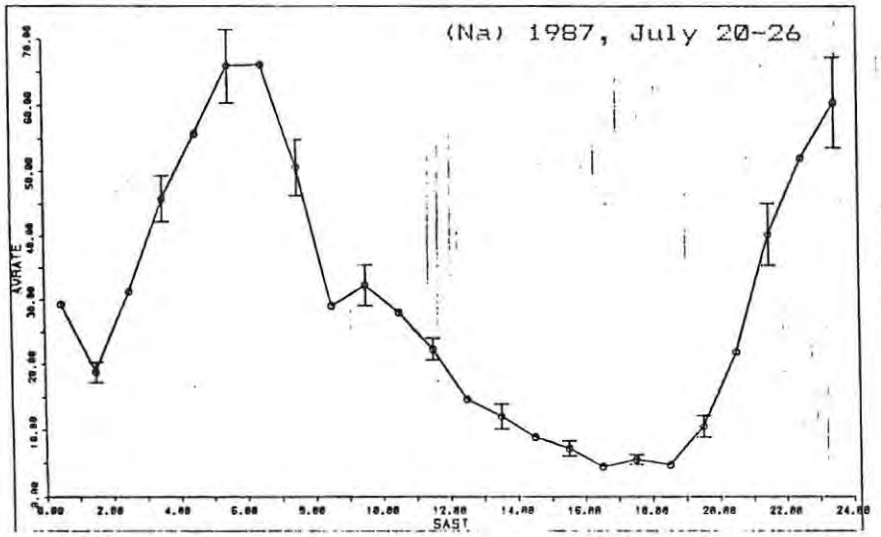
(Na) 1987, July 20-26
AVRATE
SAST

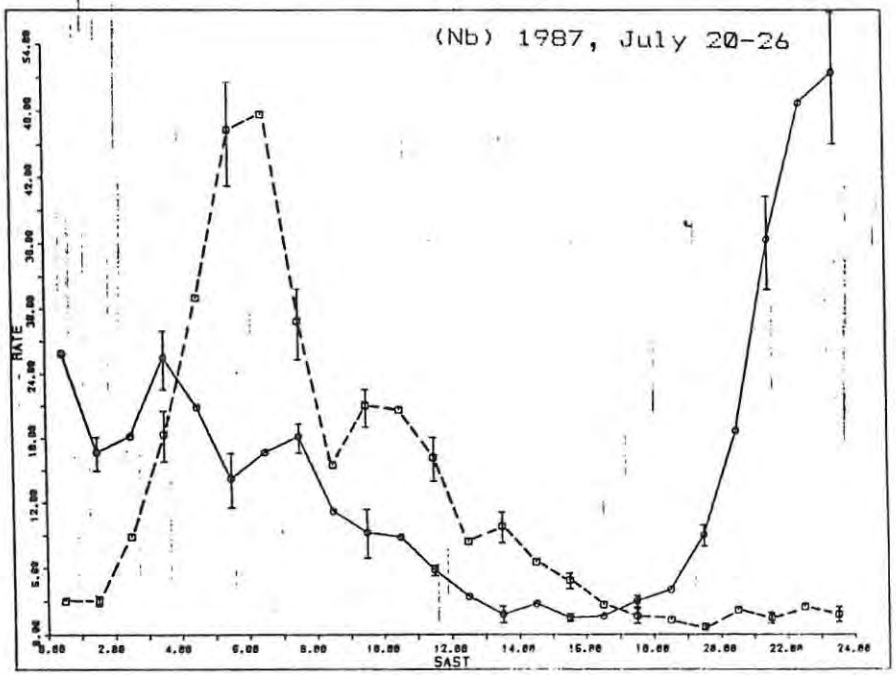
(Nb) 1987, July 20-26
RATE
SAST

Fig. 5-1 cont.

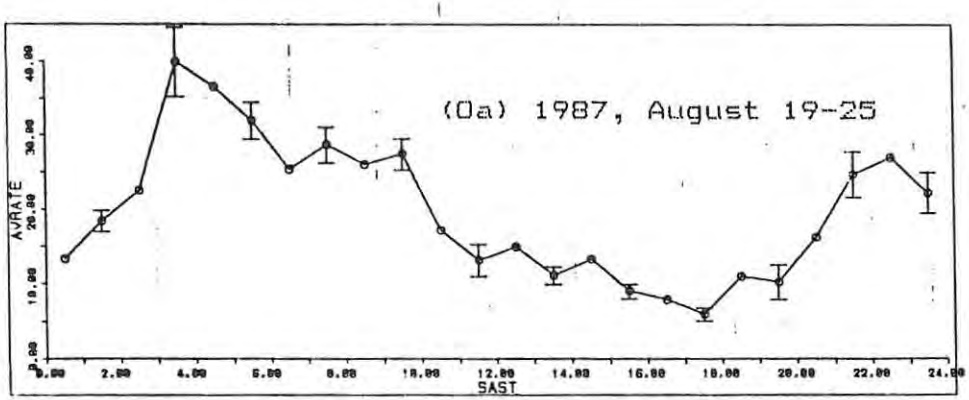
(Oa) 1987, August 19-25
AVRATE
SAST

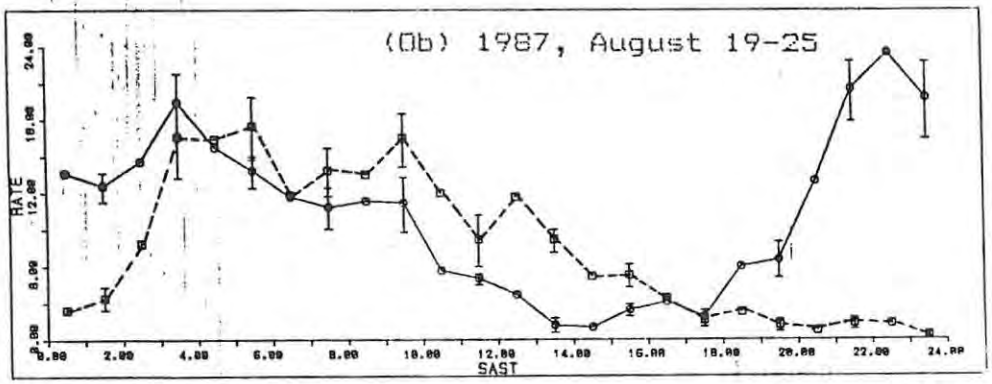
(Ob) 1987, August 19-25
RATE
SAST

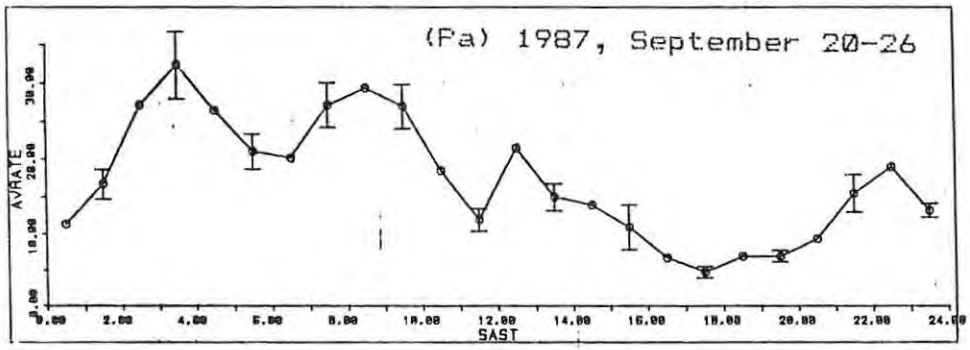
(Pa) 1987, September 20-26
AVRATE
SAST

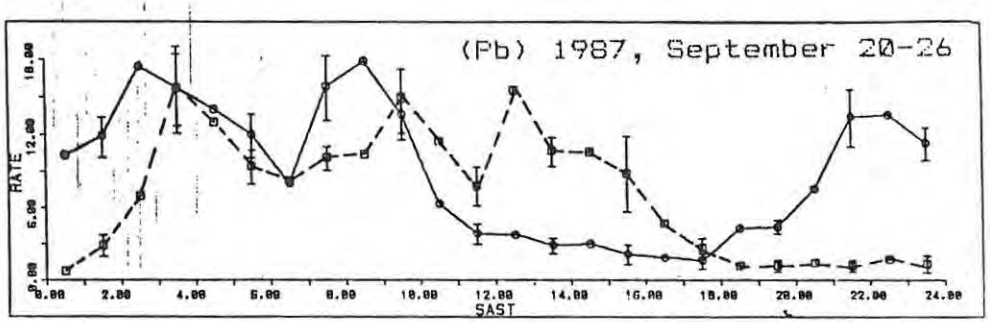
(Pb) 1987, September 20-26
RATE
SAST

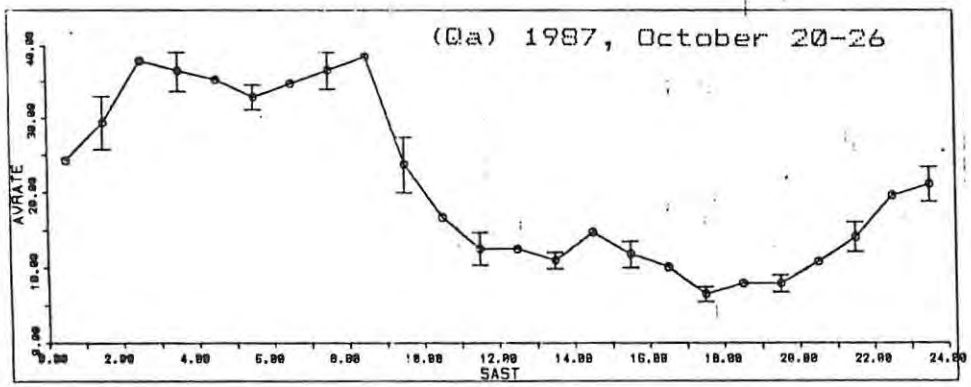
(Qa) 1987, October 20-26
AVRATE
SAST

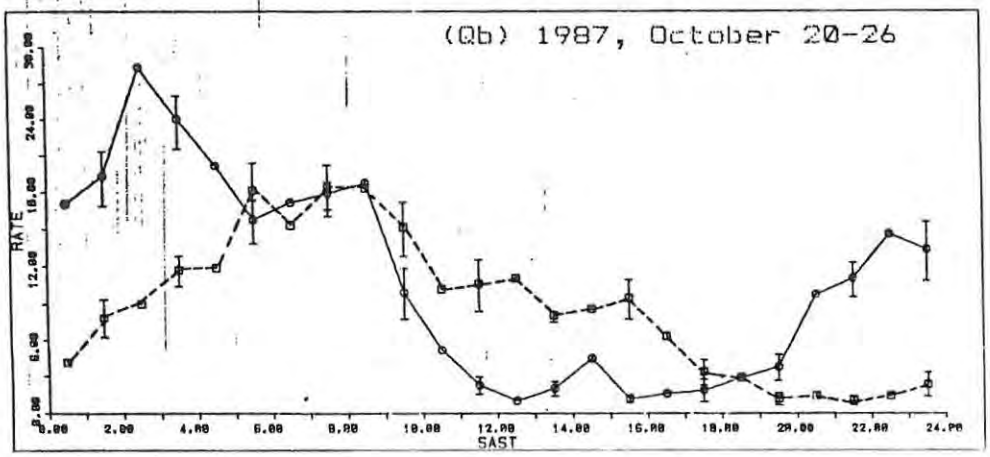
(Qb) 1987, October 20-26
RATE
SAST

Fig. 5-1 cont.

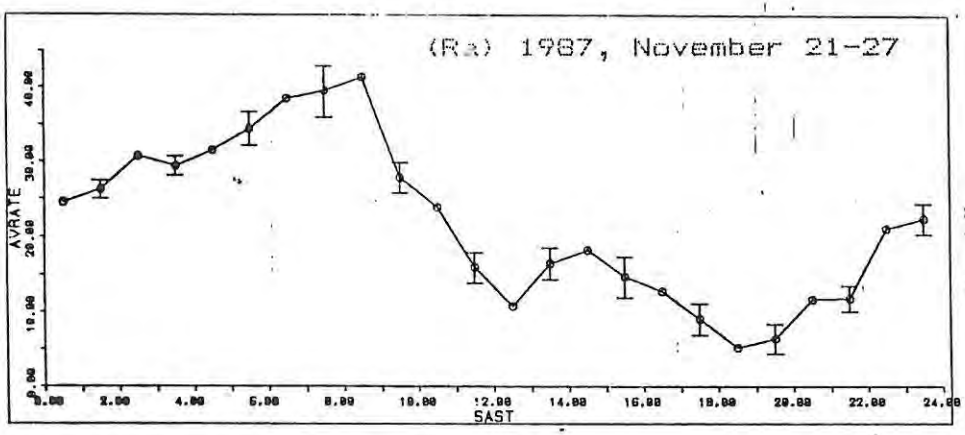
(Ra) 1987, November 21-27
AVRATE
SAST

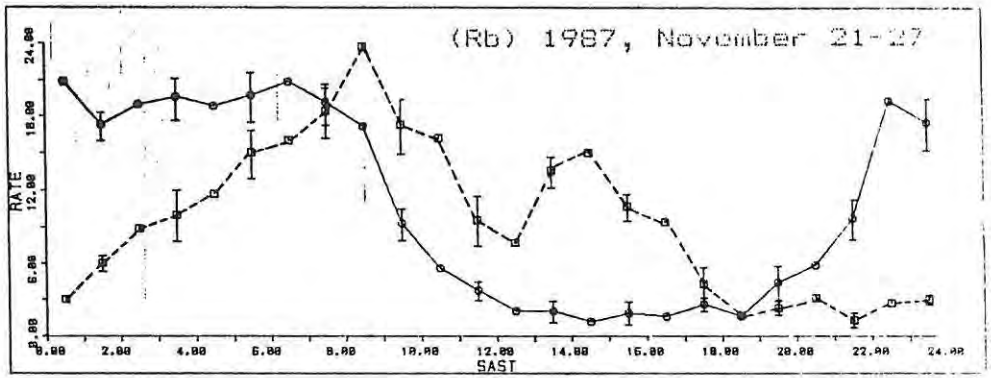
(Rb) 1987, November 21-27
RATE
SAST

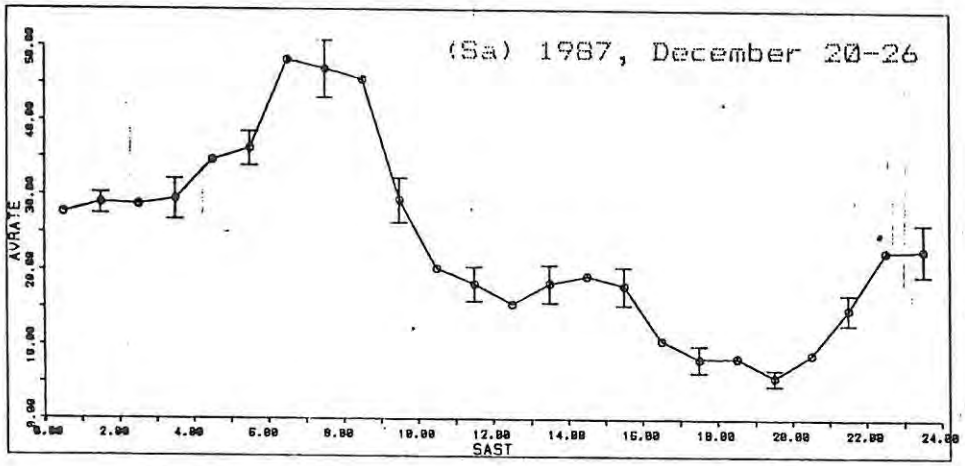
(Sa) 1987, December 20-26
AVRATE
SAST

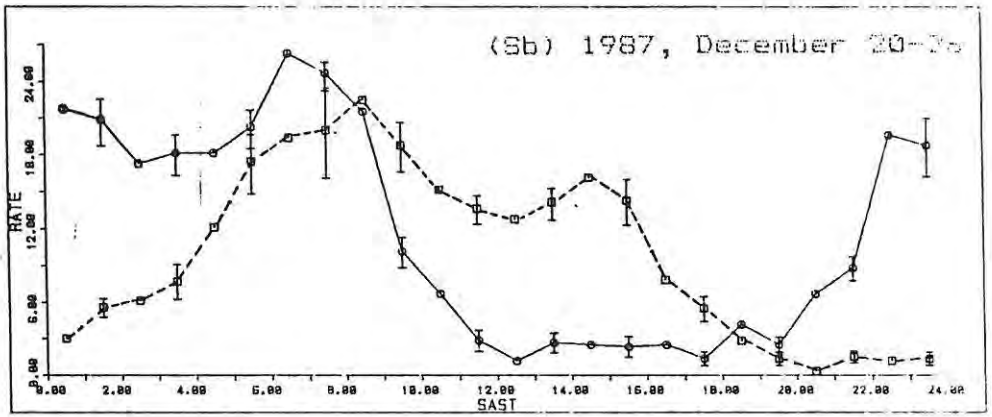
(Sb) 1987, December 20-26
RATE
SAST

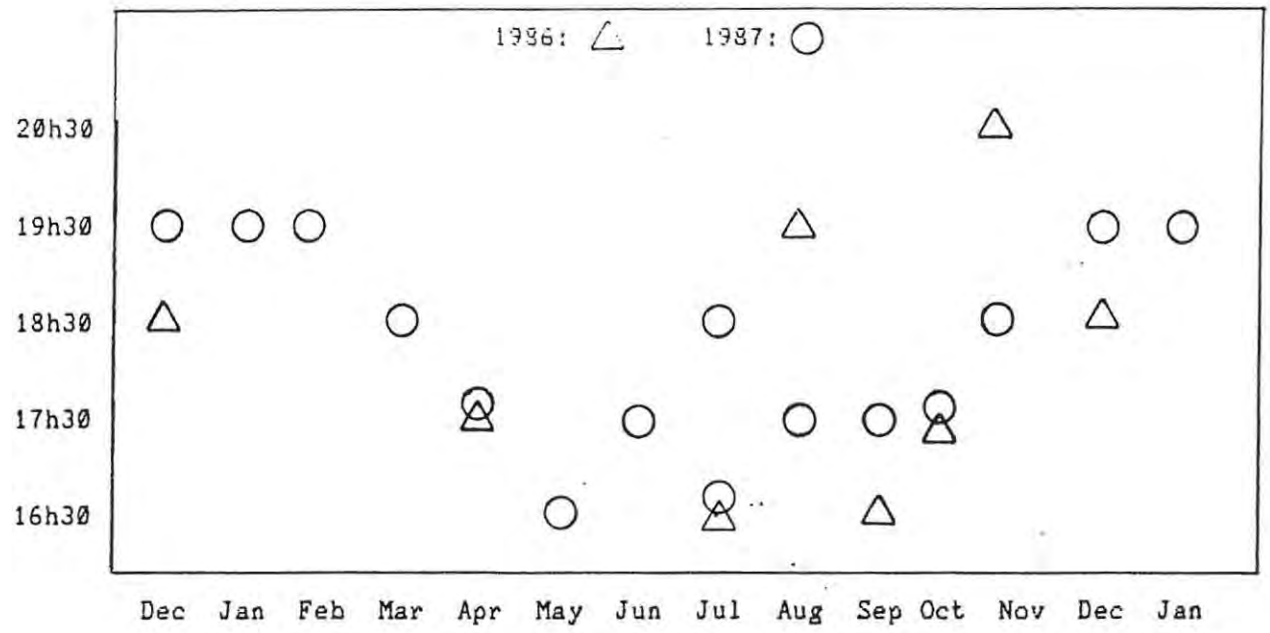

Fig. 5-2: Monthly variation of the time of diurnal minimum.

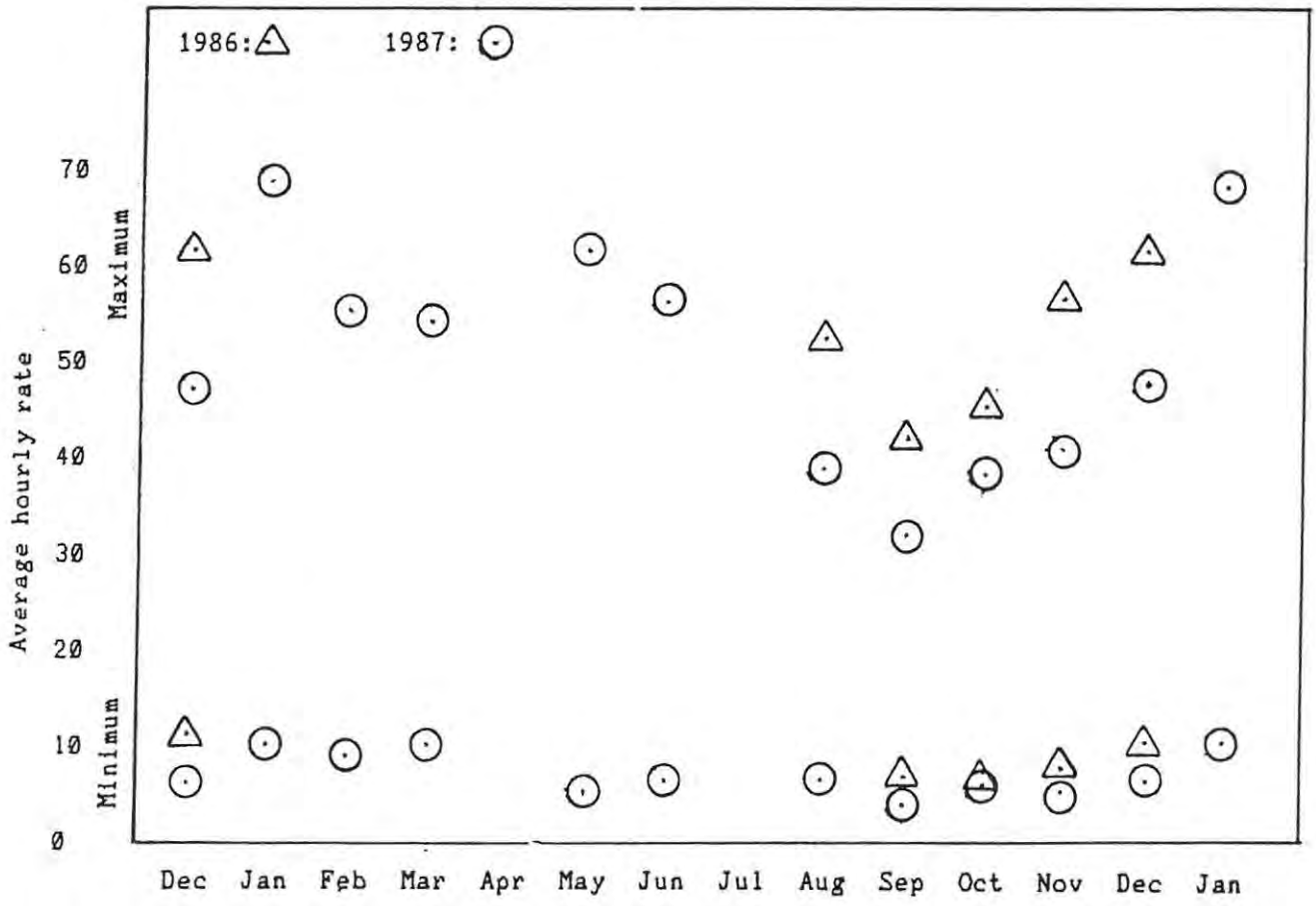

Fig. 5-3: Monthly variation of diurnal maxima and minima.

5-3: The major showers.

From Grahamstown four major annual showers are visible. Two of these, the Eta-Aquarids (May) and the Orionids (October), are associated with comet Halley. Members of the Geminid stream (December) are believed to be offspring of the asteroid 3200 Phaeton; and the remaining stream, the Delta-Aquarids (July), have no known parent body. For each major stream a list of the associated diagrams, dates over which the sporadic background was averaged, plotting programs, and program parameters is given in Table 5-1.

In this section the figures are numbered according to the order in which the showers make their annual appearance. The showers are not, however, discussed in this order; the two genetically related showers, the Eta-Aquarids and the Orionids, are discussed jointly although they occur before and after the δ-Aquarid shower, respectively.

We define the shower 'half-width' to be the number of days separating the half-maximum points on the shower rate/day curve. On this basis the widths of various streams have been estimated.

The Eta-Aquarids and the Orionids

Members of the Halley stream are among the fastest shower meteors. Velocities of 65.5 and 66.4 km s^{-1} have been measured for the Eta-Aquarids and the Orionids, respectively. Visual observations of the showers were made as early as 74 BC and 288 AD, respectively, and early astronomers noted spectacular returns of the latter during 443, 466, and 530 AD.

The main conclusions of several recent surveys of the showers have been summarized by McIntosh and Hajduk (1983). According to these workers: Both showers appear to be active for 14 days. The periods of activity are placed at $37^\circ < \lambda < 51^\circ$ for the Eta-Aquarids and $202^\circ < \lambda < 216^\circ$ for the Orionids (λ is used here to denote solar longitude). 75% of the observed maxima fall within narrow central zones at $42.5^\circ < \lambda < 47^\circ$ and $206^\circ < \lambda < 210^\circ$, respectively, centred at 45° and 208°. The activity curve is flat in these zones and the centre is marked by a small dip. Secondary maxima occur at longitudes 38° and 50°, and 203° and 215°. The positions of the maxima drift with respect to solar longitude; for the Eta-Aquarids, the average annual drift is $0.30^\circ - 0.75^\circ$, and for the Orionids $0.42^\circ - 0.92^\circ$. The maximum shower rates fluctuate from year to year, for both showers, with no definite periodicity. Annual variations in the activity of one of the showers bear no relation to the activity of the other shower, neither during the same year, nor consecutive

years. A correlation between years of minimum Orionid activity and Jupiter's 12 year orbital period exists. No such relationship is evident for the Eta-Aquarids. The flux of larger particles (corresponding to persistent echoes) is relatively stable, but large annual variations in the average echo rate are caused by a highly variable flux of smaller particles. This was inferred from the relative proportion of enduring shower echoes ($\tau > 1$ s), from year to year. Eta-Aquarid meteors produce a greater proportion of long echoes than Orionid meteors; however, because of atmospheric effects on long echoes, the discrepancy of 3.5 hours between the transit times of the showers introduces some uncertainty as to whether this indicates any real difference in the proportion of larger particles in the two showers.

Eta-Aquarids, 1986: From Fig. 5-4(a) the following features are evident: The broad central zone of activity which extended from roughly April 30 (39°) to May 11 (51°), was slightly asymmetrical about a sharp maximum at May 6 (45°), when the average shower rate (25 hr^{-1}) was roughly twice that on the days immediately prior to and after the peak. The half-width of about 4 days was bounded by half-maximum points at May 4 (43½°) and May 8 (47½°). Three secondary maxima were observed, before (April 26,36°), during (May 2, 41½°), and after (May 14, 53°) the main period of activity.

Eta-Aquarids, 1987: Fig 5-4(b) shows that during 1987 the main period of activity lasted from roughly April 28 (37°) to May 19 (57.5°), peaking sharply on May 7 (46°, average rate 38 hr^{-1}). The half-maximum points at roughly May 5 (44½°) and May 9 (48½°) give a half-width of 4 days. Eight possible secondary maxima were observed. One of these (April 24, 34°) occurred before the central zone of activity, four (May 1, 40½°; May 13, 51°; May 16, 54°; May 18, 57°) are located within this region, and the remaining three are placed much later (May 23, 61½°; May 25, 64°; May 30, 69°). However, only one of these secondary peaks (at May 30, 69°) appears in Fig. 5-5, which covers the same observing period as Fig. 5-4 (b) but is a more sensitive measure of radiant activity. This suggests that the remaining secondary peaks displayed by Fig. 5-4 (b) may be the result of our low echo rate, and if so, are spurious. From Fig. 5-5 additional local maxima at May 3 (42°), May 12 (51°), May 14(53°) and May 26 (64.5°) are evident, and this figure suggests a half-width of 6 days, from May 4 (43½°) until May 10 (49°). The equivalent of Fig. 5-5 could not be plotted for the 1986 Eta-Aquarids because direction finding was faulty.

A comparison of the (a) and (b) graphs of Figs. 5-4 and 5-7 suggests a stronger return of the shower in 1987; in that year the diurnal shower rate at maximum peaked at 62 hr^{-1}, whereas the corresponding rate for 1986 was 32 hr^{-1}. However no conclusions concerning the relative fluxes of shower meteors during the two years may be drawn from these comparisons. The reason for this is that the sporadic background for the 1986 data was averaged over dates which were not sufficiently displaced relative to the maximum, and thus contained a proportion of shower meteors. The 1987 sporadic rates were more realistic. A comparison of Figs. 5-6(a) and (b), does, however, indicate that the 1987 shower rates were up on those of the previous year, in view of the fact that a trend towards lower sporadic activity during 1987 has been noticed (see section 5-2). Figs. 5-6(a) and (b) show a diurnal peak in the total hourly rate of 83 hr^{-1} for 1986 and 114 hr^{-1} for 1987, at maximum.

The observed diurnal shower rate profile was found to agree with the predicted one within error bar limits, for both years (Figs. 5-8(a) and (b)). In each case the observed profile is asymmetrical about transit (07h40 SAST), although the asymmetry in (b) is the reverse of that in (a). This difference is not significant in view of the size of the error bars.

Orionids, 1986: Unfortunately the 1986 Orionid survey was started after the shower was already in evidence. In that year the shower peaked on October 15 (201°), displayed secondary maxima at 205°, 209° and 212°, and lasted until roughly November 2 (219°). An additional local maximum occurred after the main active period, at November 13 (230½°). All this is evident from Fig. 5-16(a). The half-width could not be determined, although the shower dropped below half its maximum strength near October 27 (213½°). Orionid activity was not strong enough to contrast sharply with the sporadic background, as shown in Fig. 5-15 for the 1987 return of the shower. This is a result of the northern declination of the radiant (δ = +17°), which is not favourably placed for observations of the shower from southern latitudes. However, the activity profile has been enhanced by counting only specular 'shower' meteors (where the meaning of 'shower' meteors is as defined in section 5-1). This is illustrated by the series of three graphs (b), (c) and (d) in Fig. 5-16, for the 1987 Orionids: as the sky-window is made smaller and smaller, thereby increasingly reducing the degree of contamination of the rate profile by non-shower echoes, the peak due to Orionid meteors improves its definition.

Orionids, 1987: From Fig. 5-16 (d) the following features are evident: Activity lasted from roughly October 7 (193°) until November 3 (220°), and reached its maximum between October 21 (207°) and October 23 (209°). The maximum has a small dip at the centre which is of doubtful

significance. The half-width was 14 days, between October 15 (201°) and October 29 (215°). Five possible secondary maxima were observed, one before (October 4, 190½°), three (October 16, 18, 29; 202°, 204°, 215°) during, and two (November 6, 9; 223°, 226°) after the central active period.

A comparison of Fig. 5-17 (a) and (b) shows that the shower was of roughly the same strength in both 1986 and 1987; in both cases the diurnal average shower rate near maximum peaked at 12 hr^{-1}. From Fig. 5-18 (a) and (b) it may be seen that for both years the observed diurnal rate curve agrees roughly with the theoretical prediction. The agreement is more approximate than for the Eta-Aquarid shower on account of the low echo rates.

Discussion

The observational evidence provided by the results of our survey will now be discussed in the light of the recent shell model for the structure of the Halley stream, proposed by McIntosh & Hajduk (1983). From our data, the following facts emerge:

(1) The two showers are not of equal length, and neither of them lasts 14 days, as suggested by the above authors (1983). During 1987 the Orionids were in evidence for slightly longer (26 days) than the Eta-Aquarids (21 days). The duration of the 1986 Orionids could not be established because the survey was started too late. The duration of the 1986 Eta-Aquarids (12 days) is unreliable because of the problem (discussed above) with sporadic background rates for that shower.

McIntosh & Hajduk (1983) have pointed out that the meteor stream does not correspond very precisely with the comet orbit. The earth's closest approach to the comet orbit in October is 0.154 AU, and 0.065 AU in May. If the meteor stream were a toroid centred on the comet orbit, the Eta-Aquarids would be expected to be much broader than the Orionids. From our data the reverse is true, suggesting that there is some flaw in the toroidal model.

(2) During both years the Eta-Aquarid maxima occurred within the central zone specified by these authors. However they were sharp, rather than flat with a central dip. Possible secondary maxima (at 36° and 53°, 1986; 51° and 53°, 1987) which were located within 3° of those listed by McIntosh & Hajduk (at 38° and 50°), occurred in both years, as well as other minor peaks which stood separate from the broad central region of activity, but which these authors do not mention.

The 1986 Orionid peak (201°) was observed well before the central zone

specified by McIntosh & Hajduk (1983). Its shape could not be ascertained. Two of the three secondary maxima (at 212½° and 205½°) observed after the 1986 peak were within 3° of that quoted by the above authors (215° and 203°). The 1987 Orionid peak was fairly flat with a possible central dip, and extended over solar longitudes in agreement with those given by these authors. Three of the local maxima observed in that year (at 202°, 204° and 215°) fall within 1° of those cited by McIntosh & Hajduk (1983).

These observations of the showers suggest that the Halley stream consists of a broad central belt of particles with a high density core, accompanied on either side by side-belts of lower density. The points of 75% maximum activity are separated by ~1 day at the May (Fig 5-5) and ~4 days at the October intersection (Fig 5-16 (d)), and the respective half-widths are ~5 and ~14 days. The earth's orbit intersects the cometary orbit at an angle of 44° and thus the thickness of the main belt, corresponding to the distance between the points of half the maximum particle number density, is roughly 0.06 AU at the May intersection and 0.17 AU at the October intersection of the stream. The respective thicknesses of the denser core, corresponding to the separation between the points of 75% maximum activity, are 0.012 AU and 0.048 AU.

There appear to have been four side belts at the 1987 October intersection, at 188°, 190½°, 223° and 226°, and at least one, at 230½°, at the 1986 October intersection. The three secondary maxima which occurred within the central region during the 1987 intersection of the stream may indicate filaments of higher density within the main belt. A similar conclusion may be drawn from the local maxima which were present in the central zone during October 1987. During 1987 May, four side belts may have been present, at 34°, 61½°, 64.5° and 69°, and two during May 1986 at 36° and 53°. Higher density filaments, corresponding to the remaining secondary peaks, appear to have been present within the broad belt during both May 1986 and May 1987.

The above features point to fine structure in the stream, and cannot easily be explained if the stream is assumed to have a circular cross-section. McIntosh & Hajduk (1983) first hypothesized a filamentary model of the stream in order to account for the observational features mentioned at the beginning of section 5-3. Clearly similar features have been evident from our own data. According to their model, the particle belt responsible for the central activity of the showers is oriented perpendicular to the plane of the comet orbit, and is 0.044 AU thick measured in that plane. A possible mechanism for the formation of such a belt, and its subsequent thickening, is explained in their paper.

(3) Changes in the positions of maximum activity, and the secondary

maxima, from 1986 to 1987 were observed. For both showers the overall maximum occurred later in 1987 than in the previous year. In general, the secondary peaks were observed at different longitudes from one year to the next. To the extent that the local peaks are real, these differences are indicative of a dynamically varying filamentary stream structure. Only the local maximum at 53° was observed in both years. The average annual shift in the maxima cannot be determined from only two years of data.

(4) The changes in the overall level of shower activity from one year to the next reflect changes in the spatial density of the stream along the cometary orbit. There was no correlation between the Eta-Aquarid activity which varied, and the Orionid activity which remained much the same during both years. This is in accordance with the observation made by McIntosh & Hajduk (1983).

(5) For both years, the proportion of long-duration echoes during the Eta-Aquarid period was greater than that during the Orionids. This fact is evident from a comparison of Fig. 5-23 (a) and (c), and Fig. 5-23 (b) and (d). This difference may not indicate the relative proportion of large particles in these showers, as it can be explained by the sunrise effect (McIntosh & Hajduk, 1977): The Orionid radiant transits at Grahamstown in relative darkness (at 04h30), as opposed to the Eta-Aquarid radiant (07h40), which transits after sunrise at the 95 km echo-surface. These authors have ascribed the higher proportion of long echoes during the daytime to a decrease in electron loss processes during the daylight hours.

The Delta-Aquarids

According to Weiss (1960), the limits of detectability for this shower are July 20 and August 14 and the flat maximum is placed between longitudes 124° and 125°. The corresponding dates cited elsewhere (eg. Ellyett & Roth, 1955; The Cambridge Encyclopedia of Astronomy, 1977) fall within the period July 15 to August 15, with the dates of maximum activity clustering around July 27 - 28 (roughly $124° < \lambda < 125°$). In view of the strength of the southern Delta-Aquarid radiant (this shower has two radiants, at $\delta = -17°$ and 0°), the stream has received surprisingly little attention from investigators. In comparison, the remaining three showers dealt with in this section have been well documented. This may be result of the unequal distribution of meteor radar facilities between the two hemispheres. Members of this stream are slower than those of the previous two showers, with measured velocities of 41 km sec^{-1}.

The shower was observed on two consecutive returns during our survey. The following facts emerge from our data:

(1) The 1986 Delta-Aquarids extended over 14 days (as shown in Fig. 5-9 (a)), from July 23 (120°) until August 5 (132°), attaining a rounded maximum (64 hr^{-1}) on July 27 (124°). The beginning and terminal dates of Fig. 5-9 (a) mark the period for which the radar was operational. The sporadic background for this graph was derived from data taken over the week August 15 - September 3, since the shower survey was not part of a longer continuous run. From the graph it is evident that the shower rate was non-zero at both July 20 (day 201) and August 9 (day 221), and so the shower may have started earlier or terminated later than these respective dates. During this part of the survey, reliable echo directions were not available. Thus a normalized hourly rate / day curve of specular echoes attributed to the radiant proper could not be plotted.

(2) Fig. 5-9 (b) shows that in 1987 the shower lasted 17 days from July 21 (118°) until August 6 (133°), attaining a broad, flat maximum (50 hr^{-1}) between July 27 (123.5°) and August 2 (129°). Shower meteors were detectable as early as July 17 and as late as August 9. A central dip in the maximum was observed on July 31 (127°). In Fig. 5-10, the normalized rate of specular echoes associated with the radiant started to rise above the background level at the dates corresponding to the half-maximum points in Fig. 5-9 (b). Fig 5-10 is a more sensitive measure of radiant activity than the latter, and shows a flat maximum extending from July 26 (122.5°) to July 31 (127°) without the central dip. This feature, and also the extent of the maximum indicated by Fig. 5-9 (b), may therefore be spurious. The shape of the second half of the shower maximum in 1987 has been obscured by the regrettable loss of data.

(3) Fig. 5-11 (a) and (b) show the diurnal variation of the total hourly rate at maximum for 1986 and 1987, respectively. Once the sporadic background had been removed, these graphs became Fig. 5-12 (a) and (b), respectively, which show that the diurnal shower rate at maximum peaked at 61 hr^{-1} in 1986 and 40 hr^{-1} in 1987. This 30% decrease corresponds to the observed overall decline in sporadic activity between the two years. We are uncertain to what extent the fall-off is the result of sunspot-related atmospheric effects which affect meteor detectability, or whether it reflects a real variation in the density of the stream along its orbit.

(4) Fig. 5-13 (a) and (b) show that there was remarkable agreement between the observed diurnal variation of the shower echo rate at maximum, and that predicted due to the southern Delta-Aquarid radiant at $\delta = -17°$. If the southern and northern radiants were of comparable

strength, the observed diurnal rate curve would be a synthesis of Fig. 4-5 (a) and (b), and it is therefore evident that the southern radiant swamps any activity of its northern counterpart. The symmetry of the observed rate curves about transit attests to the symmetry between the east and west antenna beams, as we have already mentioned in section 4-2.

(5) The expected clustering of echo points along echo lines was clearly noticeable for this shower. The reflecting points observed over several days near the maximum, in two time windows placed at the diurnal maxima are plotted in Fig. 5-14 (a). The placing of the time windows was decided after consulting Fig. 5-13. The theoretical positions of the echo lines at these times have been drawn on a transparency. In contrast, the reflecting points of sporadic echoes over a typical day of non-shower activity show no such clustering (Fig. 5-14 (b)).

The Geminids

This strong Northern Hemisphere shower is regarded as a predictable annual event by most meteor astronomers. Visual rates maximize at about 60 hr^{-1} around December 14, and visual observations of the shower span the 126 years since the Geminids were first reliably recorded in 1862 (Fox, Williams & Hughes, 1982). Radar observations of the stream, however, extend over roughly the past 40 years. We shall first discuss some of the distinctive features of the stream.

The Geminids are in evidence over the period December 2-15 (Jones & Morton, 1982). Values for the shower half-width vary between the extremes of 92 ± 5 hours (op. cit.) and 72 hours, reported as the mean of two decades of radar observations (McIntosh & Simek, 1980). The half-width depends on the limiting radio magnitude of the radar system.

Because the orbit of the Geminid stream does not make a close approach to that of Jupiter, gravitational perturbations from this planet are expected to be small, and the stream orbit should be stable. Nevertheless, measured values of the activity, width and position of the maximum are found to vary aperiodically from year to year (op. cit.). Jones (1982) has suggested that a stream composed of finer filaments would behave in this manner. In view of the comparatively recent appearance of the Geminid stream to Earth-bound observers, and the fact that no recorded event would have resulted in the formation of a new stream near that date, it is likely that gravitational perturbations from Jupiter, Venus and Earth have effected changes in the stream orbit which have brought it into intersection with that of the earth (Fox, Williams & Hughes, 1982). It is unlikely that a shower with this level of activity would have escaped attention if it had been present before the last century.

A long-recognized feature of the Geminid activity profile is its skewness with respect to solar longitude. Its rise to a maximum is generally quasi-exponential, and the fall-off afterwards is much more rapid. In an attempt to explain how this skewness arose, Fox, Williams & Hughes (1983) used Whipple's (1951) model for the ejection of dust from a parent comet to calculate the orbit of each emitted dust particle, and deduced a cross-sectional structure for the stream near the descending node (where the orbits of the earth and this stream intersect). The cross-section is oval, with a dense central bar at an angle of ~25° to the semi-major axis. This central bar is due to particles which were released near to the descending node of the stream's orbit, and is the cause of the skew rate profile. The same group (Fox et al., 1982) has suggested that this asymmetry will vary with the epoch of the observations, owing to the fact that the stream is

being swept past the orbit of the earth by gravitational effects. According to these authors (1983), the earth's orbit first began to intersect the stream early in the nineteenth century. During these early encounters the width remained constant and the activity curve was quasi-Gaussian. In about 1920 the earth started to cross the central dense bar, and the profile became skew. Initially the skewness was biased towards an early maximum (low λ), but this has changed into a bias toward a late maximum (higher λ). Early in the twenty-first century the earth's orbit will no longer intersect the central bar, and the rate profile will revert to its original quasi-Gaussian form. Thereafter, Geminid meteor activity will diminish until, finally, in the twenty-second century the orbits of the earth and the stream no longer intersect. Fox, Williams & Hughes (1983) have not investigated early records to see whether in fact their conclusions are borne out. They later add that the events outlined above may take place far slower than they had anticipated.

The date of shower maximum apparently moves later in the year as time advances. Between the first confirmed sighting (1862) and the present, there has been a shift of some 3 days. The phenomenon is the result of gravitational perturbations by the planets and also the precession of the vernal equinox (Fox, Williams & Hughes, 1982). Within the past 40 years, however, shower maxima have clustered around $\lambda = 260°$ (Jones & Morton, 1982).

The date of maximum is also strongly dependent on the size range of the meteors being observed. Webster, Kaiser & Poole (1966) found that the mass distribution index s decreases as the earth crosses the stream. This means that the earth encounters small particles before large ones, in its passage across the stream. Since the earth traverses the stream from the inside, the smaller particles must be concentrated along the inner perimeter of the orbit. This cross-sectional mass segregation would result from an initailly homogeneous mass distribution after the joint action of the Poynting-Robertson effect and the solar wind. Both of these effects reduce the orbital eccentricities of particles, and their influence is more severe for smaller meteoroids. The extent of the transverse variation of s suggests that the stream is relatively new (Jones & Morton, 1982). This group has found a mean value of 1.69 ± 0.07 for the mass distribution index.

There is a good deal of variation in the distribution of particles along the orbit of the Geminid stream, with a single maximum and minimum in the particle number density, in the ratio 2:1 (McIntosh, 1975; McIntosh & Simek, 1975). The orbital period, deduced from comparisons of the rates for successive returns of the shower, cannot be specified more accurately than 1.6 ± 0.1 yr (McIntosh & Simek, 1980).

In common with the Geminid meteor shower, the Quadrantids are also a recent phenomenon, the first reliable record being 1835 (Fox, Williams & Hughes, 1982). It is thought that, like the Geminids, the Quadrantid stream is being swept past the earth's orbit by gravitational effects. Mass segregation is observed for both showers. However the Quadrantid activity profile is Gaussian, whereas that of the Geminids is skew.

Radar observations of the Geminid shower were conducted during the returns of 1986 and 1987. A discussion of the results follows.

For both years, the average hourly rate over a 6 hour period, centred at radiant transit, was evaluated for each day of the survey. Fig. 5-19 (a) and (b) show the average echo rate remaining after subtraction of the estimated number of sporadic echoes, for 1986 and 1987, respectively. From these diagrams it is evident that the daily average shower rate rose to 25 hr^{-1} in 1986 and 35 hr^{-1} in 1987. The increase in activity is probably related to a real increase in the shower flux, in view of the tendency for rates to be lower in 1987 which we have already mentioned. For both years, the skew rate profile, which rises to a maximum more slowly than it afterwards declines, is consistent with the findings of others (eg. Webster, Kaiser & Poole, 1966; Weiss, 1959; Jones & Morton, 1982). Also evident from Fig. 5-19, is that the activity maximum was broader in 1986, with a peak on December 13 (260.5°). The 1987 peak was much sharper, and occurred on December 14 (261.5°).

Fig. 5-20 (a) [1986] and (b) [1987] show the normalized average hourly rate over the 6 hour period, of shower-echoes which satisfy the specularity condition defined earlier in the Chapter, and which are associated with meteors with radiants in a 5° square sky-window centred on the known shower radiant (112°, +32°). The broad 1986 maximum of Fig. 5-19 (a) is observed again in Fig. 5-20 (a), although the maximum is evident a day later (262°) than in Fig. 5-19 (a). Fig. 5-20 (b) reproduces the sharp 1987 peak of Fig. 5-19 (b) at the same date. The position of the radiant has been found to drift according to the relations (Jones & Morton, 1982):

$$RA = 112.3° + 1.03\ (\lambda - 261.3°)$$
$$\delta = 33.05° - 0.15\ (\lambda - 261.3°),$$

and it is possible that the small sky window together with the tight constraint on specularity may have caused true shower echoes to be excluded, since radiant drift was not allowed for. Alternatively, the position of the peak in Fig. 5-19 (a) may be due to an anomaly in the assumed background.

According to Fig. 5-20, the half-width was ~72 hours for both years. This value accords with the result of McIntosh & Simek (1980), which we cited earlier. However, Fig. 5-19 suggests that the stream was broader at the 1986 encounter (half-width ~75 hours) but narrower in 1987 (~48

hours). These values correspond to the diameters between 0.05 and 0.03 AU for the dense central core, respectively. The meteoric debris thus orbit the Sun in a fairly tight cylinder, confirming the notion that the Geminids are newly formed.

Fig. 5-21 (a) and (b) show that the diurnal peak on the day of maximum was 36 hr^{-1} in 1986 and 53 hr^{-1} in 1987. Thus the particle number densities at the respective intersections of the orbits of the stream and the earth stand in the ratio 1:1.5 (or 1:1.4 if the averages taken over the 6 hour interval are compared). This is consistent with the findings of others with regard to the structure of the stream along its orbit (eg. Simek, 1976; McIntosh, 1975; McIntoch & Simek, 1975; McIntosh & Simek, 1980). However, we can draw no conclusions concerning the periodicity of the variations of the density of the stream from only two years' data.

The observed diurnal rate curves at maximum are contrasted with the theoretical rate of underdense echoes, associated with a point radiant and for an assumed mass distribution index of 1.7, in Fig. 5-22 (a) [1986] and (b) [1987]. In both years, the coincidence between the observed and predicted rates is only approximate. Discrepancies between the two rate curves may be ascribed to the diffuseness of the radiant and the presence of a significant proportion of overdense echoes.

No second active radiant, as reported by Webster, Kaiser & Poole (1966), was observed. This group noticed a second centre of activity during 1962, displaced by about -1 hour relative to the known radiant. However it was no longer present in 1963, and no subsequent observations have confirmed its existence.

Table 5-1: Program parameters: major shower rate curves.

	DIURNAL RATES			RATE VS DAY (SOLAR LONGITUDE)									Shower	Year	Shower days used	Days of sporadic background	
	Total rate	Shower-only rate		Total rate					Shower-only rate							Before max.	After max.
Program	AVPLOT	DIFPLOT	OWL	NEWPEAK2					NEWPEAK1								
Graph of:	rate/hr vs SAST	rate/hr vs SAST	normalised obs. & predicted rate/hr vs SAST	Normalised rate in sky-window vs. day					Rate vs day								
	Fig.	Fig.	Fig.	Fig.	DT/hr	T1/hr	T2/hr	SKY/°	Fig.	DT/hr	T1/hr	T2/hr					
	5-6(a)	5-7(a)	5-8(a)						5-4(a)	4	6.3	10.3	Eta-Aqu	86	126-7	116-119	133-135
	5-23(a)												"	"			
	5-6(b)	5-7(b)	5-8(b)	5-5	4	6.7	10.7	10	5-4(b)	4	6.7	10.7	Eta-Aqu	87	127	95-100	153-159
	5-23(b)												"	"			
	5-11(a)	5-12(a)	5-13(a)						5-9(a)	2	0.1	6.1	δ-Aqu	86	207-9	-	227-234
	5-11(b)	5-12(b)	5-13(b)	5-10	2	0.7	6.7	5	5-9(b)	2.5	0.5	7.0	δ-Aqu	87	207-9	192-197	224-230
	5-23(c)	5-17(a)	5-18(a)	5-16(a)	2	4.3	6.3	10					Orionids	86	294-6	269-273	310-316
	5-23(d)	5-17(b)	5-18(b)	5-16(b)	4	3.6	7.6	20	5-15	4	2.9	6.9	Orionids	87	294-6	265-273	312-318
				5-16(c)	4	3.6	7.6	10					"	"			
				5-16(d)	4	3.6	7.6	5					"	"			
		5-21(a)	5-22(a)	5-20(a)	3	3.1	6.1	5	5-19(a)	3	3.1	6.1	Geminids	86	347-8	330-334	358-362
		5-21(b)	5-22(b)	5-20(b)	3	2.2	5.2	5	5-19(b)	3	2.2	5.2	Geminids	87	347	334-338	361-365

The following definitions occur:
T1: centre of the time-window before radiant transit, on the first day of the run.
T2: ditto, for the time-window after transit.
DT: duration of the time-window in hours.
SKY: linear dimension of the sky-window in degrees.

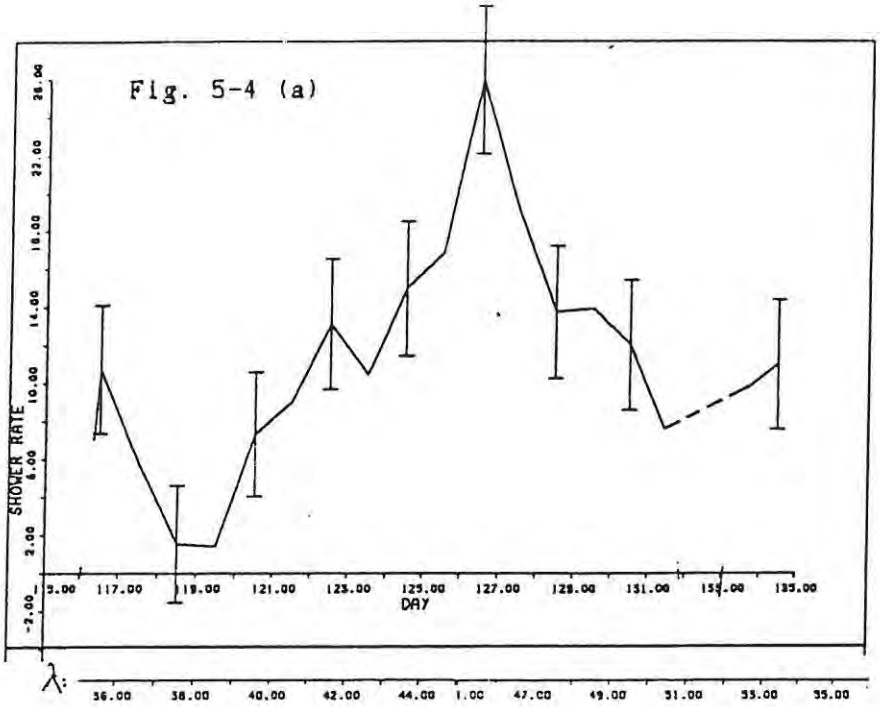

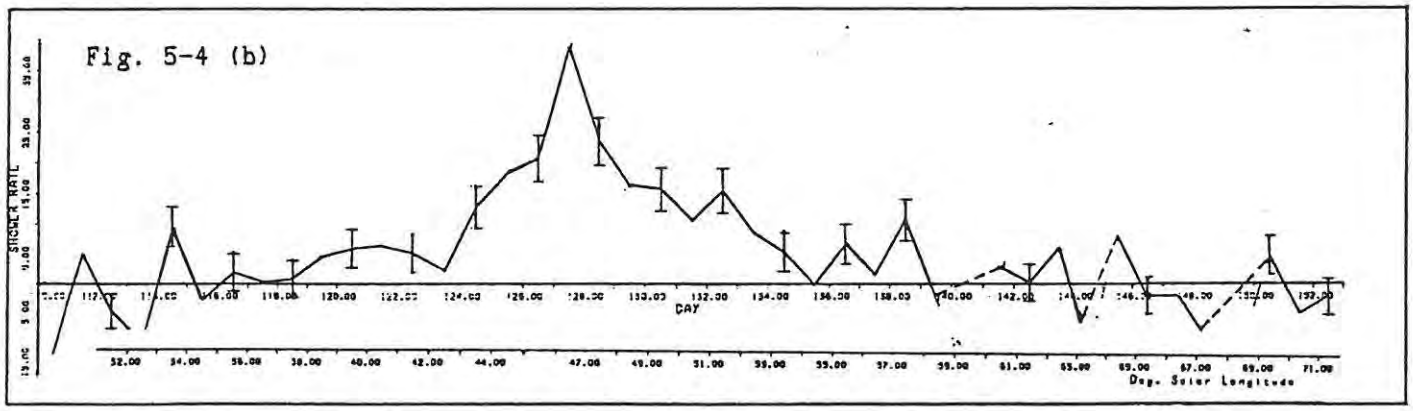

Fig 5-4: Daily variation of Eta-Aquarid shower-only hourly rate for (a) 1986 and (b) 1987. Each data point represents the mean hourly echo rate over an 8 hour interval centred on the time of radiant transit on that day. Assumed sporadic background rates have been subtracted out.

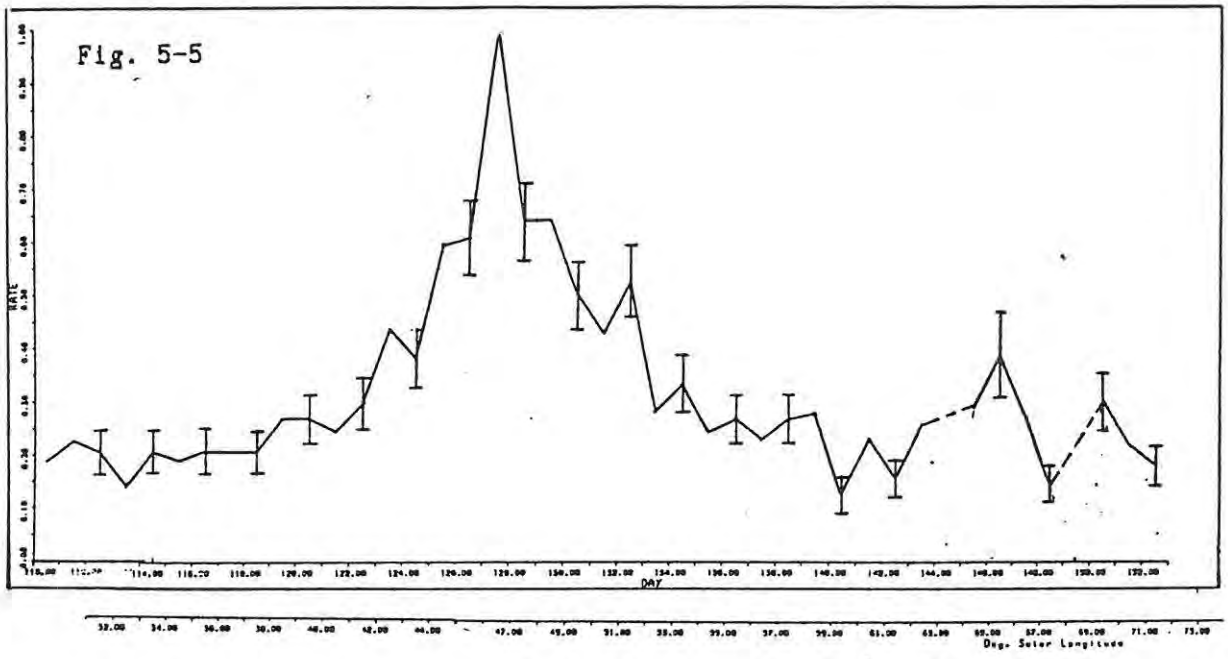

Fig 5-5: Normalised average hourly echo rates associated with a 10° square of sky centred on the Eta-Aquarid radiant in 1987, as a function of day number. Each point is the average taken over an 8 hour interval centred on the time of radiant transit on that day. No assumed background has been subtracted out.

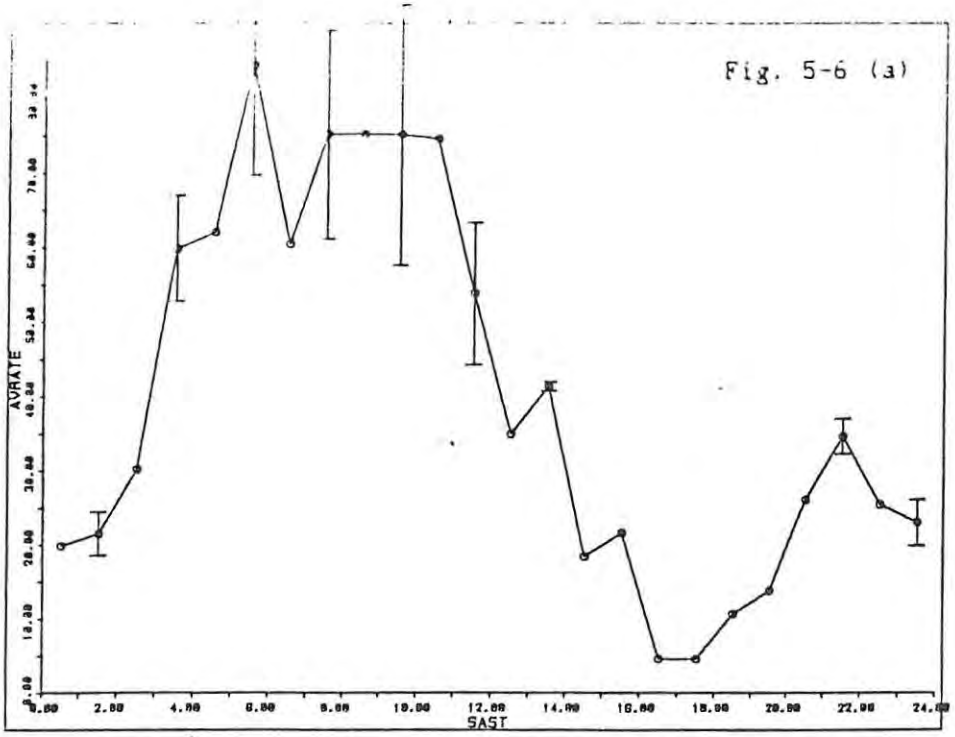

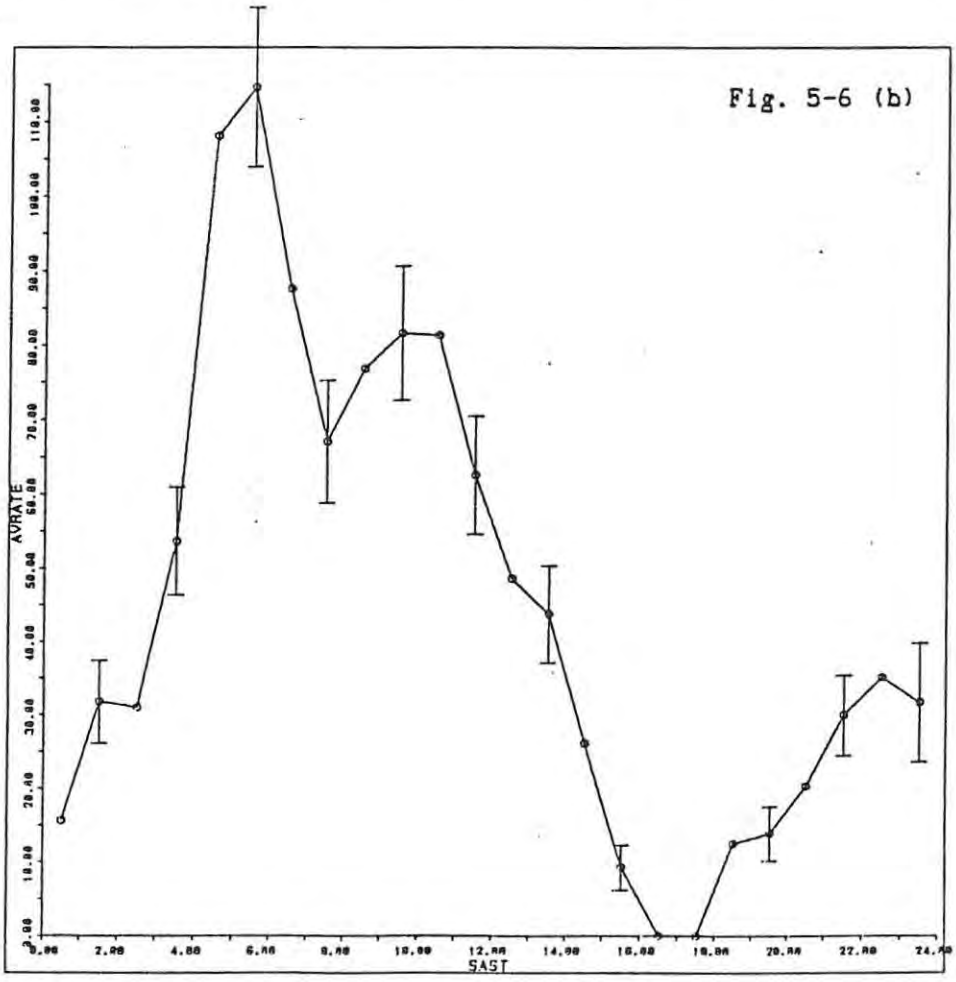

Fig 5-6: Average hourly echo rate for the days of maximum Eta-Aquarid activity as a function of SAST: (a) Days 126-7, 1986; (b) Day 127, 1987.

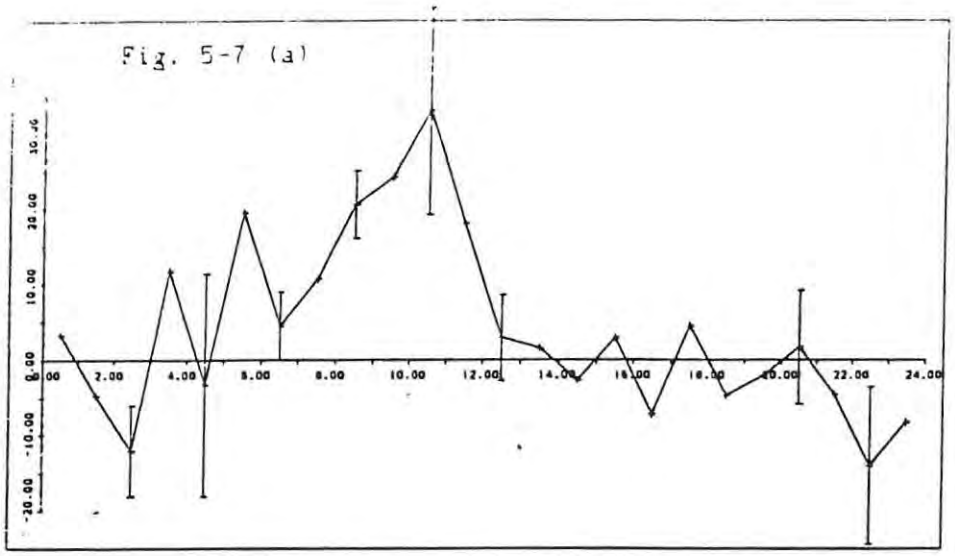

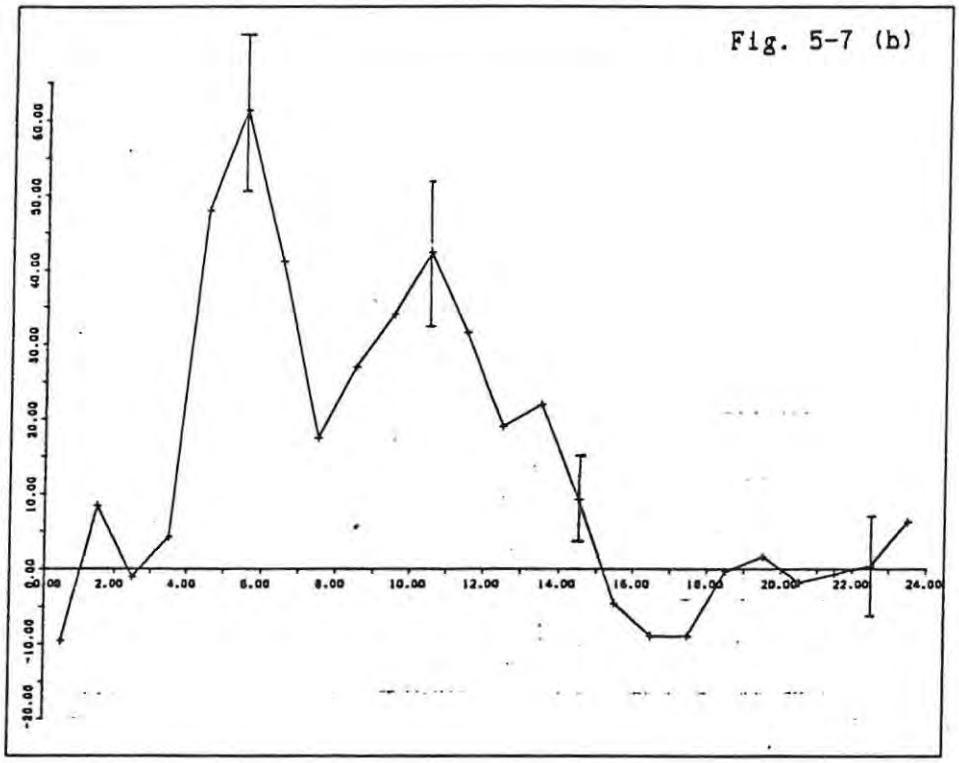

Fig 5-7: Average shower-only hourly echo rate on the days of maximum Eta-Aquarid activity as a function of SAST: (a) Days 126-7, 1986; (b) Day 127, 1987. Assumed sporadic background rates have been subtracted out.

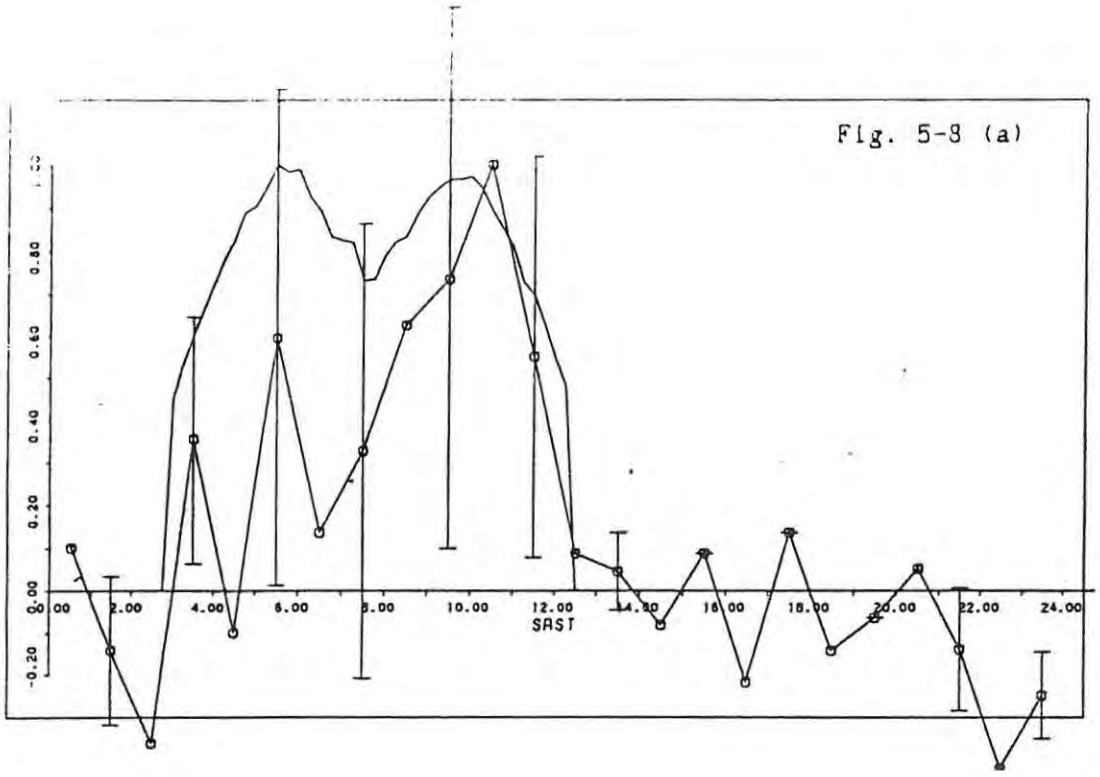

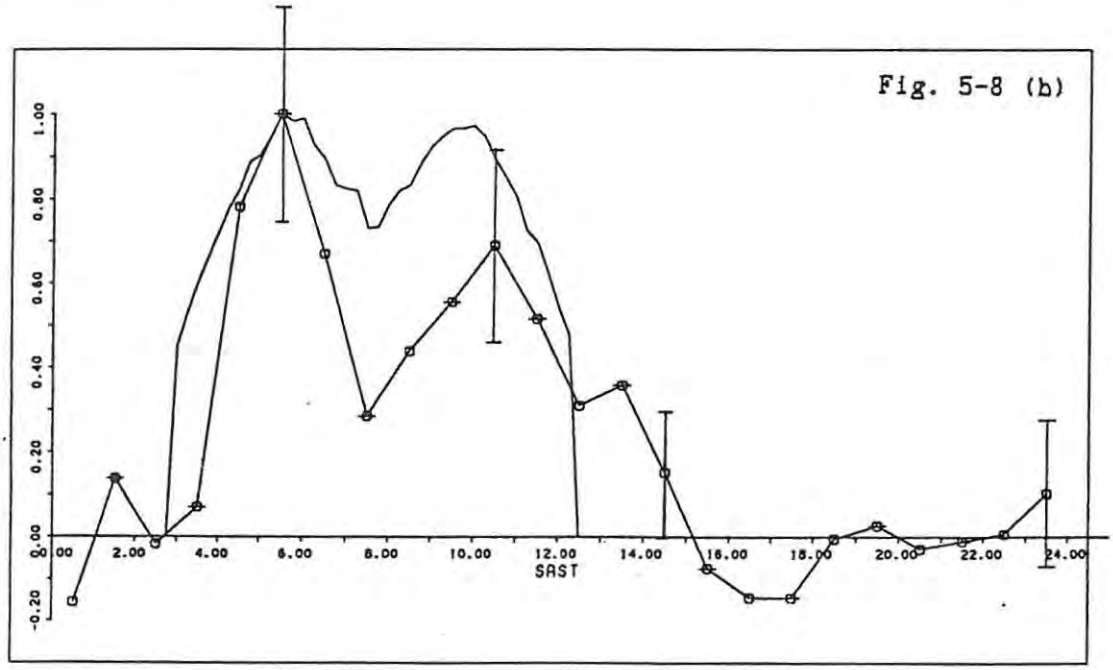

Fig 5-8: Comparison of the diurnal variation of the observed average shower-only hourly echo rate, over the days of the Eta-Aquarid maximum, with that predicted for underdense echoes associated with the shower radiant: (a) Days 126-7, 1986; (b) Day 127, 1987. The curves have been normalised.

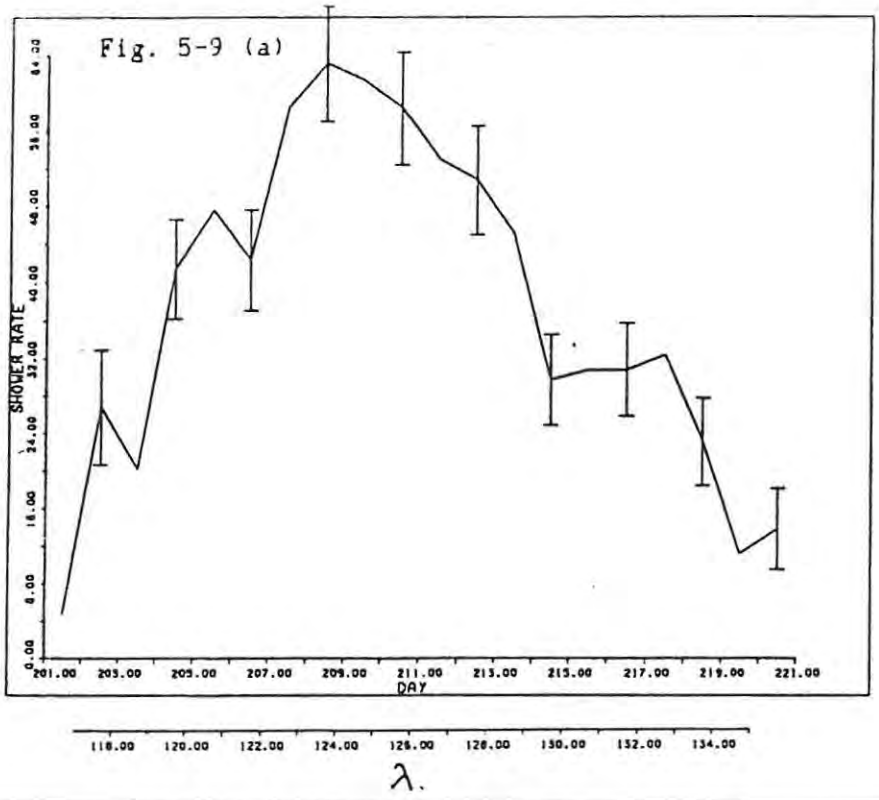

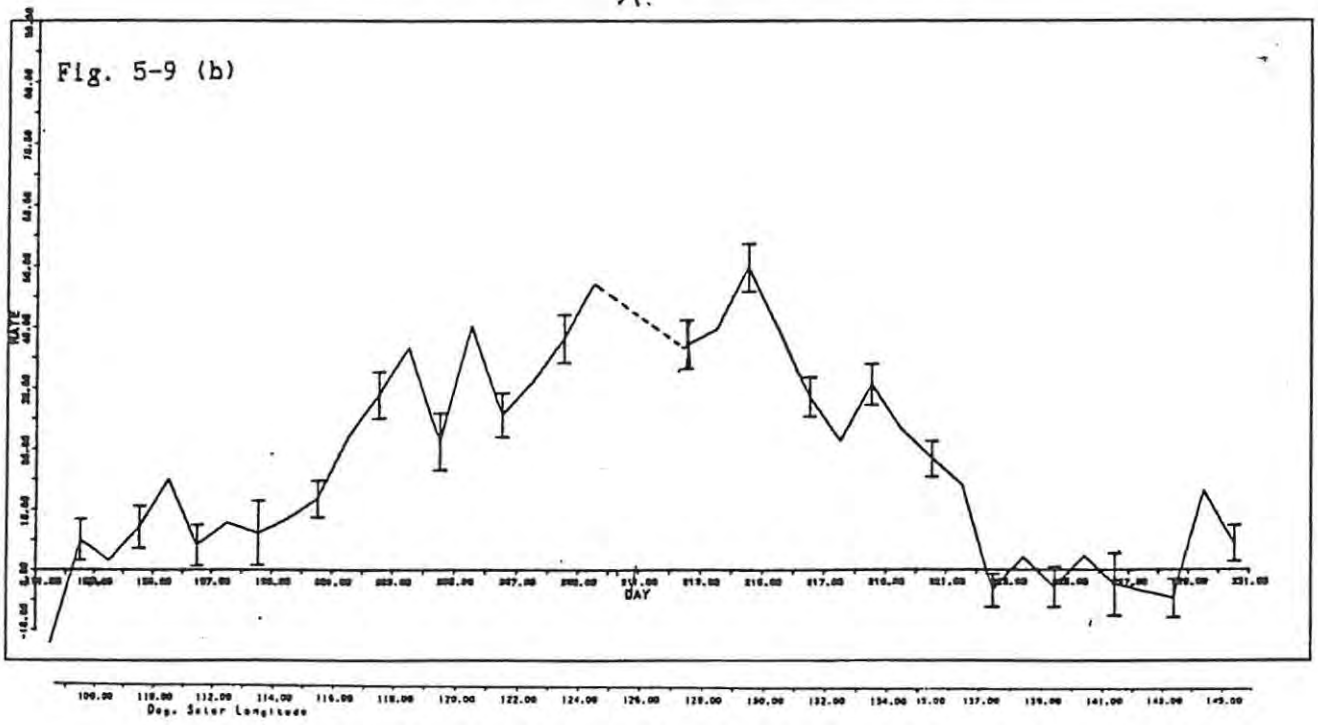

Fig 5-9: Daily variation of δ-Aquarid shower-only hourly rate for (a) 1986 and (b) 1987. Each data point represents the mean hourly echo rate taken over two time-windows, before and after radiant transit, when the diurnal echo rate is at its maximum. The duration of the time-windows was 2 hours in (a) and 2½ hours in (b). Assumed background rates have been subtracted out.

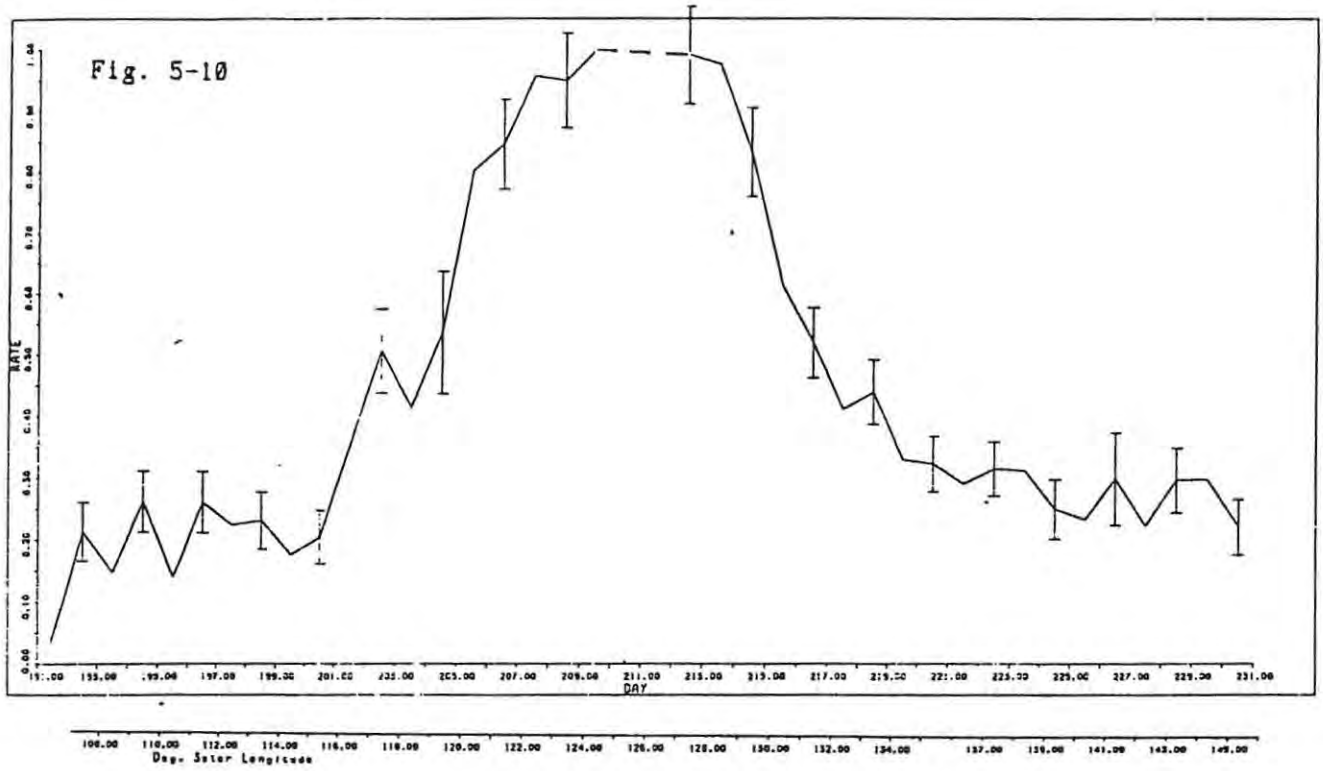

Fig 5-10: Normalised average hourly echo rates associated with a 5° square of sky centred on the southern δ-Aquarid radiant in 1987, as a function of day number. Each point is the average hourly echo rate taken over two 2½ hour time windows, as described for Fig 5-9 (b). No sporadic background has been subtracted out.

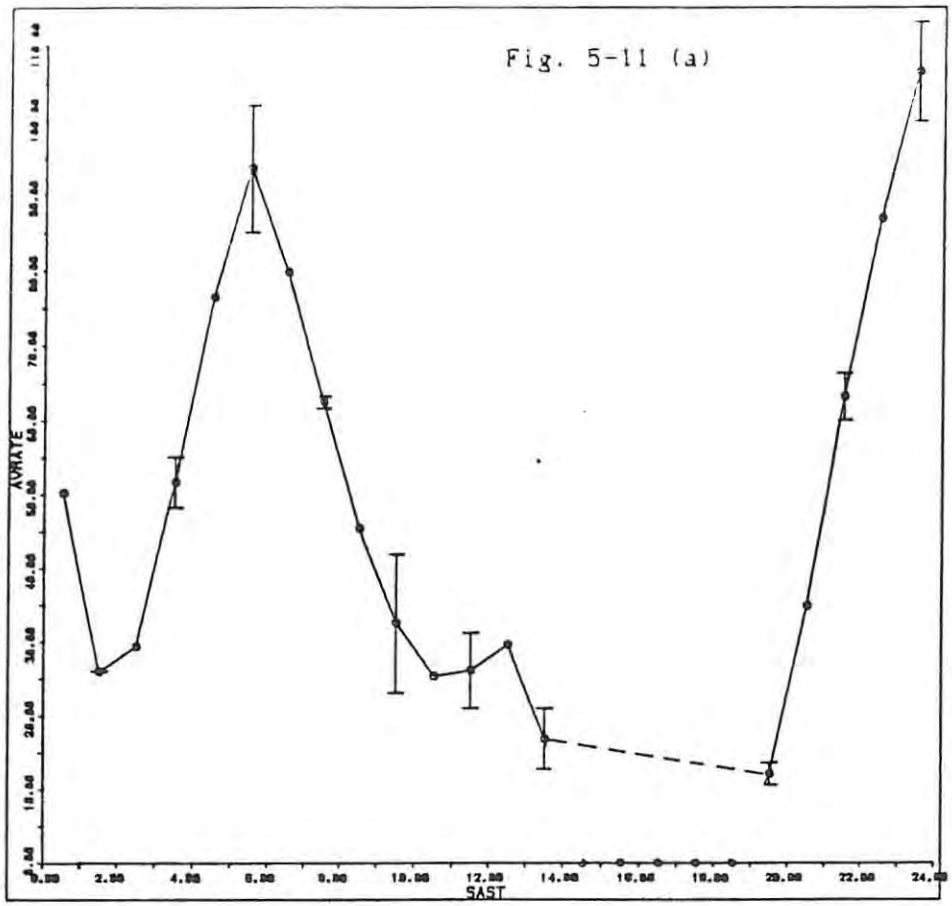

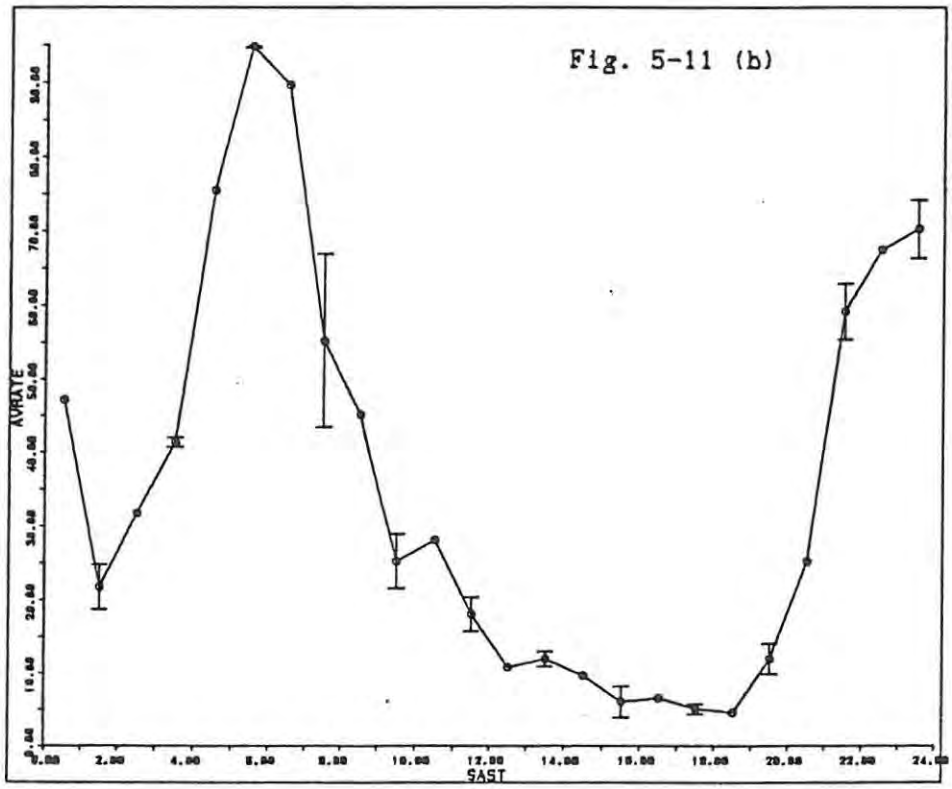

Fig. 5-11: Average hourly echo rate for the days of maximum δ-Aquarid activity, as a function of SAST: (a) Days 207-9, 1986; (b) Days 207-9, 1987.

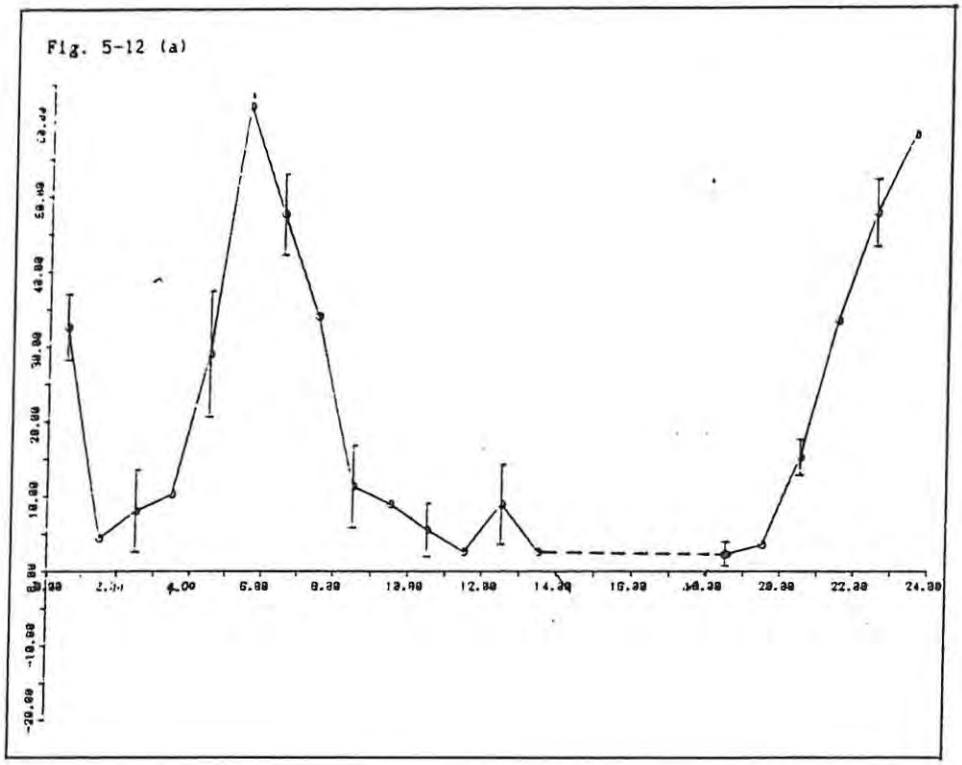

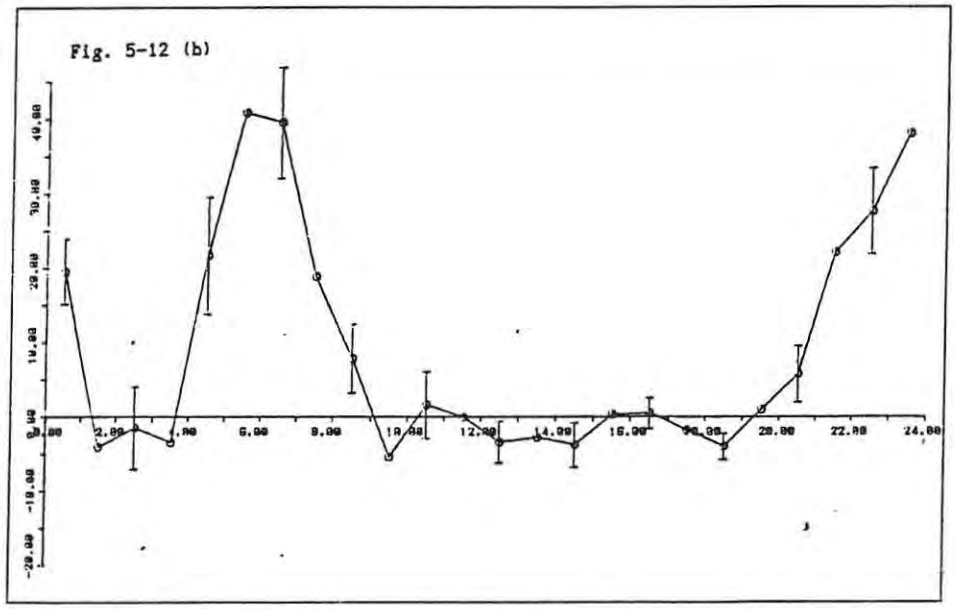

Fig 5-12: Average shower-only hourly echo rate for the days of maximum δ-Aquarid activity: (a) Days 207-9, 1986; (b) Days 207-9, 1987. Assumed sporadic background rates have been subtracted out.

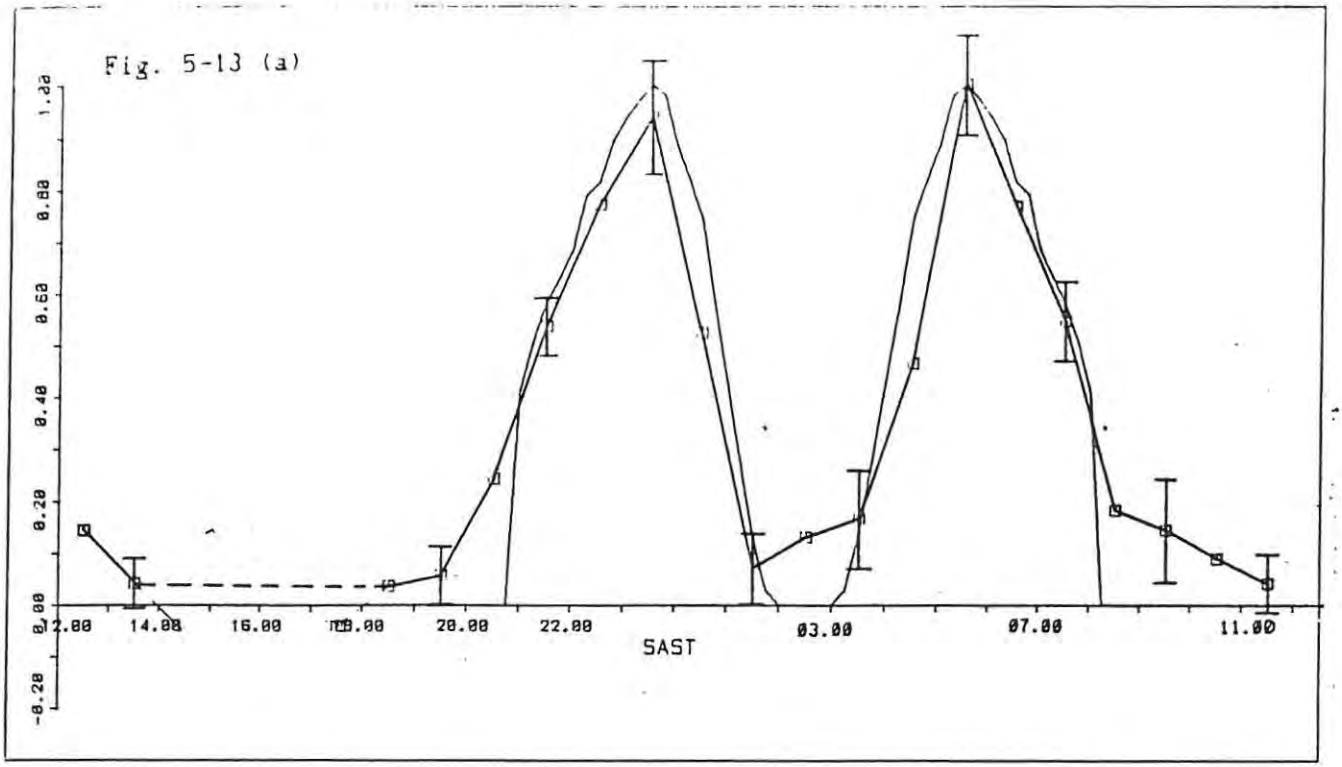

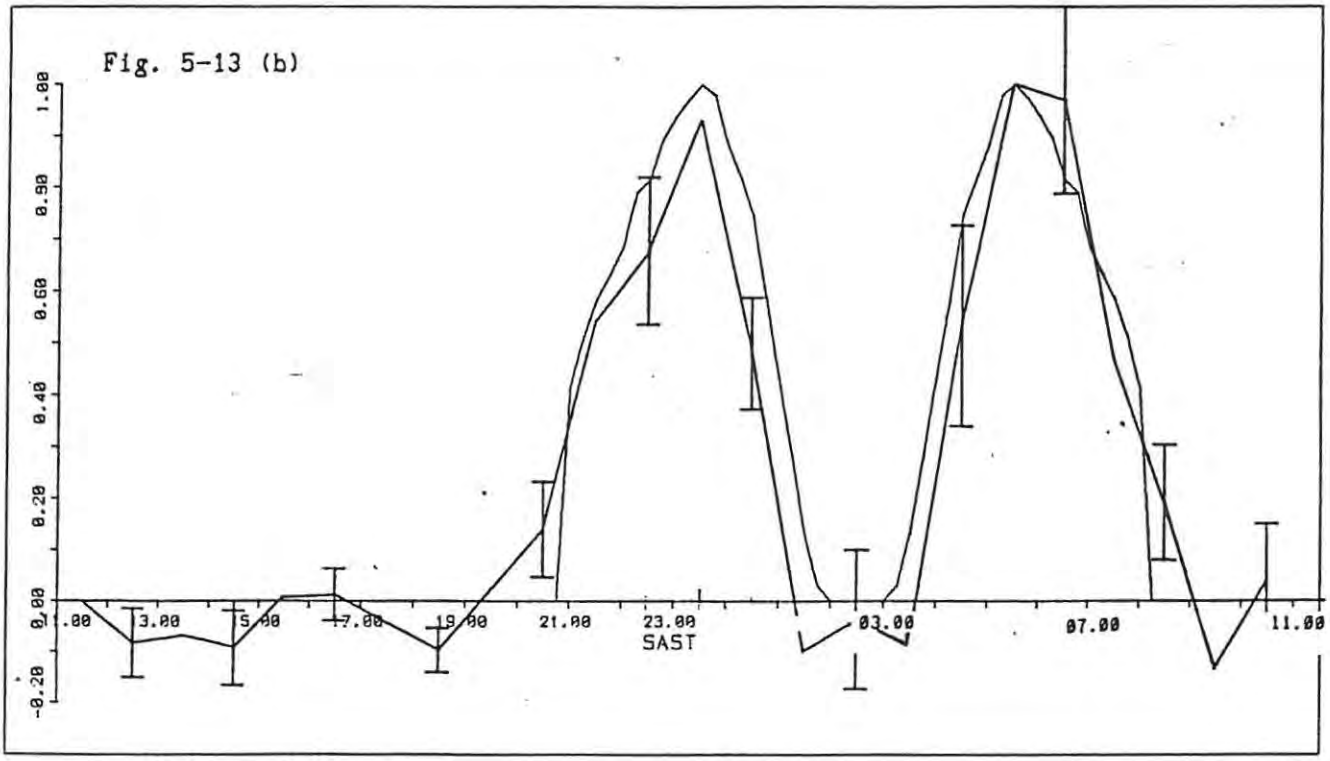

Fig 5-13: Comparison of the diurnal variation of the observed average shower-only hourly echo rates, over the days of δ-Aquarid maximum activity, with that predicted for underdense echoes associated with the southern shower radiant: (a) Days 207-9, 1986; (b) Days 207-9, 1987. The curves have been normalised.

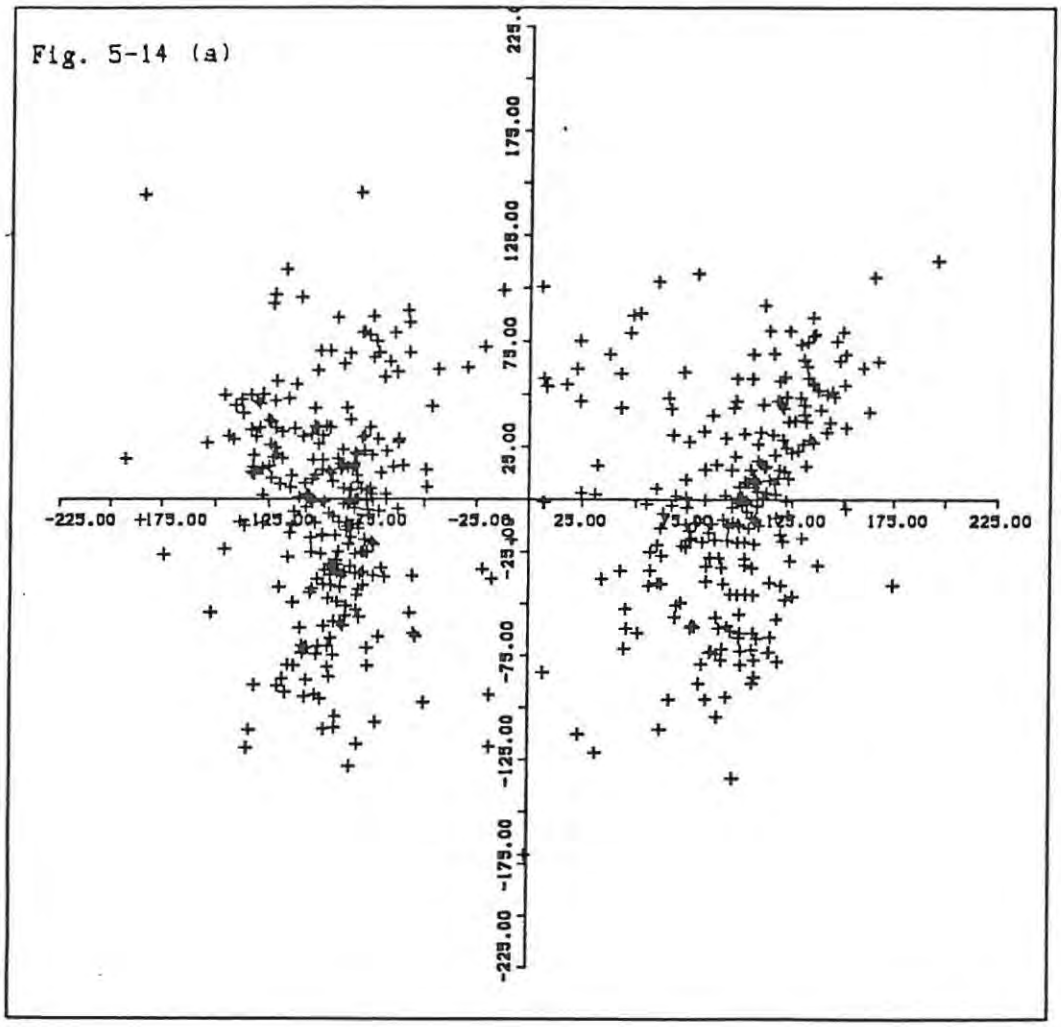

Fig 5-14: Reflection points mapped onto an echo surface at a constant height of 95 km, for (a) shower echoes associated with the southern δ-Aquarid radiant, and (b) non-shower echoes. The origin is in the observer's zenith and north is to the top of the page. Data for plot (a) are from two 24 minute time-windows centred on the diurnal δ-Aquarid maxima on each day for the period day 209-day 214, 1987. The transparency indicates the positions of the echo line at these times. Data for plot (b) are from a 24 hour period of non-shower activity (March 21, 1987).

Fig. 5-14 (b)

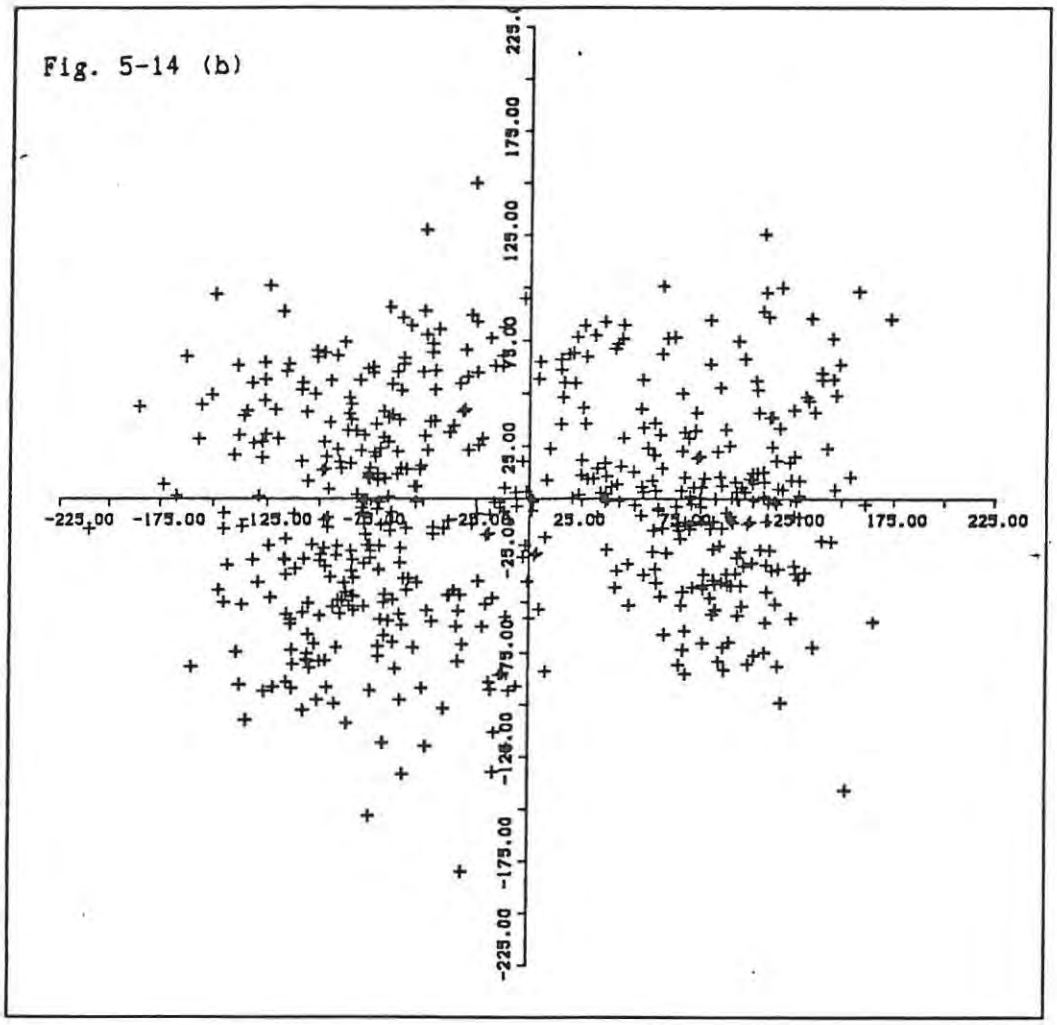
225.00
175.00
125.00
75.00
25.00
-25.00
-75.00
-125.00
-175.00
-225.00
-225.00
-175.00
-125.00
-75.00
-25.00
25.00
75.00
125.00
175.00
225.00

Fig. 5-14 (b)

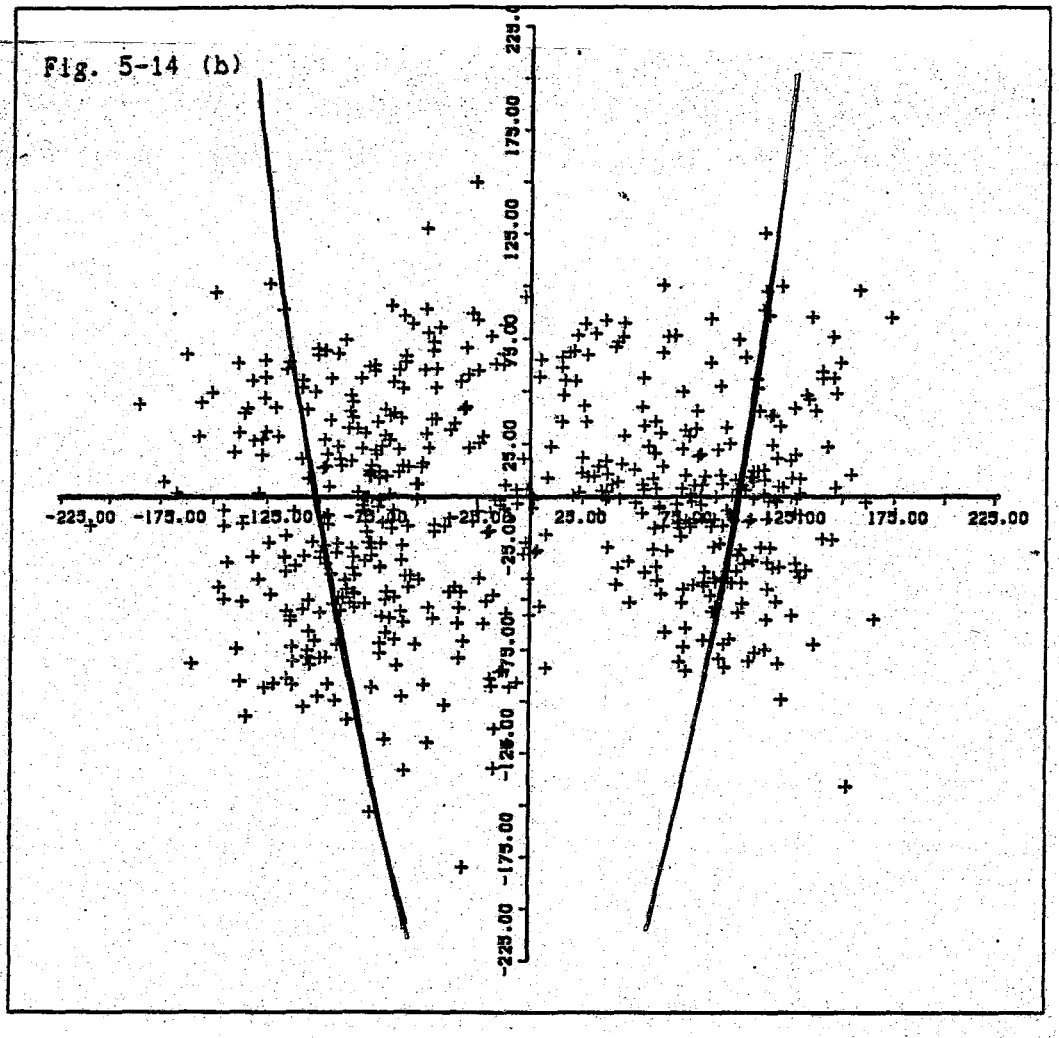
225.00
175.00
125.00
75.00
25.00
-25.00
-75.00
-125.00
-175.00
-225.00
-225.00
-175.00
-125.00
-25.00
25.00
175.00
225.00

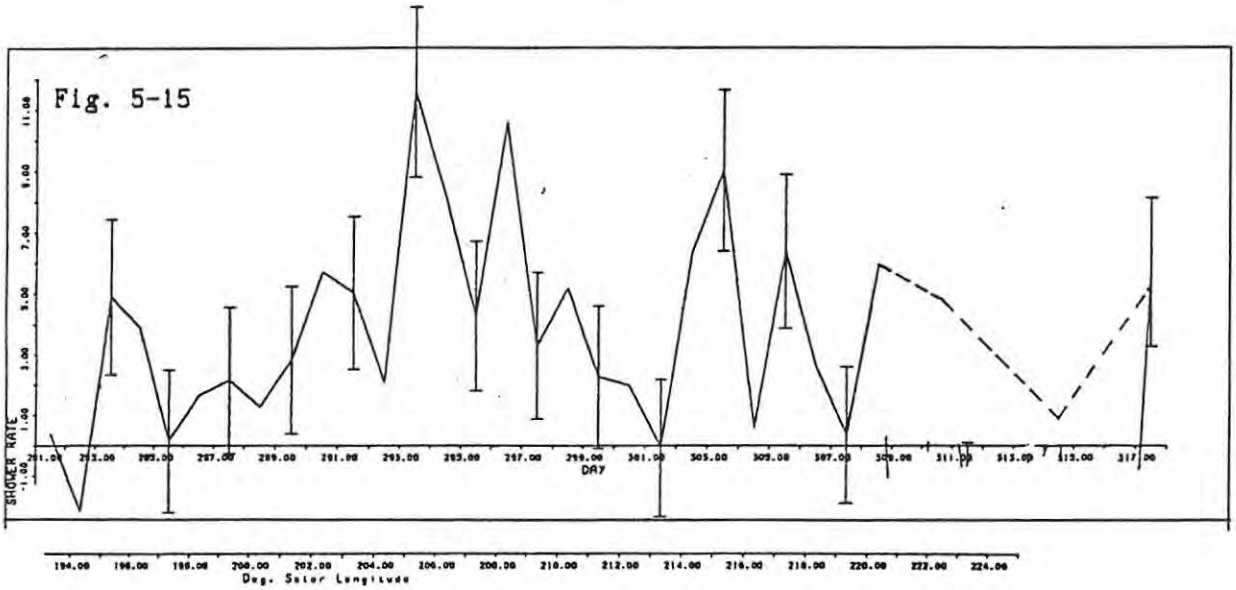

Fig 5-15: Daily variation of Orionid shower-only hourly rate for 1987. Each data point represents the mean hourly echo rate over an 8 hour period centred on the time of radiant transit on that day. An assumed sporadic background has been subtracted out.

Fig 5-16: Normalised hourly echo rates associated with a square of sky centred on the Orionid radiant, as a function of day number. Each point represents the mean hourly rate over an 8 hour period centred on the time of radiant transit on that day. Graph (a) shows the activity in a 10° square of sky for 1986, while (b), (c) and (d) show the activity in squares of variable size for 1987. The sides of the respective squares are 20°, 10° and 5°.

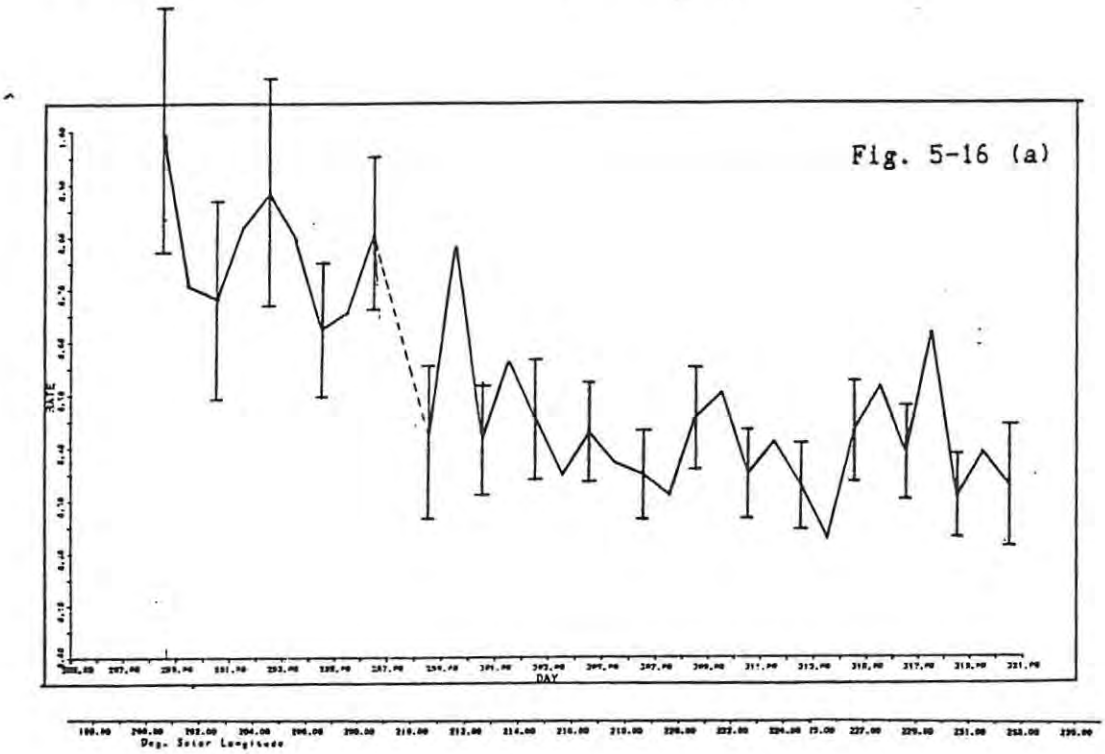

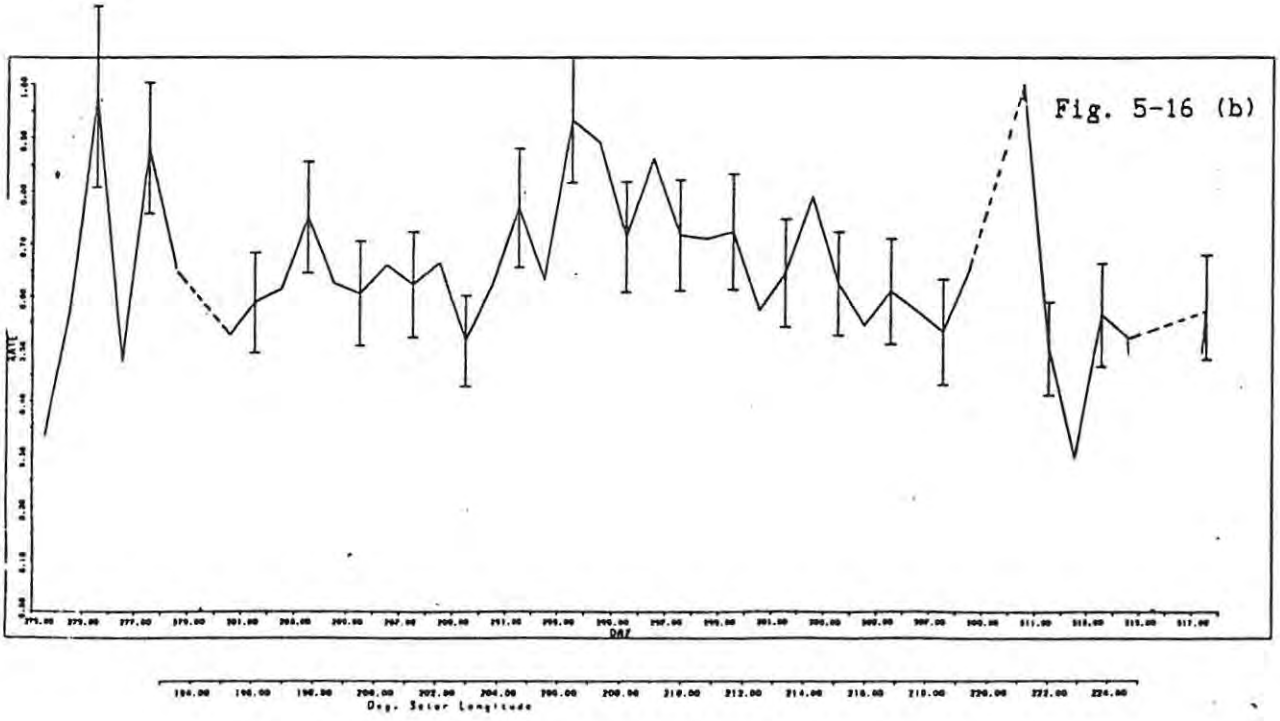

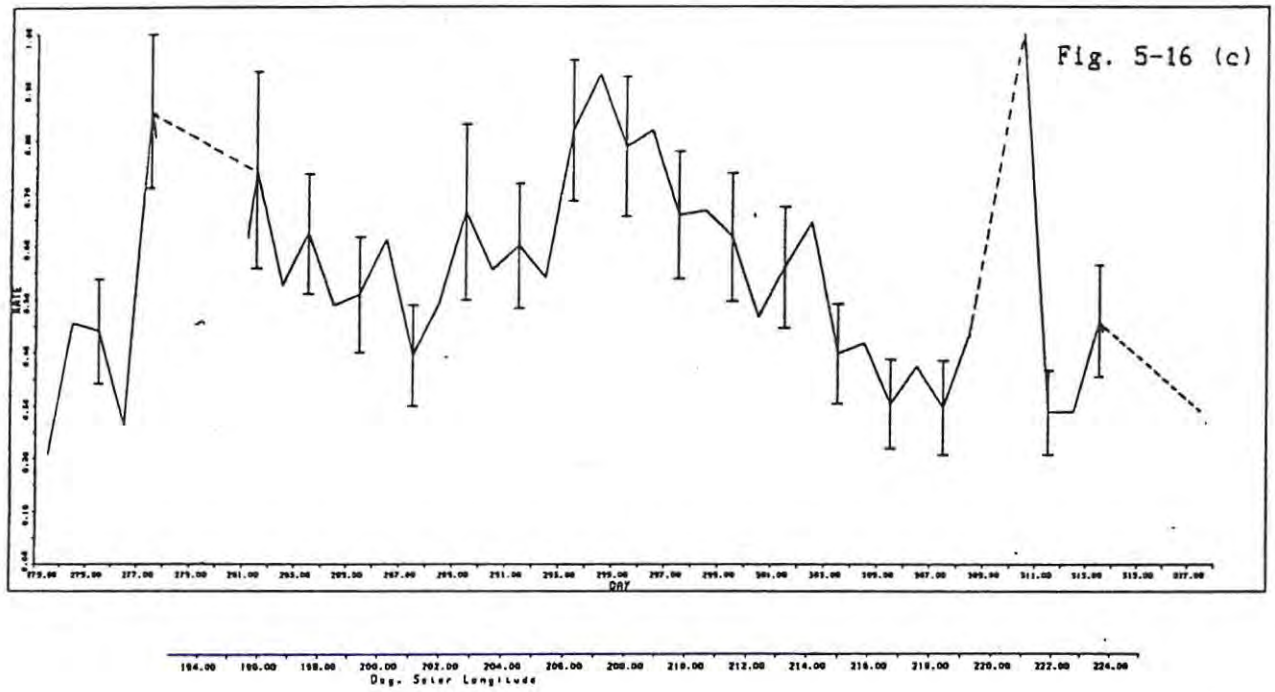

Fig. 5-16 (c)

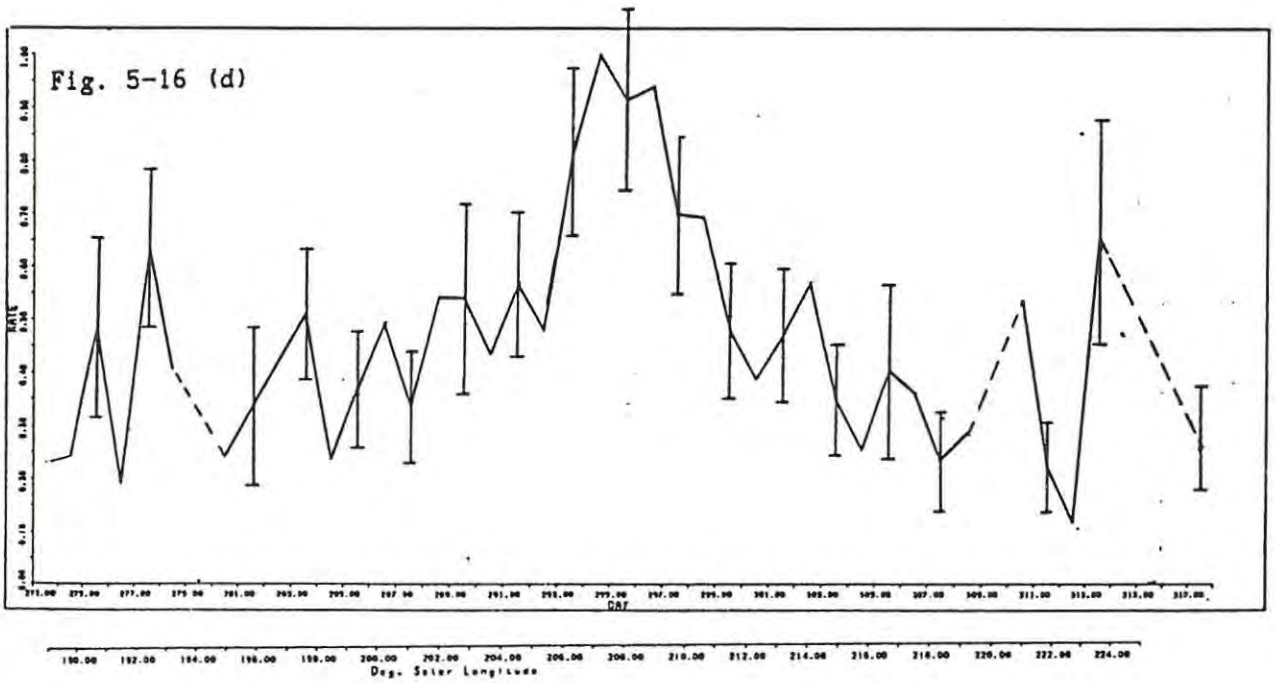

Fig. 5-16 (d)

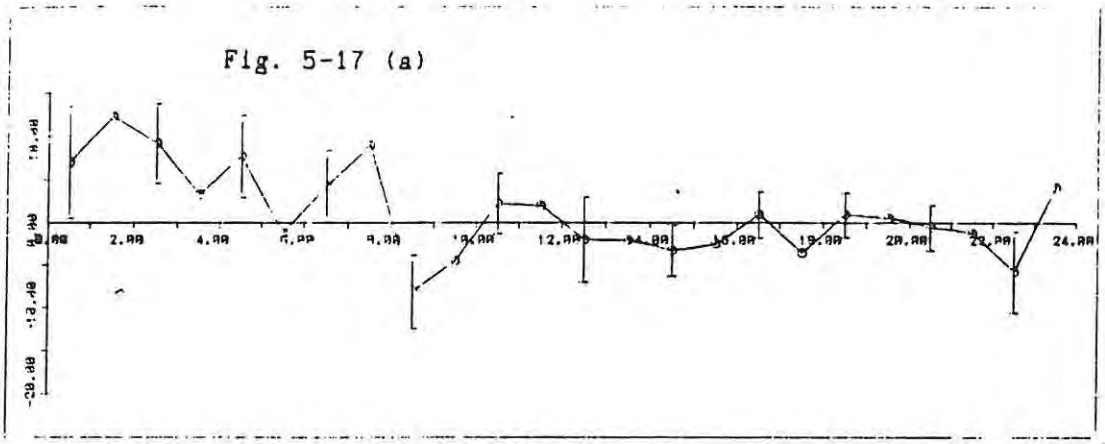

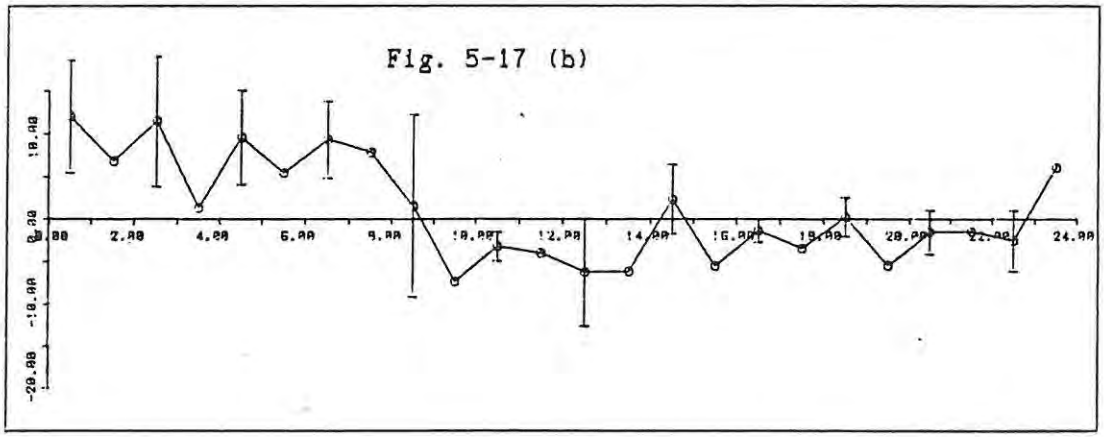

Fig 5-17: Average shower-only hourly echo rates as a function of SAST, taken over the days of maximum Orionid activity: (a) Days 294-6, 1986; (b) Days 294-6, 1987. Assumed background rates have been subtracted out.

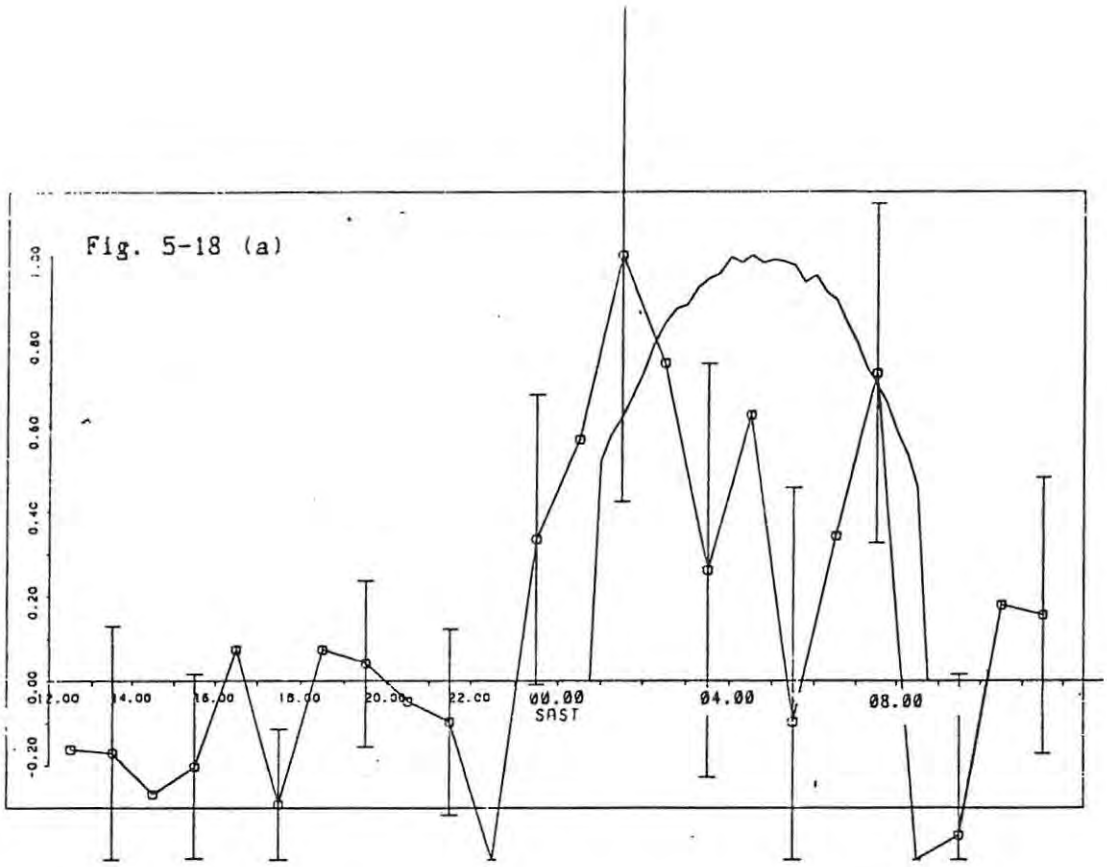

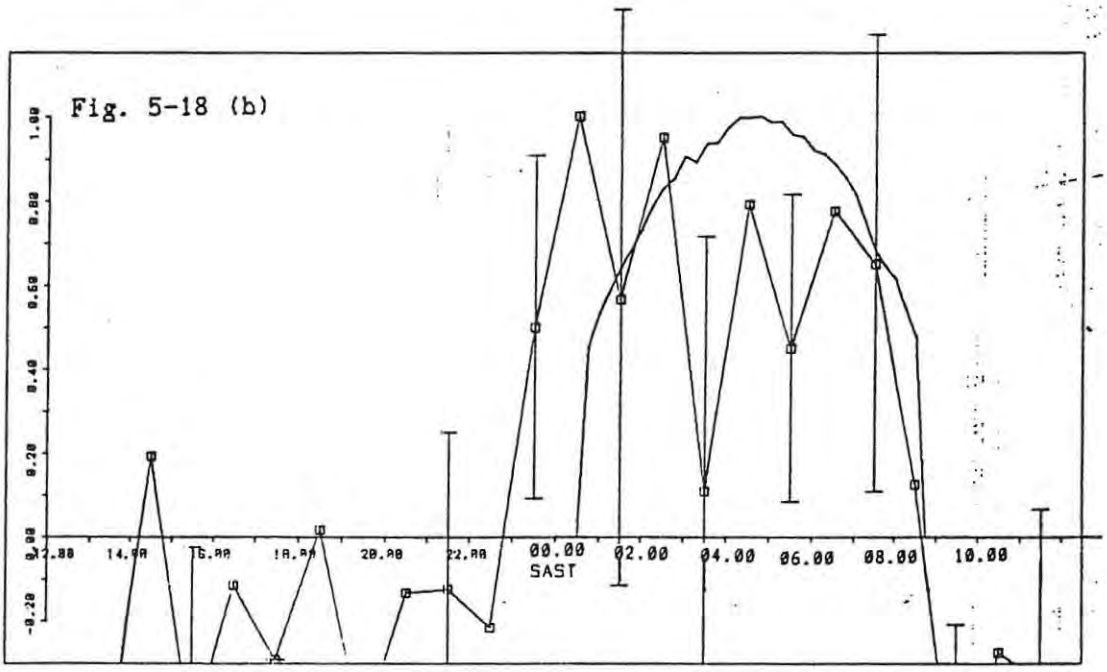

Fig 5-18: Comparison of the diurnal variation of the observed average shower-only echo rates, over the days of maximum Orionid activity, with that predicted for underdense echoes associated with the shower radiant: (a) Days 294-6, 1986; (b) Days 294-6, 1987.

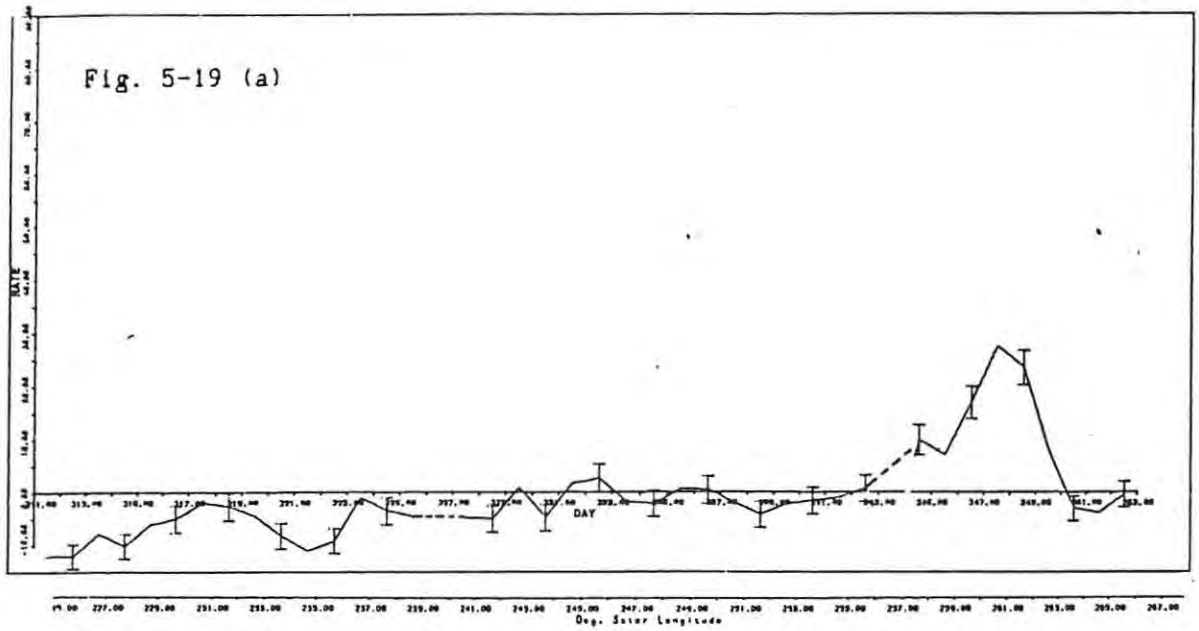

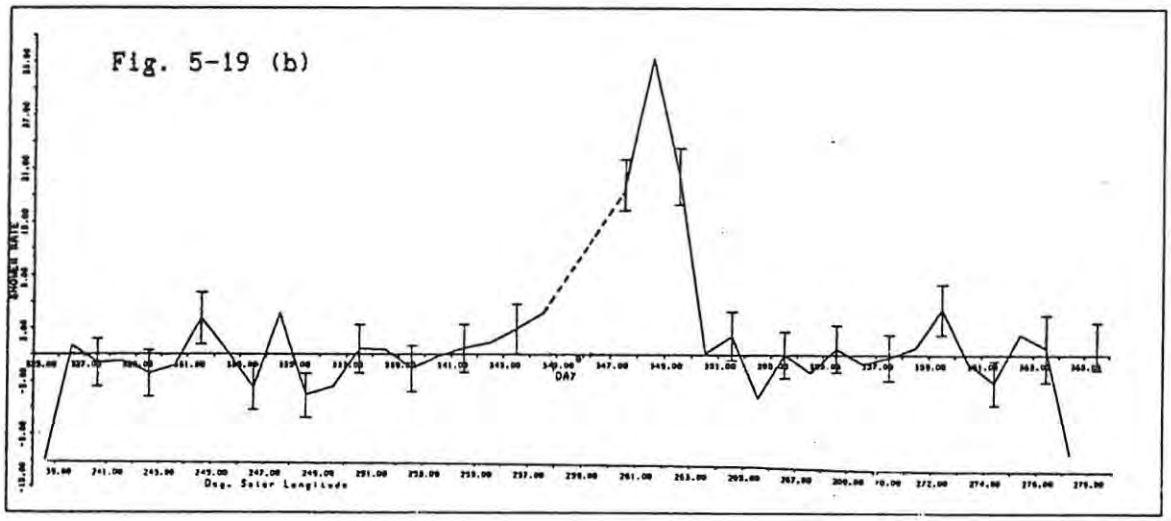

Fig 5-19: Daily variation of the Geminid shower-only hourly rate for (a) 1986 and (b) 1987. Each point represents the mean hourly echo rate taken over a 6 hour interval centred on the time of radiant transit on that day. Assumed sporadic background rates have been subtracted out.

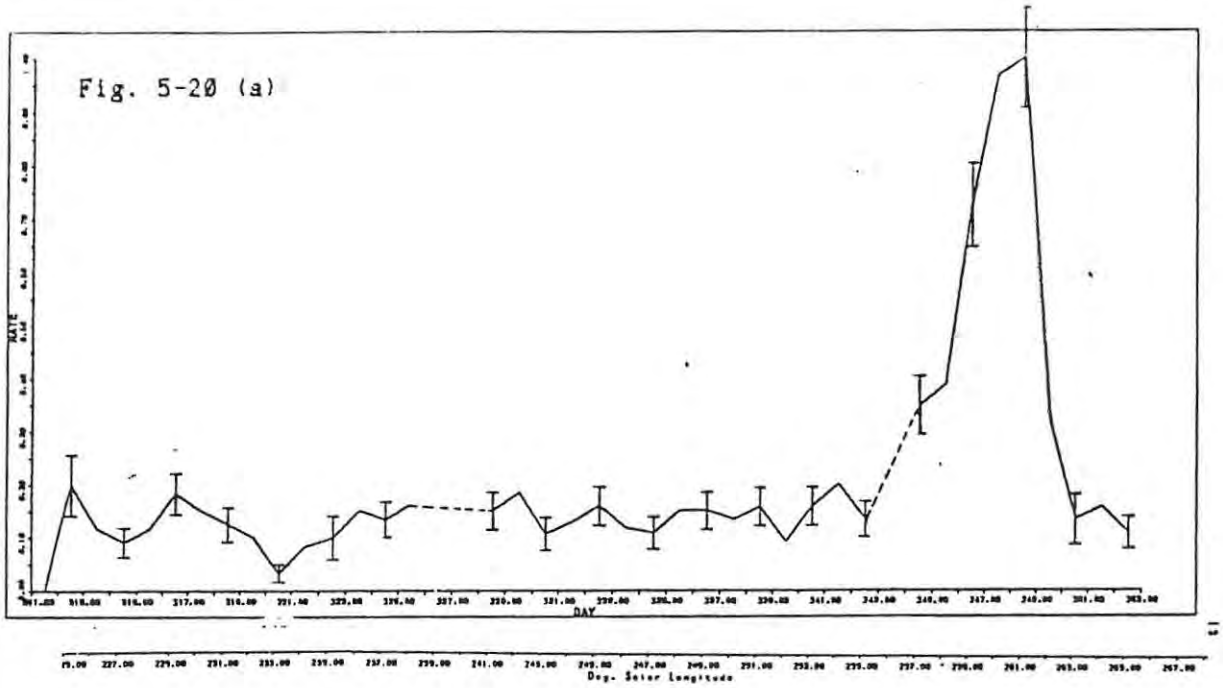

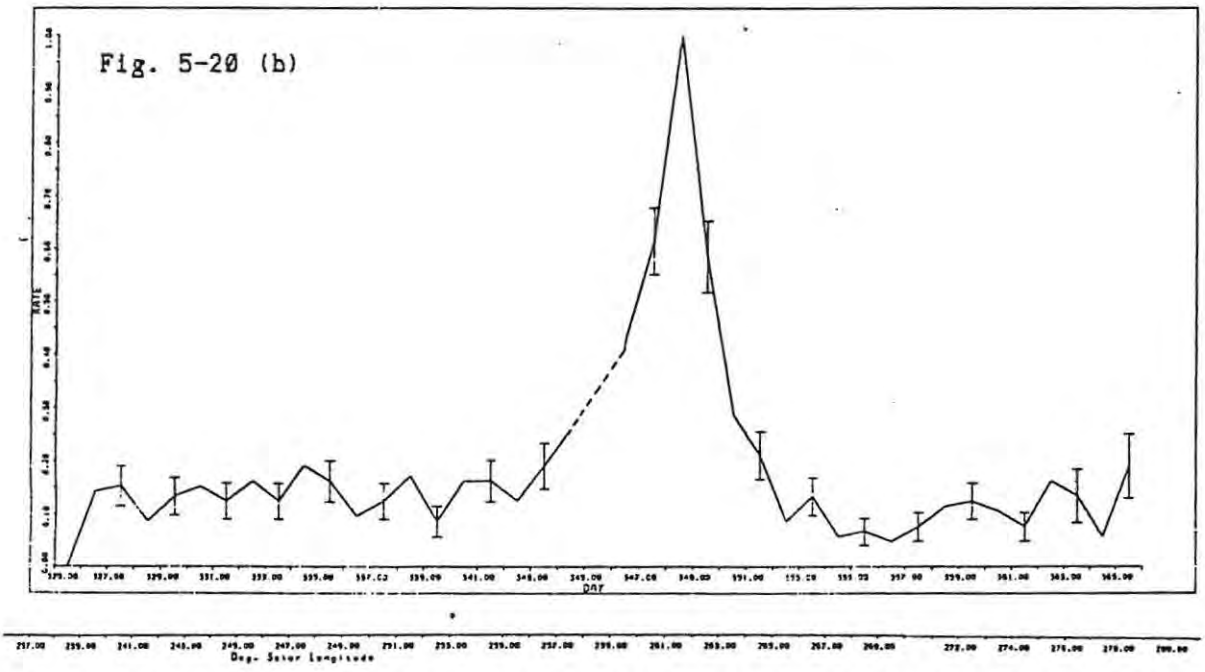

Fig. 5-20: Normalised hourly echo rates associated with a 5° square of sky centred on the Geminid radiant in (a) 1986 and (b) 1987. Each point is the average over a 6 hour time interval centred on the time of radiant transit, on that day. No sporadic background has been subtracted out.

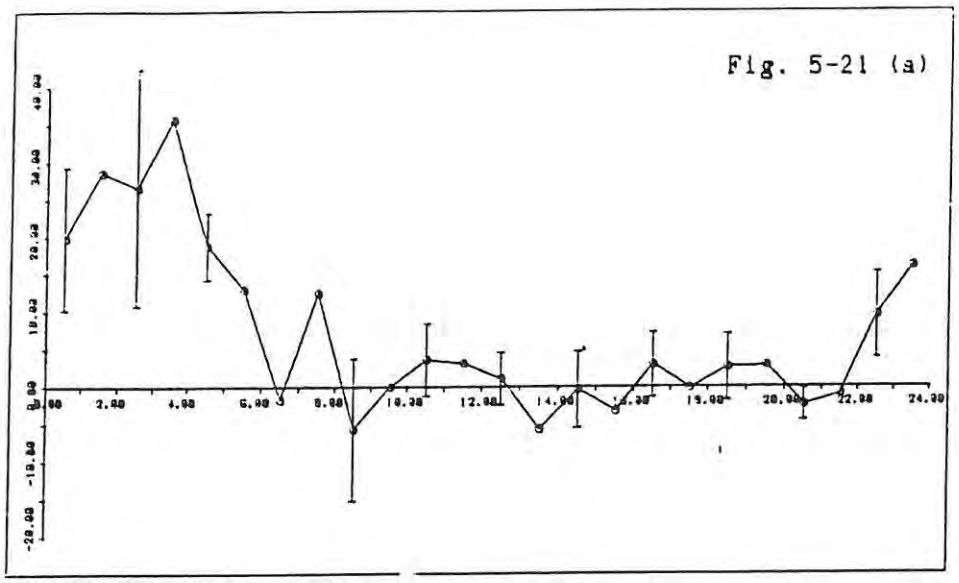

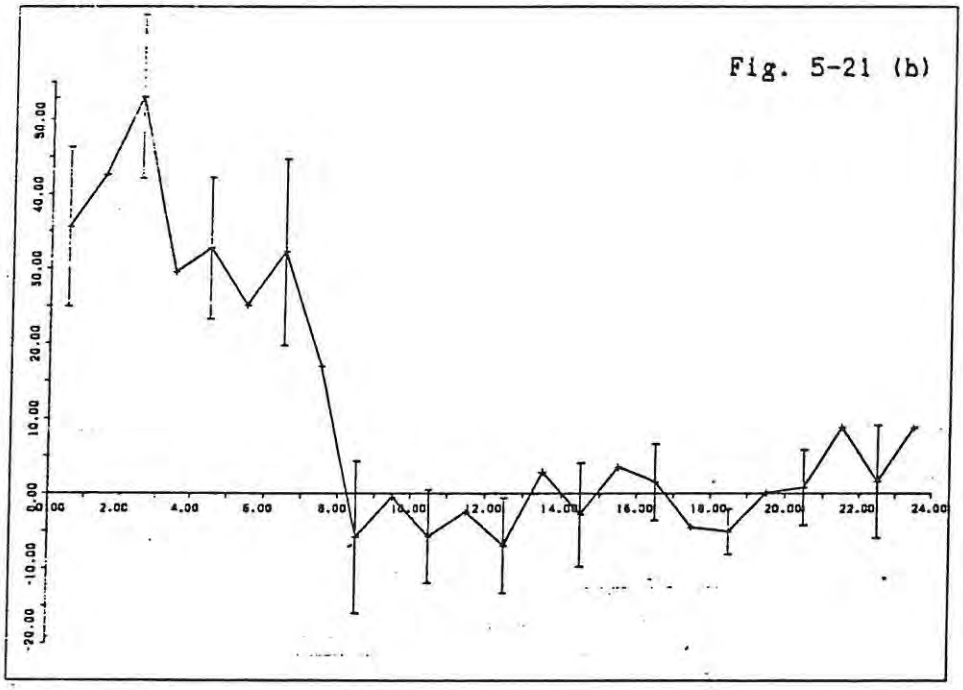

Fig. 5-21: Average shower-only hourly echo rate on the days of maximum Geminid shower activity, as a function of SAST: (a) Days 347-348, 1986; (b) Day 348, 1987.

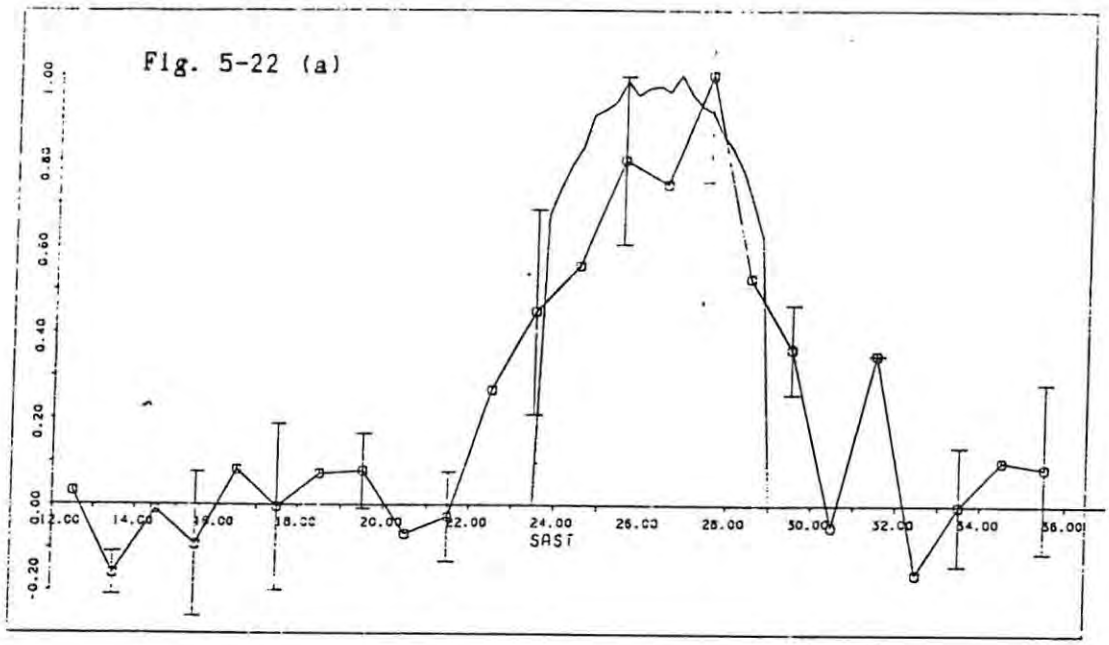

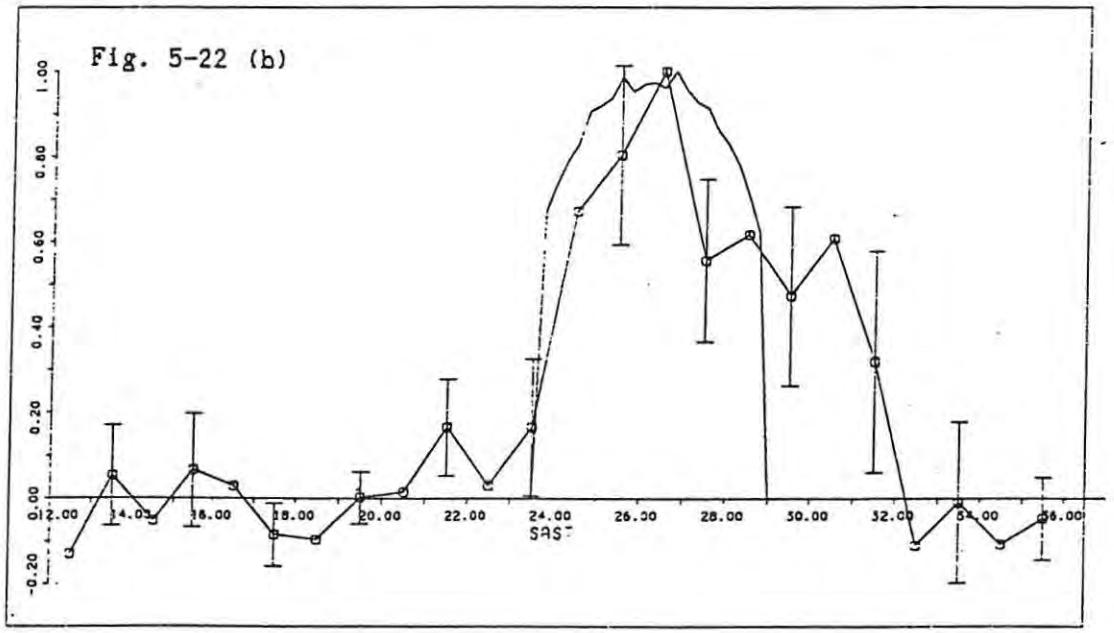

Fig 5-22: Comparison of the diurnal variation of the observed average shower -only echo rate, on the days of Geminid maximum, with that predicted for underdense echoes associated with the shower radiant: (a) Days 347-8, 1986; (b) Day 348, 1987.

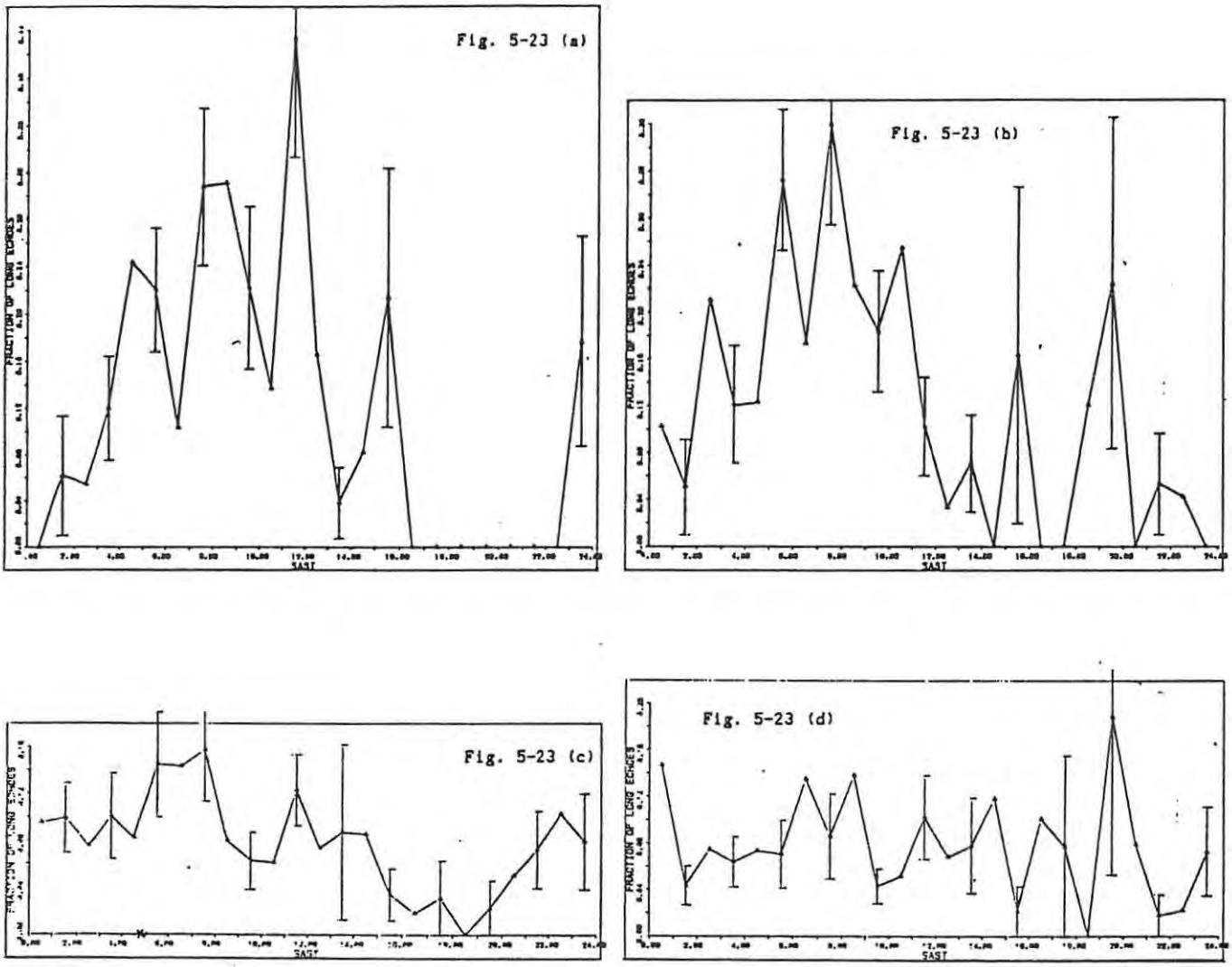

Fig 5-23: Proportion (relative to the total hourly rate) of persistent echoes (τ > 1.8 s) at shower maximum for the Eta-Aquarids: (a) day 126, 1986; (b) day 127, 1987 and the Orionids: (c) days 294-6, 1986; (d) days 294-6, 1987.

5-4: The minor showers

We have chosen to designate as 'minor' any shower which failed to produce an echo rate equal to a significant fraction of the mean non-shower rate. Such showers did not noticeably stand out against the background of sporadic meteors, and therefore their presence could not be inferred from the all-sky hourly rate versus day curves. It was hoped to detect some of these weaker showers by the technique of counting only specular echoes associated with an area of sky adjoining the position of the known shower radiant. Showers which escape detection in this way will certainly be invisible in any of the other rate curves, although they may exhibit detectable radiant structure. The results of our search for shower radiant activity are presented in Chapter 6.

Thus, by using program NEWPEAK2 to process the data gathered over the periods of expected shower activity, searches for 18 minor showers were conducted, including two weak showers which have been observed only occasionally, namely those associated with comets Grigg-Skjellerup and 1987c.

In this section our results are presented in the form of a series of rate curves, Fig. 5-24 to Fig. 5-42, inclusive. For brevity, Table 5-2 lists the showers together with the associated program parameters. Comments on each of the rate curves follow. The source of radiant coordinates and dates for the expected shower durations and maxima is the Cambridge Encyclopedia of Astronomy (1977) page 246, unless otherwise stated.

(1) Omicron-Cetids (1987): expected duration: May 13-23
expected maximum: May 15 (day 135)
radiant coordinates: (30°,-3°)

Almond (1951) has found this day-time shower to be periodic rather than annual. From Fig. 5-24, peaks on 10 and 18 May are evident (days 130 and 138). No data were collected on May 15. The observed peaks are possibly due to members of this stream, but the evidence is not strongly conclusive.

(2) Corona Australids (1987): March 14-18,
max: March 16 (day 75) (245°,-48°).

This shower has been found to be weak and of variable activity (Weiss, 1957), and has a deficiency in large meteoroids (McKinley, 1961). No activity was observed, as shown by Fig. 5-25.

(3) Alpha-Capricornids (1987): July 15-Aug 25,
max: Aug 2 (day 214) (309°,-10°).
This stream may be associated with Comet 1954 iii (McKinley, 1961). The high rates on the left of Fig. 5-26 are attributable to δ-Aquarid meteors. No α-Capricornid activity was observed.

(4) Capricornids (1987): July 10-Aug 15,
max: July 25-26 (days 206-207) (315°,-15°)
Both the proximity and the strength of the δ-Aquarid radiant have resulted in contamination from this source, so that in Fig. 5-27 any activity which might have been due to the Capricornid stream cannot be resolved.

(5) and (6) The Taurid complex.
β-Taurids (1987): June 25-July 7,
max: June 29 (day 180) (85°,+17°)
Southern and Northern Taurids (1986, 1987):
October 20-November 30, max: November 8 (day 312)
(56°,+14°) and (56°,+22°)
The β-Taurids and the Southern and Northern Taurids are members of the Taurid complex of streams, whose origin can be traced back 50 centuries. The inclinations of the stream components have undergone dispersion over 15° during this time. Comet Encke is thought to be the parent body of Taurid meteors (McKinley, 1961).

Southern and Northern Taurid meteors are observed annually in November, as they approach the Sun. In 1940 Whipple suggested that the same stream should provide a day-time shower when its members return from perhelion. His prediction was later confirmed by the discovery of a June day-time shower from Jodrell Bank in England, namely the β-Taurids (Clegg, Hughes & Lovell, 1947).

A fairly well-defined β-Taurid maximum was observed in 1987, as depicted in Fig. 5-28, extending from June 25-28 (days 176-179).

Fig. 5-39 (a) indicates a gradual rise and fall of Southern Taurid activity during 1986, between October 20 (day 293) and December 3 (day 337). Several peaks are superimposed on this broad arc, suggestive of denser filaments within the stream. An overall maximum was observed on November 12 (day 316). The activity of this stream during 1987 was characterized by three prominent maxima on November 1, 13 and 27 (305, 317 and 329). These indicate the existence of narrow regions of high particle number density separated by broader belts which are more sparsely populated.

No maximum on or near November 8 was observed for the Northern Taurids

in 1986 (Fig. 5-38 (a)). The same was true for this stream in 1987, and it is evident from Fig. 5-38 (b) that two prominent maxima were observed in that year, the stronger of the two on November 27 (329). This suggests the presence, at the 1987 intersection, of two narrow filaments, rather than a broad stream.

The four graphs 5-38 (a) & (b) and 5-39 (a) & (b) are consistent with the very broadly dispersed structure of a stream which has suffered considerable orbital dispersion over its lifetime, and has become progressively less distinct from the sporadic background. At the other extreme are the rate profiles 5-20 (a) & (b) for the Geminids, a new and compact stream which contrasts sharply with the non-shower background. Judging from the degree of definition of the maximum in Fig. 5-28, the β-Taurids have undergone less dispersion than the other members of the complex.

(7) Ophiucids (1987): June 17-26,
max: June 20 (day 171) (260°,-20°)
Fig. 5-29 shows no maximum near June 20. No shower could be detected.

(8) Iota-Aquarids (1987): July 15-August 25,
max: August 6 (338°,-15°) and (331°,-6°)
Activity proceeds from two diffuse radiants. The activity curve for the southern radiant peaks on July 28 (209) as shown in Fig. 5-30 (a). This is certainly the result of interference from the intense δ-Aquarid southern radiant which is close by. Consequently no Southern Iota-Aquarid activity can be resolved. The Northern Iota-Aquarid radiant is more favourably placed in relation to the δ-Aquarid centre, and its activity curve is shown in Fig 5-30 (b). The peak on July 25 (day 206) is probably due to δ-Aquarid meteors, but those on August 3 and 8 (215 and 220) are possibly the result of Iota-Aquarid activity.

(9) Phoenicids (1986, 1987): December 4-5 (days 338-339)
(15°,-55°)
This recently discovered night-time stream was first observed in 1956 (Weiss, 1958). Stream members have low geocentric velocities and appear as slow fileballs. An association between the Phoenicids and Comet 1819 iv Blanpain has been suggested (McKinley, 1961).

Figs. 5-31 (a) and (b) show that no hint of shower activity was observed during either year.

(10) April Lyrids (1987): April 19-24,
max: April 22 (day 112) (272°,+32°)
This highly inclined stream may be associated with Comet 1861i (McKinley, 1961). A sharp peak, 2½ times the strength of the background, was observed on April 23, as shown by Fig. 5-32. This confirms the presence of the stream.

(11) June Lyrids (1987): June 10-21,
max: June 16 (day 167) (278°,+35°)
Shower activity was detected 4 days later than the expected maximum, as shown by the strong peak on June 20 (day 171), Fig. 5-33.

(12) Leonids (1986, 1987): November 15-19,
max: November 17 (day 321) (152°,+22°)
Visual observations of this stream date back to 902 AD. Periodic enhancements in the activity every 33 years were a feature of the Leonids until 1866. These were often memorable firework displays. Since that year, however, such extreme activity maxima have not been in evidence. It is thought that the stream was strongly perturbed by Jupiter in the nineteenth century, notwithstanding the expected stability of its highly inclined retrograde orbit. Mass segregation in the stream has been reported, with the large particle flux peaking somewhat earlier that the small particles (McIntosh & Millman, 1970).

No activity was detected during either 1986 or 1987 (Fig. 5-34 (a) and (b)).

(13) Velaids (1986, 1987): December 5-January 7,
max: December 29 (day 363) (150°,-51°)
This shower was observed during both returns. In Fig. 5-35 (a) and (b) peaks occur on January 1 1987 (day '366' 1986) and December 29 1987 (day 363), respectively.

(14) Zeta-Perseids (1987): June 1-16,
max: June 8 (day 159) (59°,+22°)
Fig. 5-36 suggests weak activity during 1987. The overall maximum on June 17 (day 168) is possibly due to members of this stream.

(15) Arietids (1987): May 30-June 18,
max: June 8 (day 159) (44°,+23°)
Shower activity was detected, peaking on June 10 (day 161), as shown in Fig. 5-37. The dates corresponding to the half-maximum points were roughly June 4 and June 18.

(16) Pisces Australids (1987): July 15-August 20,
max: July 31 (day 212) (340°,-30°)
The shower radiant is situated too close to that of the δ-Aquarids for any Pisces Australid activity to be resolved. The rate curve is shown in Fig. 5-40.

(17) Sigma-Puppids (1987): max: April 23 (day 113),
(Lindblad, 1987).
It has long been suspected that a meteor stream is associated with Comet Grigg-Skjellerup. Porter predicted that shower meteors would radiate from Puppis (109°,-35°) on April 26, but members of this stream were not observed until recently. The comet's orbit has its aphelion near the orbit of Jupiter, and in 1964 this planet perturbed the comet's orbit so that it now passes very close to that of the earth. Under these circumstances, chances of observing the σ-Puppid stream are much stronger than before. Lindblad (1987) mentions that Sitarski predicted meteoric displays in 1972 and 1977 from his study of the orbital evolution of the comet. The anticipated shower would radiate from (109°,-45°) on April 23. Visual observers did observe a σ-Puppid shower in both 1972 (from 109°,-49°) and 1977, on April 23 (op.cit.). The shower appears to be characteristically short-lived and of variable strength from year to year. Its detectability is reduced by the low geocentric velocity of the σ-Puppid meteors.

Fig. 5-41 shows the rate curve which is the result of our search for the stream. No activity could be detected in 1987.

(18) Epsilon-Geminids (1987): October 14-27,
(Olsson-Steel, 1987).
The orbit of a recently discovered comet (1987c) makes its closest approach to the earth's orbit (within 0.048 AU) on October 7. This is close to the period of observed Epsilon-Geminid activity which has been given above. A comparison of the orbital parameters of both the stream and the comet strongly suggests an association between the two (op.cit.). Meteors which have arisen directly from the comet are expected to radiate from (93°,+28°), while the observed radiant for the Epsilon-Geminid stream is located at (101°,+27°) (op.cit.). In 1987 the comet preceded the earth to the point on its orbit where the two orbits make their closest approach, by about 235 days. Since debris ejected by a comet tend to lag behind the parent body (due to solar radiation pressure), Olsson-Steel (1987) predicted the possibility of a meteor storm near October 7, 1987.

The rate curve Fig. 5-42 indicates that there was no significant shower activity over this period.

5-5 Summary

The survey of the sporadic background revealed a general decrease in activity between 1986 and 1987. Rate curves of corresponding months showed greater similarity than those of adjacent months. Sporadic rates generally peaked near dawn (the 'dawn plateau') and reached a diurnal minimum near dusk, as expected. A seasonal variation in the magnitudes of the diurnal maxima was noticed. Highest rates were observed during late summer and autumn and the lowest rates during spring. During the daylight hours most of the echoes were received from the east, but the east rate had generally dropped before dusk, after which the west rate rose sharply. We attribute this phenomenon to the transit of a diffuse apex radiant. The west rate, which peaked during the dark hours, generally attained a higher diurnal maximum than the east rate. This may be due to increased D-region absorption during the daylight hours.

All four of the major showers were easily detectable. Of the minor streams, six were observed with certainty: the β-Taurids (1987), Southern Taurids (1986 & 1987), April Lyrids (1987), June Lyrids (1987), Velaids (1986 & 1987), and the Arietids (1987). A further four minor showers showed possible signs of activity, namely the Omicron-Cetids (1987), Northern Taurids (1986 & 1987), Northern Iota-Aquarids (1987), and the Zeta-Perseids (1987), and the remaining ten were not detectable at all. Clearly the Grahamstown radar is not able to resolve shower activity that does not contrast well against the sporadic background.

Chapter 6: Determination of Radiant Structure

6-1 Introduction

In the past meteor radiant data have been obtained from visual and photographic techniques. These generally involve the extrapolation of the apparent trajectories of meteors back to their points of mutual intersection. In the late 1940's Hoffmeister produced plots of radiant activity from the density of such points on the celestial sphere (Jones, 1977). A drawback of his method is that the crossing points of shower and sporadic meteor trains have no physical significance. These points cannot be distinguished from those which are relevant, and their presence degrades the image of the radiant. The method is unsuitable for large data sets because the number of intersection points, and hence the amount of computation, increases approximately as the square of the number of trains.

An alternative has been to plot the trains of individual meteors onto a gnomic projection map, where they appear as straight lines. When the lines are extended, those due to stream members have a common intersection at the shower radiant. Although this method has been used to determine stream radiants when the ratio of shower to sporadic meteors is greater than unity, the radiant of a weak shower in the presence of a strong sporadic background is difficult to locate (Jones & Morton, 1977). No information concerning shower radiant structure can be obtained in this way.

Radar methods for radiant determination generally rely on the specular reflection condition. With these methods a greater abundance of data is available than with the above techniques, although the meteor radiants deduced are usually less precise. The traditional approach has been to determine radio-meteor radiants from simultaneous observations at two or more stations. However the relative simplicity of a monostatic radar has prompted meteor astronomers to research methods for determining radiant distributions from single-station data.

To this end Clegg (1948) has described a method of establishing the positions of shower radiants which relies on the diurnal motion of the echo line through the antenna beam. Due to this motion the range of reflection points of shower echoes varies as a function of time, and from range-time plots the radiant coordinates can be deduced. The sensitivity of the method is improved by decreasing the azimuthal beam width. The overall resolution is usually some 3° (Morton & Jones, 1982), although it is considerably worse for radiants which transit far from the zenith. The method is of limited use when several centres are active, and is unsuitable for providing data on fine radiant structure.

Another technique for recovering stream radiants from single-station data has been devised by Jones & Morton (1977). The echo directions are transformed into equatorial coordinates and projected onto a plane tangential to the celestial sphere. Sporadic echoes are distributed randomly on the plane, whereas those due to meteors which emanate from a point radiant form a straight line. Any linear clustering of points therefore indicates the presence of a shower. Strong showers show up well, but again shower radiant structure cannot be deduced.

Although the radar techniques discussed above do provide means of locating centres of high activity, they fall short of allowing us to observe structural features in the distribution of meteor radiants. Our only information concerning the meteor radiant distribution is our knowledge of the distribution of echo directions. The problem of 'unscrambling' the echo directions in order to recover the distribution of radiants from single-station data has been tackled by Jones (1977) and Morton & Jones (1982). Jones' (1977) scheme of deconvolving shperical harmonic transforms has produced maps of radiant activity similar to those of Hoffmeister, whose method we have described above. However, the excessive amount of computation required by Jones' method when applied to large data sets prompted Morton & Jones (1982) to propose a different scheme. According to their method, the strength of an arbitrary radiant is determined from the number of reflecting points orthogonal to it to within 1°. Their meteor radiant maps reveal considerable fine structure in the sporadic meteor complex, and show up features only 1° wide. However, the images of stream radiants obtained in this way suffer from severe 'astigmatism', i.e. elongation along the great circle at right angles to the beam axis.

In this chapter we describe an attempt to upgrade the method of Morton & Jones (1982). By introducing a procedure of weighting each meteor echo in accordance with the beam sensitivity in the direction of the echo, we hoped to reduce the astigmatism effect. The cause of the astigmatism and our attempt to eliminate it are discussed in the following section.

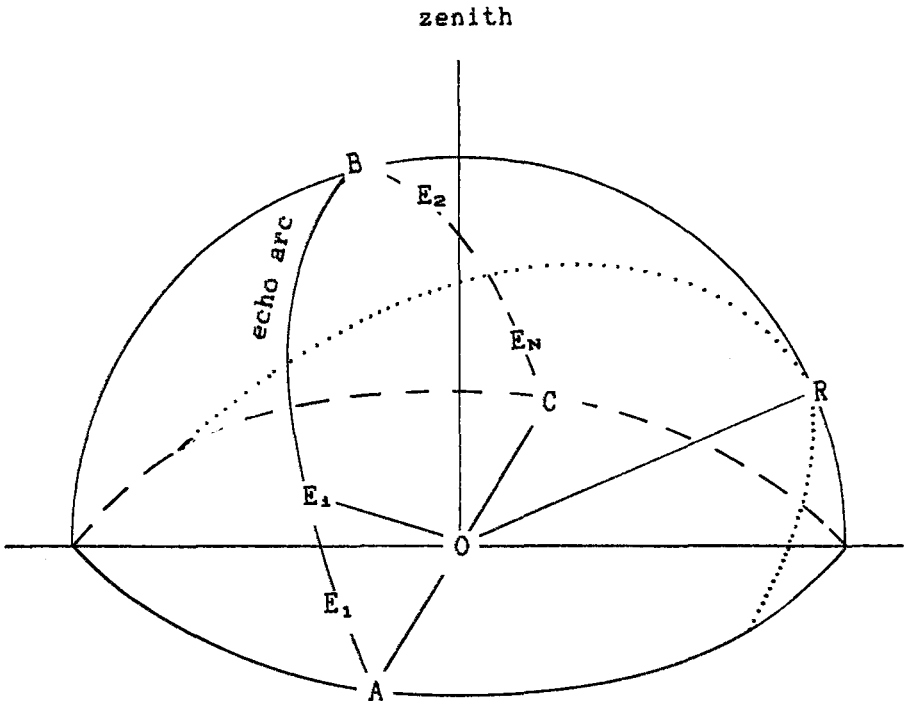

Fig 6-1: The geometry of meteor reflection. N shower meteors emanate from a radiant at R. The observer is at O. E_1, E_2, ...E_N indicate possible echo directions, and ABC is the 'echo arc'. The dotted arc, which lies in a plane orthogonal to the vector OE_i, is the locus of possible radiants for the i th meteor.

6-2 Theory

We have already dealt with the geometry of meteor reflection in Chapter 3. Fig. 6-1 illustrates the situation for the purposes of the present explanation. Let N shower meteors capable of producing the minimum detectable line density (α_{po}, see section 3-4) if incident vertically, and travelling in parallel paths, appear to emanate from a radiant at R. The arc ABC of a great circle lies orthogonal to the radiant vector OR and defines the locus of possible echo directions, indicated by E_1, E_2, ...E_N. We shall refer to ABC as the 'echo arc'. According to our scheme the actual strength of the radiant at R is N, since N reflection points lie on the associated echo arc. However, in practice the number of echoes detected will always be less than N, and at best we can arrive at only an estimator of N.

Conversely, the echo direction E_i corresponds to the arc of a great circle perpendicular to the vector OE_i, which is the locus of possible radiants for the i th meteor. According to our method, the echo registration at E_i is ascribed to radiant points all along this arc.

For a radar facility with an all-sky coverage the reflection points of shower echoes received throughout the day will be distributed uniformly around 180° of the echo arc. It should be clear from the above that any concentration of the echo directions at a point on the echo line will cause the possible radiants on the great circle orthogonal to the point to be highly weighted. This situation prevails when echo data are collected with a narrow-beam radar. Spurious, elongated regions of high activity then appear on the radiant contour maps, at right angles to the beam axis. This is the origin of the asigmatism which distorts the maps of Morton & Jones (1982).

The most suitable monostatic radar for the present purpose is one with a broad sky coverage, so that any radiant remains detectable for most of the time that it is above the horizon. This criterion is well-satisfied by the Grahamstown radar (see Chapter 4) although the beam is not isotropic. A direct consequence of the anisotropy is that the detection probability p (see Chapter 4) varies along the echo arc, so that the density of reflection points on the arc is inhomogeneous. The calculated distribution of radiants is liable to suffer from a degree of astigmatism, but this can be reduced by smoothing the uneven distribution of observed echo directions. A more homogeneous distribution can be obtained by weighting the reflection points in order to compensate for the non-uniformity of p along the echo arc.

Bearing Fig. 6-1 in mind, we proceed by dividing the echo arc into k segments. At any point on the arc, the values of ρ_w and p can be calculated from equations (4.2) and (4.13), respectively. Let Y_i

be the number of echoes received from the i th segment, at the centre of which the detection probability is p_i ($0 \leq p_i \leq 1$). The total number of shower echo-registrations is

$$\sum_{i=1}^{k} Y_i \ .$$

On average, a single registration means an incidence of $1/p_i$ meteors in the i th segment. A naive estimator of N, the total number of meteors emanating from R, is therefore

$$N_1 = \sum_{i=1}^{k} Y_i / p_i \ .$$

N_1 is the provisional strength of the radiant R. This estimator was implemented in a preliminary version of the radiant mapping program (discussed in the following section), but the contour maps exhibited spurious sharp ridges which were evidently caused by the fact that, in many cases, a large proportion of the value of N_1 came from a single registration in a segment with a very small value of p_i. It was therefore apparent that the naive estimator of N is deficient, and an alternative was sought, with the assistance of a specialist in statistics.

A detailed investigation into the statistics of the estimation has revealed that the problem is not trivial. It can be shown (Appendix 2) that the most efficient estimator of N is arrived at by (1) summing the p_i's over the echo arc at a particular time of day, and then (2) summing these quantities for the entire day. The second step is necessary to provide for the fact that the echo arc is in continuous motion across the beam, as a consequence of which the summation in step (1) will be different for each of t time-intervals. We have called the quantity

$$S_n = \sum_{i=1}^{k} p_{n\,i} \qquad \ldots(6.1)$$

the 'total detection probability over the echo arc' during the n th time-interval. The second step can be written

$$G = \sum_{n=1}^{t} S_n \qquad \ldots(6.2)$$

We have called G the 'grand total detection probability' for the radiant R in Fig. 6-1.

The best estimator of N is:

$$N_2 = \frac{\sum_{n=1}^{t} \sum_{i=1}^{k} Y_{n\,i}}{G} \qquad \ldots(6.3).$$

The numerator of (6.3) is the total number of echoes returned from the echo arc for radiant R over one day. Certain scaling constants have been ignored here, but for the purpose of comparing the activity of different radiants this is immaterial.

6-3 Method

The recovery of the meteor radiant distribution from the distribution of reflection points is performed as follows: We first select a region of the celestial sphere in which we define a regular grid of possible point radiants. The estimator of N for each point is then calculated from equation (6.3), although we count the number of echoes returned from an belt of finite width and centred on the echo arc, rather than from a discrete arc. This is because of an uncertainty of ~2° in the observed echo directions which causes the reflection points to stray from the echo arc. Long echoes which produce multiple registrations will be the cause of unwanted ridges on a contour map of the intensity of meteoric flux, at right angles to the echo direction. Any echo which occurs within ~2 seconds of the previous one is therefore ignored.

The present method was put into effect by writing the Fortran program, SKYMAP, which is listed in Appendix 1. The workings of the program are given in some detail below.

SKYMAP maps meteor radiant activity contours, normalized to a maximum value of 10, onto a projection of the celestial sphere. The main functions of the program have been assigned to five different 'modules':

MODULE A involves an interactive session with the operator. He chooses the position and the size of the region of the celestial sphere which is to be mapped, and whether to weight the echoes or leave them unweighted. Values for several other parameters whose purpose is explained below, are chosen. The operator specifies the days of the year for which meteor activity is to be monitored.

MODULE B reads echo data from O-files (see Chapter 4) into an array. Echo directions ecxeeding 70° in elevation are ignored, as are 'ambiguous' echoes (see Chapter 4). The echo direction of an enduring echo which has produced several consecutive registrations, is taken as that belonging to the first registration. For each selected echo, the data array finally contains: the local sidereal time (LST) of occurrence, the corresponding local standard time (SAST), altitude, and azimuth.

MODULE C calculates the 'grand total detection probability' G for each radiant in the chosen grid. It first generates a two-dimensional array of M possible meteor radiants. The coarseness of this grid is chosen by the operator. We label these possible radiants rad(1), rad(2), ...rad(M) for the purpose of the present explanation.

If the option of weighting the meteor echoes has been chosen, the

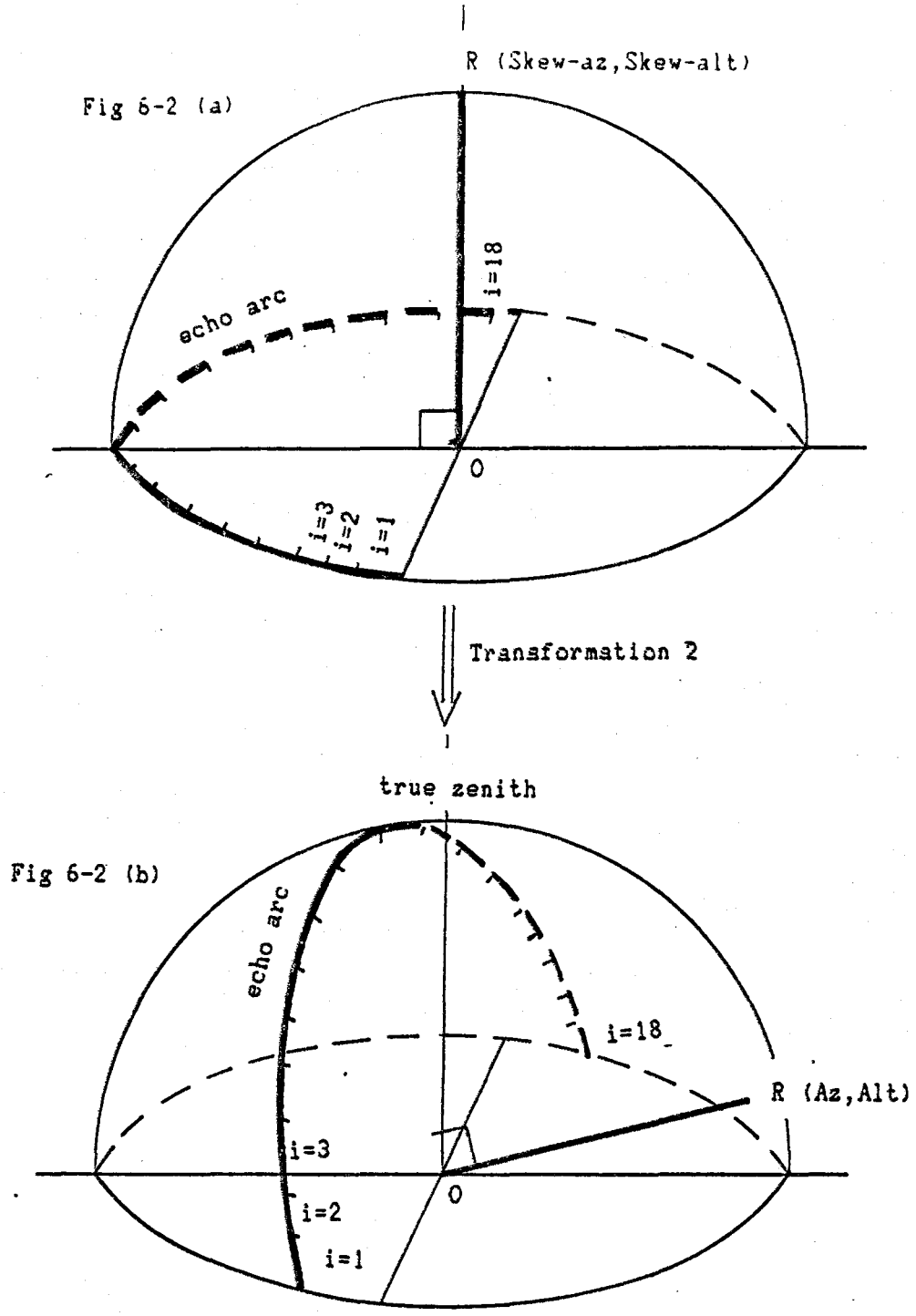

Fig 6-2: (a) When the radiant at R is regarded as the 'north pole' of a 'skew' coordinate system, the echo arc appears to an observer at O in the skew system as coincident with the 'equator'. The division of the echo arc into 18 equal segments is shown. Transformation 2 transforms each skew-coordinate pair (Skew-az, Skew-alt) for points on the echo arc to normal coordinates (Az, Alt) in a frame centred on O, with the true zenith vertically above the observer. The effect of the coordinate transformation is shown in (b).

program implements equation (6.1) and then (6.2) for each of the M possible radiants, otherwise G for each radiant is set equal to unity. We shall refer to the implementation of these two equations as steps (1) and (2), respectively. Their stepwise execution is involved:

Step (1): The day is divided into 24 one-hour time-windows, which we label tw(1), tw(2), ...tw(24). The LST at the centre of each time-window is calculated; it is utilised by the first of two coordinate transformations which follow.

Consider now the procedure for tw(1): 'Transformation (1)' transforms the coordinates of rad(1) from the equatorial (RA,Dec) to the horizontal system (Az,Alt). Transformation (1) is preliminary to establishing the relative disposition of the echo arc to the antenna beam, so that ρ_w may be evaluated at points along the arc. A second coordinate transformation must be applied before we know the (Az,Alt) of points along the echo arc. First, rad(1) is treated as the north pole of a 'skew' horizontal coordinate system. This situation is illustrated in Fig. 6-2 (a). For an observer O at the origin of the 'skew' system, rad(1) appears in the zenith and the echo arc as a half-circle coincident with the horizon and spanning the range of Skew-azimuths from 0 to 180°. All points on the arc have a Skew-altitude of zero. Second, the echo arc is divided into 18 equal segments. The central skew-coordinates of each 10° segment are known, and these are then transformed back to the 'normal' horizontal system by 'transformation (2)'. The effect of transformation (2) is illustrated in Fig. 6-2 (b). Equation (4.2) can now be used to calculate the value of ρ_w at the azimuth and altitude corresponding to each of the 18 points, and the detection probability p for each point is easily obtained from equation (4.13).

In our discussion of the detection probability (Chapter 4) we have not yet taken into account the fact that an arbitrary meteor is more likely to be detected if it is incident vertically than if it enters the atmosphere obliquely. This is referred to as the 'cos X effect' where X is the radiant-zenith angular distance. To allow for this each value of p should be multiplied by $(\cos X)^{s-1}$. Assuming that $s \sim 2$, a correction factor of cosX has been adopted here.

We shall call the final value of the detection probability at the centre of the i th segment of the echo line associated with rad(1), during tw(1), $p_{1\,1\,i}$. The general case is $p_{m\,n\,i}$, where the subscript m denotes the radiant ($1 \leq m \leq M$), n the time-window ($1 \leq n \leq 24$) and i the segment of the echo line ($1 \leq i \leq 18$). Now we are in a position to implement equation (6.1). The total detection probability over the echo line for rad(1), during tw(1) is expressed as

$$S_{1\ 1} = \sum_{i=1}^{18} p_{1\ 1\ i} \qquad \ldots(6.4).$$

The general expression for (6.4) is

$$S_{m\ n} = \sum_{i=1}^{18} p_{m\ n\ i} \qquad \ldots(6.5).$$

where the subscripts have retained their meanings. $S_{1\ 1}$ is the final result of step (1), for tw(1) and rad(1). The quantities $S_{2\ 1}$, $S_{3\ 1}$, ...$S_{M\ 1}$ are then calculated for the radiants rad(2), rad(3), ...rad(M), during tw(1).

In this manner a value of $S_{m\ n}$ is computed for each radiant, for each of the 24 time-windows. The final result of Step (1) is a M x 24 matrix:

$$\begin{matrix} S_{1\ 1} & S_{1\ 2} & S_{1\ 3} & \ldots S_{1\ 24} \\ S_{2\ 1} & S_{2\ 2} & S_{2\ 3} & \ldots S_{2\ 24} \\ \vdots & & & \\ S_{M\ 1} & S_{M\ 2} & S_{M\ 3} & \ldots S_{M\ 24} \end{matrix}$$

Step (2): The final step in the weighting of echoes involves calculating G for each of rad(1) ...rad(M). This is done by implementing equation (6.2) for each row of the above matrix:

$$G_m = \sum_{n=1}^{24} S_{m\ n} \qquad \ldots(6.6).$$

MODULE D performs a specularity check for each echo in the data array, by comparing the echo direction with the position of every radiant in the grid in succession.

The (RA,Dec) of rad(1) are transformed to the (Az,Alt) corresponding to the LST of the first echo in the data array, echo(1). If the angular distance between the two is within x degrees of a right angle, Y_1, the number of registrations associated with rad(1), is incremented by 1 (we refer to the final value of Y_1 as the **strength** or the **weighting** of rad(1)). The 'specularity parameter' x is chosen by the operator during module A. The (RA,Dec) of rad(2) are then transformed to (Az,Alt) at the LST of echo(1) and the test for orthogonality is carried out. If rad(2) and echo(1) are orthogonal to within x degrees, Y_2, the strength of rad(2), is incremented by 1. In this way echo(1) is tested for orthogonality against each of the M radiants, and the weightings Y_1, ...Y_M are incremented only when the specularity condition is satisfied.

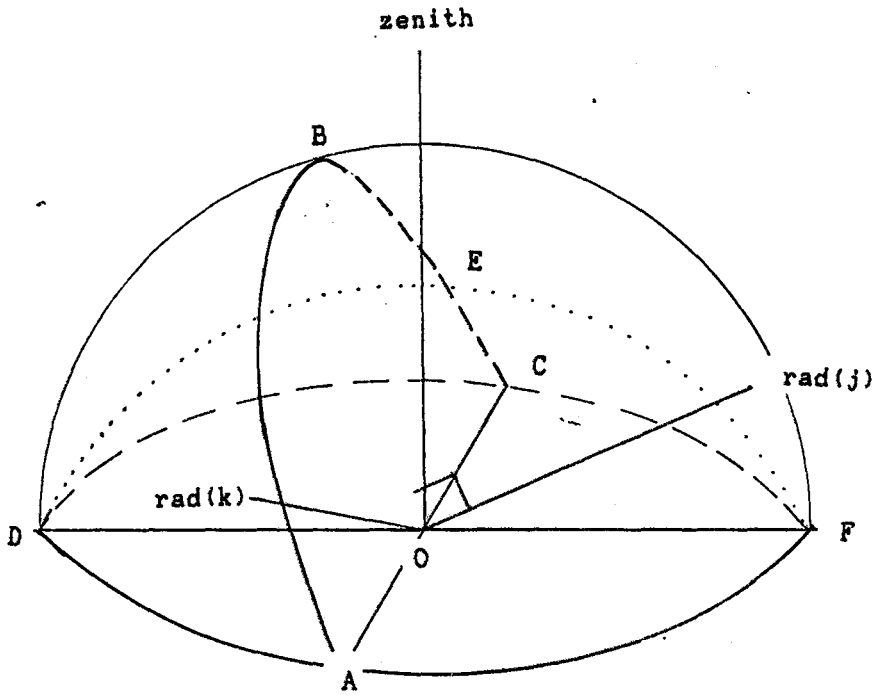

Fig 6-2 (c) ABC is the echo arc associated with rad(j), and the dotted arc DEF is that associated with rad(k). The echo at their intersection, E, could be due to a meteor from either radiant. Both Y_j and Y_k will be incremented as a result of the echo at E.

After every echo has been tested for specularity against every radiant, the final number of echo registrations associated with the j th radiant, Y_j, represents the number of echoes which it is **possible** to associate with rad(j). An echo which is orthogonal to rad(j) need not necessarily be due to a meteor which has emanated from rad(j), but could just as easily be due to rad(k) whose echo arc intersects that associated with rad(j) (see Fig. 6-2 (c)). Both Y_j and Y_k will be incremented as a result of the echo at E in this diagram. Clearly then, the present method does no more than exclude counting meteors which **cannot** have emanated from a particular radiant. This ambiguity represents unavoidable 'noise' that appears to be associated with any single-station reduction of radiant structure.

The final result of Module D is, for each radiant, the numerator of equation (6.3): namely, the total number of echo registrations which it is possible to associate with a radiant point on the grid, given the constraints on specularity. We shall omit the summation signs present in the numerator of (6.3) and call these quantities Y_1, Y_2, ...Y_M.

MODULE E: The estimator of N is calculated from (6.3), for each radiant of the grid. If the 'weighting' option has been selected, the values of G_m obtained from (6.6) are used. Otherwise, $G_m = 1$, m=1,M. The estimator of N for each radiant is

$$N_{2_m} = \frac{Y}{G_m} \quad , \; m= 1, \; M. \quad \ldots(6.7).$$

The values of N_{2_m} are fed into a contour plotting program. Contour maps of radiant activity are presented and discussed in the following section.

6-4 Results

In this section we present the results of our investigation into possible radiant structure associated with each of the 22 meteor showers discussed in Chapter 5. Generally, radiant activity was monitored for the day of the observed shower maximum, although for the cases where no distinct maximum was evident from our own rate curves, the dates cited by the Cambridge Encyclopedia of Astronomy (1977) were used. We have included only those maps which positively suggest the presence of shower radiant structure. All of the contour maps presented in subsections 6-4-1 and 6-4-2 were plotted without weighting the echoes to correct for the beam anisotropy. The effects of the echo-weighting procedure are presented and discussed in 6-4-3.

We shall refer to the region circumscribed by by the highest contour (which corresponds to 90% of the maximum activity on a particular map) as the 'shower radiant'. The positions of the various radiant centres are given in equatorial coordinates to the nearest 0.5°. The expected radiant coordinates for each of the 22 showers appear in Chapter 5. The reader should note that our contour maps have been plotted with the declination **decreasing** vertically upwards and the right ascension **increasing** to the right, whereas in conventional astronomical maps the reverse is true.

6-4-1 Major showers

Eta-Aquarids: May 7, 1987.
Fig. 6-3 shows that a near-circular radiant of diameter ~4° and centred at (338°,-2½°), was observed. Surrounding the radiant is an area of high activity, part of which extends as a short bar to the east of north. The sporadic background shows considerable structure. A corresponding map for 1986 could not be plotted because the echo directions were faulty.

Delta-Aquarids: July 27-28, 1986 and 1987.
Strong, slightly elliptical radiants were observed in both years, and are illustrated clearly by Figs. 6-4 and 6-5, respectively. Their respective centres are at (337½°,-18°) and (337½°,-18½°). Both centres are ~6° in length and ~4° across. The general area of strong shower activity was elongated along an axis parallel to the north-south meridian in 1986, but the axis of elongation was somewhat skew with respect to the meridian in 1987. The slight rotation of the axis in 1987 is attributable to missing data from the west lobe of the beam, which was lost for one of the days due to a power failure. The sense of the rotation is compatable with a preponderance of echoes from the the east beam, and is evidence that the observed elongation of the radiant

in both years is a case of genuine astigmatism.

The strength of the shower radiant is indicated by the absence of fine structure in the surrounding sporadic background, and by the strength of this radiant in relation to secondary activity maxima which may represent 'noise'. Indeed, the strength of the southern radiant (shown here) is such that any activity due to the Northern Delta-Aquarids is completely undetectable. The fact that absolute values of the flux cannot be assigned to the contours is a weakness of the present method. This point is raised again in subsection 6-4-4.

We hoped to witness the development of the shower radiant by mapping the region of sky in its vicinity on each of the 8 days prior to the 1987 maximum. The results of this are shown in Figs. 6-6 (a) to (h). No active centre could be discerned on July 19 (a), but by July 20 (b) recognisable structure was in evidence near to the expected radiant position. By July 21 (c) the radiant had evidently grown in strength and diameter, but the centre of activity then became more diffuse, and remained so over July 22 (d) and July 23 (e). A dual radiant was present on July 23. On July 24 (f) the shower radiant was once again strong and unmistakeable, consisting of a single active centre. Although this state of affairs prevailed over the final two days before the overall maximum, the activity contours were more ordered on July 25 (g) and somewhat disarranged on July 26 (h). The maps (f), (g) and (h) show a day-by-day drift of the radiant centre to the north-east, from (334°,-19°) to (337°,-17½°).

Orionids: October 21-22, 1986 and 1987.
The shower radiant was observed in both years, as shown in Figs. 6-7 and 6-8. The 1986 radiant was irregularly shaped, had the dimensions ~8° x ~4°, and was centred at (93½°,16°). In the following year it was a rough ellipse with semi- major and minor axes of ~ 4° and ~3°, respectively, and centred at (94½°,16°). In both years the main active region was elongated at an angle of ~45° to the north-south meridian. The Orionid maps show considerable fine structure in the sporadic meteor complex, in contrast to those of the stronger Delta-Aquarids.

Geminids: December 14, 1986 and 1987.
Figs. 6-9 and 6-10 show up the strong Geminid radiant for both years. The near-circular radiant (diameter ~4° in both cases) was centred at (113½°,30°) in 1986 and at (114°,30°) in 1987. Both maps show 'spokes' of intermediate activity (contour 3) radiating outwards. The observed strength of the radiant is remarkable in view of the fact that it transits at an elevation of only 27°.

Figs. 6-3 to 6-10: meteor radiant activity in the vicinity of the active centres of the four major showers. In each case the echoes are unweighted.

Figs. 5-24 to 5-42 show, for each minor shower, the normalised hourly echo rate associated with a SKY° square of sky centred on the shower radiant, as a function of day number. Each data point represents the average over two time-windows which span the period of the expected daily shower maximum. Each time-window has duration DT. The parameters DT and SKY are listed in Table 5-2.

Table 5-2: Program parameters: minor shower rate curves.
The parameters DT, T1, T2 and SKY have the same meaning as in Table 5-1.

	RATE VS DAY (SOLAR LONGITUDE)					Shower	Year
Program:	NEWPEAK2						
Graph of:	Normalised rate/hr in sky-window vs. day						
	Fig.	DT/hr	T1/hr	T2/hr	SKY/°		
	5-24	4	9.8	13.8	10	o-Cetids	87
	5-25	2	2.5	9.9	10	Cor.Australids	87
	5-26	4	23.7	5.7	5	α-Capricornids	87
	5-27	2.5	23.2	5.2	10	Capricornids	87
	5-28	4	10.8	14.8	10	ß-Taurids	87
	5-29	3	22.2	4.2	10	Ophiucids	87
	5-30(a)	2.5	2.2	8.2	5	Iota-Aqu.(S)	87
	5-30(b)	4	2.7	6.7	5	Iota-Aqu.(N)	87
	5-31(a)	3	18.1	2.1	5	Phoenicids	86
	5-31(b)	3	18.0	2.0	10	Phoenicids	87
	5-32	1	5.4	6.4	5	April Lyrids	87
	5-33	1	1.9	2.9	5	June Lyrids	87
	5-34(a)	2	7.0	9.0	10	Leonids	86
	5-34(b)	2	7.0	9.0	10	Leonids	87
	5-35(a)	4	0.2	8.2	5	Velaids	86
	5-35(b)	4	0.3	8.3	10	Velaids	87
	5-36	3	10.6	13.6	5	Zeta-Perseids	87
	5-37	3	9.6	12.6	5	Arietids	87
	5-38(a)	4	0.1	4.1	5	Taurids (N)	86
	5-38(b)	4	0.1	4.1	10	Taurids (N)	87
	5-39(a)	4	0.1	4.1	5	Taurids (S)	86
	5-39(b)	4	0.1	4.1	10	Taurids (S)	87
	5-40	3	0.7	6.7	5	Pisces Austr.	87
	5-41	2	14.9	21.9	10	Sigma Puppids	87
	5-42	2	6.7	8.7	10	Epsilon Gemin.	87

Fig 5-24: Omicron Cetids, 1987.

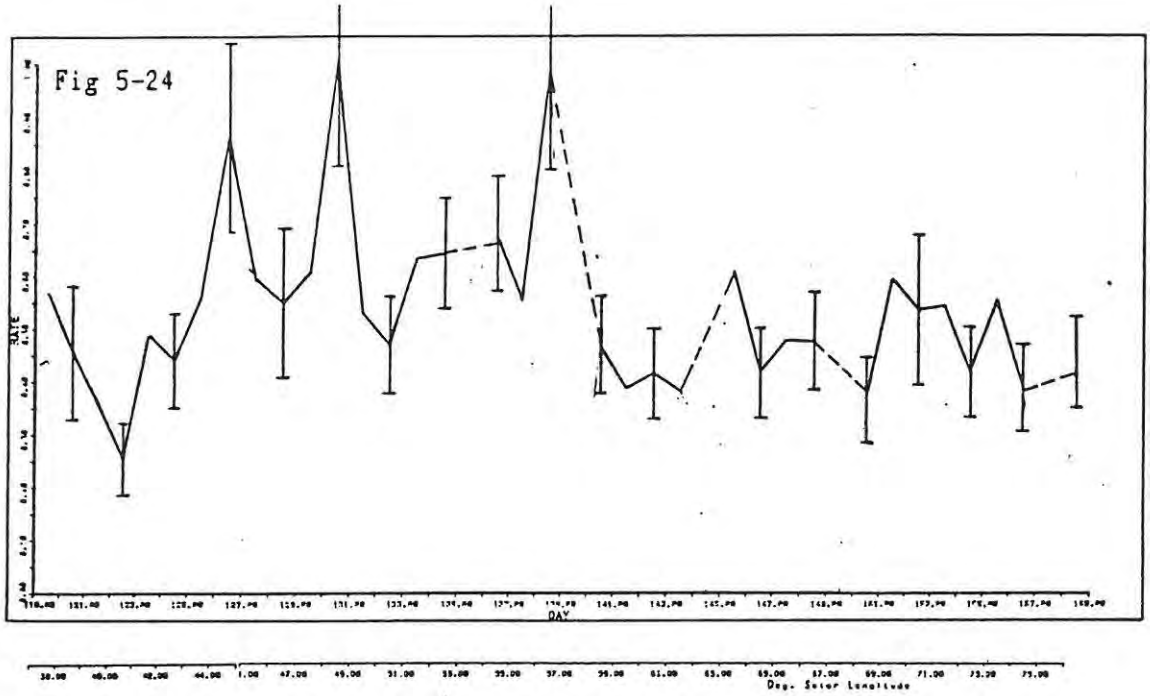

Fig 5-25: Corona Australids, 1987.

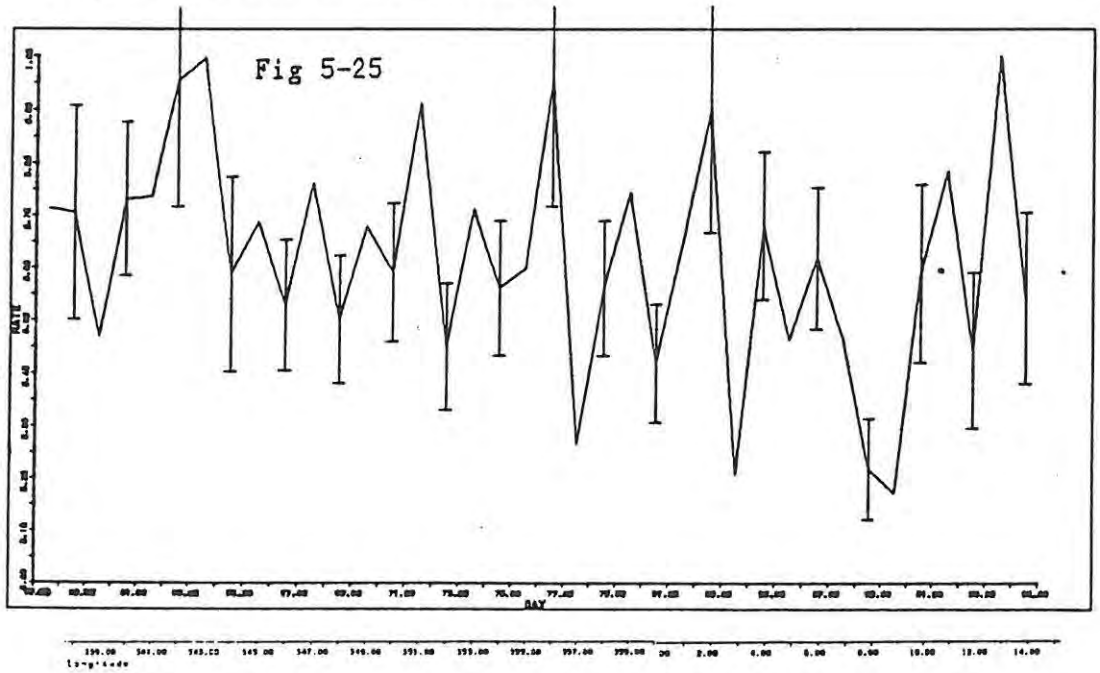

Fig 5-26: Alpha Capricornids, 1987.

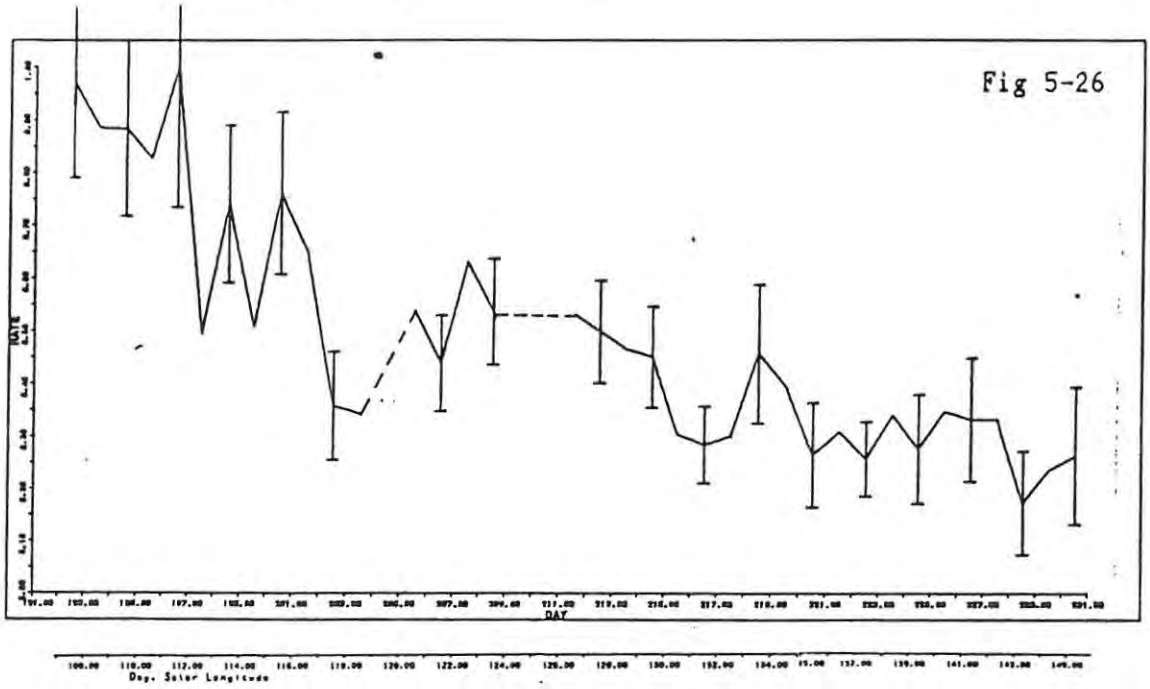

Fig 5-27: Capricornids, 1987.

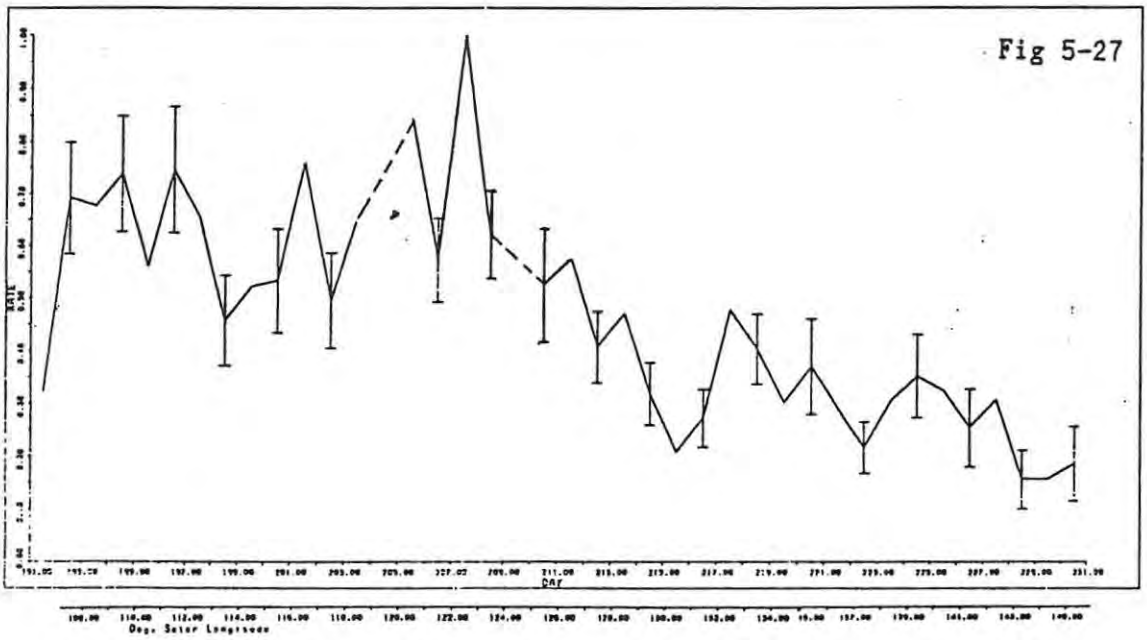

Fig 5-28: β-Taurids, 1987.

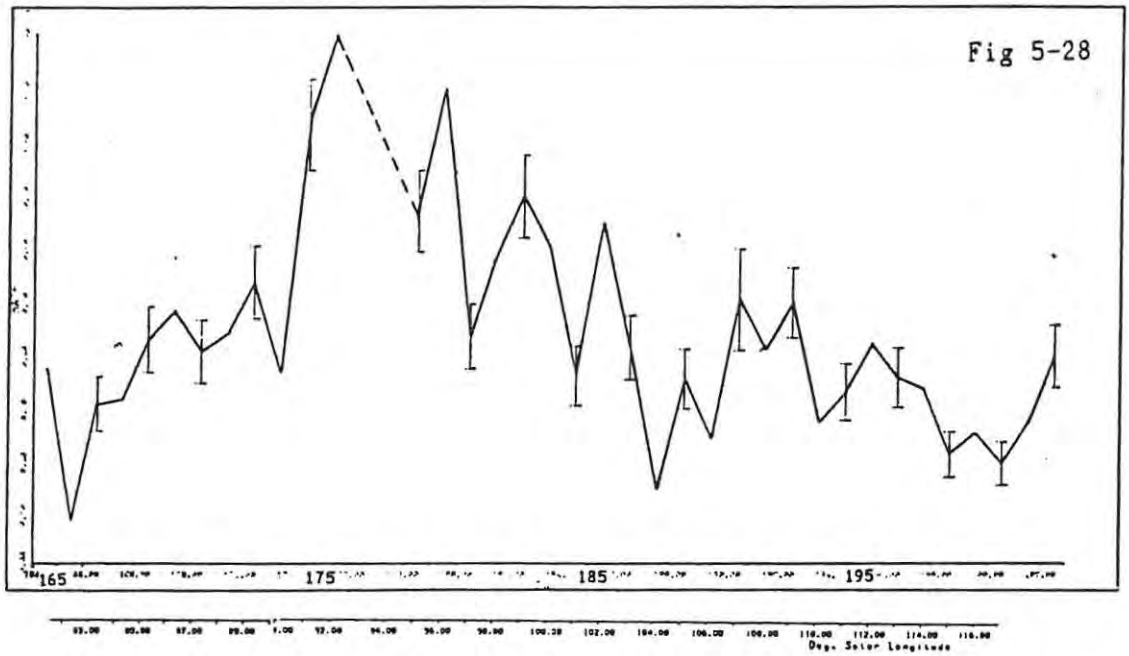

Fig 5-29: Ophiucids, 1987.

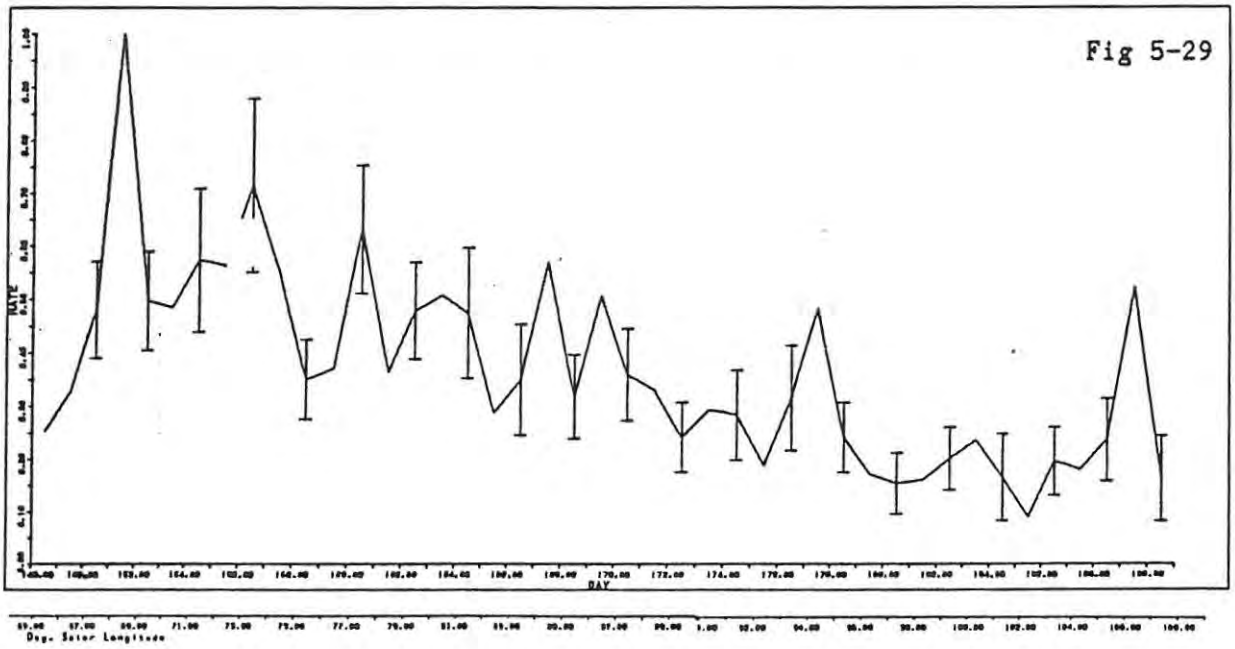

Fig 5-30: Iota Aquarids, 1987: southern radiant (a) and northern radiant (b).

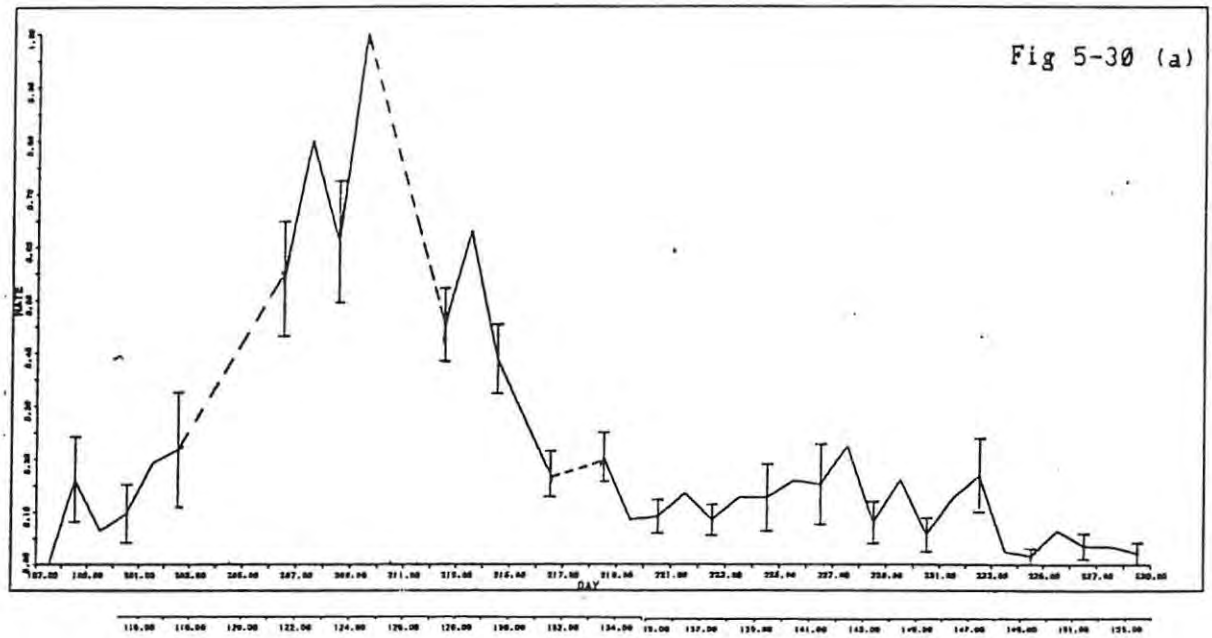

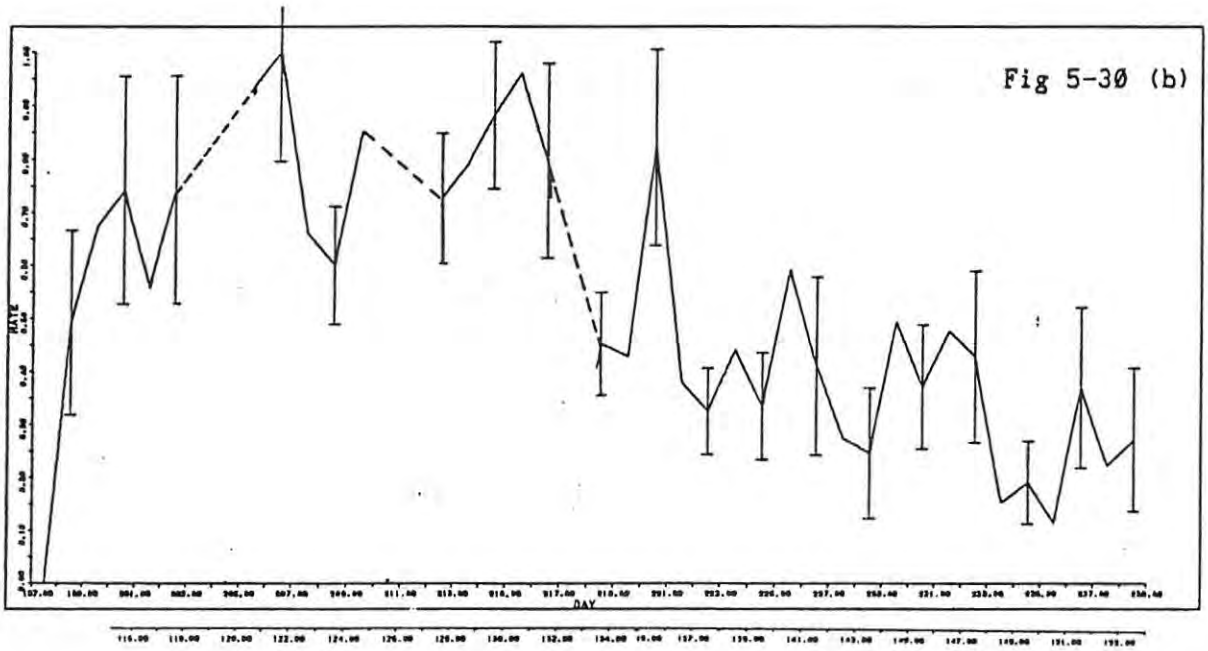

Fig 5-31: Phoenicids: (a) 1986 and (b) 1987.

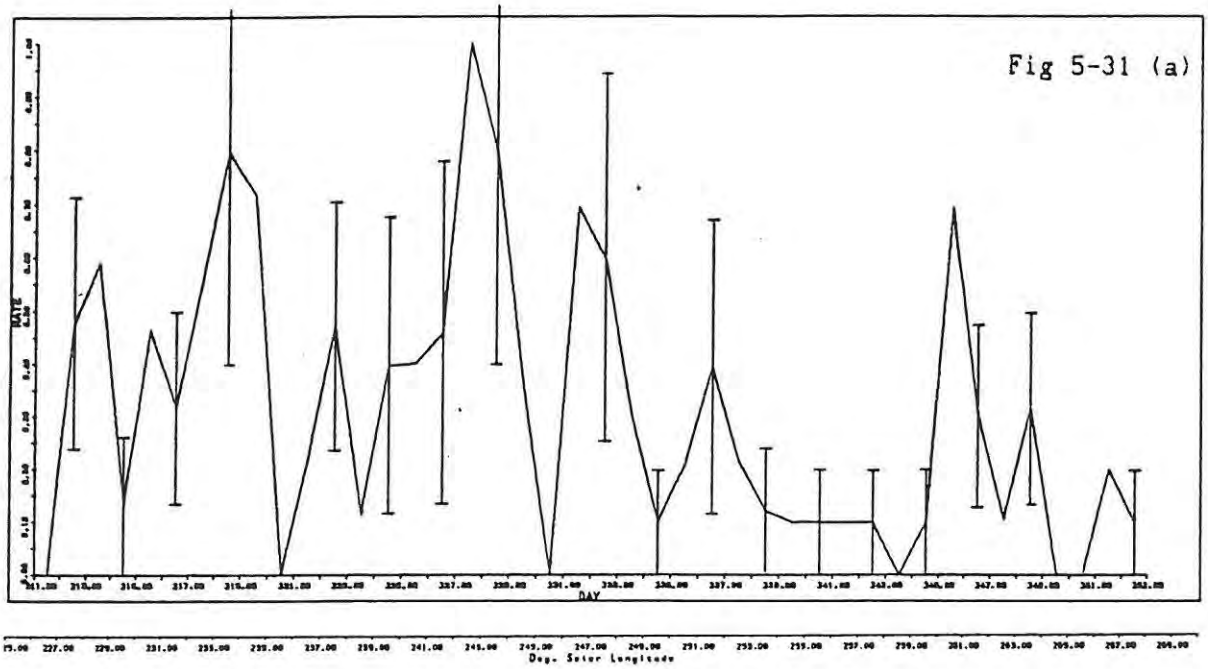

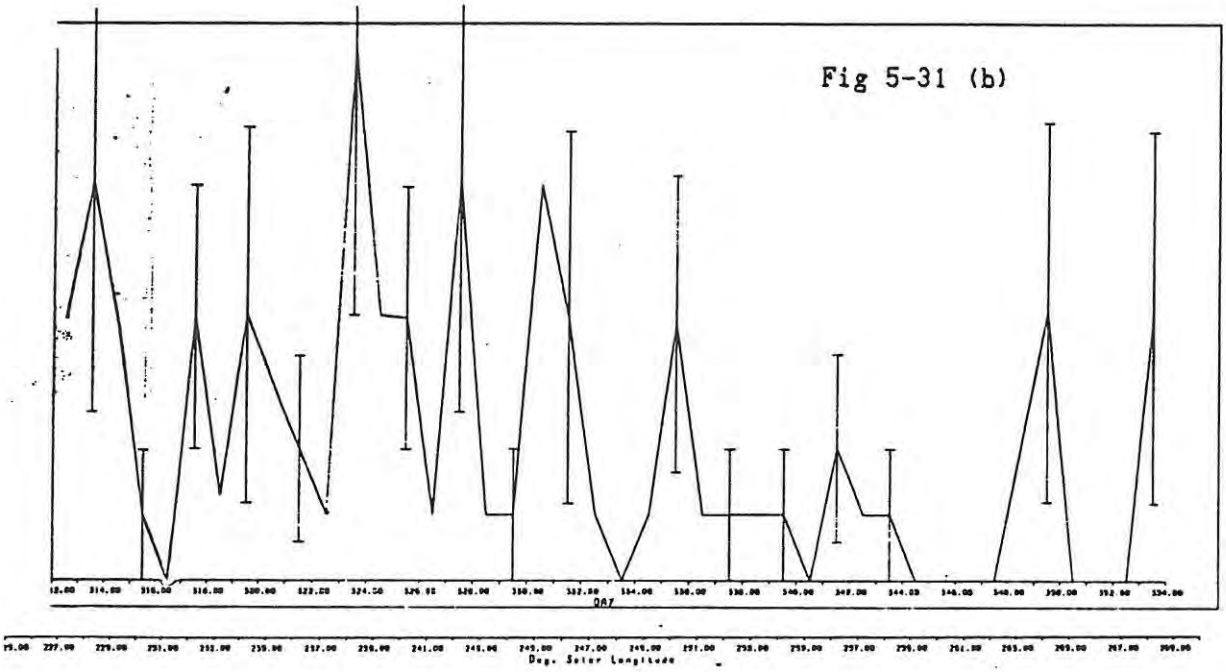

Fig 5-32: April Lyrids, 1987.

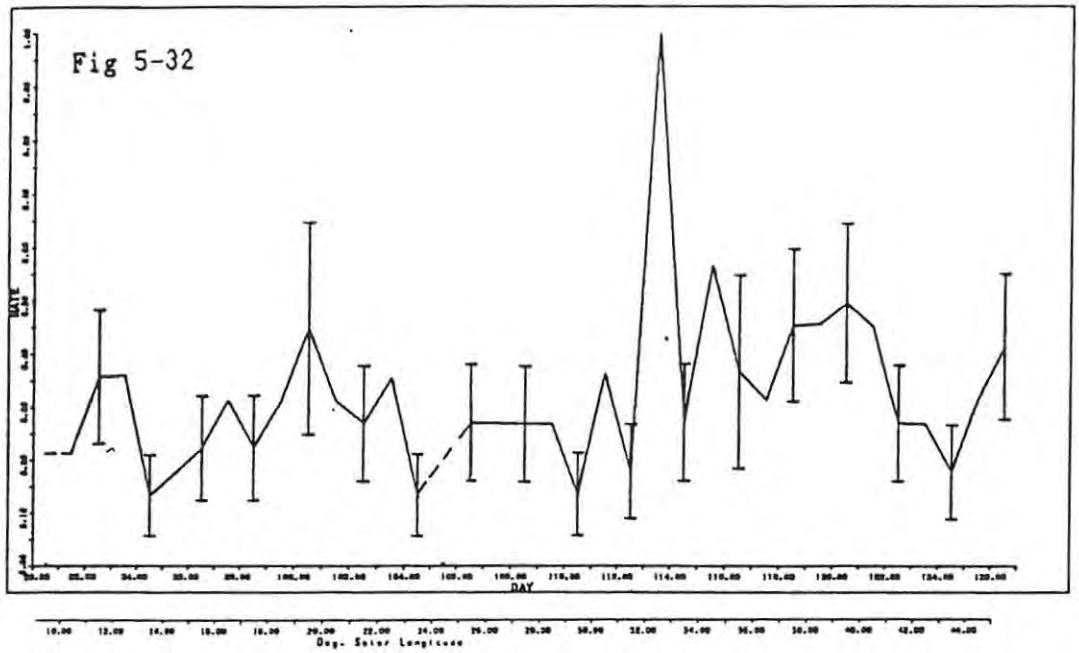

Fig 5-33: June Lyrids, 1987.

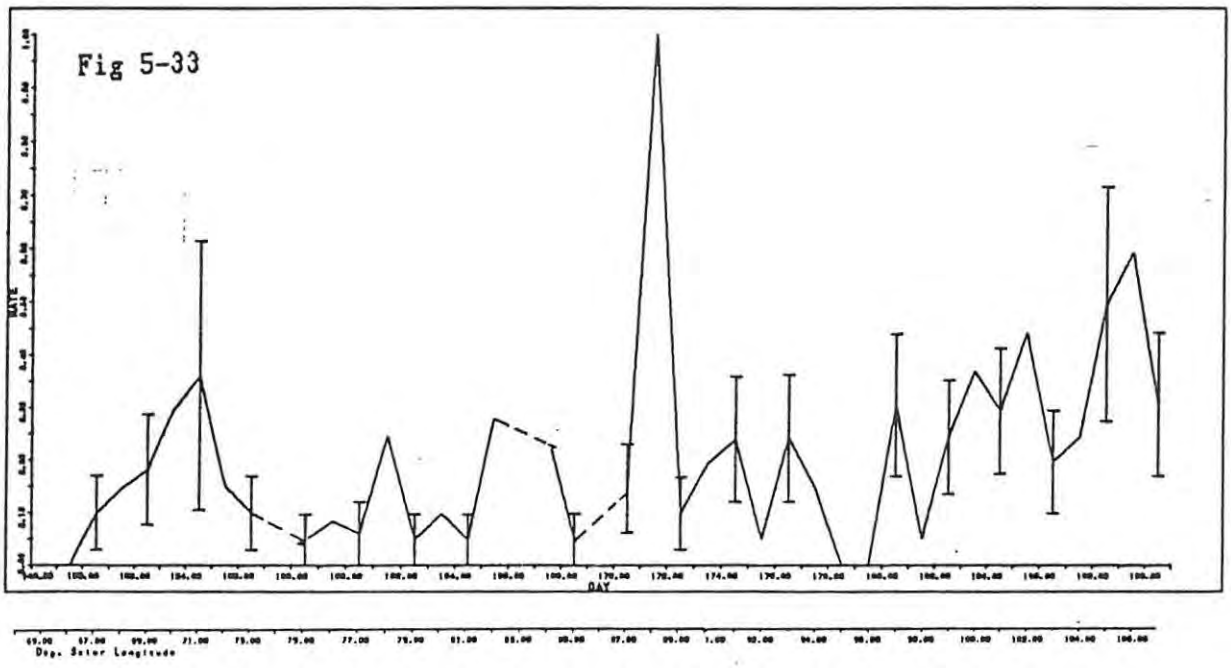

Fig 5-34: Leonids, (a) 1986 and (b) 1987.

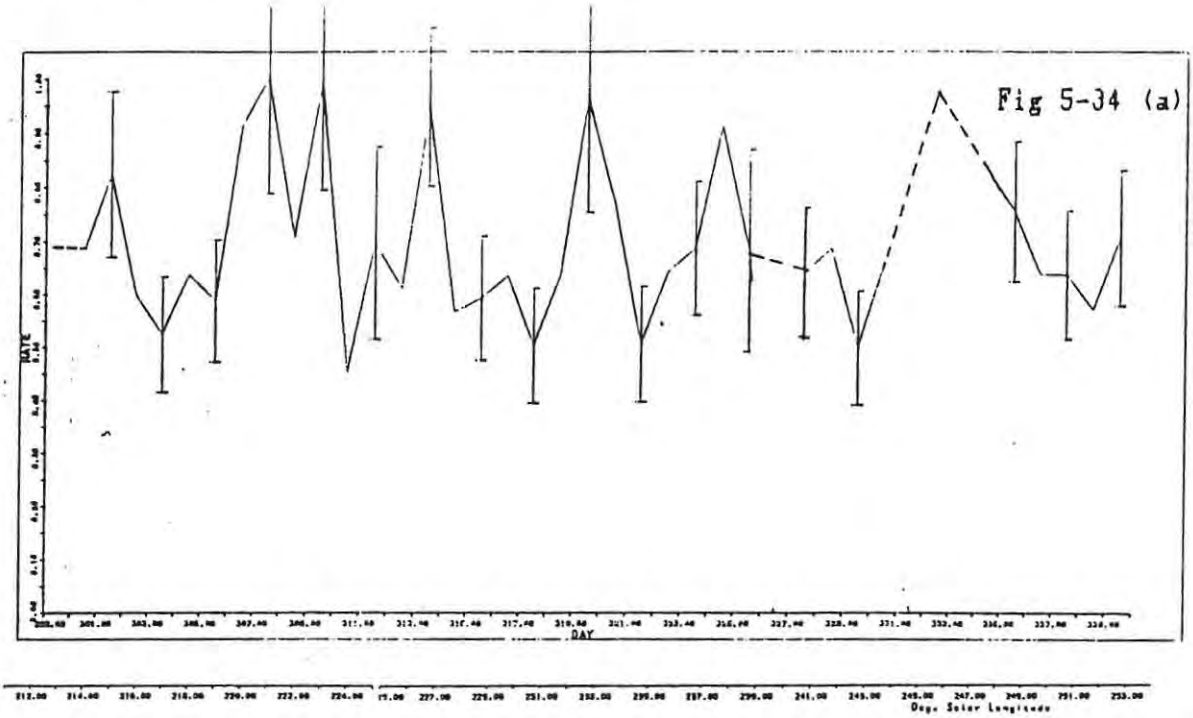

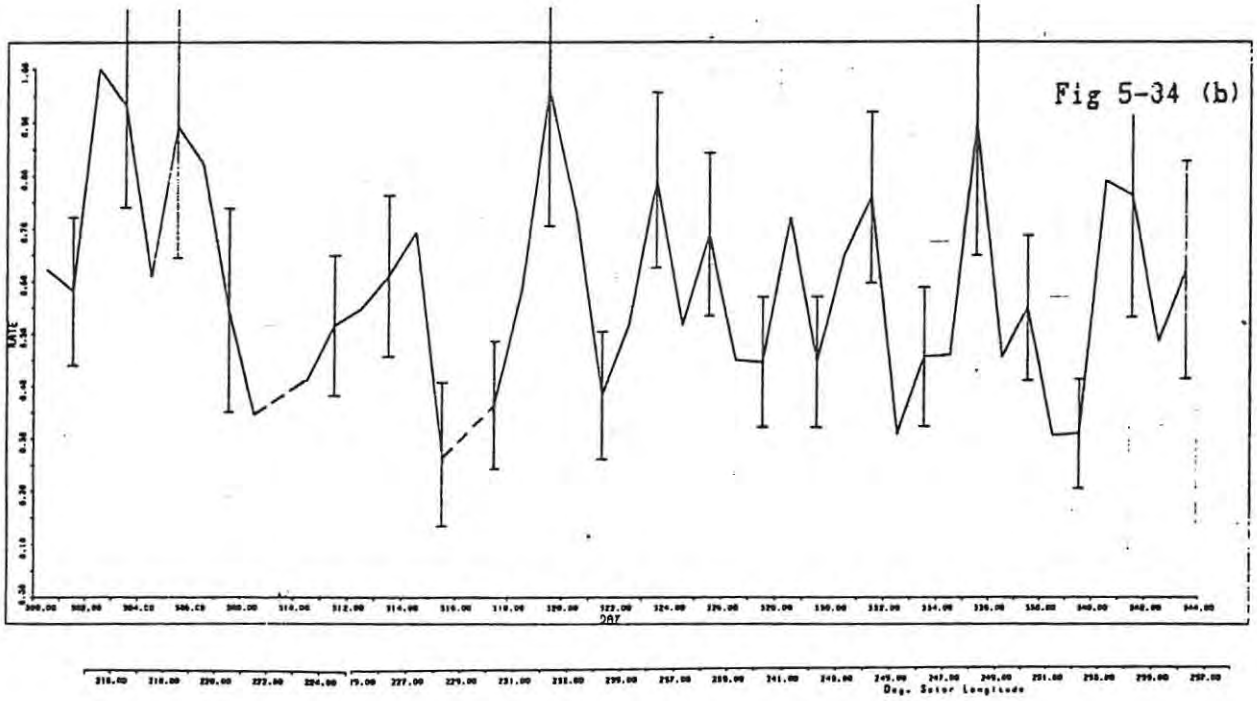

Fig 5-35: Velaids, (a) 1986-1987 and (b) 1987-1988.

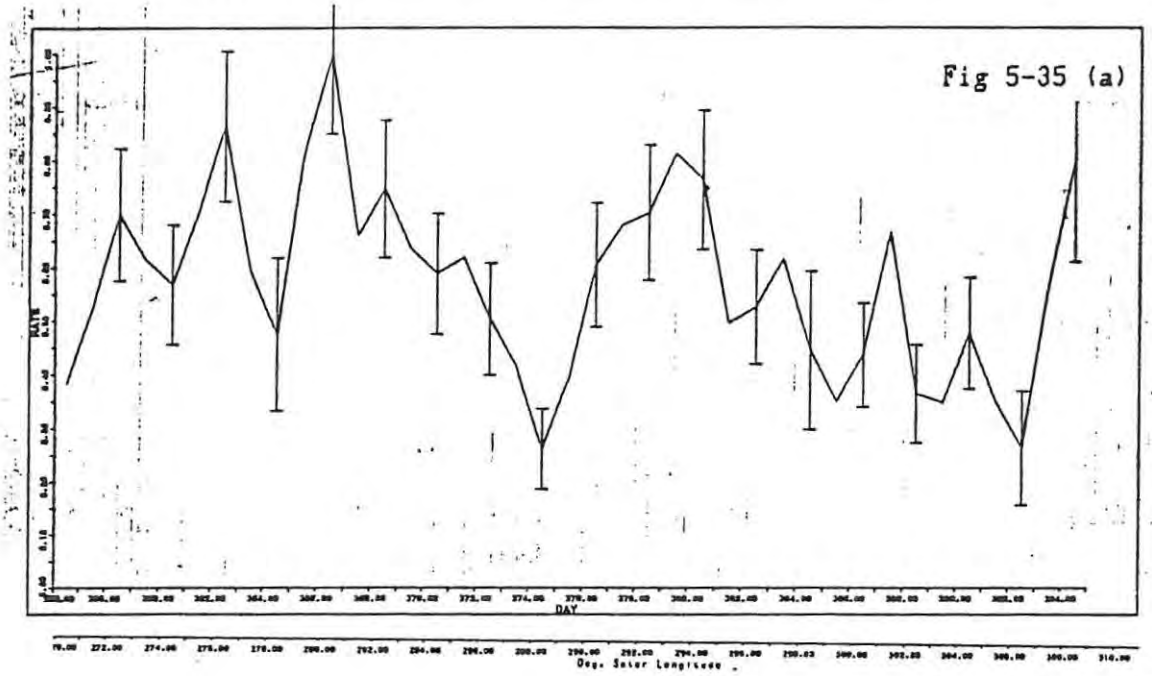

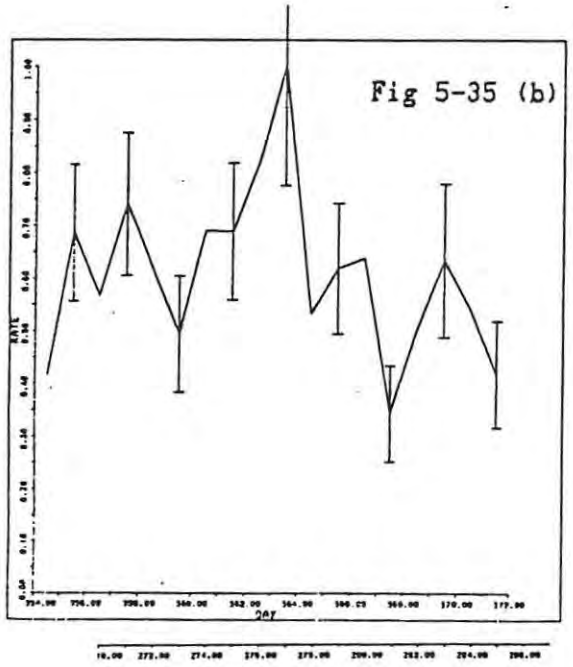

Fig 5-36: Zeta-Perseids, 1987.

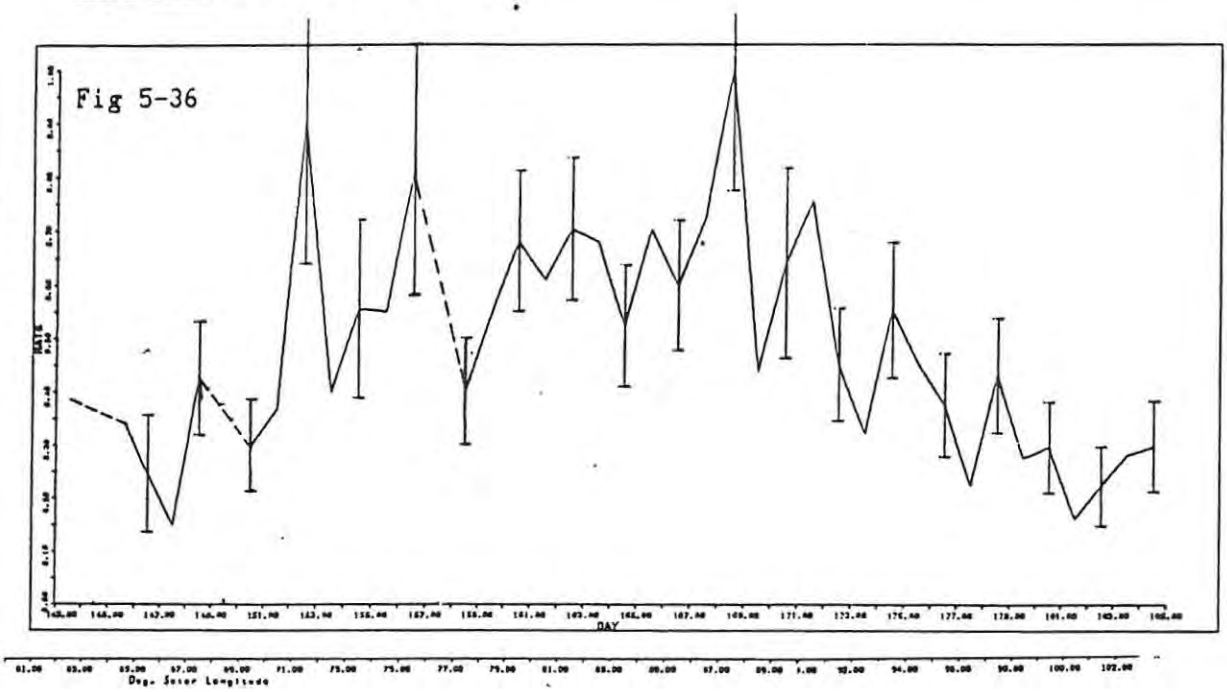

Fig 5-37: Arietids, 1987.

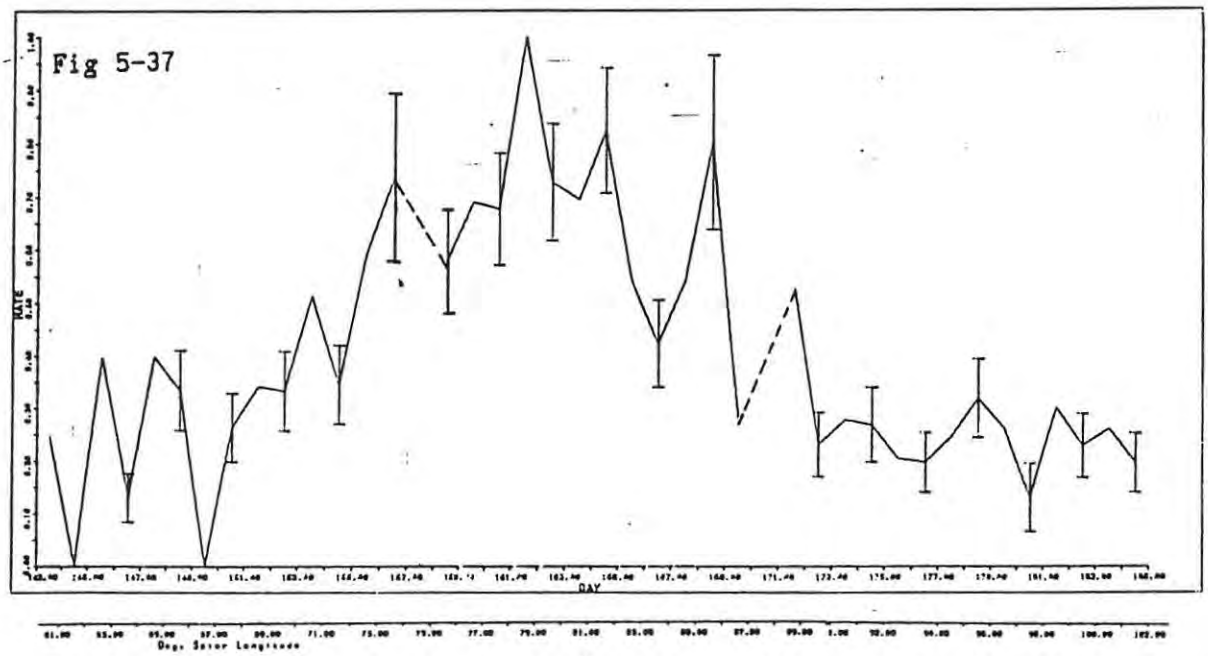

Fig 5-38: Northern Taurids, (a) 1986 and (b) 1987.

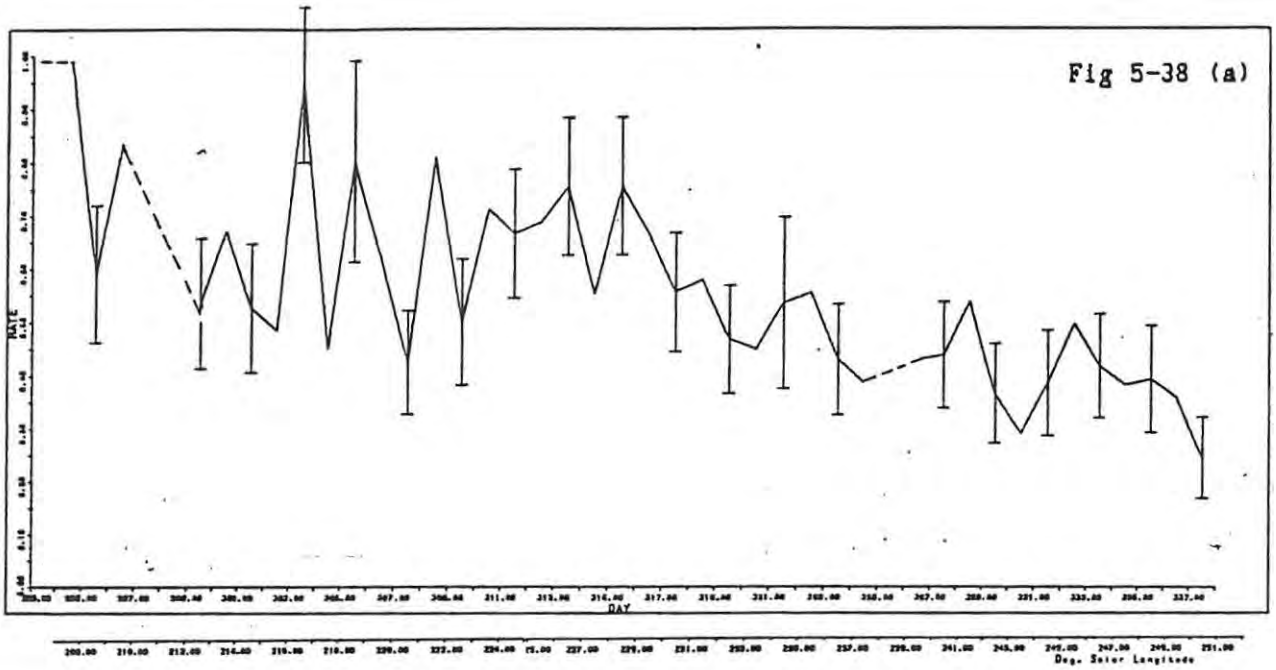

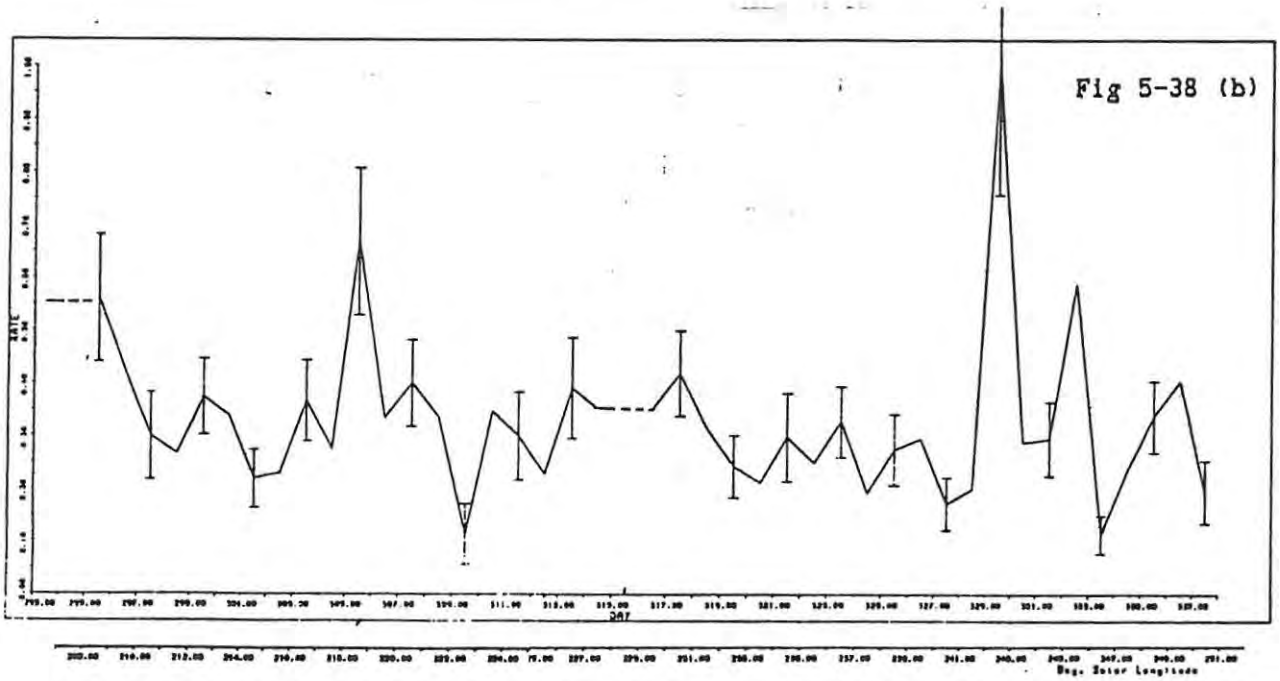

Fig 5-39: Southern Taurids, (a) 1986 and (b) 1987.

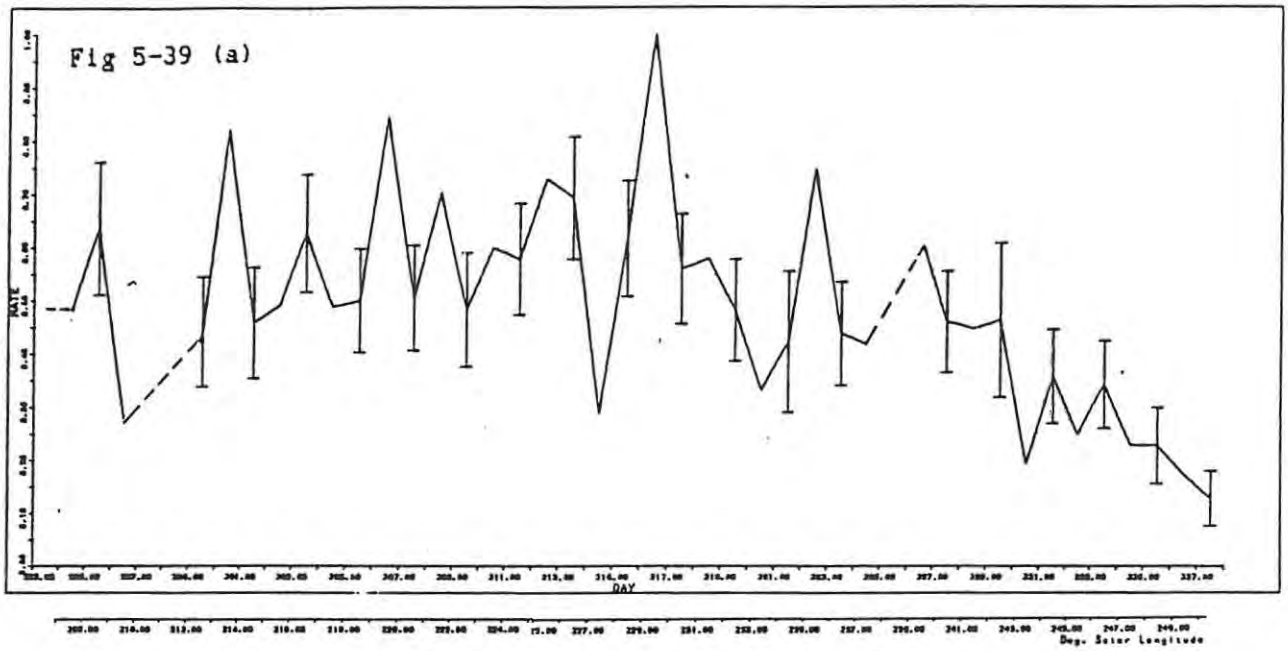

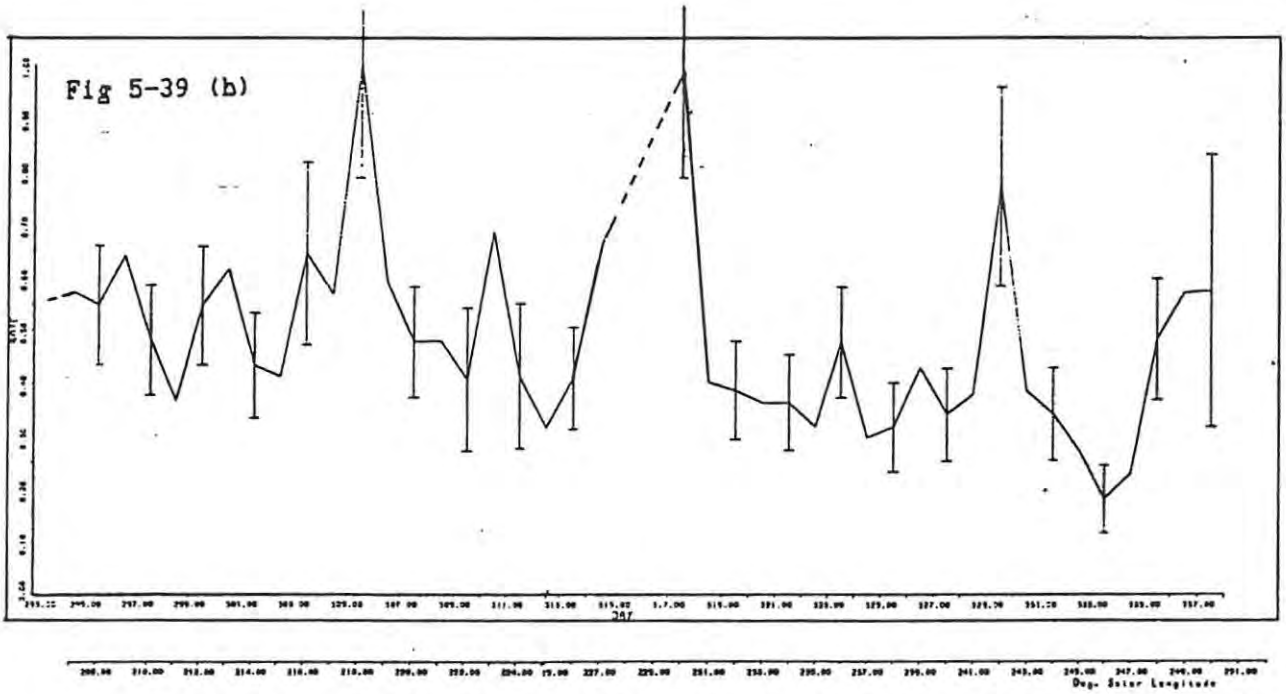

Fig 5-40: Pisces Australids, 1987.

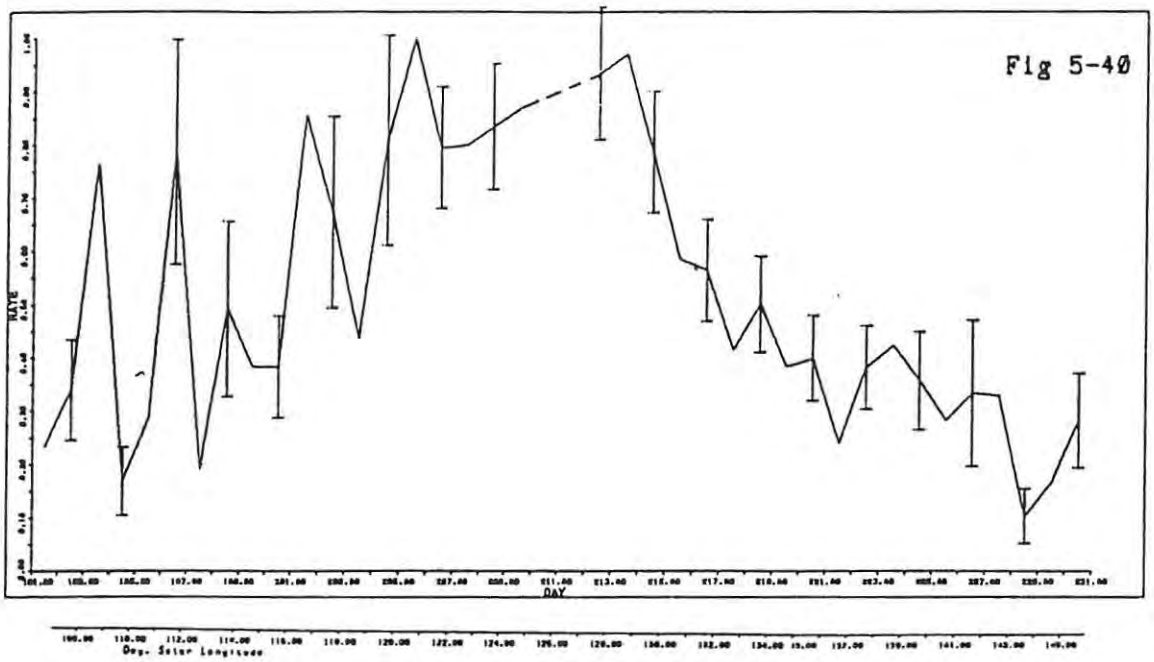

Fig 5-41: Sigma Puppids, 1987.

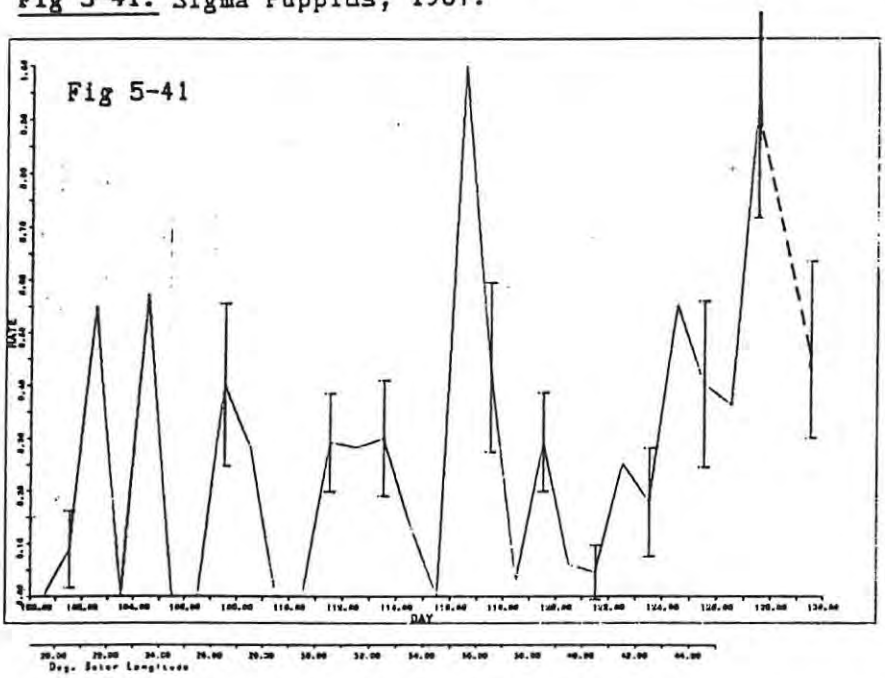

Fig 5-42: Epsilon Geminids, 1987.

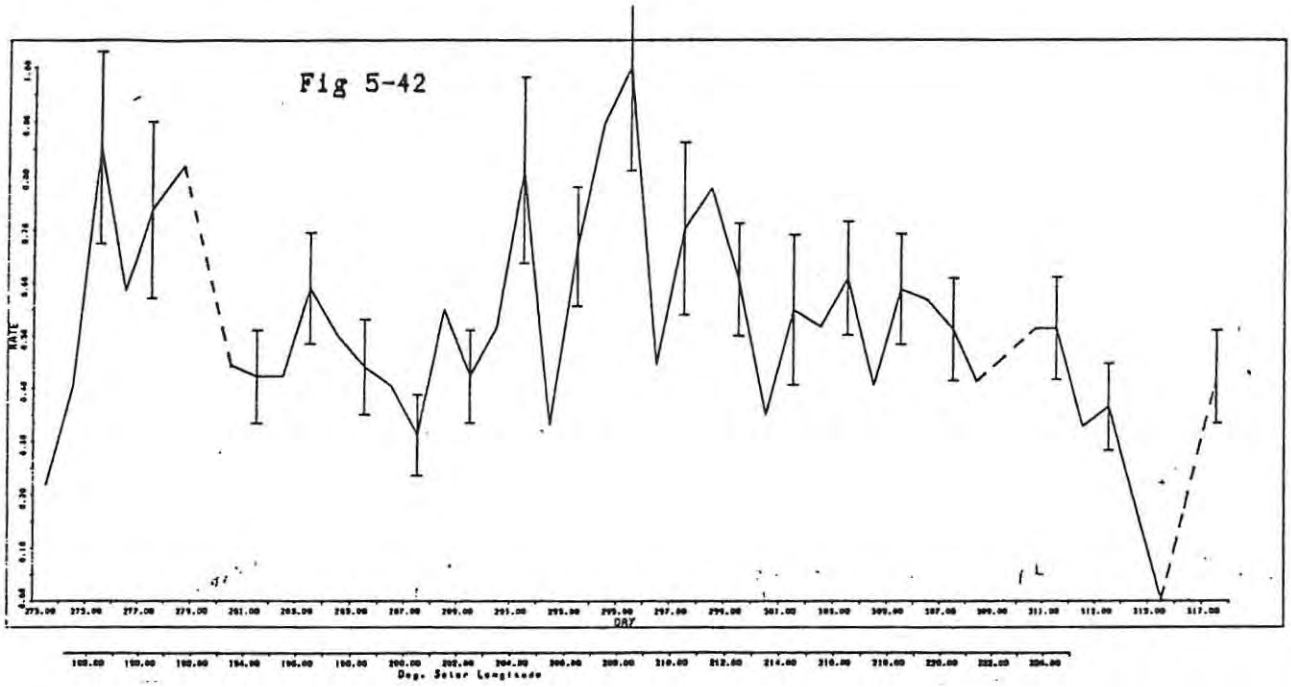

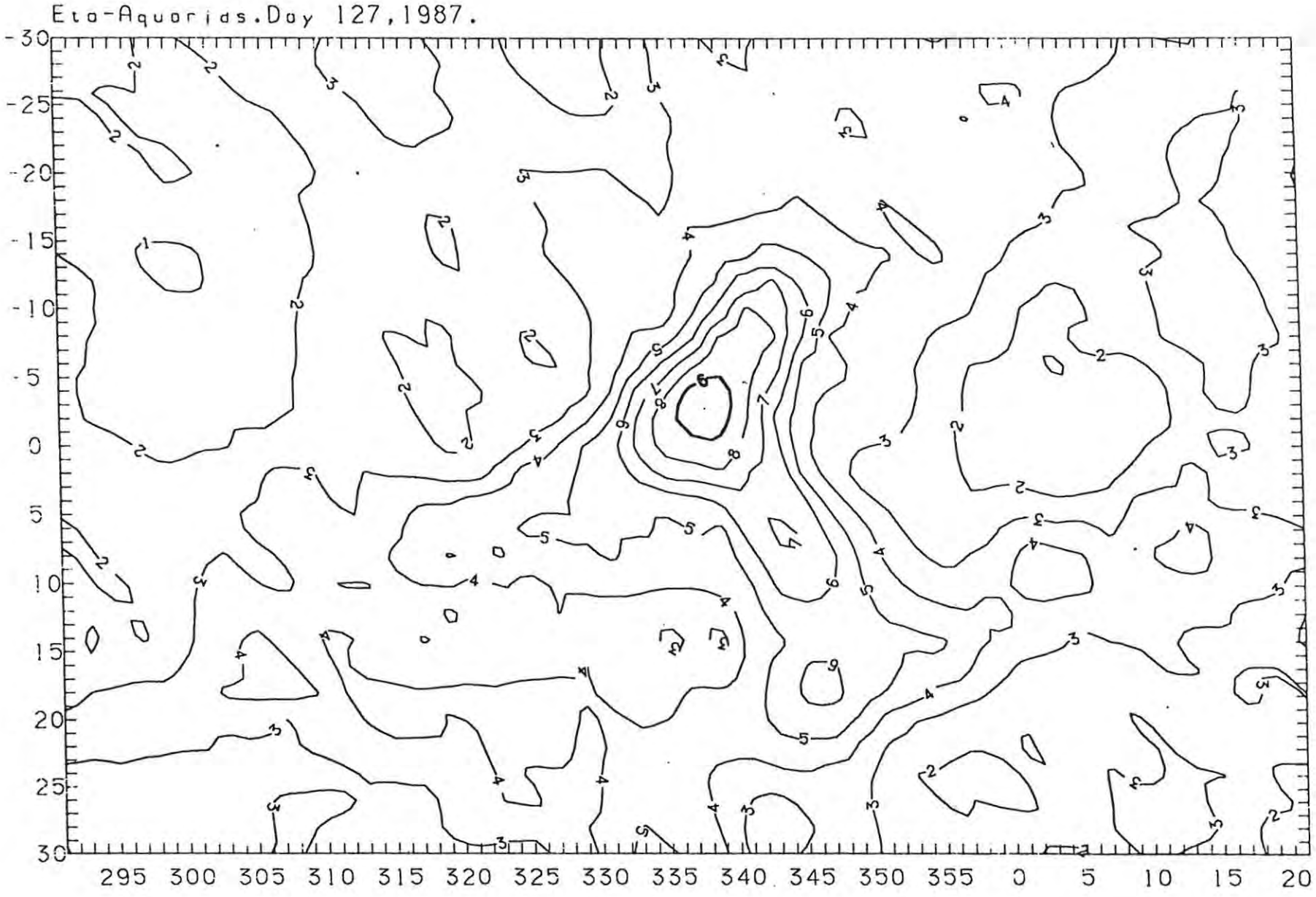
Eta-Aquarids.Day 127,1987.
-30
-25
-20
-15
-10
-5
0
5
10
15
20
25
30
295 300 305 310 315 320 325 330 335 340 345 350 355 0 5 10 15 20

Fig 6-3

Fig 6-4

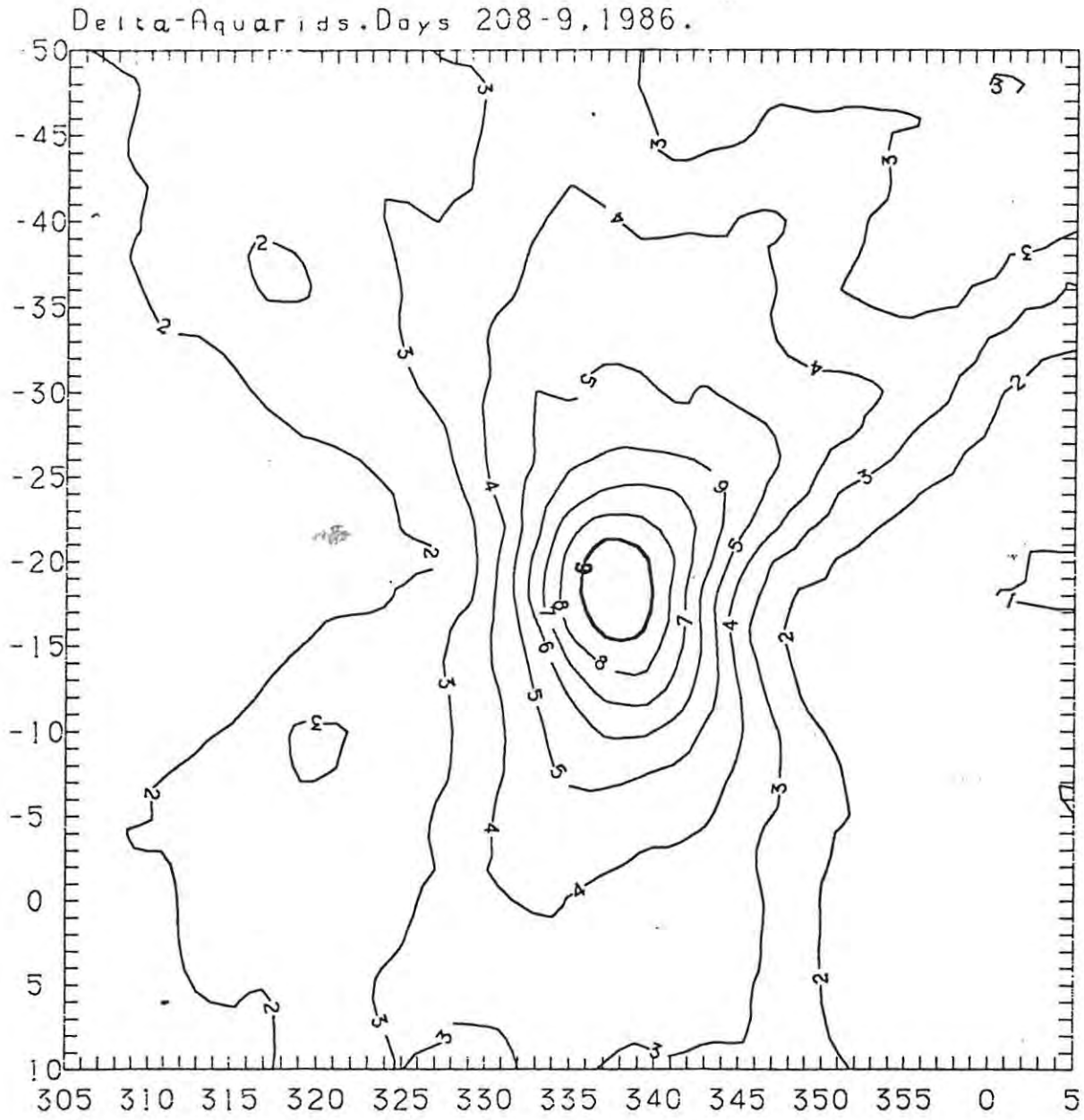
Delta-Aquarids.Days 208-9,1986.
-50
-45
-40
-35
-30
-25
-20
-15
-10
-5
0
5
10
305 310 315 320 325 330 335 340 345 350 355 0 5

Fig 6-5

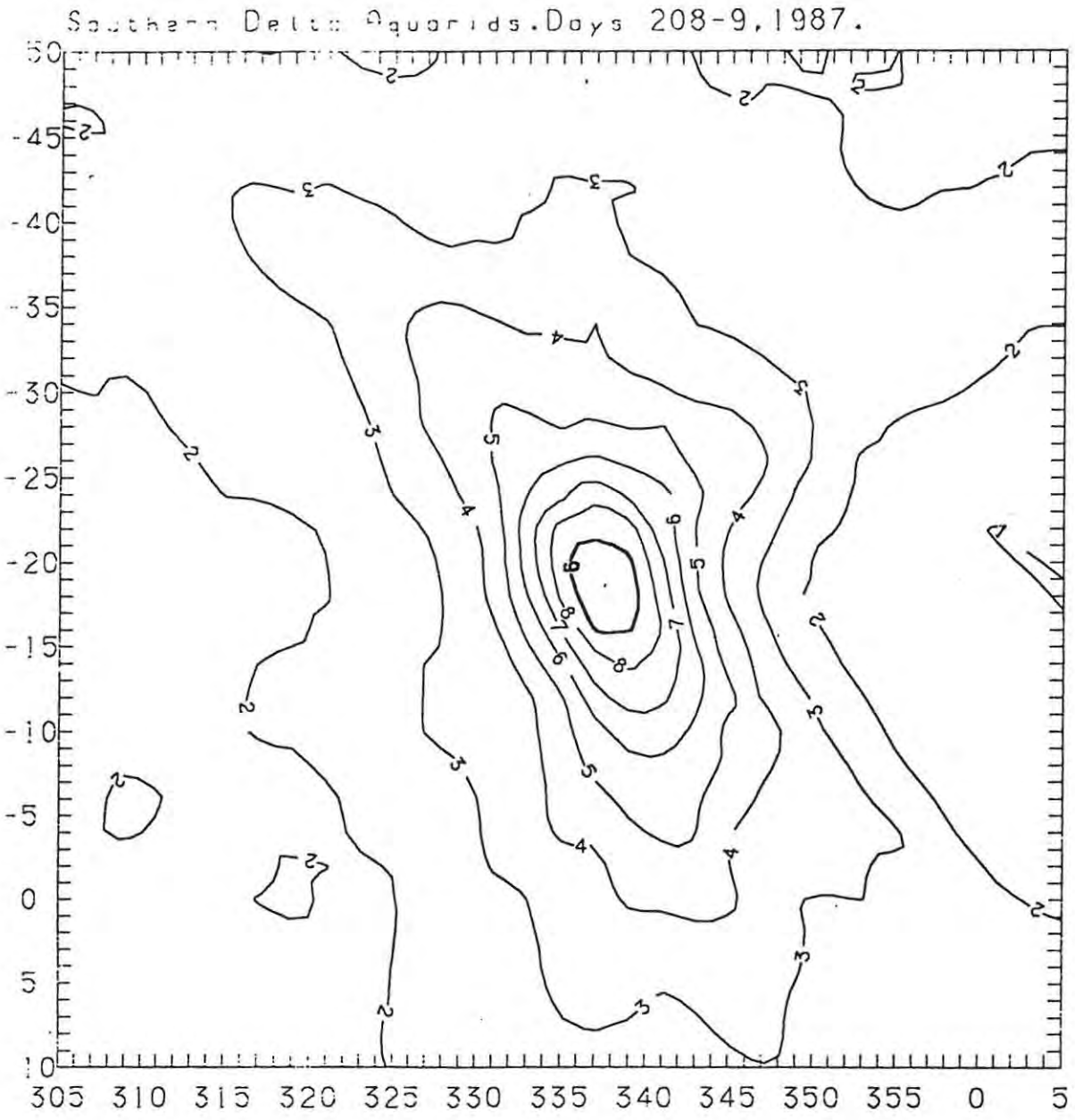
Southern Delta Aquarids.Days 208-9,1987.
-50
-45
-40
-35
-30
-25
-20
-15
-10
-5
0
5
10
305 310 315 320 325 330 335 340 345 350 355 0 5

Fig 6-6: (a) to (h) show the development of the southern δ-Aquarid radiant over successive days immediately before shower maximum.

Fig 6-6 (a)

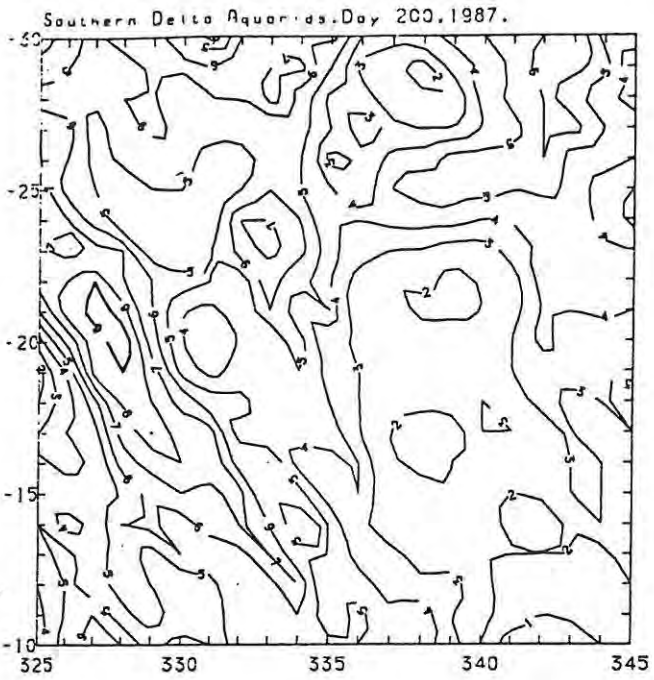

Fig 6-6 (b)

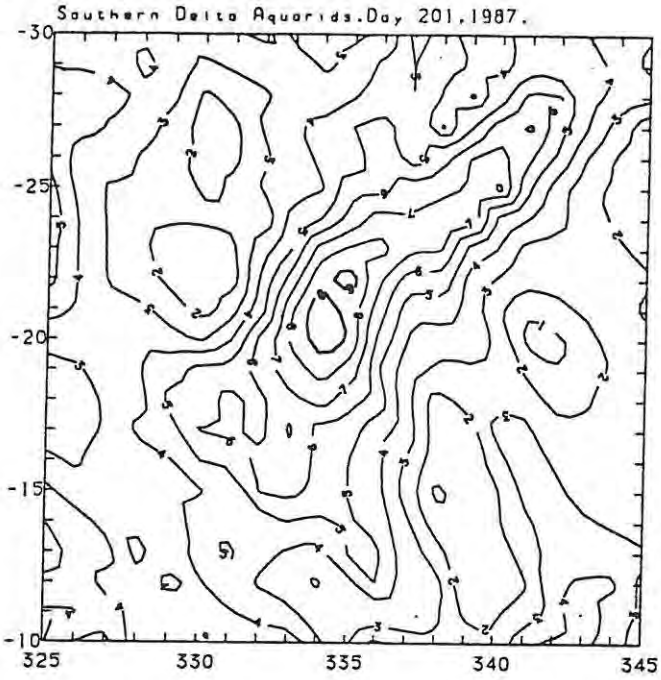

Fig 6-6 (c)

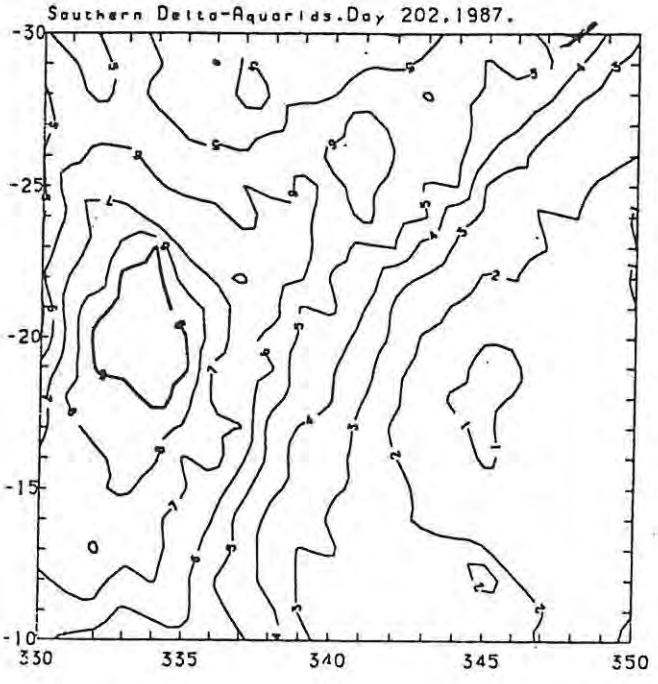

Fig 6-6 (d)

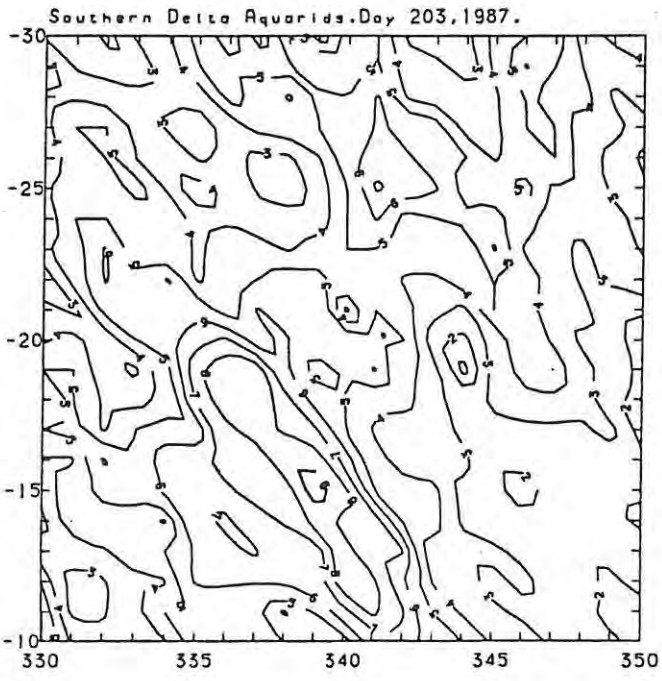

Fig 6-6 (e)

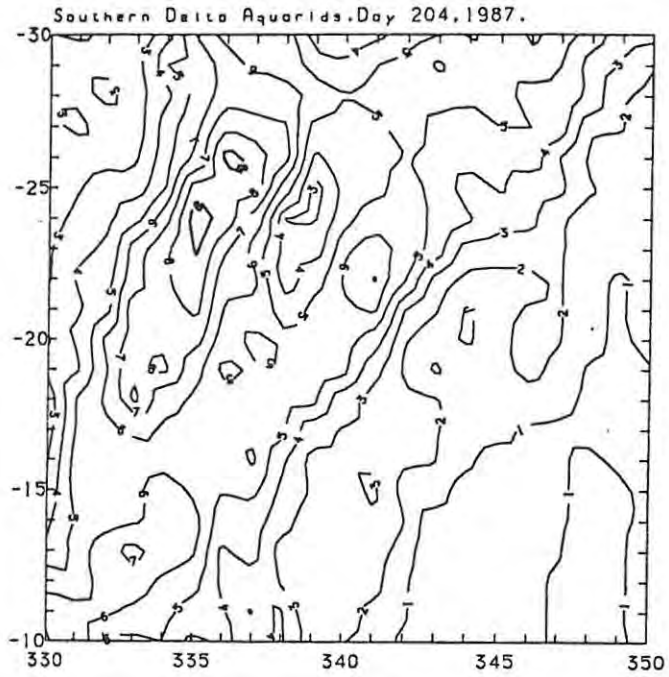

Fig 6-6 (f)

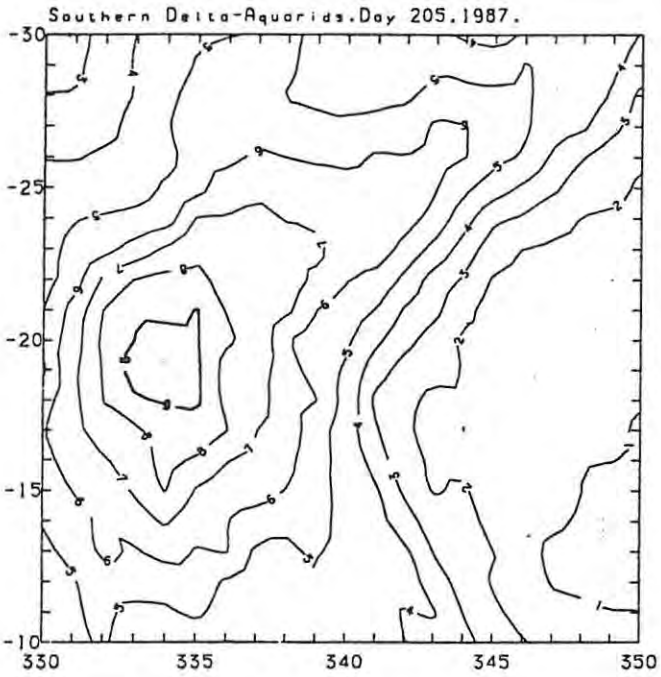

Fig 6-6 (g)

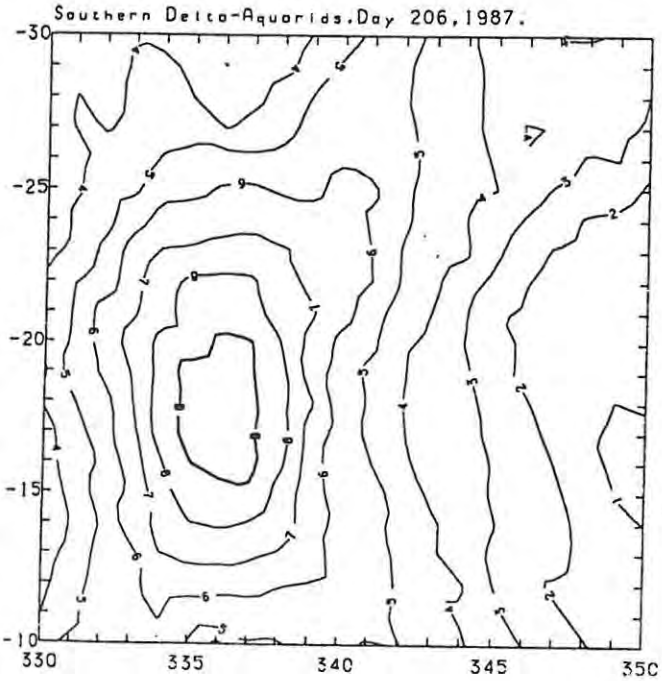

Fig 6-6 (h)

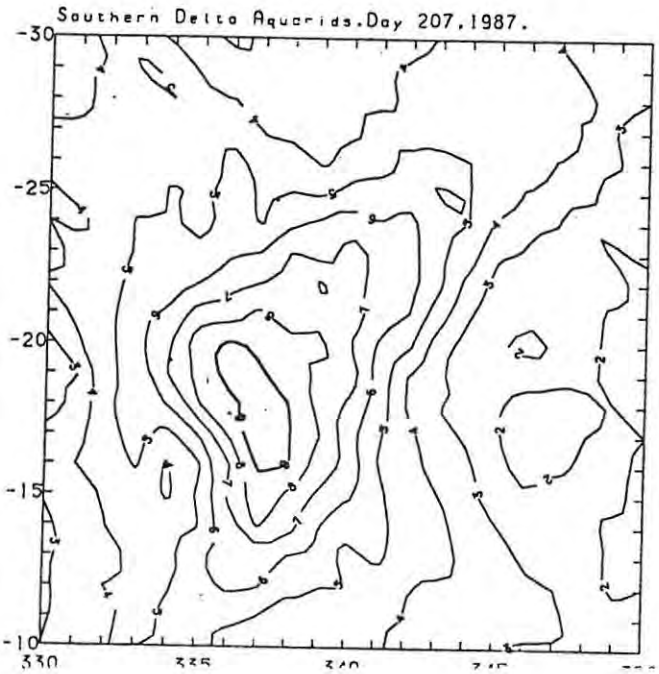

Fig 6-7

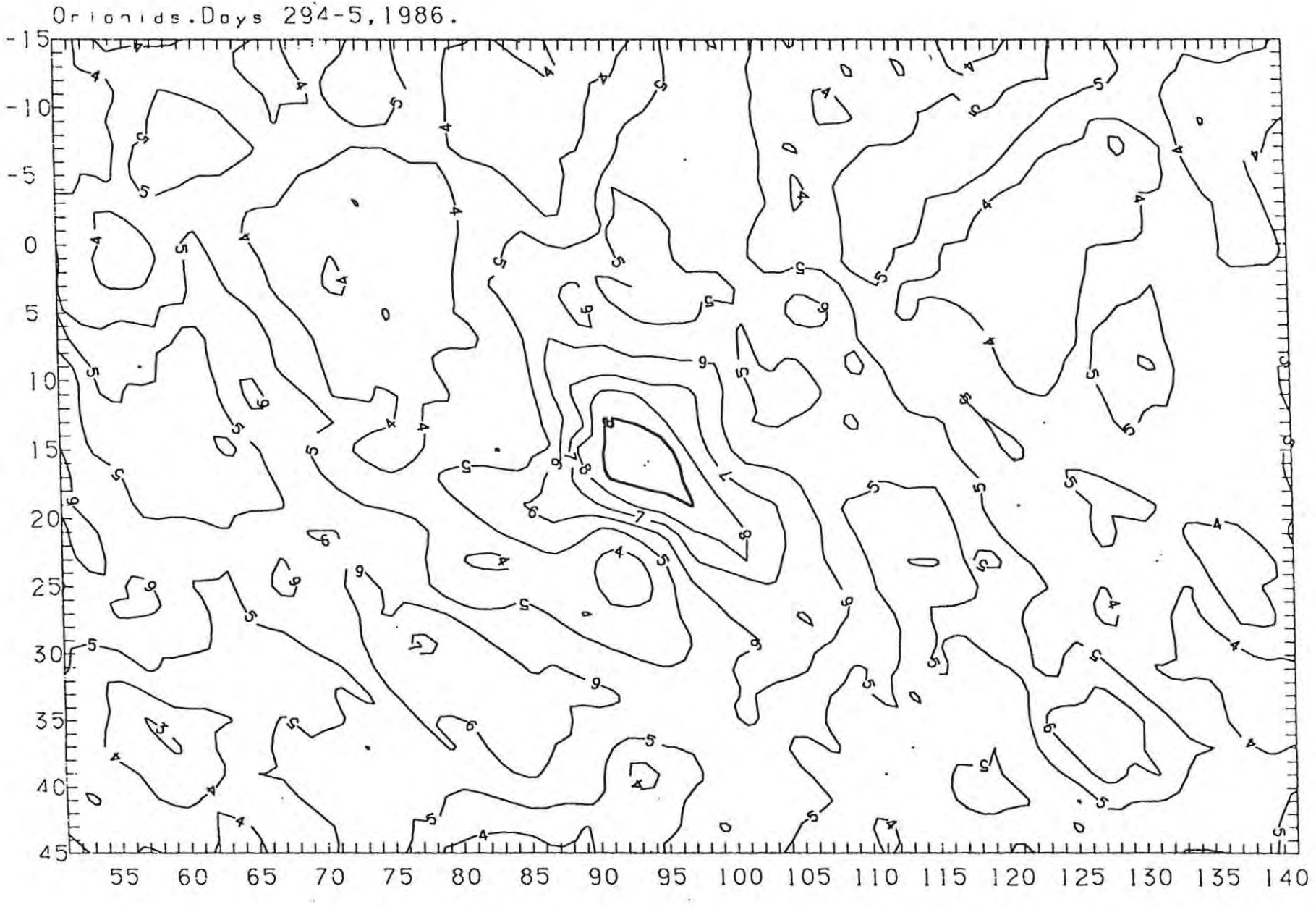
Orionids.Days 294-5,1986.
-15
-10
-5
0
5
10
15
20
25
30
35
40
45
55 60 65 70 75 80 85 90 95 100 105 110 115 120 125 130 135 140

Fig 6-8

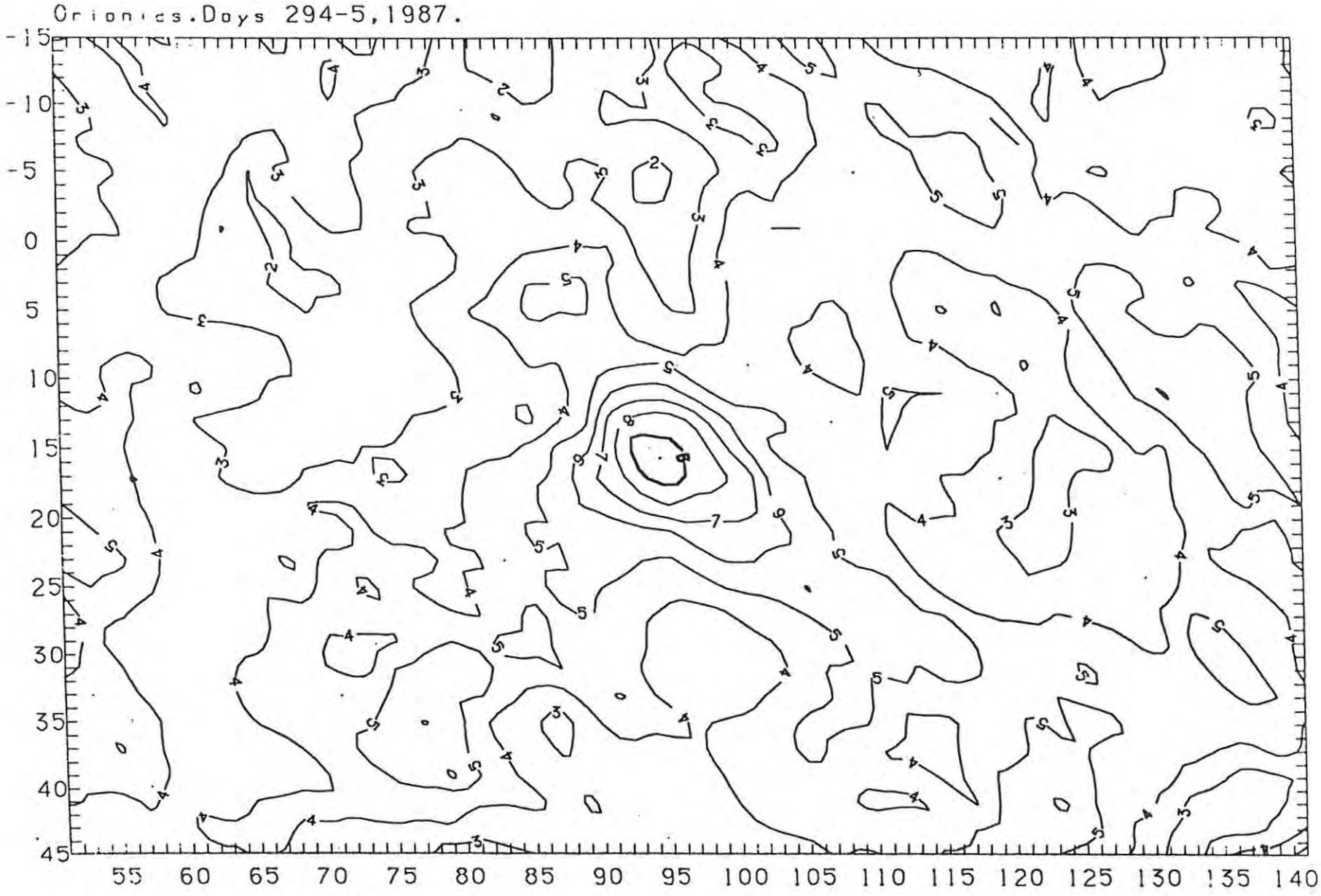
Orionics.Days 294-5,1987.
-15
-10
-5
0
5
10
15
20
25
30
35
40
45
55 60 65 70 75 80 85 90 95 100 105 110 115 120 125 130 135 140

Fig 6-9

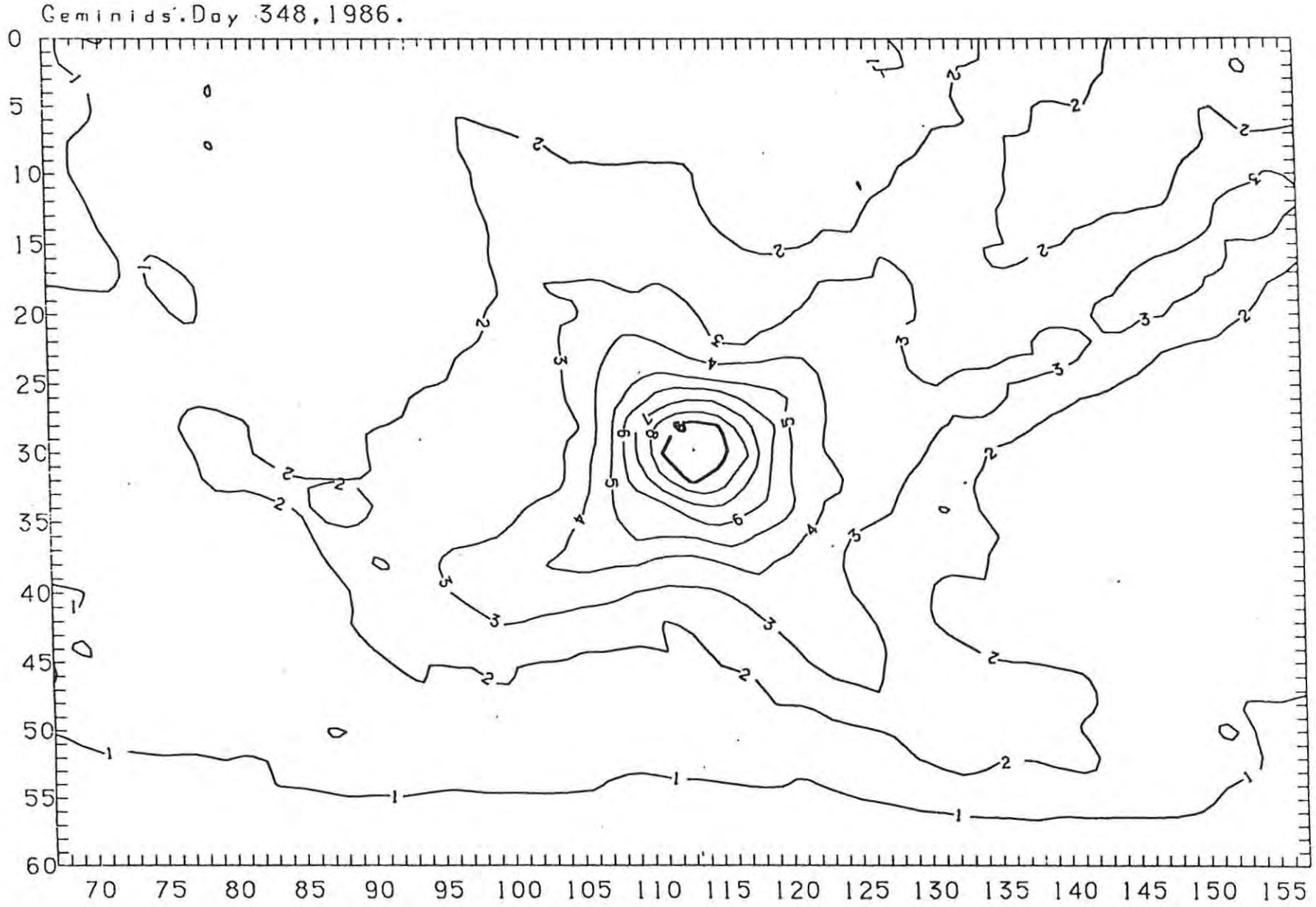
Geminids.Day 348,1986.
0
5
10
15
20
25
30
35
40
45
50
55
60
70 75 80 85 90 95 100 105 110 115 120 125 130 135 140 145 150 155

Fig 6-10

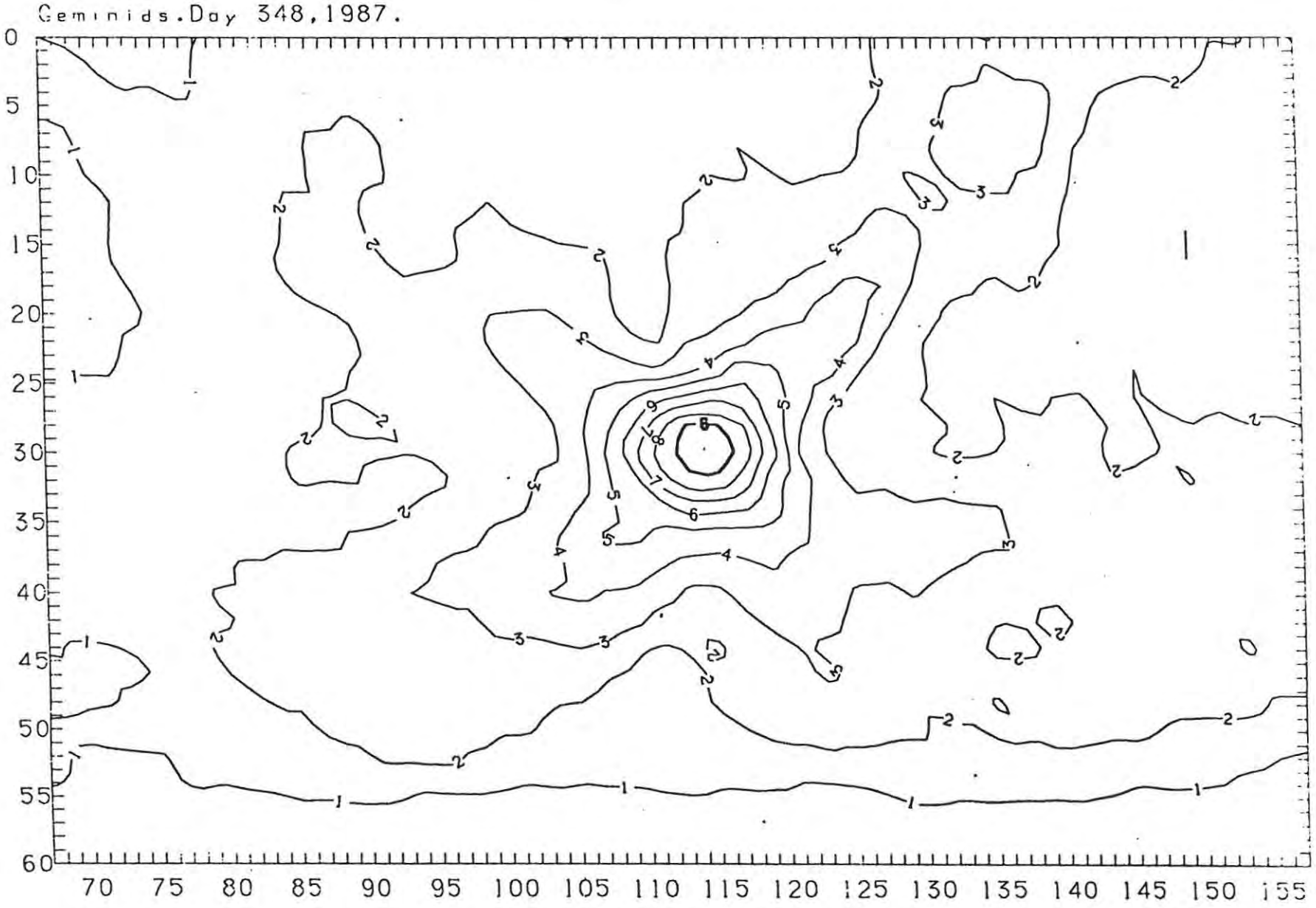
Geminids.Day 348,1987.
0
5
10
15
20
25
30
35
40
45
50
55
60
70 75 80 85 90 95 100 105 110 115 120 125 130 135 140 145 150 155

6-4-2: Minor showers

April Lyrids: April 23, 1987.
From Fig. 6-11 it is evident that an active centre was present at (274°,31°), close to the expected position of the radiant. Another centre of comparable strength is present at the top right of the contour map. We cannot establish from the present method whether only one, or both of the radiants is a genuine centre of shower activity (see 6-4-4).

Arietids: June 10, 1987.
A strong near-circular radiant (diameter ~2°), centred at at (43½°,23°), was observed (Fig. 6-12). We feel confident that this active centre is genuinely due to stream members, in view of its proximity to the catalogued position of the radiant. A secondary, crescent-shaped centre is present at (46°,20½°).

Beta-Taurids: June 25, 1987.
Fig. 6-13 shows an irregularly shaped radiant centred at (74°,15½°). This is far removed from the catalogued radiant position, and the radiant may be spurious.

Taurids: November 17, 1987.
We see from Fig. 6-14 that two regions of enhanced activity were present in the general vicinity of the northern and southern stream radiants. Approximate coordinates of these centres are, respectively, (52°,28°) and (64°,10°). Both are located on a high 'plateau'. We cannot be certain that these possible radiants are due to stream members.

Phoenicids: December 4-5, 1986 and 1987.
The broad regions of maximum activity in Figs. 6-15 (a) and (b) are possibly due to Phoenicid meteors. Again, we are unable to know this with any certainty. It is interesting that both maps show a ridge running horizontally at a declination of about -55°.

Velaids: January 1, 1987 and 1988.
Both Figs. 6-16 (a) and (b) show regions of enhanced activity to the south-west of the position of the expected radiant. Because of this displacement and also the magnitude of the 'noise' peaks, we cannot attribute these maxima to the Velaid shower with certainty. Fig. 6-16 (a) shows the sporadic fine structure in greater detail than (b). This is because a coarser radiant grid was used (b) than in (a), in the running of the program SKYMAP.

Our search for radiant structure associated with the remaining minor showers produced results which were not indicative of the presence of shower activity.

Figs. 6-11 to 6-16: meteor radiant activity in the vicinity of the active centres of some of the minor showers. The echoes have not been weighted.

Fig 6-11

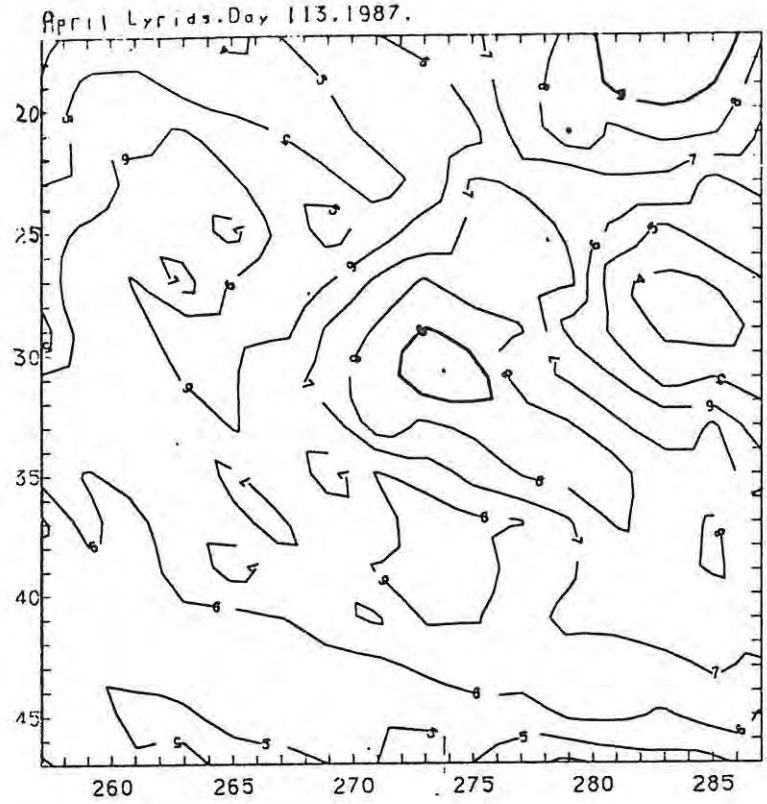

Fig 6-12

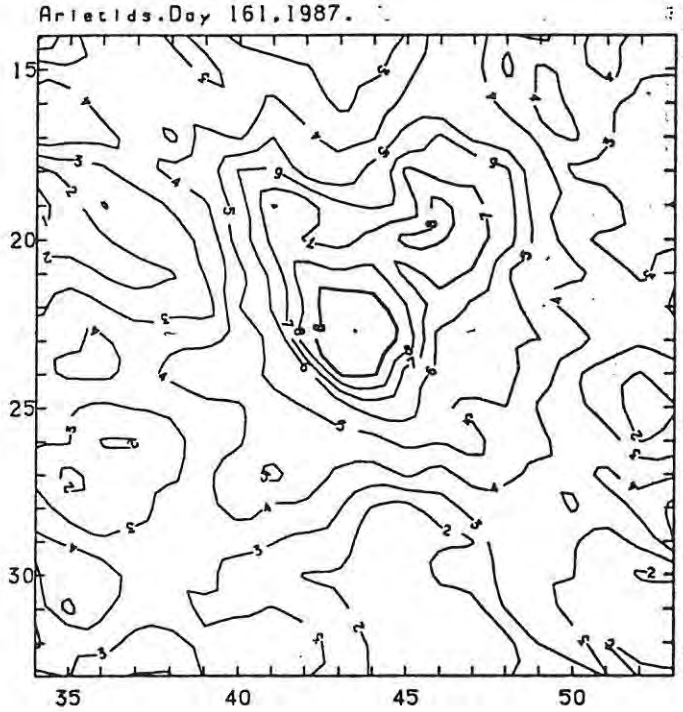

Fig 6-13

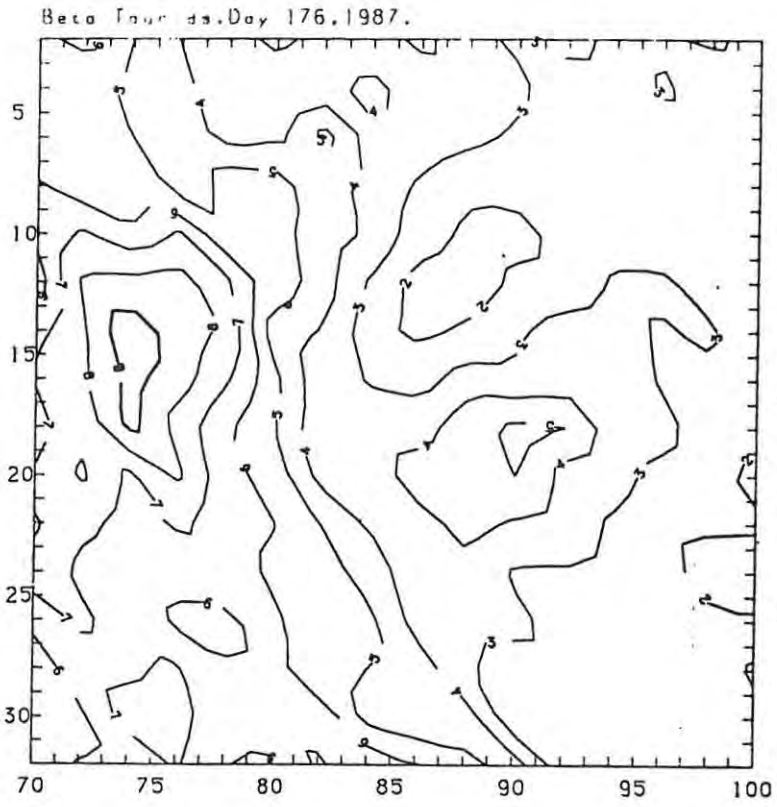

Fig 6-14

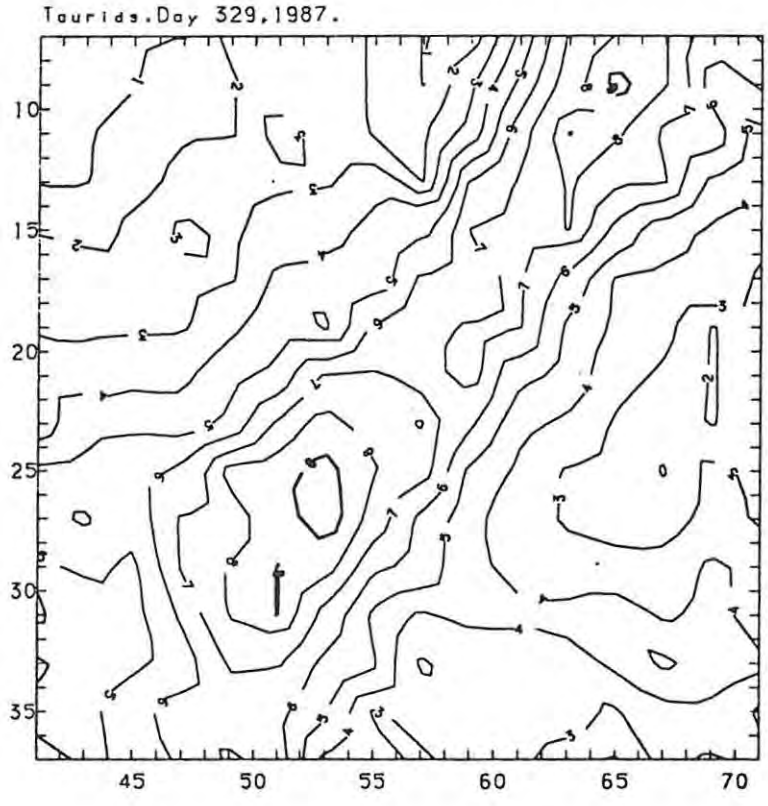

Fig 6-15 (a)

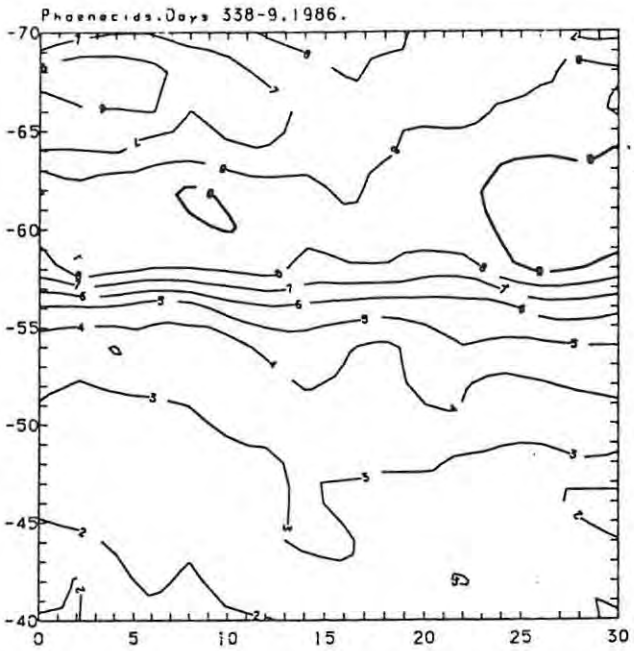

Fig 6-15 (b)

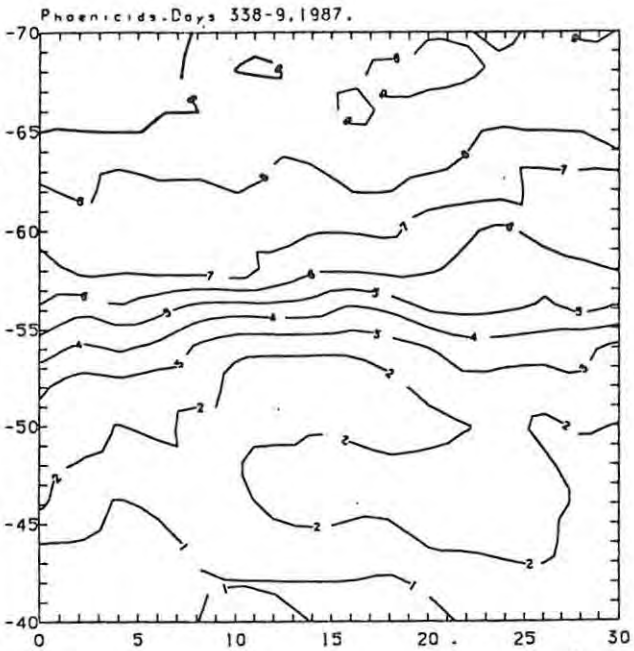

Fig 6-16 (a)

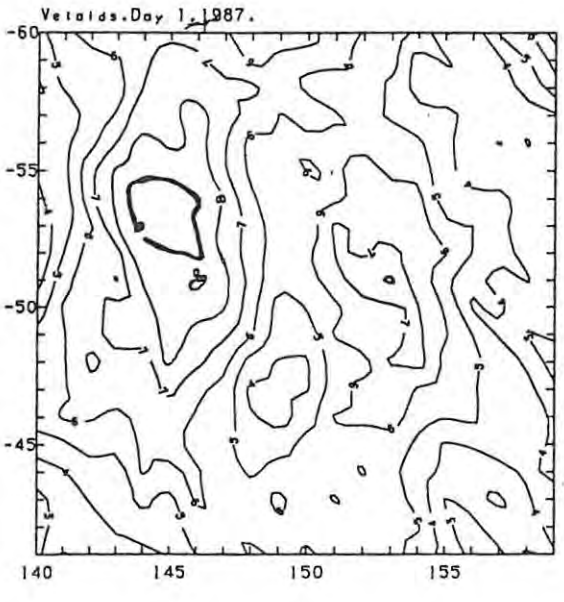

Fig 6-16 (b)

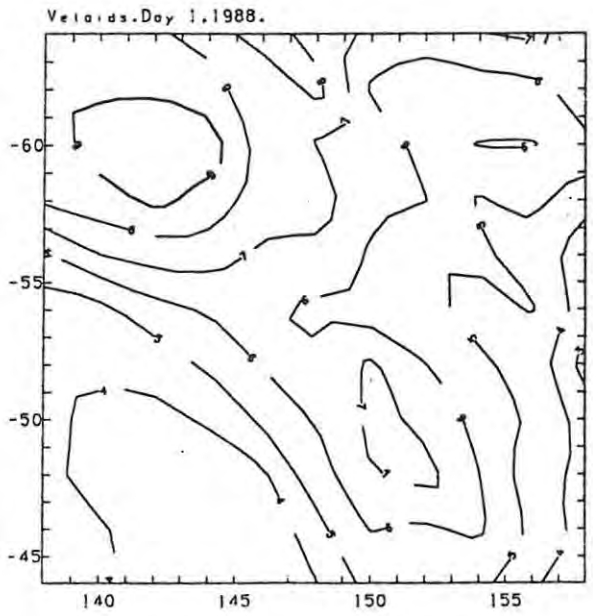

6-4-3: Echo-weighting

The results of the weighting procedure which we discussed earlier in this chapter are presented in Figs. 6-17 to 6-22. Figs. 6-17, 6-18, 6-19 and 6-20 are the weighted versions of Figs. 6-3, 6-4, 6-7 and 6-9, respectively. Comparisons between each of the weighted and unweighted maps reveal that our procedure did not alter the Eta-Aquarid (6-17) or the Delta-Aquarid (6-18) radiant maps significantly. However, in the case of the Orionids (6-19) and the Geminids (6-20), the weighting procedure actually introduced a noticeable new type of distortion into the maps.

From our discussion of the 'cosX effect' (section 6-3) it is apparent that the grand total detection probability depends strongly on this term. The effect of the weighting procedure on the radiant maps therefore depends largely upon the variation of the term cosX, between the upper and lower limits of the map. The variation of the mean value of cosX as a function of the radiant declination is relatively gradual over regions of the celestial sphere which transit near to the zenith, but is much more rapid over those regions which do not rise well above the observer's horizon.

It follows that the distortion, due to the cosX term, of features in the weighted maps of the four major showers (Figs 6-17 to 6-20) increases in the following order: δ-Aquarids, Eta-Aquarids, Orionids, Geminids. In Fig 6-20 we see the most extreme example of this distortion for the 1986 Geminids: the activity contours have been compressed into a narrow strip near the lower border of the map. The effect is less pronounced in Fig 6-19; although the contour 9 appears at the bottom of the map, the Orionid radiant is nevertheless visible at the centre (contour 5). The variation of cosX has affected the δ- and Eta-Aquarid maps (Figs 6-17 & 6-18) only slightly.

An obvious way of minimising the difference between the upper and lower values of cosX, without altering the computer program, is to map a smaller area of sky. This is shown Fig. 6-21, which is in fact a map of the central region of Fig. 6-7. In Fig. 6-21 (a) the echoes have been weighted while in (b) they have not. The extrema of cosX for Fig. 6-21 are 0.84 and 0.45, and the ratio of these quantities is ~1.9 (compared with ~4.5 for Fig. 6-7). Consequently the degree of distortion between (a) and (b) of Fig. 6-21 is not as great as that between Figs. 6-19 and 6-7.

We finally made the inclusion of cosX in the calculation of p optional, and the result is illustrated by Fig. 6-22, for the 1986 Geminids. This map is an obvious improvement on Fig. 6-20, although it is somewhat 'noisier' than the unweighted version, Fig. 6-9. However, G_m for

radiants which barely rise above the northern horizon is small whether or not the cosX factor is taken into account, and the two sharp peaks which occur at the bottom of both Figs 6-20 and 6-22 are probably artefacts arising from this fact. All three of these maps were drawn from identical data.

In the case of the δ-Aquarid radiant map (Fig 6-18), which shows definite atigmatism, our echo-weighting procedure was ineffective. As we have already indicated, since this phenomenon arises from the uneven clustering of reflection points, an effective countermeasure would be to redistribute the echo directions more homogeneously along the entire echo arc. However, the method of dividing the total number of echo registrations associated with a given radiant by G_m does not have the desired effect of smoothing the distribution of reflection points. Although this technique is unsuitable for radiant mapping, it may be used for determining the strengths of of widely separated radiants where the association between any of the radiant points and a particular echo direction is unambiguous. Clearly the method as it stands is in need of further development.

6-4-4: Discussion

In this chapter we have presented the results of our search for radiant activity associated with twenty-two meteor streams in the form of contour maps of radiant intensity, and also our attempt to rid these maps of possible distortions arising from the anisotropic radar antenna beam.

Well-defined, strong radiants were observed for the four major showers. Definite radiant structure was observed for only one minor shower, the Arietids (1987). Active centres which were possibly due to a further five minor showers, were observed: the April Lyrids (1987), Beta-Taurids (1987), Taurids (1987), Phoenicids (1986 & 1987), and the Velaids (1987 & 1988). No radiants for the remaining minor showers could be detected. The maps reveal considerable structure in the sporadic radiant complex, and some features (eg. the horizontal ridge in Figs. 6-15 (a) and (b)) were observed in both years.

Astigmatism is not immediately apparent in several of the unweighted contour maps (eg. Figs. 6-3, 6-9, 6-10), and even in those which do show definite astigmatism, the effect is much less marked than in the radiant activity maps produced by Morton & Jones (1982). Our echo-weighting procedure in its present form did little to improve the maps which did show slight astigmatism (eg. the Delta-Aquarids, 1986 & 1987), and in some cases (eg. the Orionids and Geminids) introduced

unwanted serious distortions rather than removing any which might have existed. The most serious distortions are attributable to the 'cosX effect', and were mitigated once this factor was omitted in the calculation of the detection probability. In any case it is clear that the method breaks down completely for radiants which graze the northern horizon.

The penalty for normalizing the radiant maps is the loss of information on the absolute strengths of the respective shower radiants. Their **relative** strengths can be inferred, however, from the amount of sporadic noise which is present. Any strongly active centre will drown the islands of noise beneath contour level 1. Even if no shower is active, the level of radiant intensity on our maps must of necessity rise above contour 9, because of normalization. This makes weaker showers difficult to detect, particularly when multiple centres are present.

Our method should be capable of determining radiant positions to within ~2°. This figure is also the approximate uncertainty in any echo direction. Indeed, the five radiant centres which were determined with certainty are within ~2° of the catalogued positions (see Chapter 5).

Figs. 6-17 to 6-22 illustrate the effect of our echo-weighting procedure on the radiant activity contour maps for the major showers.

Fig 6-17
Eta Aquarids. Day 127, 1987.

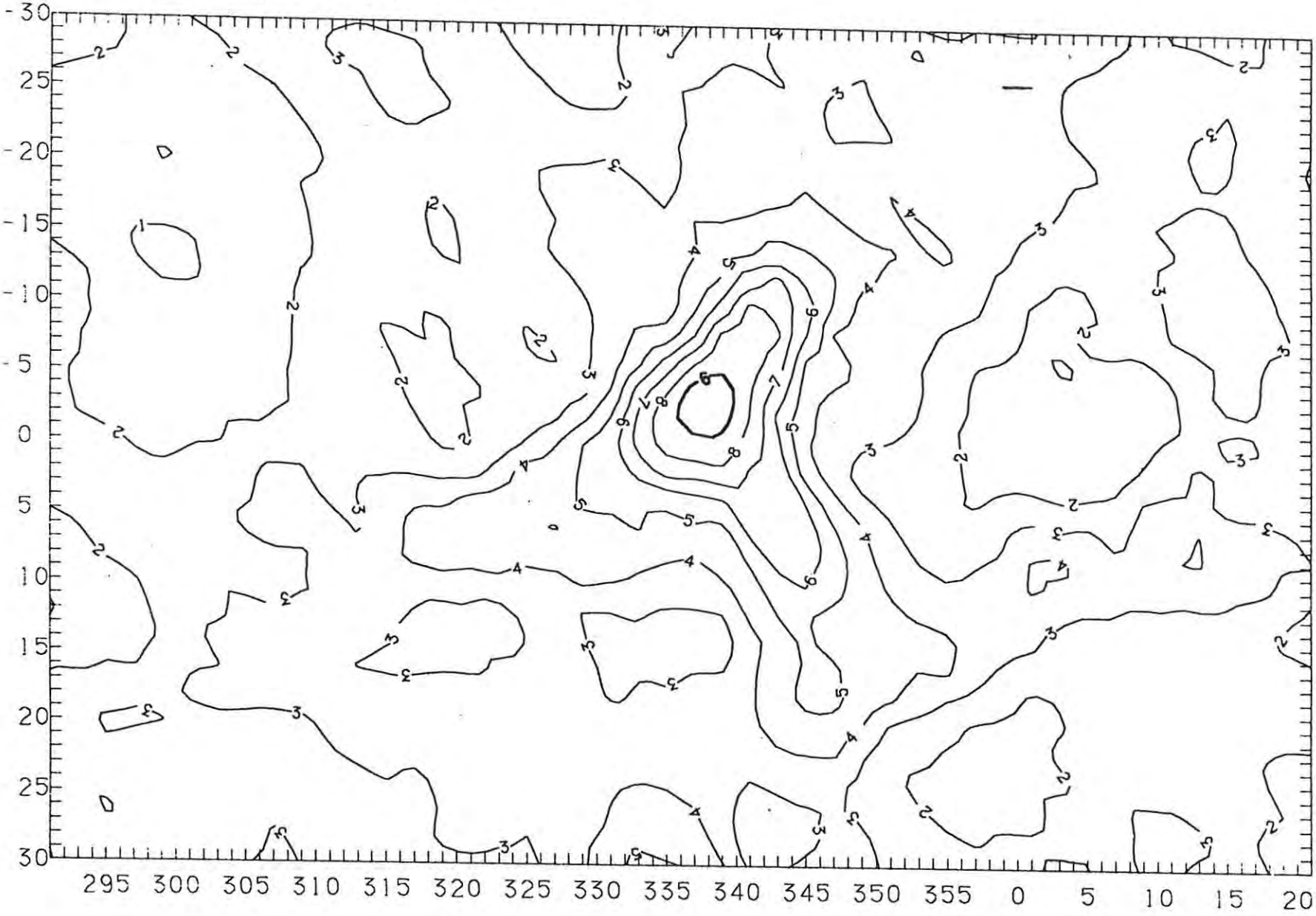

Fig 6-18

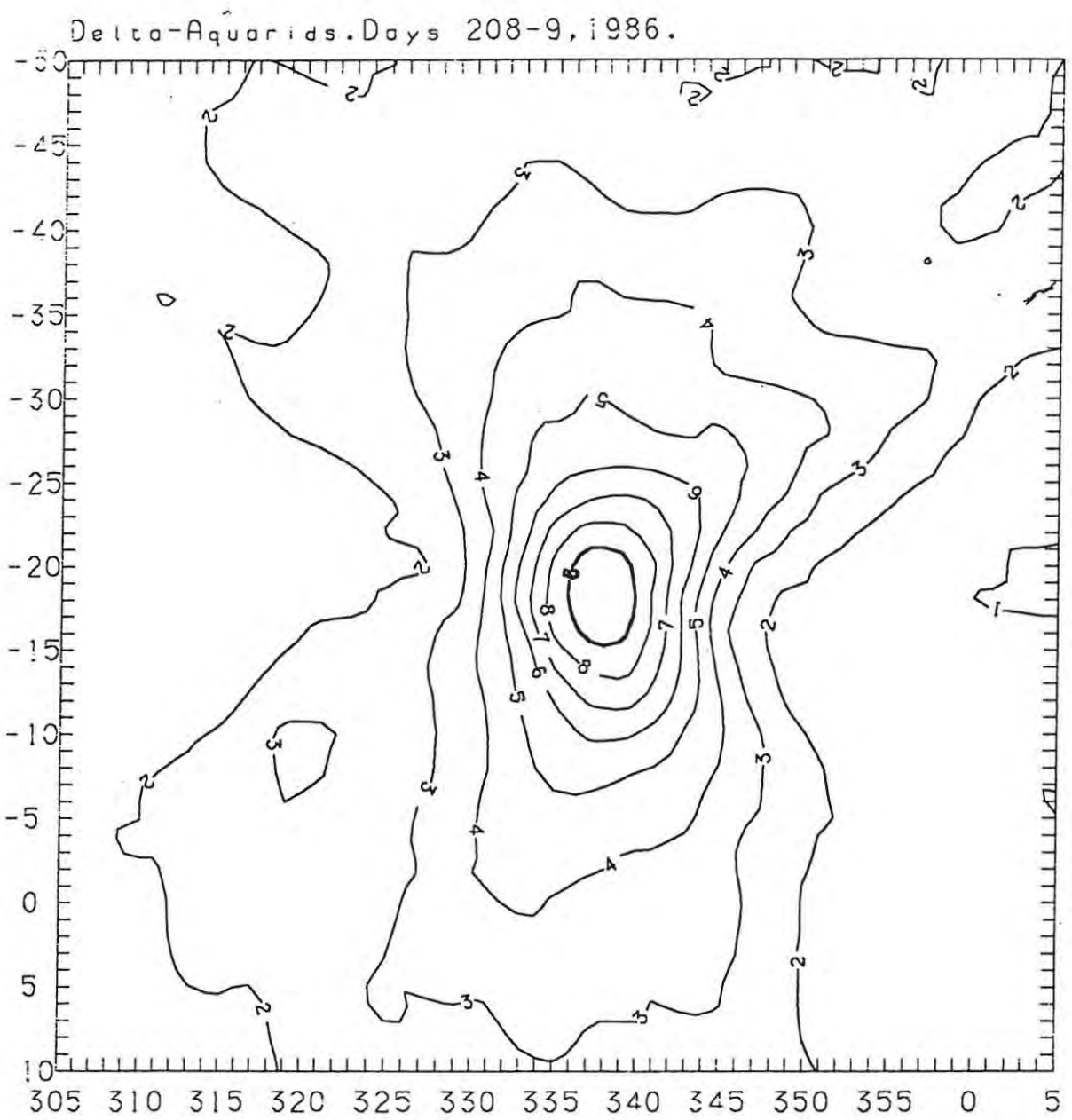
Delta-Aquarids. Days 208-9, 1986.
-50
-45
-40
-35
-30
-25
-20
-15
-10
-5
0
5
10
305
310
315
320
325
330
335
340
345
350
355
0
5

Fig 6-19

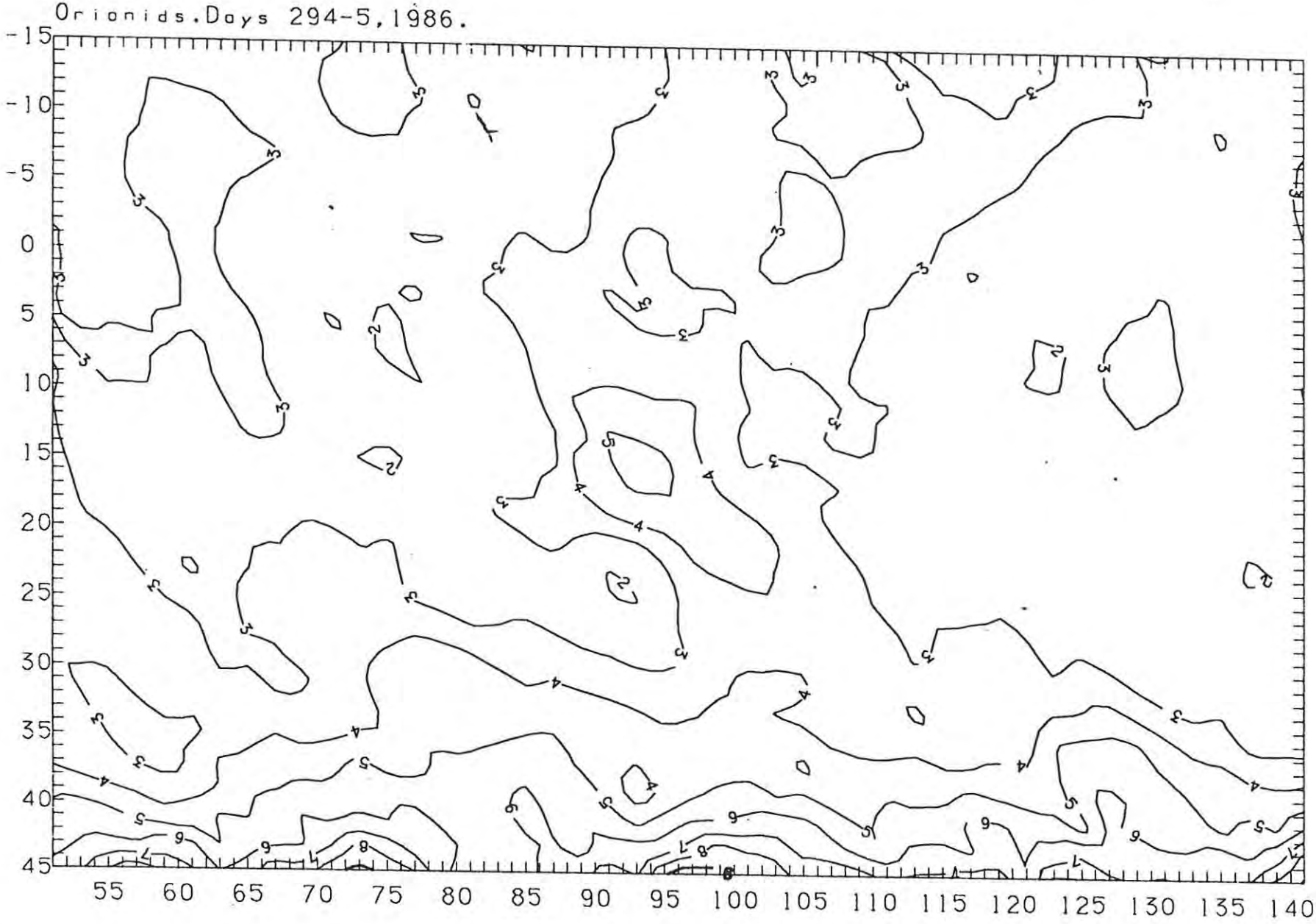
Orionids.Days 294-5,1986.
-15
-10
-5
0
5
10
15
20
25
30
35
40
45
55 60 65 70 75 80 85 90 95 100 105 110 115 120 125 130 135 140

Fig 6-20

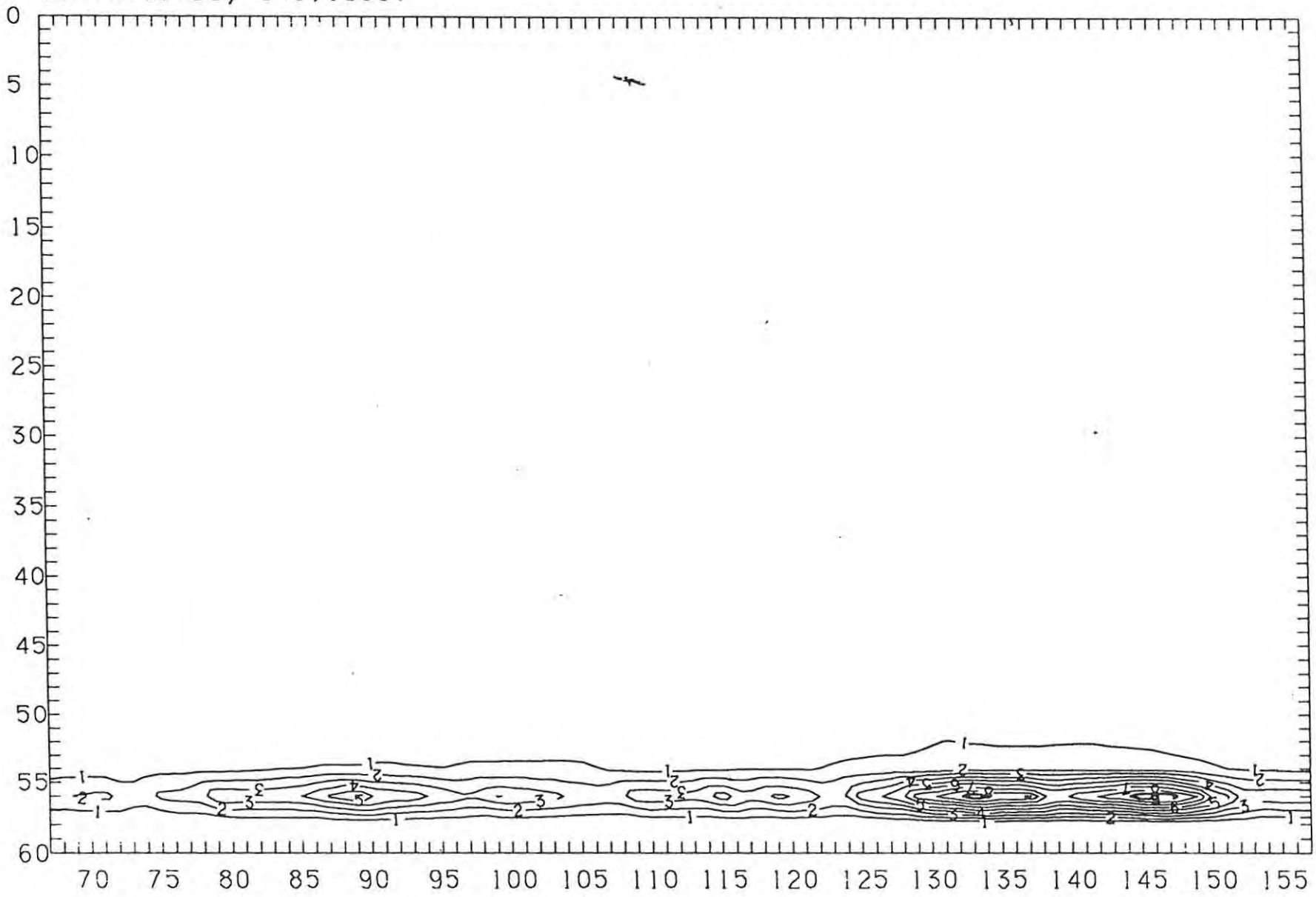
Geminids.Day 348,1986.
0
5
10
15
20
25
30
35
40
45
50
55
60
70 75 80 85 90 95 100 105 110 115 120 125 130 135 140 145 150 155

Fig 6-21 (a)

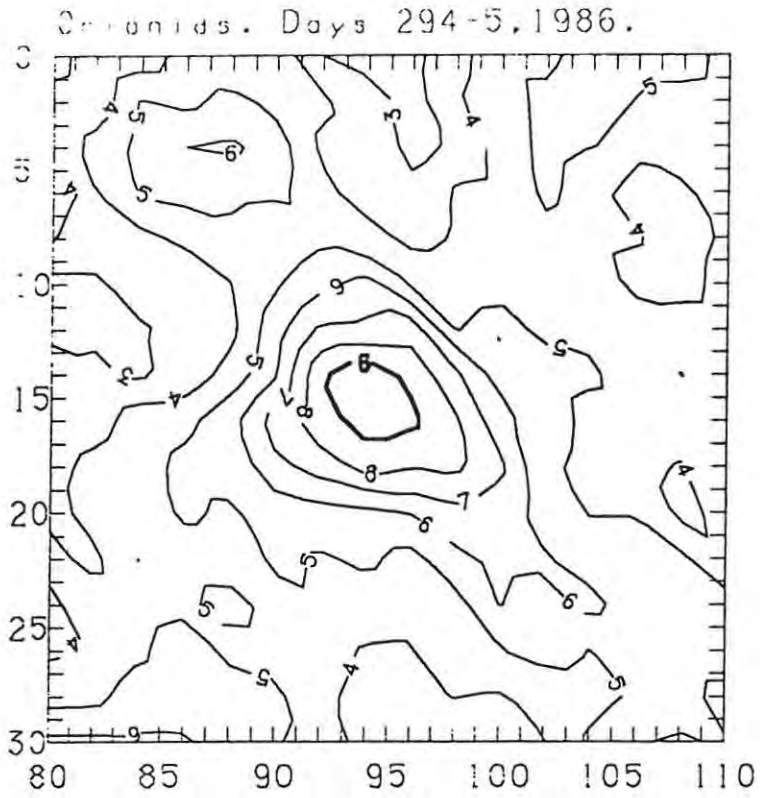

Fig 6-21 (b)

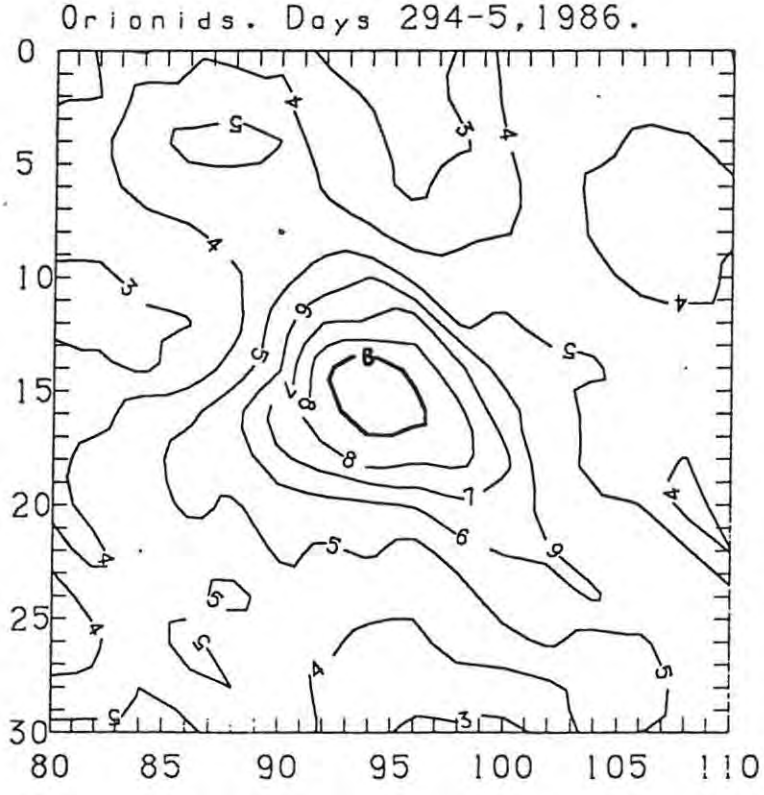

Fig 6-21: (a) unweighted and (b) weighted echoes.

Fig 6-22: Echoes weighted but the factor cosX excluded.

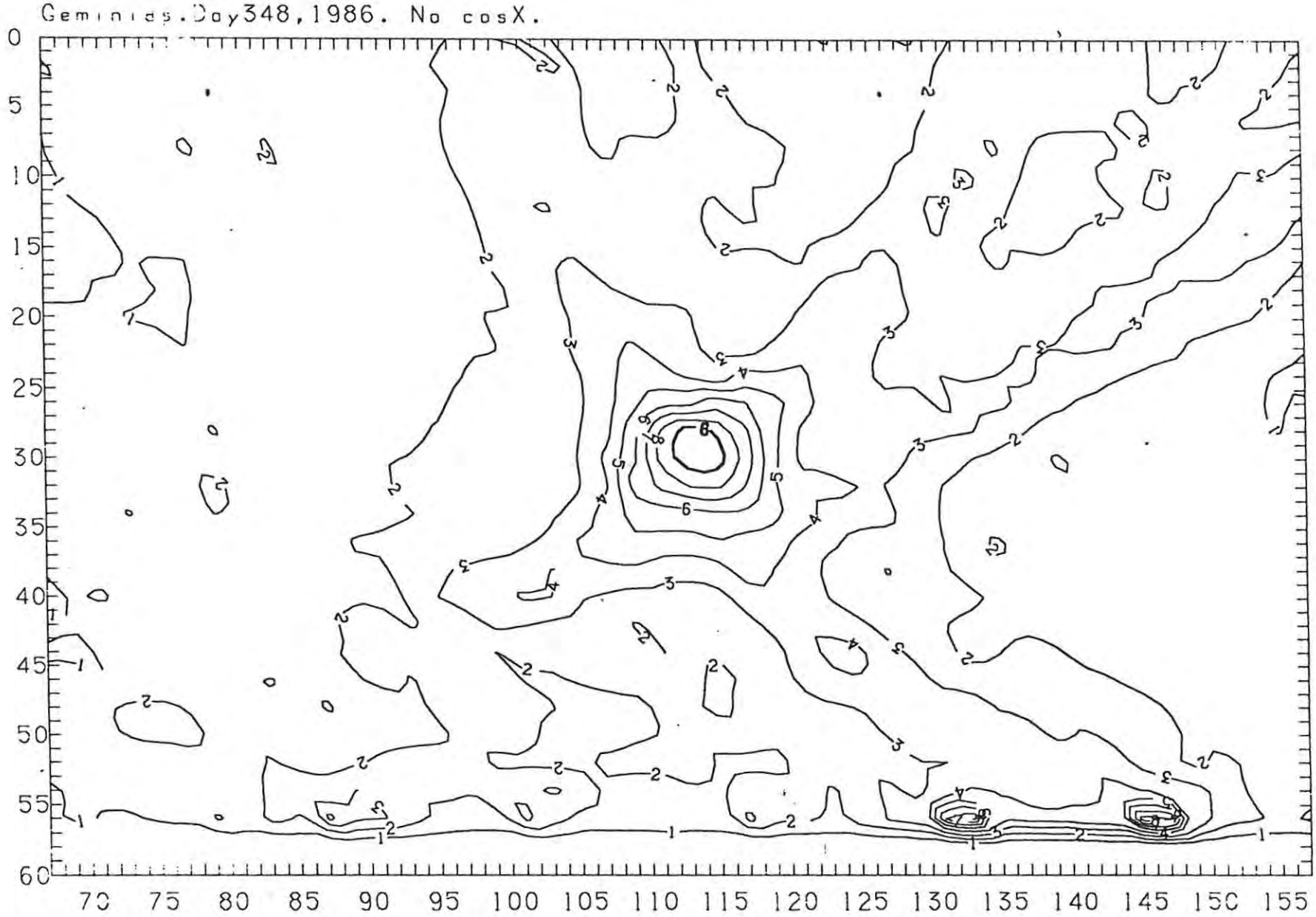

Chapter 7: Concluding Remarks

7.1: Summing up

We have presented a general rate survey of 20 Southern Hemisphere meteor streams and the sporadic meteor background, for the period 1986 April to 1988 January. A method of recovering the distribution of meteor radiants from the echo directions, based on that of Morton & Jones (1982), has been described and implemented, to produce maps of radiant activity. This method, when used in conjunction with a non-isotropic antenna beam, produces spurious elongation of features ('astigmatism') on the maps. Although this effect is not severe with the broad-beamed antenna system, we have described a method of compensating for anisotropy by weighting the echoes in accordance with the beam sensitivity in the echo directions, which we hoped would rid the maps of the remaining astigmatism. The procedure as implemented had little effect on astigmatism while introducing other artefacts into the maps.

Our results indicate that the radar at Grahamstown will have considerable potential once it has been upgraded. The most immediate improvement envisaged is a new data logging system, which will discriminate against noise spikes by performing an on-site spectral analysis of all received signals. Thus it will soon be possible to operate the radar for 100% of every hour, and also to lower the minimum echo amplitude threshold considerably, since noise data will no longer occupy disc space. The lower threshold means improved system sensitivity. In the long-term, fitting each channel with an independent receiver will further enhance the sensitivity. By transmitting at two closely spaced frequencies, it will be possible to calculate the range and hence the heights of reflection points.

7.2: Suggestions for further research

The work presented in this thesis has laid the groundwork for further investigation into the weighting procedure; although echo-weighting did not improve the contour maps as we had hoped, there is every indication that a refinement of the method will lead to better results. Further research into the problem is certainly merited. The fact that a number of assumptions have to be made in arriving at p_i (Chapter 4) is not critical, since proper compensation should involve only slight corrections to the unweighted maps.

An enhanced system sensitivity will provide a greater abundance of

data, which may enable some of the weaker showers for which the results of the present survey are inconclusive, to be detected. It will therefore be worthwhile to investigate the rate profiles and possible radiant structure associated with these showers, once the upgraded radar system becomes operational. Height-distribution studies represent an avenue of research that has not yet been explored, and it is likely that this will form the basis of another research project.

APPENDICES

Appendix 1 contains listings of the eleven Fortran programs described in Chapters 4, 5 & 6.


```
      PROGRAM RATE
C     ============
C
C     GENERAL PROGRAM FOR COMPUTATION OF HOURLY METEOR RATES;
C     AZBINS REMAIN LUMPED; DOES AMPLITUDE DISTRIBUTION IN EACH BIN.
C
C     Written by DAVID G.ROUX, 1986.
C     Revised by D.G.R., 29 December 1987.
C
C
      DIMENSION CAZALT(9,12),R(9),R1(9),R2(9),DR(9),AREA(9),
     *CPSQK(9,12),HRSQK(9,12),SECLINE(14),KTH(10),HR(10),C(10),
     *AMPBIN(10,9,12),MIDAZ(12),MIDALT(12),RBIN(10,9,12),FISH(11),
     *DEADT(5),AT(5),BT(5),TA(5),TB(5)
      CHARACTER*2 GEN,PS,FFILE,LFILE,DISCNO,GENF,GENL,F23
      CHARACTER F24*3,DISC*3,FLNM(1601)*7,FILETD*27,RFILE*9,
     *ANS*1,NAS*1
      INTEGER EHR,WHR
C-------------------------------------------------------------------------------
      CALL FILENAME(FLNM,ILF)
C-------------------------------------------------------------------------------
      WRITE(6,'(X,A)')'ENTER FIRST DAY, LAST DAY'
      READ(5,*)IFID,ILAD
      PI=3.141593
      PTF=0.25
      FLAG=0
      IHR0=-1
      OT3=0
      OTM=0
      WRITE(6,'(X,A23)') 'PRINT ALTAZ BINS? (Y/N)'
      READ(5,'(A1)') ANS
      IF(ANS.EQ.'Y')WRITE(6,'(X,A)')'LUMP TOGETHER THE AZIMITH
     * BINS? (Y/N)'
      READ(5,'(A)')NAS
      KTH(1)=25
      KTH(2)=35
      KTH(3)=39
      KTH(4)=45
      KTH(5)=55
      KTH(6)=77
      KTH(7)=86
      KTH(8)=96
      KTH(9)=106
      KTH(10)=116
      DO J=1,9
      AJ=J
      IF(AJ.EQ.1)THEN
      AJ=AJ+1E-4
      ELSE
      AJ=AJ
      END IF
      R1(J)=90*(COSD(AJ*10)/SIND(AJ*10))
      R2(J)=90*(COSD((AJ-1)*10)/SIND((AJ-1)*10))
      R(J)=0.5*(R1(J)+R2(J))
      DR(J)=R2(J)-R1(J)
      AREA(J)=2*PI*R(J)*DR(J)*0.3333
      END DO
      RFILE='R'//FLNM(1)(2:3)//FLNM(1)(6:7)//FLNM(ILF)(2:3)//
     *FLNM(ILF)(6:7)
      OPEN(UNIT=2,FILE=RFILE,FORM='FORMATTED',STATUS='NEW')
```

```
      WRITE(2,'(X,A9)')RFILE
      WRITE(2,'(X,A6,2X,10(3X,I3))')'THRESH',(KTH(K),K=1,10)
      DO J=1,9
      MIDALT(J)=(10*(J-1))+5
      END DO
      IF(NAS.EQ.'Y')THEN
      DO I=1,3
      MIDAZ(I)=(30*(I-1))+15
      END DO
      ELSE
      DO I=1,12
        IF(I.LE.6)THEN
        MIDAZ(I)=(30*(I-1))+15
        ELSE
        MIDAZ(I)=(30*(7-I))+15
        END IF
      END DO
      END IF
C-----------------------------------------------------------------
      DO IFL=1,1601
      IF (FLNM(IFL).EQ.'Z') STOP
      OPEN(UNIT=1,FILE='DUA1:[USER.GRAHAM]'//FLNM(IFL),
     *READONLY,FORM='FORMATTED',STATUS='OLD',IOSTAT=IOS1,ERR=99)
      READ(1,'(X,A)') FILETD
      READ(1,*)(SECLINE(I),I=1,14)
      GEN=FLNM(IFL)(6:7)
15    FRA=0
      READ(1,*,END=98)IAD,IDAY,HRS,NS,FRA,
     *IAMP,FAVE,RAVE,DMIN1,WV,ALT,AZ
      IF(IDAY.LT.IFID.OR.IDAY.GT.ILAD)GO TO 15
C     ALGORITHM FOR FAULTY CH4
      IF(GEN.EQ.'03',OR.GEN.EQ.'02')THEN
      F23=FLNM(IFL)(2:3)
      F24=FLNM(IFL)(2:4)
        IF(GEN.EQ.'03')THEN
        IF(F23.EQ.'11',OR.F23.EQ.'12',OR.F24.EQ.'09B',
     *  OR.F24.EQ.'10B',OR.F24.EQ.'13A',OR.F24.EQ.'14A')DMIN1=0.1
        END IF
        IF(GEN.EQ.'02')THEN
        IF(F23.EQ.'09',OR.F23.EQ.'10',OR.F23.EQ.'11',
     *  OR.F23.EQ.'12',OR.F24.EQ.'07B',OR.F24.EQ.'08B')DMIN1=0.1
        END IF
      END IF
C-----------------------------------------------------------------
      DAY=IDAY
      AMP=IAMP
      DO I=2,12
      IF(SECLINE(I).EQ.99)NOUTS=I-2
      END DO
      OT=NOUTS*SECLINE(1)
      OTM=OTM + ((FLOAT(NS)+76.8)/3840)
      IF(FRA.EQ.0) GOTO 15
      IHR=INT(HRS)
C-----------------------------------------------------------------
      IF(IHR0.EQ.-1)GOTO 16
      IF(IHR.NE.IHR0) THEN
      OUT=OT
      F=60/(60-OUT-OTM)
      DO K=1,10
      HR(K)=C(K)*F
```



```
      END DO
      HRL=CL*F
         IF(IHR.EQ.0) THEN
         DAY1=DAY-1
         ELSE
         DAY1=DAY
         END IF
       IF(OUT.LE.30.AND.F.LT.0)WRITE(6,'(X,I3,X,A,X,I2,X,A)')
     *DAY1,'HOUR',IHR0,'NEGATIVE RATE'
       IF(DAY1.GE.IFID.AND.DAY1.LE.ILAD)
     *WRITE(2,'(X,F4.0,X,I2,X,11(X,F5.1))')
     *DAY1,IHR0,(HR(K),K=1,10),HRL
       IF(NAS.EQ.'N')THEN
       LETZT=12
       ELSE
       LETZT=3
       END IF
       IF(ANS.EQ.'Y'.AND.OUT.LE.30)THEN
       DO I=1,LETZT
       DO J=1,9
       DO K=1,10
       RBIN(K,J,I)=AMPBIN(K,J,I)*F
       END DO
       CPSQK(J,I)=CAZALT(J,I)/AREA(J)
       HRSQK(J,I)=CPSQK(J,I)*F*1E5
       IF(CAZALT(J,I).NE.0)WRITE(2,'(X,A3,X,I5,X,A3,X,I5,X,
     *10(X,F5.1),X,F7.2)')'AZ',MIDAZ(I),'ALT',
     *MIDALT(J),(RBIN(K,J,I),K=1,10),HRSQK(J,I)
       END DO
       END DO
       WHR=INT(WESTAZ*F)
       EHR=INT(EASTAZ*F)
       DO N=1,11
       FISH(N)=0.0
       END DO
       WRITE(2,'(X,A3,2X,I4,X,A3,2X,I4,X,10(X,F5.1),X,F7.2)')
     *'WES',WHR,'EAS',EHR,(FISH(N),N=1,11)
       END IF
       OTM=0
       OT3=0
16     DO I=1,12
       DO J=1,9
       DO K=1,10
       AMPBIN(K,J,I)=0
       END DO
       CAZALT(J,I)=0
       END DO
       END DO
       DO K=1,10
       C(K)=0
       END DO
       CL=0
       EASTAZ=0
       WESTAZ=0
       END IF
C-----------------------------------------------------------------
       IF(IHR0.EQ.-1)GOTO 45
       HRS1=HRS0+((76.8+NS0)/230400)
       DHRS=HRS-HRS1
45     IF(DHRS.GT..0005.OR.IHR0.EQ.-1)THEN
```

```
          DO K=1,10
          IF(AMP.GE.KTH(K))C(K)=C(K)+1
          END DO
          IF(ABS(DMIN1).GE.0.050.OR.ANS.EQ.'N')GO TO 46
          IF(AZ.GT.0.AND.AZ.LT.90)AZNEW=AZ
          IF(AZ.GT.90)AZNEW=180-AZ
          IF(AZ.LT.0.AND.AZ.GT.-90)AZNEW=-AZ
          IF(AZ.LT.-90)AZNEW=180+AZ
          IF(NAS.EQ.'Y')I=INT(AZNEW/30)+1
          J=INT(0.1*ALT)+1
          IF(AZ.GT.0)THEN
          EASTAZ=EASTAZ+1
          IF(NAS.EQ.'N')I=INT(AZ/30)+1
          ELSE
          WESTAZ=WESTAZ+1
          IF(NAS.EQ.'N')I=INT(ABS(AZ/30))+7
          END IF
          CAZALT(J,I)=CAZALT(J,I)+1
          DO K=1,10
          IF(AMP.GE.KTH(K))AMPBIN(K,J,I)=AMPBIN(K,J,I)+1
          END DO
46        FLAG=1
          ELSE
          IF(FLAG.EQ.1)CL=CL+1
          WRITE(6,'(X,A,X,I5)')'ADDRESS',IAD0
          FLAG=0
          END IF
50        HRS0=HRS
          NS0=NS
          IHR0=INT(HRS0)
          IAD0=IAD
          GO TO 15
C-------------------------------------------------------------
1000      END DO
99        IF(IOS1.EQ.29)THEN
          WRITE(6,'(X,A,A)')FLNM(IFL), 'NOT FOUND.'
          ELSE
          WRITE(6,'(X,A,I2)')'ERR NO ',IOS1
          END IF
          GO TO 1000
98        CLOSE(UNIT=1)
          GO TO 1000
          END
```



```
          PROGRAM AVRATE1
C         ==============
C         AVERAGE HOURLY METEOR RATES AND STD DEV OF THE MEAN. DOES NO
C         PLOTTING BUT GENERATES AN A-FILE.
C
C         Written by David G. Roux, September 1986.
C
          DIMENSION ARRAY(11,0:23),R(11),C(0:23),AVER(11,0:23),
         *SQ(11,0:23),SD(11,0:23)
          CHARACTER RFILE*9,AVFILE*12,SCRATCH*9,ZONK*120,G1*1,G2*2,RFILEL*16
          WRITE(6,'(X,A25)')'NAME OF RFILE? (9 DIGITS)'
          READ(5,'(A9)')RFILE
          WRITE (6,'(X,A)')RFILE
          OPEN(UNIT=1,FILE=RFILE,FORM='FORMATTED',STATUS='OLD')
          DO I=0,23
          DO J=1,11
          ARRAY(J,I)=0
          AVER(J,I)=0
          SQ(J,I)=0
          R(J)=0
          END DO
          C(I)=0
          END DO
          READ(1,'(A)')SCRATCH
          READ(1,'(A)')ZONK
10        READ(1,*,END=20)IDAY,IHR,(R(J),J=1,11)
          DO J=1,11
          ARRAY(J,IHR)=ARRAY(J,IHR)+R(J)
          SQ(J,IHR)=SQ(J,IHR)+R(J)**2
          END DO
          C(IHR)=C(IHR)+1
          GO TO 10
20        AVFILE='A'//RFILE(2:9)
          WRITE(6,'(X,A)')AVFILE
          OPEN(UNIT=2,FILE=AVFILE,FORM='FORMATTED',STATUS='NEW')
          WRITE(2,'(X,A12)')AVFILE
          WRITE(2,'(X,A)')ZONK
          DO I=0,23
          DO J=1,11
          IF(C(I).EQ.0)THEN
          AVER(J,I)=0
          SD(J,I)=0
          ELSE
          AVER(J,I)=ARRAY(J,I)/C(I)
          IF(C(I).NE.1)THEN
          SD(J,I)=((SQ(J,I)/(C(I)*(C(I)-1)))-(AVER(J,I)**2/(C(I)-1)))**0.5
          ELSE
          SD(J,I)=SQRT(AVER(J,I))
          END IF
          END IF
          END DO
          INEW=I+1
          WRITE(2,'(X,I2,X,11(X,F5.1))')INEW,(AVER(J,I),J=1,11)
          WRITE(2,'(4X,11(X,F5.1))')(SD(J,I),J=1,11)
          WRITE(3,'(X,I2,X,11(X,F8.1))')INEW,(ARRAY(J,I),J=1,11)
          WRITE(4,'(X,F5.0)')C(I)
          END DO
          STOP
          END
```

```
      PROGRAM AVRATE2
C     ===============
C
C     AVERAGE HOURLY METEOR RATES OVER SEVERAL DAYS AND DISTRIBUTED
C     ABOVE 10 THRESHOLD AMPLITUDES (1)FOR ALL ECHO DIRECTIONS AND
C     (2)WITHIN EACH LUMPED OR UNLUMPED AZALT BIN.
C
C     Written by David G. Roux, Grahamstown, 1987.
C
      DIMENSION ARRAY(11,0:23),BALT(9),BAZ(12),B(11),R(11),C(0:23),
     *SQ(11,0:23),SD(11,0:23),BARRAY(11,9,12,0:23),
     *SQWR(0:23),SQER(0:23),BAVER(11,9,12,0:23),SDB(11,9,12,0:23),
     *SQB(11,9,12,0:23),AVW(0:23),AVE(0:23),SDWR(0:23),SDER(0:23),
     *AVER(11,0:23),SUMWR(0:23),SUMER(0:23),W(11,0:23),X(0:23),
     *Y(0:23),Z(11,9,12,0:23),LUMPAMP(11,9,12),CK(0:23),CC(0:23),
     *SQAVER(11,0:23)
      CHARACTER RFILE*9,AVFILE*12,SCRATCH*9,ZONK*120,
     *ZA*3,TLA*3,ANS*1,SNA*1
      INTEGER H,BAZ,BALT,AZ,ALT
      WRITE(6,'(X,A25)')'NAME OF RFILE? (9 DIGITS)'
      READ(5,'(A9)')RFILE
      WRITE(6,'(X,A)')'HAVE ALTAZ BINS BEEN GENERATED IN THE RFILE?
     *(Y/N)'
      READ(5,'(A1)')SNA
      WRITE(6,'(X,A)')'LUMP TOGETHER THE HOURS FOR AMP. DISTR.?
     *(Y/N)'
      READ(5,'(A1)')ANS
      OPEN(UNIT=1,FILE=RFILE,FORM='FORMATTED',STATUS='OLD')
      DO I=0,23
      DO J=1,11
      ARRAY(J,I)=0
      AVER(J,I)=0
      SQ(J,I)=0
      R(J)=0
      END DO
      C(I)=0
      END DO
      DO H=0,23
      DO I=1,3
      DO J=1,9
      DO K=1,11
      BARRAY(K,J,I,H)=0
      SQB(K,J,I,H)=0
      LUMPAMP(K,J,I)=0
      END DO
      END DO
      END DO
      SUMWR(H)=0
      SUMER(H)=0
      SQWR(H)=0
      SQER(H)=0
      END DO
      READ(1,'(A)')SCRATCH
      READ(1,'(A)')ZONK
10    READ(1,*,END=20)IDAY,IHR,(R(J),J=1,11)
      C(IHR)=C(IHR)+1
      DO J=1,11
      ARRAY(J,IHR)=ARRAY(J,IHR)+R(J)
      SQ(J,IHR)=SQ(J,IHR)+R(J)**2
```



```
      END DO
      IF(SNA.EQ.'Y')THEN
15    READ(1,'(X,A3,2X,I4,X,A3,2X,I4,X,10(X,F5.1),X,F7.2)')
     *ZA,AZ,TLA,ALT,(B(K),K=1,11)
      IF(ZA.EQ.'WES')THEN
      SUMWR(IHR)=SUMWR(IHR)+AZ
      SUMER(IHR)=SUMER(IHR)+ALT
      SQWR(IHR)=SQWR(IHR)+AZ**2
      SQER(IHR)=SQER(IHR)+ALT**2
      GO TO 10
      ELSE
        IF(AZ.GE.0)THEN
        I=((AZ-15)/30)+1
        ELSE
        I=7-((AZ+15)/30)
        END IF
      J=((ALT-5)/10)+1
      DO K=1,11
      BARRAY(K,J,I,IHR)=BARRAY(K,J,I,IHR)+B(K)
      SQB(K,J,I,IHR)=SQB(K,J,I,IHR)+B(K)**2
      END DO
      END IF
      IF(ZA.EQ.'WES')THEN
      GO TO 10
      ELSE
      GO TO 15
      END IF
      ELSE
      GO TO 10
      END IF
20    AVFILE='A'//RFILE(2:9)
      OPEN(UNIT=2,FILE=AVFILE,FORM='FORMATTED',STATUS='NEW')
      WRITE(2,'(X,A)')AVFILE
      WRITE(2,'(X,A)')ZONK
      DO I=0,23
      DO J=1,11
      IF(C(I).EQ.0)THEN
      AVER(J,I)=0
      SD(J,I)=999
      AVW(I)=0
      AVE(I)=0
      SDWR(I)=999
      SDER(I)=999
      ELSE
      AVER(J,I)=ARRAY(J,I)/C(I)
      AVW(I)=SUMWR(I)/C(I)
      AVE(I)=SUMER(I)/C(I)
      IF(C(I).NE.1)THEN
      CK(I)=C(I)-1
      CC(I)=C(I)*(C(I)-1)
      SQAVER(J,I)=AVER(J,I)**2
      W(J,I)=(SQ(J,I)/(C(I)*(C(I)-1)))-
     *(AVER(J,I)**2/(C(I)-1))
      SD(J,I)=W(J,I)**0.5
      X(I)=(SQWR(I)/(C(I)*(C(I)-1)))-
     *(AVW(I)**2/(C(I)-1))
      SDWR(I)=X(I)**0.5
      Y(I)=(SQER(I)/(C(I)*(C(I)-1)))-
     *(AVE(I)**2/(C(I)-1))
      SDER(I)=Y(I)**0.5
```

```
 ELSE
 SD(J,I)=999
 SDWR(I)=999
 SDER(I)=999
 END IF
 END IF
 END DO
 IF(SNA.EQ.'Y')THEN
 WRITE(2,'(X,I2,2(X,A,X,F5.1),X,11(X,F5.1))')I,
*'WEST RATE',AVW(I),'EAST RATE',AVE(I),(AVER(J,I),J=1,11)
 WRITE(2,'(14X,F5.1,11X,F5.1,X,11(X,F5.1))')SDWR(I),
*SDER(I),(SD(J,I),J=1,11)
 WRITE(4,'(X,I2,X,F5.0)')I,C(I)
 WRITE(3,'(X,I2,X,13(X,F6.1))')I,X(I),Y(I),(W(J,I),J=1,11)
 WRITE(7,'(X,I2,X,13(X,F7.0))')I,CC(I),CK(I),(SQAVER(J,I),
*J=1,11)
 WRITE(7,'(20X,11(X,F7.0))')(SQ(J,I),J=1,11)
 ELSE
 WRITE(2,'(X,I2,11(X,F5.1))')I,(AVER(J,I),J=1,11)
 END IF
 END DO
 IF(ANS.EQ.'Y')THEN
 DO I=1,3
    IF(I.LT.6)THEN
    BAZ(I)=(30*(I-1))+15
    ELSE
    BAZ(I)=(30*(7-I))-15
    END IF
 DO J=1,9
 DO K=1,11
 DO H=0,23
 LUMPAMP(K,J,I)=LUMPAMP(K,J,I)+BARRAY(K,J,I,H)
 END DO
 END DO
 BALT(J)=(10*(J-1))+5
 WRITE(2,'(X,A,X,I4,X,A,X,I2,X,11(X,I6))')'AZ',BAZ(I),'ALT',
*BALT(J),(LUMPAMP(K,J,I),K=1,11)
 END DO
 END DO
 ELSE
 DO H=0,23
 DO I=1,3
 DO J=1,9
 DO K=1,11
 IF(C(H).EQ.0)THEN
 BAVER(K,J,I,H)=0
 SDB(K,J,I,H)=999
 ELSE
 BAVER(K,J,I,H)=BARRAY(K,J,I,H)/C(H)
 IF(C(H).NE.1)THEN
 Z(K,J,I,H)=(SQB(K,J,I,H)/(C(H)*(C(H)-1)))-
*(BAVER(K,J,I,H)**2/(C(H)-1))
 SDB(K,J,I,H)=Z(K,J,I,H)**0.5
 ELSE
 SDB(K,J,I,H)=999
 END IF
 END IF
 END DO
 IF(I.LE.6)THEN
 BAZ(I)=(30*(I-1))+15
```



```
 ELSE
 BAZ(I)=(30*(7-I))-15
 END IF
 BALT(J)=(10*(J-1))+5
 IF(BAVER(11,J,I,H).NE.0.AND.SNA.EQ.'Y')THEN
 WRITE(2,'(X,I2,X,A,X,I4,X,A,X,I2,X,11(X,F5.1))')H,'AZ',
*BAZ(I),'ALT',BALT(J),(BAVER(K,J,I,H),K=1,11)
 WRITE(2,'(9X,A,8X,11(X,F5.1))')'SD',(SDB(K,J,I,H),K=1,11)
 WRITE(3,'(X,11(X,F8.1))')(Z(K,J,I,H),K=1,11)
 ELSE
 CONTINUE
 END IF
 END DO
 END DO
 END DO
 END IF
 STOP
 END
```

```
      PROGRAM AVPLOT
C     ==============
C     AVERAGE HOURLY METEOR RATE PLOTTING PROGRAM
C     Accepts data of uniform format from an R-file.
C     Written by David G. Roux, 1986.
C     Revised by D.G.R., 29 December 1987. Renamed AVPLOT on
C     January 6 1988.
      DIMENSION ARRAY(11,24),R(11),C(24),AVER(11,24),
     *SQ(11,24),SD(11,24),FK1(24),FK2(24)
      CHARACTER RFILE*9,SCRATCH*9,ZONK*120
      REAL X(30),Y(30),E(30),LHS
      LOGICAL DAVID
C-----------------------------------------------------------------------
      YMAX=0
7     WRITE(6,'(X,A25)')'NAME OF RFILE? (9 DIGITS)'
      READ(5,'(A9)')RFILE
      IF(RFILE.EQ.'Z')STOP
      WRITE(6,'(X,A)')'PLOT (1)AV HR RATE ABOVE AMP. LEVEL K2; LEVEL
     *K1, OR PLOT (2) AV HR RATE ABOVE A SINGLE LEVEL? (ENTER1/2)'
      READ(5,*)ANS
      IF(ANS.EQ.2)THEN
      WRITE(6,'(X,A)')'PLOT GRAPH OF ECHOES ABOVE LEVEL K; ENTER K'
      READ(5,*)K
      ELSE
      WRITE(6,'(X,A)')'PLOT HR ABOVE LEVEL K2; HR ABOVE LEVEL K1.
     *ENTER K2,K1'
      READ(5,*)K2,K1
      END IF
      WRITE(6,'(X,A)')'Enter Y-axis scale'
      READ(5,*)YSCAL
      VSCAL=1/YSCAL
      CALL START_PLOT(DAVID)
      OPEN(UNIT=1,FILE=RFILE,FORM='FORMATTED',STATUS='OLD')
      DO I=1,24
      DO J=1,11
      ARRAY(J,I)=0
      AVER(J,I)=0
      SQ(J,I)=0
      R(J)=0
      END DO
      C(I)=0
      END DO
      READ(1,'(A)')SCRATCH
      READ(1,'(A)')ZONK
10    READ(1,*,END=20)IDAY,IHR,(R(J),J=1,11)
      IHR=IHR+1
      DO J=1,11
      ARRAY(J,IHR)=ARRAY(J,IHR)+R(J)
      SQ(J,IHR)=SQ(J,IHR)+R(J)**2
      END DO
      C(IHR)=C(IHR)+1
      GO TO 10
20    DO I=1,24
      DO J=1,11
      IF(C(I).EQ.0)THEN
      AVER(J,I)=0
      SD(J,I)=SQRT(AVER(J,I))
      ELSE
      AVER(J,I)=ARRAY(J,I)/C(I)
      IF(C(I).NE.1)THEN
```



```
      SD(J,I)=((SQ(J,I)/(C(I)*(C(I)-1)))-(AVER(J,I)**2/(C(I)-1)))**0.5
      ELSE
      SD(J,I)=SQRT(AVER(J,I))
      END IF
      END IF
      END DO
      X(I)=I-0.5
      IF(ANS.EQ.2)THEN
      Y(I)=AVER(K,I)
      E(I)=SD(K,I)
      ELSE
      IF(AVER(K1,I).NE.0)Y(I)=AVER(K2,I)/AVER(K1,I)
      IF(AVER(K1,I).NE.0)FK1(I)=SD(K1,I)/AVER(K1,I)
      IF(AVER(K2,I).NE.0)FK2(I)=SD(K2,I)/AVER(K2,I)
      E(I)=((FK1(I)**2+FK2(I)**2)**0.5)*Y(I)
      END IF
      WRITE(6,*)X(I),Y(I),E(I)
      END DO
      DO I=1,24
      IF(Y(I).GE.YMAX)YMAX=Y(I)
      END DO
C     START PLOTTING ROUTINE
      CALL FACTOR(0.7)
      CALL PLOT(1.0,1.0,-3)
      IF(ANS.EQ.2)THEN
      DIV=YMAX/YSCAL
      TOP=INT(DIV)+1
      FTOP=TOP*YSCAL
      BTOP=TOP+1
      X(25)=0.0
      X(26)=1.0
      Y(25)=0.0
      Y(26)=YSCAL
      CALL AXIS(0.0,0.0,'SAST',-4,24.0,0.0,0.0,1.0)
      CALL AXIS(0.0,0.0,'AVRATE',6,TOP,90.0,0.0,YSCAL)
      CALL LINE(X,Y,24,1,1,6)
      DO I=24,2,-2
      LHS=X(I)-0.2
      RHS=X(I)+0.2
      YU=VSCAL*(Y(I)+E(I))
      YL=VSCAL*(Y(I)-E(I))
      IF(YL.GT.0.AND.YU.LT.90)THEN
      CALL PLOT(LHS,YL,3)
      CALL PLOT(RHS,YL,2)
      CALL PLOT(X(I),YL,3)
      CALL PLOT(X(I),YU,2)
      CALL PLOT(LHS,YU,3)
      CALL PLOT(RHS,YU,2)
      END IF
      END DO
      ELSE
      DIV=YMAX/YSCAL
      TOP=INT(DIV)+1
      BTOP=TOP+1
      X(25)=0.0
      X(26)=1.0
      Y(25)=0.0
      Y(26)=YSCAL
      CALL AXIS(0.0,0.0,'SAST',-4,24.0,0.0,0.0,1.0)
      CALL AXIS(0.0,0.0,'FRACTION OF LONG ECHOES',23,
```

```
*TOP,90.0,0.0,YSCAL)
 CALL LINE(X,Y,24,1,1,4)
 DO I=24,2,-2
 LHS=X(I)-0.2
 RHS=X(I)+0.2
 YU=VSCAL*(Y(I)+E(I))
 YL=VSCAL*(Y(I)-E(I))
 IF(YL.GT.-10)THEN
 CALL PLOT(LHS,YL,3)
 CALL PLOT(RHS,YL,2)
 CALL PLOT(X(I),YL,3)
 CALL PLOT(X(I),YU,2)
 CALL PLOT(LHS,YU,3)
 CALL PLOT(RHS,YU,2)
 END IF
 END DO
 END IF
 CALL PLOT(-1.0,-1.0,3)
 CALL PLOT(-1.0,BTOP,2)
 CALL PLOT(24.2,BTOP,2)
 CALL PLOT(24.2,-1.0,2)
 CALL PLOT(-1.0,-1.0,2)
 CALL END_PLOT
 CLOSE(UNIT=1)
 STOP
 END
```



```
      PROGRAM DIFFPLOT
C     ================
C-----SUBTRACTS SPORADIC BACKGROUND HOURLY RATES FROM SHOWER HOURLY RATES
C
C     Written by David G. Roux, Ght, 1986.
C
      DIMENSION DIFFER(11,24),R1(11),R2(11),SD1(11),SD2(11),SD(11,24)
      CHARACTER FILE1*19,FILE2*19,SCRATCH1*19,SCRATCH2*19,
     *ZONK1*120,ZONK2*120
      REAL X(30),Y(30),E(24),LHS
      LOGICAL DAVE
      YMAX=0
5     WRITE(6,'(X,A27)')'NAME OF AVFILE1? (9 DIGITS)'
      READ(5,'(A)')FILE1
      IF(FILE1.EQ.'Z')STOP
      WRITE(6,'(X,A27)')'NAME OF AVFILE2? (9 DIGITS)'
      READ(5,'(A)')FILE2
      WRITE(6,'(X,A)')'PLOT ECHOES ABOVE THE KTH LEVEL; ENTER K'
      READ(5,*)K
      CALL START_PLOT(DAVE)
      OPEN(UNIT=1,FILE=FILE1,FORM='FORMATTED',STATUS='OLD')
      OPEN(UNIT=2,FILE=FILE2,FORM='FORMATTED',STATUS='OLD')
      DO I=1,24
      DO J=1,11
      DIFFER(J,I)=0
      SD(J,I)=0
      END DO
      END DO
      READ(1,'(A)')SCRATCH1
      READ(1,'(A)')ZONK1
      READ(2,'(A)')SCRATCH2
      READ(2,'(A)')ZONK2
      WRITE(3,'(A)')ZONK1
10    READ(1,*,END=15)I,(R1(J),J=1,11)
      READ(1,*)(SD1(J),J=1,11)
15    READ(2,*,END=20)I,(R2(J),J=1,11)
      READ(2,*)(SD2(J),J=1,11)
      DO J=1,11
      DIFFER(J,I)=R1(J)-R2(J)
      SD(J,I)=SD1(J)+SD2(J)
      END DO
      X(I)=I-0.5
      Y(I)=DIFFER(K,I)
      E(I)=SD(K,I)
      WRITE(6,*)X(I),Y(I),E(I)
      GO TO 10
20    DO I=1,24
      IF(Y(I).GE.YMAX)YMAX=Y(I)
      END DO
      DIV=YMAX/5
      TOP=INT(DIV)+5
      BTOP=TOP-2
C     START PLOTTING ROUTINE
      CALL FACTOR(0.7)
      CALL PLOT(1.0,5.0,-3)
      X(25)=0.0
      X(26)=1.0
      Y(25)=0.0
      Y(26)=5.0
      CALL AXIS(0.0,0.0,' ',-1,24.0,0.0,0.0,1.0)
```

```
      CALL AXIS(0.0,-4.0,' ',1,TOP,90.0,-20.0,5.0)
      CALL LINE(X,Y,24,1,1,6)
      DO I=23,1,-2
      LHS=X(I)-0.1
      RHS=X(I)+0.1
      YU=0.2*(Y(I)+E(I))
      YL=0.2*(Y(I)-E(I))
      IF(YL.GT.-19)THEN
      CALL PLOT(LHS,YL,3)
      CALL PLOT(RHS,YL,2)
      CALL PLOT(X(I),YL,3)
      CALL PLOT(X(I),YU,2)
      CALL PLOT(LHS,YU,3)
      CALL PLOT(RHS,YU,2)
      END IF
      END DO
      CALL PLOT(-1.0,-5.0,3)
      CALL PLOT(-1.0,BTOP,2)
      CALL PLOT(24.5,BTOP,2)
      CALL PLOT(24.5,-5.0,2)
      CALL PLOT(-1.0,-5.0,2)
      CALL END_PLOT
      CLOSE(UNIT=1)
      CLOSE(UNIT=2)
      STOP
      END
```



```
      PROGRAM EASTWEST
C     =================
C     Plots either (a) West rate - east rate; or
C                  (b) West and east rates superimposed.
C     Input must be of non-uniform format (contain azalt bins),
C     and is the output of RATE.
C     Written by David Roux, December 1986.
C     Revised by D.G.R., December 1987.
      DIMENSION C(24),Y(24),
     *SQWR(24),SQER(24),SUMWR(24),SUMER(24),W(11,24),X(24),
     *AVW(24),AVE(24),SDWR(24),SDER(24)
      CHARACTER RFILE*9,SCRATCH*9,ZONK*120,
     *ZA*3,TLA*3,ANS*1
      INTEGER H,AZ,ALT
      REAL DX(26),DY(26),LHS,EXY(24)
      DYMAX=0
      DYMIN=0
      LINTYPE=1
      FLAG=0
7     WRITE(6,'(X,A25)')'NAME OF RFILE? (9 DIGITS)'
      READ(5,'(A9)')RFILE
      IF(RFILE.EQ.'Z')STOP
      WRITE(6,'(X,A)')'Plot difference (W-E), or W and E rates? (D,W)'
      READ(5,'(A)')ANS
      OPEN(UNIT=1,FILE=RFILE,FORM='FORMATTED',STATUS='OLD')
      DO I=1,24
      C(I)=0
      END DO
      DO H=1,24
      SUMWR(H)=0
      SUMER(H)=0
      SQWR(H)=0
      SQER(H)=0
      END DO
      READ(1,'(A)')SCRATCH
      READ(1,'(A)')ZONK
10    READ(1,*,END=20)IDAY,IHR
      IHR=IHR+1
      C(IHR)=C(IHR)+1
15    READ(1,'(X,A3,2X,I4,X,A3,2X,I4)')
     *ZA,AZ,TLA,ALT
      IF(ZA.EQ.'WES')THEN
      SUMWR(IHR)=SUMWR(IHR)+AZ
      SUMER(IHR)=SUMER(IHR)+ALT
      SQWR(IHR)=SQWR(IHR)+AZ**2
      SQER(IHR)=SQER(IHR)+ALT**2
      GO TO 10
      END IF
      IF(ZA.EQ.'WES')THEN
      GO TO 10
      ELSE
      GO TO 15
      END IF
20    DO I=1,24
      DO J=1,11
      IF(FLAG.EQ.0)THEN
      IF(C(I).EQ.0)THEN
      AVW(I)=0
      AVE(I)=0
      SDWR(I)=0
```

```
      SDER(I)=0
      ELSE
      AVW(I)=SUMWR(I)/C(I)
      AVE(I)=SUMER(I)/C(I)
      IF(C(I).NE.1)THEN
      X(I)=(SQWR(I)/(C(I)*(C(I)-1)))-
     *(AVW(I)**2/(C(I)-1))
      SDWR(I)=X(I)**0.5
      Y(I)=(SQER(I)/(C(I)*(C(I)-1)))-
     *(AVE(I)**2/(C(I)-1))
      SDER(I)=Y(I)**0.5
      ELSE
      SDWR(I)=0
      SDER(I)=0
      END IF
      END IF
      END IF
      END DO
      IF(ANS.EQ.'D')THEN
      DY(I)=AVW(I)-AVE(I)
      EXY(I)=(SDWR(I)**2+SDER(I)**2)**0.5
      END IF
100   IF(ANS.EQ.'W')THEN
      IF(FLAG.EQ.0)THEN
      DY(I)=AVW(I)
      EXY(I)=SDWR(I)
      INTEQ=6
      ELSE
      DY(I)=AVE(I)
      EXY(I)=SDER(I)
      INTEQ=3
      LINTYPE=-1
      END IF
      END IF
      DX(I)=I-0.5
      IF(DY(I).GE.DYMAX)DYMAX=DY(I)
      IF(DY(I).LT.DYMIN)DYMIN=DY(I)
      END DO
      IF(FLAG.EQ.1)ANS='A'
      DIV=DYMAX/3
      TOP=INT(DIV)+1
      BTOP=TOP+1
      BDIV=DYMIN/3
      IF(ANS.EQ.'D')THEN
      BOT=INT(BDIV)-1
      ELSE
      BOT=0
      END IF
      YORIG=-1*(BOT-1)
      BBOT=-1*YORIG
      AXLEN=TOP-BOT
      FVAL=BOT*3
C     START OF PLOTTING ROUTINE
      CALL EPSPLOT(UNIT 3,'X')
      CALL FACTOR(0.7)
      CALL PLOT(1.0,YORIG,-3)
      DX(25)=0.0
      DX(26)=1.0
      DY(25)=0.0
      DY(26)=3.0
```



```
      CALL LINE(DX,DY,24,1,LINTYPE,INTEQ)
      DO I=24,2,-2
      LHS=DX(I)-0.1
      RHS=DX(I)+0.1
      YU=0.33*(DY(I)+EXY(I))
      YL=0.33*(DY(I)-EXY(I))
      CALL PLOT(LHS,YL,3)
      CALL PLOT(RHS,YL,2)
      CALL PLOT(DX(I),YL,3)
      CALL PLOT(DX(I),YU,2)
      CALL PLOT(LHS,YU,3)
      CALL PLOT(RHS,YU,2)
      END DO
      FLAG=1
      IF(ANS.EQ.'W')GO TO 20
      CALL AXIS(0.0,0.0,'SAST',-4,24.0,0.0,0.0,1.0)
      CALL AXIS(0.0,BOT,'RATE',4,AXLEN,90.0,FVAL,3.0)
      CALL PLOT(-1.0,BBOT,3)
      CALL PLOT(-1.0,BTOP,2)
      CALL PLOT(25.0,BTOP,2)
      CALL PLOT(25.0,BBOT,2)
      CALL PLOT(-1.0,BBOT,2)
      CALL ENDPLOT
      CLOSE (UNIT 1)
      STOP
      END
```

```
      PROGRAM OWL
C     ===========
C     So - called because the first graph looked like an owl.
C     Plots to EPSON graphs of theoretical rate and  of
C     observed rate of major showers.
C     Written by David Roux, Jan.1987.
      CHARACTER UO*1,ANS*1,SNA*2
      DIMENSION RO(-36:36,44)
      COMMON /CCOORD/ SBO, CBO, SBP, CBP, SB1, CB1, AO, AP, A1
      REAL X(200),YU(200),YO(200),XX(30),YY(30),EE(30),
     *PX(200),PYU(200),PYO(200),PXX(30),PYY(30),PEE(30),LHS
      LOGICAL DAVE
      PI=3.14159
      OPEN(UNIT=1,FILE='RHO',FORM='FORMATTED',STATUS='OLD')
      DO 100 IC=1,44
      READ(1,*) Z,(RO(IA,IC),IA=0,18)
       DO 100 IA=0,18
       RO(-IA,IC)=RO(IA,IC)
       RO(36-IA,IC)=RO(IA,IC)
100    RO(IA-36,IC)=RO(IA,IC)
      SBO=0.8358
      CBO=0.5490
      SBP=-0.5490
      CBP=0.8358
250   WRITE(6,'(X,A)')'ENTER STATRTING TIME (INTEGRAL HOUR)'
      READ(5,*)ST
      WRITE(6,'(X,A)')
     *'ENTER TIME OF RADIANT TRANSIT, DECLINATION. (HOURS, DEGREES)'
      READ(5,*)T,DEC
      TH=3E-12
      S=1.8
      WRITE(6,'(X,A)')
     *'PLOT WHICH OF THE FOLLOWING: UNDERDENSE (UN)? OR OVERDENSE (OV)?'
      READ(5,'(A2)')SNA
      CALL START_PLOT(DAVE)
      SB1=SIND(DEC)
      CB1=COSD(DEC)
      AO=0
      AP=0
      IF(SNA.EQ.'UN')UO='U'
      IF(SNA.EQ.'OV')UO='O'
      DD=0.25
      NPTS=(24/DD)+1
350   RMAX=0
      DO N=1,97
      X(N)=(N-1)*DD
      TRT=X(N)-T
      IF(TRT.LT.-12.0)TRT=TRT+24
      IF(TRT.GT.12.0)TRT=TRT-24
      A1=TRT*15
      CALL COORD(A2,B2)
      IF(B2.LE.015)THEN
      RATE=0
      GO TO 550
      END IF
      CHI=90-B2
      AR=A2
      E=S-1
      EX=E
      IF (UO.EQ.'O') EX=4*E
```



```
      CCE=COSD(CHI)**E
      SC=SIND(CHI)
      F2=CCE/SQRT(SC*SC+.0313)
      F1=7E3*TH*(1+1.25/E)
      EL=0
      F3=0
      A=AR+95
      PHI=-90
      IAS=NINT(A/5)
      IAF=IAS+34
      TCHI=TAND(CHI)
       DO J=IAS,IAF
       JAG=J
       IF(I.LT.-36) JAG=I+72
       IF(I.GT.36) JAG=I-72
       IF(I.LT.-108)JAG=I+144
       IF(I.GT.108) JAG=I-144
       PHI=PHI+5
       CDA=COSD(PHI)
       TC=TCHI*CDA
       C=ATAN(TC)
       IC=NINT(90*C/PI)
       CDA1=COSD(PHI-2.5)
       CDA2=COSD(PHI+2.5)
       TC1=TCHI*CDA1
       TC2=TCHI*CDA2
       C1=ATAN(TC1)
       C2=ATAN(TC2)
       CC1=COS(C1)
       CC2=COS(C2)
       SC1=SIN(C1)
       SC2=SIN(C2)
       RS1=(1E5*(SQRT(4225-4096*CC1*CC1)-64*SC1))*CC1
       RS2=(1E5*(SQRT(4225-4096*CC2*CC2)-64*SC2))*CC2
       DL=SQRT(RS1**2+RS2**2-1.9924*RS1*RS2)
       EL=EL+DL
       F3=F3+(RO(IA,IC)**EX)*DL
110   END DO
      RATE=3600*F1*F2*F3
      IF(RATE.GT.RMAX)RMAX=RATE
550   IF(UO.EQ.'U')YU(N)=RATE
      IF(UO.EQ.'O')YO(N)=RATE
      END DO
      DO M=1,NPTS
      IF(UO.EQ.'U')YU(M)=YU(M)/RMAX
      IF(UO.EQ.'O')YO(M)=YO(M)/RMAX
      END DO
      CLOSE(UNIT=1)
      CALL GANJA(XX,YY,EE)
      OFF=ST-1
      DO I=1,24
      K=I+OFF
      IF(K.GT.24)THEN
      K=K-24
      PXX(I)=XX(K)+24
      PYY(I)=YY(K)
      PEE(I)=EE(K)
      ELSE
      PXX(I)=XX(K)
      PYY(I)=YY(K)
```

```
      PEE(I)=EE(K)
      END IF
      END DO
      DO I=1,97
      K=(ST/DD)+I
      IF(K.GT.97)THEN
      K=K-96
      PX(I)=X(K)+24
      ELSE
      PX(I)=X(K)
      END IF
      PYU(I)=YU(K)
      PYO(I)=YO(K)
      WRITE(6,'(X,A,X,A,I3,3(X,F6.2))')'THEOR:','I=',I,PX(I),
     *PYU(I),PYO(I)
      END DO
      DO L=1,30
      WRITE(6,'(X,A,X,A,I2,F6.2,X,F7.5)')'OBSERVED:','L=',L,PXX(L),
     *PYY(L)
      END DO
C     START PLOTTING ROUTINE (THEORETICAL RATE)
      CALL FACTOR(0.8)
      CALL PLOT(1.0,3.0,-3)
      ST=ST-1
      PX(NPTS+1)=ST
      PX(NPTS+2)=1.0
      PYU(NPTS+1)=0.0
      PYU(NPTS+2)=0.1
      PYO(NPTS+1)=0.0
      PYO(NPTS+2)=0.1
      CALL AXIS(0.0,0.0,'SAST',-4,24.0,0.0,ST,1.0)
      CALL AXIS(0.0,-2.0,' ',1,12.0,90.0,-0.2,0.1)
      IF(SNA.EQ.'UN')CALL LINE(PX,PYU,NPTS,1,0,1)
      IF(SNA.EQ.'OV')CALL LINE(PX,PYO,NPTS,1,0,1)
C     START PLOTTING ROUTINE (OBSERVED RATE)
      PXX(25)=ST
      PXX(26)=1.0
      PYY(25)=0.0
      PYY(26)=0.1
      CALL LINE(PXX,PYY,24,1,1,3)
      DO I=24,2,-2
      PXX(I)=PXX(I)-ST
      LHS=PXX(I)-0.2
      RHS=PXX(I)+0.2
      YUP=10*(PYY(I)+PEE(I))
      YL=10*(PYY(I)-PEE(I))
      CALL PLOT(LHS,YL,3)
      CALL PLOT(RHS,YL,2)
      CALL PLOT(PXX(I),YL,3)
      CALL PLOT(PXX(I),YUP,2)
      CALL PLOT(LHS,YUP,3)
      CALL PLOT(RHS,YUP,2)
      END DO
      CALL PLOT(-1.0,-3.0,3)
      CALL PLOT(-1.0,11.5,2)
      CALL PLOT(24.5,11.5,2)
      CALL PLOT(24.5,-3.0,2)
      CALL PLOT(-1.0,-3.0,2)
      CALL END_PLOT
      CLOSE(UNIT=1)
```



```
      STOP
      END
      SUBROUTINE COORD (A2 , B2)
C     ================
C
C     This subroutine converts the longitude-like (A1) and
C     the latitude-like (B1) coordinates of a point on a sphere
C     into the corresponding coordinates (A2,A2) in a different
C     coordinate system that is specified by the coordinates
C     of its origin (A0,B0) and its north pole (AP,BP) in
C     the original coordinate system. The range of A2 will
C     be from 0 to 360 degrees and B2 from -90 to +90 degrees.
C
C     All arguments are in degrees
C
C     Ref: Methods of Experimental Physics Vol 12 part C
C     by Meeks, p 311.
C
      COMMON /CCOORD/ SB0, CB0, SBP, CBP, SB1, CB1, A0, AP, A1
C
C     Longitude-like:A0=0,    A1=HA,  A2=az,  AP=0
C     Latitude-like: B0=56.7, B1=dec, B2=alt, BP=-33.3
        SB2 = SBP*SB1 + CBP*CB1*COSD(AP - A1)
        SB2 = MAX(-0.99999,MIN(0.99999,SB2))
        B2 = ASIND(SB2)
        CB2 = COSD(B2)
        SAA = SIND(AP - A1)*CB1/CB2
        CAA = (SB1 - SB2*SBP)/(CB2*CBP)
        CBB = SB0/CBP
        SBB = SIND(AP - A0)*CB0
        SA2 = SAA*CBB - CAA*SBB
        CA2 = CAA*CBB + SAA*SBB
        IF (CA2 .LE. 0.0) THEN
            A2 = 2.0*ATAN2D((1.0 - CA2),SA2)
          ELSE
            A2 = 2.0*ATAN2D(SA2,(1.0 + CA2))
        END IF
        IF (A2 .LE. 0.0) A2 = A2 + 360.0
        RETURN
      END
      SUBROUTINE GANJA(XX, YY, EE)
C     ============================
C     SUBTRACTS SPORADIC BACKGROUND HOURLY RATES FROM SHOWER HOURLY RATES
C     DOES PLOT ON THE SCREEN; S STANDS FOR 'SCREEN'
      DIMENSION DIFFER(11,24),R1(11),R2(11),SD1(11),SD2(11),SD(11,24)
      CHARACTER FILE1*19,FILE2*19,SCRATCH1*19,SCRATCH2*19,
     *ZONK1*120,ZONK2*120
      REAL XX(30),YY(30),EE(24),LHS
5     WRITE(6,'(X,A27)')'NAME OF AVFILE1? (9 DIGITS)'
      READ(5,'(A)')FILE1
      IF(FILE1.EQ.'Z')STOP
      WRITE(6,'(X,A27)')'NAME OF AVFILE2? (9 DIGITS)'
      READ(5,'(A)')FILE2
      WRITE(6,'(X,A)')'PLOT ECHOES ABOVE THE KTH LEVEL; ENTER K'
      READ(5,*)K
      OPEN(UNIT=1,FILE=FILE1,FORM='FORMATTED',STATUS='OLD')
      OPEN(UNIT=2,FILE=FILE2,FORM='FORMATTED',STATUS='OLD')
      DO I=1,24
      DO J=1,11
      DIFFER(J,I)=0
```

```
      SD(J,I)=0
      END DO
      END DO
      READ(1,'(A)')SCRATCH1
      READ(1,'(A)')ZONK1
      READ(2,'(A)')SCRATCH2
      READ(2,'(A)')ZONK2
      WRITE(3,'(A)')ZONK1
      YYMAX=0
10    READ(1,*,END=15)I,(R1(J),J=1,11)
      READ(1,*)(SD1(J),J=1,11)
15    READ(2,*,END=20)I,(R2(J),J=1,11)
      READ(2,*)(SD2(J),J=1,11)
      DO J=1,11
      DIFFER(J,I)=R1(J)-R2(J)
      IF(SD1(J).NE.999.0.AND.SD2(J).NE.999.0)THEN
      SD(J,I)=SD1(J)+SD2(J)
      ELSE
      SD(J,I)=0
      END IF
      END DO
      XX(I)=I-0.5
      YY(I)=DIFFER(K,I)
      EE(I)=SD(K,I)
      IF(YY(I).GT.YYMAX)YYMAX=YY(I)
      GO TO 10
20    CONTINUE
      DO I=1,24
      WRITE(6,'(X,A,I2,X,F6.2)')'I=',I,YY(I)
      YY(I)=YY(I)/YYMAX
      EE(I)=EE(I)/YYMAX
      END DO
      WRITE(6,'(X,A,F6.2)')'YYMAX=',YYMAX
      END
```



```
      PROGRAM ECHOPLOT
C     ================
C
C     ECHOPLOT asks for two time windows placed symmetrically about radiant
C     transit; one before and one after, corresponding to the echoline
C     intersecting the most sensitive part of the antenna beam. The time
C     window duration which you enter balances on these two times. The
C     coordinates of the echoes located during these two periods of peak
C     shower activity are then plotted onto the echo surface at 95 km.
C     For the period before transit only negative Azimuth echoes
C     are plotted to ensure that sporadic meteors do not
C     degrade the echoline that should hopefully become evident.
C     The centre of each time window is shifted 4 minutes
C     earlier each successive day.

C     Written by David Roux, Rhini, September 1987.
C     ----------------------------------------------------------------------
C
      DIMENSION SECLINE(14)
      CHARACTER*2 GEN,PS,FFILE,LFILE,DISCNO,GENF,GENL,F23
      CHARACTER DISC*3,FLNM(16001)*7,FILETD*27,
     *ANS*1,F24*3,PLOTFL*9
      REAL X(10000),Y(10000)
      LOGICAL DAVID
C-----------------------------------------------------------------------
      CALL FILENAME(FLNM,ILF)
C-----------------------------------------------------------------------
      WRITE(6,'(X,A)')'SAST BEFORE TRANSIT? (DECIMAL OF AN HOUR)'
      READ(5,*)T1
      WRITE(6,'(X,A)')'SAST AFTER TRANSIT? (DECIMAL OF AN HOUR)'
      READ(5,*)T2
      WRITE(6,'(X,A)')'DURATION OF TIME WINDOW? (DEC. OF HOUR)'
      READ(5,*)DT
      WRITE(6,'(A)')'$PEN NO.? (1, 2 OR 3)'
      READ(5,*)IPEN
      WRITE(6,'(A)')'PLOTTER SYMBOL? (INTEGER)'
      READ(5,*)ISYM
      CALL START_PLOT(DAVID)
      N=0
      IHR0=-1
C-----------------------------------------------------------------------
      DO IFL=1,16001
      IF(FLNM(IFL).EQ.'Z')GO TO 3000
      OPEN(UNIT=1,FILE='DUA1:[USER.GRAHAM]'//FLNM(IFL),READONLY,
     *FORM='FORMATTED',STATUS='OLD',IOSTAT=IOS1,ERR=99)
      PLOTFL='E'//FFILE//GENF//LFILE//GENL
      OPEN(UNIT=2,FILE=PLOTFL,FORM='FORMATTED',STATUS='NEW')
      READ(1,'(X,A)')FILETD
      READ(1,*)(SECLINE(I),I=1,14)
      GEN=FLNM(IFL)(6:7)
15    FRA=0
      READ(1,*,END=98)IAD,IDAY,HRS,NS,FRA,IAMP,
     *FAVE,RAVE,DMIN1,WV,ALT,AZ
      IF(IHR0.EQ.-1)GO TO 16
      IF(IDAY.GT.IDAY0)THEN
      T1=T1-0.0667
      T2=T2-0.0667
      ELSE
      CONTINUE
```

```
      END IF
16    T1A=T1-(DT/2)
      T1B=T1+(DT/2)
      T2A=T2-(DT/2)
      T2B=T2+(DT/2)
C     PROVISION FOR FAILURE IN CH4
      IF(GEN.EQ.'03'.OR.GEN.EQ.'02')THEN
      F23=FLNM(IFL)(2:3)
      F24=FLNM(IFL)(2:4)
        IF(GEN.EQ.'03')THEN
        IF(F23.EQ.'11'.OR.F23.EQ.'12'.OR.F24.EQ.'09B'.
     *  OR.F24.EQ.'10B'.OR.F24.EQ.'13A'.OR.F24.EQ.'14A')DMIN1=0.1
        END IF
        IF(GEN.EQ.'02')THEN
        IF(F23.EQ.'09'.OR.F23.EQ.'10'.OR.F23.EQ.'11'.
     *  OR.F23.EQ.'12'.OR.F24.EQ.'07B'.OR.F24.EQ.'08B')DMIN1=0.1
        END IF
      END IF
C-----------------------------------------------------------------
      IF(FRA.EQ.0)GO TO 15
      IF(ABS(DMIN1).GE.0.050)GO TO 15
      IF(IHR0.EQ.-1)GO TO 20
      HRS1=HRS0+((76.8+NS0)/230400)
      DHRS=HRS-HRS1
20     IHR0=INT(HRS)
      IF((HRS.GE.T1A.AND.HRS.LE.T1B.AND.AZ.LT.0).OR.(HRS.GE.
     *T2A.AND.HRS.LE.T2B.AND.AZ.GT.0))THEN
        IF(DHRS.GT.0.0005.OR.IHR0.EQ.-1)THEN
        IF(ALT.GE.22)THEN
        N=N+1
        X(N)=95*(COSD(ALT)/SIND(ALT))*SIND(AZ)
        Y(N)=95*(COSD(ALT)/SIND(ALT))*COSD(AZ)
        WRITE(6,*)X(N),Y(N),N
        WRITE(2,'(X,F7.2,X,F7.2)')X(N),Y(N)
        END IF
        END IF
      END IF
      HRS0=HRS
      NS0=NS
      IDAY0=IDAY
      GO TO 15
C-----------------------------------------------------------------
1000  END DO
99    IF(IOS1.EQ.29)THEN
      WRITE(6,'(X,A,A)')FLNM(IFL),'NOT FOUND'
      ELSE
      WRITE(6,'(X,A,I2)')'ERR NO',IOS1
      END IF
      GO TO 1000
98    CLOSE(UNIT=1)
      GO TO 1000
C     START OF PLOTTING ROUTINE
3000  CALL FACTOR(0.98)
      CALL NEWPEN(IPEN)
      CALL PLOT(1.0,1.0,-3)
      X(N+1)=-225.0
      X(N+2)=25.0
      Y(N+1)=-225.0
      Y(N+2)=25.0
      CALL AXIS(0.0,9.0,' ',-1,18.0,0.0,-225.0,25.0)
```



```
CALL AXIS(9.0,0.0,' ',1,18.0,90.0,-225.0,25.0)
CALL LINE(X,Y,N,1,-1,ISYM)
CALL PLOT(-1.0,-1.0,3)
CALL PLOT(-1.0,18.5,2)
CALL PLOT(19.0,18.5,2)
CALL PLOT(19.0,-1.0,2)
CALL PLOT(-1.0,-1.0,2)
CALL END_PLOT
STOP
END
```

```
      PROGRAM NEWPEAK1
C     ================
C
C     Newpeak1 plots to LASER the normalized hourly echo rate versus date,
C     averaged over two time windows each day, both of which are centred on the
C     times of maximum shower activity of a particular day, one before and the
C     other after radiant transit. Both windows are shifted four minutes
C     earlier every next day.
C     Written by David Roux, October 1987. Platonic idealist.
C     Revised by D.G.R., January 1988.
C
      DIMENSION SECLINE(14),B1(0:12),B2(0:12)
      CHARACTER*2 GEN,PS,FFILE,LFILE,DISCNO,GENF,GENL,F23
      CHARACTER DISC*3,FLNM(16001)*7,FILETD*27,
     *ANS*1,F24*3
      REAL X(390),Y(390),PX(390),PY(390),ERR(390),PERR(390),
     *LHS,PXX(390)
      LOGICAL DAVE
C-----------------------------------------------------------------------
      CALL FILENAME(FLNM,ILF)
C-----------------------------------------------------------------------
      WRITE(6,'(X,A)')'Duration of time window? (integral hours)'
      READ(5,*)DT
      WRITE(6,'(X,A)')'SAST before transit? (decimal of an hour)'
      READ(5,*)T1
      WRITE(6,'(X,A)')'SAST after transit?  (decimal of an hour)'
      READ(5,*)T2
      WRITE(6,'(X,A)')'Enter sporadic background rates to be removed'
      WRITE(6,'(X,A)')' from following hours: if the upper limit of'
      WRITE(6,'(X,A)')' the window before transit is in hour n, then '
      WRITE(6,'(X,A)')' enter background rates for the hours n, n-1,'
      WRITE(6,'(X,A)')' n-2, ...until n-(dt+4). (dt+5 quantities requ.)'
      IDT=DT+4
      READ(5,*)(B1(I),I=0,IDT)
      WRITE(6,'(X,A)')'Ditto, for the window after transit.
     *(d.h. (DT+5) Zahlen sind verlangen)'
      READ(5,*)(B2(I),I=0,IDT)
      WRITE(6,'(X,A)')'Scale of Y-axis: counts per cm? (Norm = 5)'
      READ(5,*)YSCALA
      CALL START_PLOT(DAVE)
      SPOR1=0
      SPOR2=0
      KZ1=0
      KZ2=0
      OTM1=0
      OTM2=0
      YMIN=0
      YMAX=0
      IHRO=-1
C-----------------------------------------------------------------------
      DO IFL=1,16001
      IF(FLNM(IFL).EQ.'Z')GO TO 3000
      OPEN(UNIT=1,FILE='DUA1:[USER.GRAHAM]'//FLNM(IFL),READONLY,
     *FORM='FORMATTED',STATUS='OLD',IOSTAT=IOS1,ERR=99)
      READ(1,'(X,A)')FILETD
      READ(1,*)(SECLINE(I),I=1,14)
      GEN=FLNM(IFL)(6:7)
      DO I=1,12
      IF(SECLINE(I).EQ.99)NOUTS=I-2
      END DO
```



```
15    FRA=0
      READ(1,*,END=98)IAD,IDAY,HRS,NS,FRA,IAMP,
     *FAVE,RAVE,DMIN1,WV,ALT,AZ
      IF(IHRO.EQ.-1)THEN
      ST=IDAY
      T10=T1
      T20=T2
      IF(T10.GE.24)T10=T10-24
      IF(T20.GE.24)T20=T20-24
      GO TO 16
      END IF
      IF(IDAY.LT.ST)IDAY=IDAY+365
C-----------------------------------------------------------------------
      IF(IDAY.NE.IDAYO)THEN
      DELTA1A=INT(T1A)+1-T1A
      DELTA1B=T1B-INT(T1B)
      IF(T1B.GT.T1BO)THEN
      U1B=T1B-25
      ELSE
      U1B=T1B
      END IF
      IDAV1=INT(T1BO)-INT(U1B)
      DO N=0,3
      IF(IDAV1.EQ.N)THEN
      NQ=DT+N
      SPOR1B=DELTA1B*B1(N)
      SPOR1A=DELTA1A*B1(NQ)
      L=N+1
      M=NQ-1
      DO J=L,M
      SPOR1=SPOR1+B1(J)
      END DO
      SPOR1=SPOR1+SPOR1A+SPOR1B
      END IF
      END DO
C     Echoes in window 2
      DELTA2A=(INT(T2A)+1)-T2A
      DELTA2B=T2B-INT(T2B)
      IF(T2B.GT.T2BO)THEN
      U2B=U2B-25
      ELSE
      U2B=T2B
      END IF
      IDAV2=INT(T2BO)-INT(U2B)
      DO N=0,3
      IF(IDAV2.EQ.N)THEN
      NQ=DT+N
      SPOR2B=DELTA2B*B2(N)
      SPOR2A=DELTA2A*B2(NQ)
      L=N+1
      M=NQ-1
      DO J=L,M
      SPOR2=SPOR2+B2(J)
      END DO
      SPOR2=SPOR2+SPOR2A+SPOR2B
      END IF
      END DO
      TOUT1=OTAT+OTM1+OUT1
      TOUT2=OTPT+OTM2+OUT2
      F1=(60*DT)/((60*DT)-TOUT1)
```

```
      F2=(60*DT)/((60*DT)-TOUT2)
      HR1=((KZ1*F1)-SPOR1)/DT
      HR2=((KZ2*F2)-SPOR2)/DT
      HKZ1=KZ1/2
      HKZ2=KZ2/2
      IF(KZ1.LT.HKZ2)THEN
      Y(IDAY0)=HR2
      IF(Y(IDAY0).LT.-12)Y(IDAY0)=-12
      ERR(IDAY0)=(KZ2**0.5)*F2/DT
      END IF
      IF(KZ2.LT.HKZ1)THEN
      Y(IDAY0)=HR1
      IF(Y(IDAY0).LT.-12)Y(IDAY0)=-12
      ERR(IDAY0)=(KZ1**0.5)*F1/DT
      END IF
      IF(KZ1.GE.HKZ2.AND.KZ2.GE.HKZ1)THEN
      KZT=KZ1+KZ2
      FT=(60*2*DT)/((60*2*DT)-TOUT1-TOUT2)
      Y(IDAY0)=((KZT*FT)-SPOR1-SPOR2)/(DT*2)
      IF(Y(IDAY0).LT.-12)Y(IDAY0)=-12
      ERR(IDAY0)=((KZT**0.5)*FT)/(DT*2)
      END IF
      X(IDAY0)=IDAY0+0.5
      KZ1=0
      KZ2=0
      OTM1=0
      OTM2=0
      SPOR1=0
      SPOR2=0
      T1=T1-0.0656
      T2=T2-0.0656
      END IF
C-----------------------------------------------------------------------
16    T1A=T1-(DT/2)
      T1B=T1+(DT/2)
      T2A=T2-(DT/2)
      T2B=T2+(DT/2)
      IF(T1A.LT.0)T1A=T1A+24
      IF(T2A.LT.0)T2A=T2A+24
      IF(T1B.LT.0)T1B=T1B+24
      IF(T2B.LT.0)T2B=T2B+24
      IF(T1A.GE.24)T1A=T1A-24
      IF(T2A.GE.24)T2A=T2A-24
      IF(T1B.GE.24)T1B=T1B-24
      IF(T2B.GE.24)T2B=T2B-24
C-----------------------------------------------------------------------
      IF(IHR0.EQ.-1)THEN
      T1B0=T1B
      T2B0=T2B
      END IF
      IF(FRA.EQ.0)THEN
        IF(T1A.GT.T1B)THEN
        IF((HRS.GE.T1A.AND.HRS.LT.24).OR.(HRS.LE.T1B))OTM1=
     *  OTM1+((NS+76.8)/3840)
        ELSE
        IF(HRS.GE.T1A.AND.HRS.LE.T1B)OTM1=OTM1+((NS+76.8)/3840)
        END IF
        IF(T2A.GT.T2B)THEN
        IF((HRS.GE.T2A.AND.HRS.LT.24).OR.(HRS.LE.T2B))OTM2=
     *  OTM2+((NS+76.8)/3840)
```



```
        ELSE
        IF(HRS.GE.T2A.AND.HRS.LE.T2B)OTM2=OTM2+((NS+76.8)/3840)
        END IF
      IDAY0=IDAY
      GO TO 15
      END IF
      IF(IHR0.EQ.-1)GO TO 20
      IF(T1A.GT.T1B)THEN
        IF((HRS.GE.T1A.AND.HRS.LT.24).OR.(HRS.LE.T1B))THEN
        HRS1=HRS0+((76.8+NS0)/230400)
        DHRS=HRS-HRS1
        END IF
      ELSE
        IF(HRS.GE.T1A.AND.HRS.LE.T1B)THEN
        HRS1=HRS0+((76.8+NS0)/230400)
        DHRS=HRS-HRS1
        END IF
      END IF
      IF(T2A.GT.T2B)THEN
        IF((HRS.GE.T2A.AND.HRS.LT.24).OR.(HRS.LE.T2B))THEN
        HRS1=HRS0+((76.8+NS0)/230400)
        DHRS=HRS-HRS1
        END IF
      ELSE
        IF(HRS.GE.T2A.AND.HRS.LE.T2B)THEN
        HRS1=HRS0+((76.8+NS0)/230400)
        DHRS=HRS-HRS1
        END IF
      END IF
20    IF(T1A.GT.T1B)THEN
        IF((HRS.GE.T1A.AND.HRS.LT.24).OR.(HRS.LE.T1B))THEN
        IF(DHRS.GT.0.0005.OR.IHR0.EQ.-1)THEN
        IF(IAMP.GE.25)KZ1=KZ1+1
        ELSE
        WRITE(6,'(X,A,I5)')'ADDRESS:',IAD0
        END IF
        OTM1=OTM1+((NS+76.8)/3840)
        OTAT=NOUTS*SECLINE(1)*DT
        END IF
      ELSE
        IF(HRS.GE.T1A.AND.HRS.LE.T1B)THEN
        IF(DHRS.GT.0.0005.OR.IHR0.EQ.-1)THEN
        IF(IAMP.GE.25)KZ1=KZ1+1
        ELSE
        WRITE(6,'(X,A,I5)')'ADDRESS:',IAD0
        END IF
        OTM1=OTM1+((NS+76.8)/3840)
        OTAT=NOUTS*SECLINE(1)*DT
        END IF
      END IF
      IF(T2A.GT.T2B)THEN
        IF((HRS.GE.T2A.AND.HRS.LT.24).OR.(HRS.LE.T2B))THEN
        IF(DHRS.GT.0.0005.OR.IHR0.EQ.-1)THEN
        IF(IAMP.GE.25)KZ2=KZ2+1
        ELSE
        WRITE(6,'(X,A,I5)')'ADDRONK:',IAD0
        END IF
        OTM2=OTM2+((NS+76.8)/3840)
        OTPT=NOUTS*SECLINE(1)*DT
        END IF
```

```
      ELSE
        IF(HRS.GE.T2A.AND.HRS.LE.T2B)THEN
        IF(DHRS.GT.0.0005.OR.IHR0.EQ.-1)THEN
        IF(IAMP.GE.25)KZ2=KZ2+1
        ELSE
        WRITE(6,'(X,A,I5)')'ADDRESS:',IAD0
        END IF
        OTM2=OTM2+((NS+76.8)/3840)
        OTPT=NOUTS*SECLINE(1)*DT
        END IF
      END IF
      HRS0=HRS
      IHR0=INT(HRS0)
      NS0=NS
      IDAY0=IDAY
      IAD0=IAD
      GO TO 15
C-----------------------------------------------------------------
1000  END DO
99    IF(IOS1.EQ.29)THEN
      WRITE(6,'(X,A,A)')FLNM(IFL),'NOT FOUND'
      ELSE
      WRITE(6,'(X,A,I2)')'ERR NO',IOS1
      END IF
      GO TO 1000
98    CLOSE(UNIT=1)
      GO TO 1000
C     PLOTTING ARRAY CREATED
3000  DO K=ST,IDAY0
      J=K-ST+1
      PX(J)=X(K)
      PXX(J)=PX(J)-ST
      IF(PX(J).GT.365)PX(J)=PX(J)-365
      PY(J)=Y(K)
      IF(PY(J).GT.YMAX)YMAX=PY(J)
      IF(PY(J).LE.YMIN)YMIN=PY(J)
      PERR(J)=ERR(K)
      WRITE(3,*)J,PX(J),PY(J),PERR(J)
      END DO
      PTS=IDAY0-ST
      TDIV=YMAX/YSCALA
      BDIV=YMIN/YSCALA
      TOP=INT(TDIV)+1
      IF(YMIN.LT.0)THEN
      BOT=INT(BDIV)-1
      ELSE
      BOT=0
      END IF
      AXLEN=TOP+ABS(BOT)
      TFRME=TOP+1
      BFRME=BOT-1
      YORIG=ABS(BOT)+1
      FIRSTV=BOT*YSCALA
      VSCALA=1/YSCALA
      WRITE(6,'(X,F10.1)')YMAX,YMIN,PTS,TDIV,BDIV,TOP,BOT,
     *AXLEN,TFRME,BFRME,YORIG,FIRSTV,VSCALA
C     START OF PLOTTING ROUTINE
      CALL FACTOR(0.5)
      CALL PLOT(1.0,YORIG,-3)
      PX(PTS+1)=ST
```



```
      PX(PTS+2)=1.0
      PY(PTS+1)=0.0
      PY(PTS+2)=YSCALA
      CALL AXIS(0.0,0.0,'DAY ',-3,PTS,0.0,ST,1.0)
      CALL AXIS(0.0,BOT,'SHOWER RATE',11,AXLEN,90.0,FIRSTV,YSCALA)
      NPTS=PTS
      ZOLA=PTS+2
      CALL LINE(PX,PY,NPTS,1,0,6)
      NNN=NPTS
      DO I=NNN,2,-2
      LHS=PXX(I)-0.2
      RHS=PXX(I)+0.2
      YUP=VSCALA*(PY(I)+PERR(I))
      YL=VSCALA*(PY(I)-PERR(I))
      CALL PLOT(LHS,YL,3)
      CALL PLOT(RHS,YL,2)
      CALL PLOT(PXX(I),YL,3)
      CALL PLOT(PXX(I),YUP,2)
      CALL PLOT(LHS,YUP,3)
      CALL PLOT(RHS,YUP,2)
      END DO
      CALL PLOT(-1.0,BFRME,3)
      CALL PLOT(-1.0,TFRME,2)
      CALL PLOT(ZOLA,TFRME,2)
      CALL PLOT(ZOLA,BFRME,2)
      CALL PLOT(-1.0,BFRME,2)
      CALL END_PLOT
      STOP
      END
```

```
      PROGRAM NEWPEAK2
C     ================
C
C     NEWPEAK2  plots the hourly rate versus date of echoes in two time
C     windows symmetrical about transit, and belonging to an area of sky
C     close to the known shower radiant.
C
C     Written by David Roux, Grahamstown, 1987.
C
      COMMON /CCOORD/ SB0,CB0,SBP,CBP,SB1,CB1,A0,AP,A1
      DIMENSION SECLINE(14)
      CHARACTER*2 GEN,PS,FFILE,LFILE,DISCNO,GENF,GENL,F23
      CHARACTER DISC*3,FLNM(16001)*7,FILETD*60,YEAR*4,
     *ANS*1,F24*3,OPT*1
      REAL X(400),Y(400),PX(400),PY(400),ERR(400),PERR(400),
     *LHS,PXX(400),LST
      INTEGER RA(20),HA(20),DEC(20)
      LOGICAL DAVE
C-----------------------------------------------------------------------
      CALL FILENAME(FLNM,ILF)
C-----------------------------------------------------------------------
      WRITE(6,'(X,A)')'Duration of time window? (integral hours)'
      READ(5,*)DT
      WRITE(6,'(X,A)')'SAST before transit? (decimal of an hour)'
      READ(5,*)T1
      WRITE(6,'(X,A)')'SAST after transit?  (decimal of an hour)'
      READ(5,*)T2
      WRITE(6,'(X,A)')'Enter max. time allowed between echoes (between
     * 0 and 1 hour, in hours)'
      READ(5,*)GAP
      WRITE(6,'(X,A)')'Include the option of rejecting one of the two
     * time windows? (Y/N)'
      READ(5,'(A)')OPT
      IF(OPT.EQ.'N')GO TO 3
      WRITE(6,'(X,A)')'Enter rejection parameter, IREJ. Window 1 is '
      WRITE(6,'(X,A)')'rejected if KZ1 is less than KZ2/IREJ, etcetera'
      READ(5,*)IREJ
3     WRITE(6,'(X,A)')'Enter side of square section of sky, int.degrees'
      WRITE(6,'(X,A)')' maximium = 20'
      READ(5,*)ISKY
      WRITE(6,'(X,A)')' Enter Right Ascension and Declination of a '
      WRITE(6,'(X,A)')' point radiant; RA,DEC. The point lies at bottom'
      WRITE(6,'(X,A)')' left of a ISKY squ. section of sky. Int. deg.'
      READ(5,*)RA(1),DEC(1)
      WRITE(6,'(X,A)')'Assign a single echo to only one radiant point?
     *(Y/N)'
      READ(5,'(A)')ANS
      WRITE(6,'(X,A)')'Enter lowest allowed radiant altitude, ILAA'
      READ(5,*)ILAA
      CALL START_PLOT (DAVE)
      KZ1=0
      KZ2=0
      OTM1=0
      OTM2=0
      OUT1=0
      OUT2=0
      YMAX=0
      IHR0=-1
      DO I=1,ISKY
      RA(I)=RA(1)+(I-1)
```



```
      DEC(I)=DEC(1)+1-I
      END DO
      XOG=0
C-----------------------------------------------------------------------
      DO IFL=1,16001
      IF(FLNM(IFL).EQ.'Z')GO TO 3000
      OPEN(UNIT=1,FILE='DUA1:[USER.GRAHAM]'//FLNM(IFL),READONLY,
     *FORM='FORMATTED',STATUS='OLD',IOSTAT=IOS1,ERR=99)
      READ(1,'(X,A)')FILETD
      YEAR=FILETD(38:41)
      READ(1,*)(SECLINE(I),I=1,14)
      GEN=FLNM(IFL)(6:7)
      DO I=1,12
      IF(SECLINE(I).EQ.99)NOUTS=I-2
      END DO
15    FRA=0
      READ(1,*,END=98)IAD,IDAY,HRS,NS,FRA,IAMP,
     *FAVE,RAVE,DMIN1,WV,ALT,AZ
      FLAG=0
C
C     Algorithm for faulty channel 4 during sep. 03.
C
      IF(GEN.EQ.'03'.OR.GEN.EQ.'02')THEN
      F23=FLNM(IFL)(2:3)
      F24=FLNM(IFL)(2:4)
         IF(GEN.EQ.'03')THEN
         IF(F23.EQ.'11'.OR.F23.EQ.'12'.OR.F24.EQ.'09B'.
     *   OR.F24.EQ.'10B'.OR.F24.EQ.'13A'.OR.F24.EQ.'14A')DMIN1=0.1
         END IF
         IF(GEN.EQ.'02')THEN
         IF(F23.EQ.'09'.OR.F23.EQ.'10'.OR.F23.EQ.'11'.
     *   OR.F23.EQ.'12'.OR.F24.EQ.'07B'.OR.F24.EQ.'08B')DMIN1=0.1
         END IF
      END IF
C-----------------------------------------------------------------------
      IF(IHR0.EQ.-1)THEN
      SKT=IDAY
      T10=T1
      T20=T2
      IF(T10.GE.24)T10=T10-24
      IF(T20.GE.24)T20=T20-24
      GO TO 16
      END IF
      IF(IDAY.LT.SKT)THEN
      IDAY=IDAY+365
      XOG=1
      END IF
C-----------------------------------------------------------------------
      IF(IDAY.NE.IDAY0)THEN
      TOUT1=OTAT+OTM1+OUT1
      TOUT2=OTPT+OTM2+OUT2
      IF(OPT.EQ.'Y')THEN
      F1=(60*DT)/((60*DT)-TOUT1)
      F2=(60*DT)/((60*DT)-TOUT2)
      HR1=((KZ1*F1))/DT
      HR2=((KZ2*F2))/DT
      HKZ1=KZ1/IREJ
      HKZ2=KZ2/IREJ
      IF(KZ1.LT.HKZ2)THEN
      Y(IDAY0)=HR2
```

```
      ERR(IDAY0)=(KZ2**0.5)*F2/DT
      END IF
      IF(KZ2.LT.HKZ1)THEN
      Y(IDAY0)=HR1
      ERR(IDAY0)=(KZ1**0.5)*F1/DT
      END IF
      ELSE
      HKZ1=0
      HKZ2=0
      END IF
      IF(KZ1.GE.HKZ2.AND.KZ2.GE.HKZ1)THEN
      KZT=KZ1+KZ2
      FT=(60*2*DT)/((60*2*DT)-TOUT1-TOUT2)
      Y(IDAY0)=((KZT*FT))/(DT*2)
      ERR(IDAY0)=((KZT**0.5)*FT)/(DT*2)
      END IF
      X(IDAY0)=IDAY0+0.5
      KZ1=0
      KZ2=0
      OTM1=0
      OTM2=0
      OUT1=0
      OUT2=0
      T1=T1-0.0656
      T2=T2-0.0656
      END IF
C-----------------------------------------------------------------
16    T1A=T1-(DT/2)
      T1B=T1+(DT/2)
      T2A=T2-(DT/2)
      T2B=T2+(DT/2)
      IF(T1A.LT.0)T1A=T1A+24
      IF(T2A.LT.0)T2A=T2A+24
      IF(T1B.LT.0)T1B=T1B+24
      IF(T2B.LT.0)T2B=T2B+24
      IF(T1A.GE.24)T1A=T1A-24
      IF(T2A.GE.24)T2A=T2A-24
      IF(T1B.GE.24)T1B=T1B-24
      IF(T2B.GE.24)T2B=T2B-24
C-----------------------------------------------------------------
      IF(IHR0.EQ.-1)THEN
      T1B0=T1B
      T2B0=T2B
      END IF
      IF(FRA.EQ.0.OR.ABS(DMIN1).GE.0.05)THEN
        IF(T1A.GT.T1B)THEN
        IF((HRS.GE.T1A.AND.HRS.LT.24).OR.(HRS.LE.T1B))OTM1=
     *  OTM1+((NS+76.8)/3840)
        ELSE
        IF(HRS.GE.T1A.AND.HRS.LE.T1B)OTM1=OTM1+((NS+76.8)/3840)
        END IF
        IF(T2A.GT.T2B)THEN
        IF((HRS.GE.T2A.AND.HRS.LT.24).OR.(HRS.LE.T2B))OTM2=
     *  OTM2+((NS+76.8)/3840)
        ELSE
        IF(HRS.GE.T2A.AND.HRS.LE.T2B)OTM2=OTM2+((NS+76.8)/3840)
        END IF
      IDAY0=IDAY
      GO TO 15
      END IF
```



```
      IF(IHR0.EQ.-1)GO TO 20
      IF(T1A.GT.T1B)THEN
        IF((HRS.GE.T1A.AND.HRS.LT.24).OR.(HRS.LT.T1B))THEN
        HRS1=HRS0+((76.8+NS0)/230400)
        DHRS=HRS-HRS1
        IF(DHRS.GT.GAP)THEN
        IF((HRS0.GE.T1A.AND.HRS0.LT.24).OR.(HRS0.LT.T1B))
     *  OUT1=OUT1+(DHRS*60)
        END IF
        END IF
      ELSE
        IF(HRS.GE.T1A.AND.HRS.LT.T1B)THEN
        HRS1=HRS0+((76.8+NS0)/230400)
        DHRS=HRS-HRS1
        IF(DHRS.GT.GAP)THEN
        IF(HRS0.GE.T1A.AND.HRS0.LT.T1B)OUT1=OUT1+(DHRS*60)
        END IF
        END IF
      END IF
      IF(T2A.GT.T2B)THEN
        IF((HRS.GE.T2A.AND.HRS.LT.24).OR.(HRS.LT.T2B))THEN
        HRS1=HRS0+((76.8+NS0)/230400)
        DHRS=HRS-HRS1
        IF(DHRS.GT.GAP)THEN
        IF((HRS0.GE.T2A.AND.HRS0.LT.24).OR.(HRS0.LT.T2B))
     *   OUT2=OUT2+(DHRS*60)
        END IF
        END IF
      ELSE
        IF(HRS.GE.T2A.AND.HRS.LT.T2B)THEN
        HRS1=HRS0+((76.8+NS0)/230400)
        DHRS=HRS-HRS1
        IF(DHRS.GT.GAP)THEN
        IF(HRS0.GE.T2A.AND.HRS0.LT.T2B)OUT2=OUT2+(DHRS*60)
        END IF
        END IF
      END IF
20    IF(T1A.GT.T1B)THEN
        IF((HRS.GE.T1A.AND.HRS.LT.24).OR.(HRS.LE.T1B))THEN
        OTM1=OTM1+((NS+76.8)/3840)
        OTAT=NOUTS*SECLINE(1)*DT
        IF(DHRS.GT.0.0005.OR.IHR0.EQ.-1)THEN
        IF(IAMP.GE.25)THEN
        FLAG=1
        GO TO 700
        END IF
        ELSE
        WRITE(6,'(X,A,I5)')'ADDRESS:',IAD0
        END IF
        END IF
      ELSE
        IF(HRS.GE.T1A.AND.HRS.LE.T1B)THEN
        OTM1=OTM1+((NS+76.8)/3840)
        OTAT=NOUTS*SECLINE(1)*DT
        IF(DHRS.GT.0.0005.OR.IHR0.EQ.-1)THEN
        IF(IAMP.GE.25)THEN
        FLAG=1
        GO TO 700
        END IF
        ELSE
```

```
        WRITE(6,'(X,A,I5)')'ADDRESS:',IAD0
        END IF
        END IF
      END IF
      IF(T2A.GT.T2B)THEN
        IF((HRS.GE.T2A.AND.HRS.LT.24).OR.(HRS.LE.T2B))THEN
        OTM2=OTM2+((NS+76.8)/3840)
        OTPT=NOUTS*SECLINE(1)*DT
        IF(DHRS.GT.0.0005.OR.IHR0.EQ.-1)THEN
        IF(IAMP.GE.25)THEN
        FLAG=2
        GO TO 700
        END IF
        ELSE
        WRITE(6,'(X,A,I5)')'ADDRONK:',IAD0
        END IF
        END IF
      ELSE
        IF(HRS.GE.T2A.AND.HRS.LE.T2B)THEN
        OTM2=OTM2+((NS+76.8)/3840)
        OTPT=NOUTS*SECLINE(1)*DT
        IF(DHRS.GT.0.0005.OR.IHR0.EQ.-1)THEN
        IF(IAMP.GE.25)THEN
        FLAG=2
        GO TO 700
        END IF
        ELSE
        WRITE(6,'(X,A,I5)')'ADDRESS:',IAD0
        END IF
        END IF
      END IF
      IF(FLAG.EQ.0)GO TO 750
C-----------------------------------------------------------------------
C     Coordinate transformations; 1)from (HA,Dec) to (Az,Alt), and
C     2) from the echo (Az,alt) to (skew-Az,skew-alt).
C-----------------------------------------------------------------------
700   IF(YEAR.EQ.'1987'.AND.XOG.EQ.0) THEN
      TDN=IDAY+365
      ELSE
      TDN=IDAY
      END IF
      ABC=0.06556*TDN
      ST=6.625+ABC
      DO N=0,10
      DEF=(N*24)+17.375
      GHI=((N-1)*24)+17.375
      IF(ABC.LT.DEF.AND.ABC.GE.GHI)ST=ST-(N*24)
      END DO
      SAST=HRS
      LST=ST+1.7667+((SAST-2)*1.0027379)
      IF(LST.GE.24)LST=LST-24
      DO I=1,ISKY
      DO J=1,ISKY
      HA(J)=(LST*15)-RA(J)
      A1=HA(J)
      B1=DEC(I)
      A0=0
      B0=56.7
      AP=0
      BP=-33.3
```



```
      SB0=0.8358
      CB0=0.5490
      SBP=-0.5490
      CBP=0.8358
      SB1=SIND(B1)
      CB1=COSD(B1)
      CALL COORD(A2,B2)
      IF(B2.LE.ILAA)GO TO 740
      A0=A2+90
      B0=0
      AP=A2
      BP=B2
      A1=AZ
      B1=ALT
      SB0=SIND(B0)
      CB0=COSD(B0)
      SBP=SIND(BP)
      CBP=COSD(BP)
      SB1=SIND(B1)
      CB1=COSD(B1)
      CALL COORD(A2,B2)
      IF(B2.LE.1.25.AND.B2.GT.-1.25)THEN
      IF(FLAG.EQ.1)KZ1=KZ1+1
      IF(FLAG.EQ.2)KZ2=KZ2+1
      IF(ANS.EQ.'Y')GO TO 750
      END IF
740   END DO
      END DO
C-----------------------------------------------------------------------
750   HRS0=HRS
      IHR0=INT(HRS0)
      NS0=NS
      IDAY0=IDAY
      IAD0=IAD
      GO TO 15
C-----------------------------------------------------------------------
1000  END DO
99    IF(IOS1.EQ.29)THEN
      WRITE(6,'(X,A,A)')FLNM(IFL),'NOT FOUND'
      ELSE
      WRITE(6,'(X,A,I2)')'ERR NO',IOS1
      END IF
      GO TO 1000
98    CLOSE(UNIT=1)
      GO TO 1000
C     PLOTTING ARRAY CREATED
3000  DO K=SKT,IDAY0
      IF(Y(K).GT.YMAX)YMAX=Y(K)
      END DO
      DO K=SKT,IDAY0
      Y(K)=Y(K)/YMAX
      ERR(K)=ERR(K)/YMAX
      J=K-SKT+1
      PX(J)=X(K)
      PXX(J)=PX(J)-SKT
      PY(J)=Y(K)
      PERR(J)=ERR(K)
      END DO
      PTS=IDAY0-SKT
C     START OF PLOTTING ROUTINE
```

```
CALL FACTOR(0.5)
CALL PLOT(1.0,1.0,-3)
PX(PTS+1)=SKT
PX(PTS+2)=1.0
PY(PTS+1)=0.0
PY(PTS+2)=0.05
CALL AXIS(0.0,0.0,'DAY ',-3,PTS,0.0,SKT,1.0)
CALL AXIS(0.0,0.0,'RATE',4,20.0,90.0,0.0,0.05)
NPTS=PTS
ZOLA=PTS+2
CALL LINE(PX,PY,NPTS,1,0,6)
NNN=NPTS
DO I=NNN,2,-2
LHS=PXX(I)-0.2
RHS=PXX(I)+0.2
YUP=20*(PY(I)+PERR(I))
YL=20*(PY(I)-PERR(I))
IF(YL.GE.0.AND.YUP.LE.32)THEN
CALL PLOT(LHS,YL,3)
CALL PLOT(RHS,YL,2)
CALL PLOT(PXX(I),YL,3)
CALL PLOT(PXX(I),YUP,2)
CALL PLOT(LHS,YUP,3)
CALL PLOT(RHS,YUP,2)
END IF
END DO
CALL PLOT(-1.0,-1.0,3)
CALL PLOT(-1.0,21.0,2)
CALL PLOT(ZOLA,21.0,2)
CALL PLOT(ZOLA,-1.0,2)
CALL PLOT(-1.0,-1.0,2)
CALL END_PLOT
STOP
END
```



```
      PROGRAM SKYMAP
C     ==============
C
C     This program generates M point radiants in a JSKY x ISKY degree
C     section of sky. It reads the data from D - files into an array.
C     An echo is singled out, and if the echo direction is orthogonal
C     to any of the M possible radiants, the 'weight' of that radiant
C     is incremented by 1. The final 'weight' of each radiant is mul-
C     tiplied by a factor, based on the detection probability of meteor
C     echoes at different points on the celestial sphere, in order to
C     compensate for the anisotropy of the antenna beam pattern.
C     The following echo is then singled out, etcetera. Echo directions
C     with altitudes greater or equal to 70 degrees are rejected as
C     are ambiguous echoes.
C
C     The program was written by David G. Roux, around September 1987.
C     Revised by D.G.R. during January and February 1988.
C
      DIMENSION SECLINE(14),DATA(5,100000)
      COMMON /CCOORD/ SBO, CBO, SBP, CBP, SB1, CB1, AO, AP, A1
      CHARACTER*2 GEN,PS,FFILE,LFILE,DISCNO,GENF,GENL,F23
      CHARACTER F24*3,DISC*3,FLNM(16001)*7,JUNK*37,TYD*8,
     *ANS*1,SNAIL*1,CONGO*1
      REAL RA(61),HA(61),DEC(61),DECRA(61,61),LA,LN,NEKOS,LST,
     *MAX,CFM(61,61),TA(0:23),TB(0:23),TMID(0:23),ELST(0:23),
     *PRB(61,61,0:23),SRALT(61,61,0:23),ROUX(61,61)
      INTEGER YEAR,IDECRA(61,61),IQK(61,61)
C-----------------------------------------------------------------------
C     MODULE A: Interactive session.
C     ========
C
      CALL FILENAME(FLNM,ILF)
      WRITE(6,'(X,A)')'Enter first day, last day.'
      READ(5,*)IFID,ILAD
      WRITE(6,'(X,A)')'No. degrees between pts on radiant grid?'
      READ(5,*)NDEG
      WRITE(6,'(X,A)')'Enter length (RA) of sky window.
     *(max.=NDEG x 60 deg)'
      READ(5,*)JSKY
      JSKY=(JSKY/NDEG)+1
      WRITE(6,'(X,A)')'Enter breadth (dec) of window
     *(max.=NDEG x 60 deg)'
      READ(5,*)ISKY
      ISKY=(ISKY/NDEG)+1
      TAG=0
      IDX=NDEG
      IDY=-NDEG
      NPTSX=JSKY
      NPTSY=ISKY
      ZAIRE=0
      KAK=0
      MAX=0.0
      KSQE=0
      IQ=0
      DO N=0,23
      DO I=1,ISKY
      DO J=1,JSKY
      PRB(J,I,N)=0
      END DO
      END DO
```

```
      END DO
      DO I=1,ISKY
      DO J=1,JSKY
      ROUX(J,I)=0
      IQK(J,I)=0
      DECRA(J,I)=0
      END DO
      END DO
      WRITE(6,'(X,A)')'Enter the Risht Ascension and Declination of'
      WRITE(6,'(X,A)')' a point radiant. This point will lie at the'
      WRITE(6,'(X,A)')' BOTTOM left-hand corner of a JSKY by ISKY deg.'
      WRITE(6,'(X,A)')' section of sky.'
      WRITE(6,'(X,A)')' RA, Dec in integral degrees.'
      READ(5,*)RA(1),DEC(1)
      WRITE(6,'(X,A)')'Weisht the echoes? (Y/N)'
      READ(5,'(A)')ANS
      WRITE(6,'(X,A)')'Enter lowest allowed radiant altitude'
      READ(5,*)ILAA
      WRITE(6,'(X,A)')'Use 'COORD' or the separation formua? (C/S)'
      READ(5,'(A)')SNAIL
      WRITE(6,'(X,A)')'Include cosX effect? (Y/N)'
      READ(5,'(A)')CONGO
      WRITE(6,'(X,A)')CONGO
      WRITE(6,'(X,A)')SNAIL
      WRITE(6,'(X,A)')'Specularity parameter (degrees)?'
      READ(5,*)SPECP
      ALIM=90+SPECP
      ZLIM=90-SPECP
      IRA1=RA(1)
      IDEC1=DEC(1)
      IHR=-1
      ROM=0.7491
      RP=150000
      PI=3.14159
      HPI=PI/2
C-----------------------------------------------------------------------
C     MODULE B: Data are read from D-files into an array.
C     ========
C
      DO IFL=1,16001
      WRITE(6,*)IFL
      IF(FLNM(IFL).EQ.'Z')GO TO 2000
      OPEN(UNIT=1,FILE='DUA1:[USER.GRAHAM]'//FLNM(IFL),
     *READONLY,FORM='FORMATTED',STATUS='OLD',IOSTAT=IOS1,ERR=99)
      READ(1,'(X,A37,I4,X,A8)')JUNK,YEAR,TYD
      READ(1,*)(SECLINE(I),I=1,14)
      GEN=FLNM(IFL)(6:7)
15    FRA=0
      READ(1,*,END=98)IAD,IDAY,HRS,NS,FRA,IAMP,FAVE,RAVE,DMIN1,
     *WV,ALT,AZ
      IF(IDAY.LT.IFID.OR.IDAY.GT.ILAD)GO TO 15
      IF(FRA.EQ.0.OR.ALT.GE.70)GO TO 15
C
C-----Algorithm for faulty channel 4 during gen. 03 and 02.
C
      IF(GEN.EQ.'03'.OR.GEN.EQ.'02')THEN
      F23=FLNM(IFL)(2:3)
      F24=FLNM(IFL)(2:4)
         IF(GEN.EQ.'03')THEN
         IF(F23.EQ.'11'.OR.F23.EQ.'12'.OR.F24.EQ.'09B'.
```



```
     *   OR.F24.EQ.'10B'.OR.F24.EQ.'13A'.OR.F24.EQ.'14A')DMIN1=0.1
         END IF
         IF(GEN.EQ.'02')THEN
         IF(F23.EQ.'09'.OR.F23.EQ.'10'.OR.F23.EQ.'11'.
     *   OR.F23.EQ.'12'.OR.F24.EQ.'07B'.OR.F24.EQ.'08B')DMIN1=0.1
         END IF
       END IF
C-----End of algorithm.
       IF(IHR.EQ.-1)THEN
         IF(IFID.NE.ILAD)THEN
         IDAY00=IDAY+1
         ELSE
         IDAY00=IDAY
         END IF
       IF(IDAY00.GT.365)IDAY00=IDAY00-365
       END IF
       IF(ABS(DMIN1).GE.0.05)THEN
         IF(IHR.EQ.-1)IHR=INT(HRS)
         HRS0=HRS
         GO TO 15
       END IF
       IF(IHR.NE.-1)THEN
       HRS1=HRS0+((76.8+NS0)/230400)
       DHRS=HRS-HRS1
       IF(DHRS.LE.0.0005)GO TO 15
       END IF
C
C      Local Sidereal Time as a function of Solar Time and day number
C      is calculated.
C      Longitude=26.5 degrees East (1.7667 hours), ST, Greenwich,
C      00:00 Hrs 0 Jan 1986, taken as 6.6244 Hrs.
C
600    IF(TAG.EQ.1)IDAY=IDAY00
       IF(YEAR.EQ.1987)THEN
       TDN=IDAY+365
       ELSE
       TDN=IDAY
       END IF
       ABC=0.06571*TDN
C      Sidereal time at 0:00 UT at Greenwich as function of day number.
       ST=6.6244+ABC
       DO JN=0,10
       DEF=(JN*24)+17.375
       GHI=((JN-1)*24)+17.375
       IF(ABC.LT.DEF.AND.ABC.GE.GHI)ST=ST-(JN*24)
       END DO
       IF(TAG.EQ.0)THEN
       SAST=HRS
       LST=ST+1.7667+((SAST-2)*1.0027379)
       IF(LST.GE.24)LST=LST-24
       ELSE
       SAST=TMID(NP)
       ELST(NP)=ST+1.7667+((SAST-2)*1.0027379)
       IF(ELST(NP).GE.24)ELST(NP)=ELST(NP)-24
       TAG=0
       GO TO 2020
       END IF
       IQ=IQ+1
       DATA(1,IQ)=LST
       DATA(2,IQ)=HRS
```

```
      DATA(3,IQ)=ALT
      DATA(4,IQ)=AZ
      DATA(5,IQ)=IAD
      IHR=INT(HRS)
      NSO=NS
      HRSO=HRS
      GO TO 15
1000  END DO
99    IF(IOS1.EQ.29)THEN
      WRITE(6,'(X,A,A)')FLNM(IFL),'NOT FOUND.'
      ELSE
      WRITE(6,'(X,A,I2)')'ERR NO ',IOS1
      END IF
      GO TO 1000
98    CLOSE(UNIT=1)
      GO TO 1000
C-------------------------------------------------------------------------------
C     MODULE C: 'Grand total detection probability' is computed for each
C     ========    radiant.
C
2000  DO I=1,ISKY
      DEC(I)=DEC(1)+NDEG-(I*NDEG)
      END DO
      DO J=1,JSKY
      RA(J)=RA(1)-NDEG+(J*NDEG)
      END DO
      DO N=0,23
      TA(N)=N
      TB(N)=TA(N)+1.0
      TMID(N)=TA(N)+0.5
      TAG=1
      NP=N
      GO TO 600
2020  END DO
      IF(ANS.EQ.'Y')THEN
      DO N=0,23
      DO I=1,ISKY
      IF(I.EQ.20)WRITE(6,*)I
      DO J=1,JSKY
      EHA=(ELST(N)*15)-RA(J)
      A1=EHA
      B1=DEC(I)
2040  A0=0
      B0=56.7
      AP=0
      BP=-33.3
      SB0=0.8358
      CB0=0.5490
      SBP=-0.5490
      CBP=0.8358
      SB1=SIND(B1)
      CB1=COSD(B1)
      CALL COORD(A2,B2)
      RAZ=A2
      RALT=B2
      IF(B2.LE.0)THEN
      PRB(J,I,N)=0
      GO TO 2050
      END IF
      SRALT(J,I,N)=SIND(B2)
```



```
      SA2=SIND(A2)
      CA2=COSD(A2)
      SB2=SIND(B2)
      CB2=COSD(B2)
      CASB=CA2*SB2
      CACB=CA2*CB2
      DO M=1,18
      A1=(M*10)-5
      B1=0
      AP=90
      BP=RALT
      A0=90+ATAN2D(SA2,-CASB)
      B0=ASIND(CACB)
      SB0=SIND(B0)
      CB0=COSD(B0)
      SBP=SIND(BP)
      CBP=COSD(BP)
      SB1=SIND(B1)
      CB1=COSD(B1)
C     Skew Az and skew alt to 'normal' (Az,alt).
      CALL COORD(A2,B2)
      AZE=A2
      ALTE=B2
C
C     Calculate range - weighted rho for a particular Azimuth and
C     Altitude, and hence the probability of meteor detection at
C     the centre of a 10 degree segment of the echo line.
      CC=COSD(ALTE)
      SC=SIND(ALTE)
      R=1E5*(SQRT(4225-4096*CC*CC)-64*SC)
      RP2=2*RP
      IF(R.GT.RP.AND.R.LT.RP2)W=(RP2-R)/RP
      IF(R.LE.RP)W=R/RP
      IF(R.GE.RP2)W=0
      CT=CC*COSD(AZE)
      STSQ=1-CT*CT
      F=COS(HPI*CT)
      XT=SIN(2*0.333*PI*SC)
      XR=XT
      G=4*F*F*XT*XR/STSQ
      Q=R**1.5
      RO=W*ABS(G/Q)*1E7/ROM
      IF(ABS(RO).GE.0.178)THEN
      LA=ALOG(RO)/2.30259
      CBA=32.49-57.76*LA*LA
      LN=0.5*(-5.7+SQRT(CBA))
      NEKOS=10**LN
      ELSE
      NEKOS=0
      END IF
      IF(NEKOS.LT.0)NEKOS=0
      PRB(J,I,N)=PRB(J,I,N)+NEKOS
      END DO
      IF(CONGO.EQ.'Y')PRB(J,I,N)=PRB(J,I,N)*SRALT(J,I,N)
2050  END DO
      END DO
2060  END DO
C     Now sum the probabilities for each hour of the day.
      DO I=1,ISKY
      DO J=1,JSKY
```

```
      DO N=0,23
      ROUX(J,I)=ROUX(J,I)+PRB(J,I,N)
      END DO
      END DO
      END DO
      ELSE
      DO I=1,ISKY
      DO J=1,JSKY
      ROUX(J,I)=1
      END DO
      END DO
      END IF
C-----------------------------------------------------------------------
C     MODULE D: Each radiant is weighted according to the number of
C     ========  echo reflection points located on the associated
C               echo line.
C
      DO K=1,IQ
      KAK=KAK+1
      IF(KAK.EQ.5)THEN
      WRITE(6,'(X,A,I7)')'IQ=',K
      KAK=0
      END IF
      LST=DATA(1,K)
      HRS=DATA(2,K)
      ALT=DATA(3,K)
      AZ=DATA(4,K)
      IAD=DATA(5,K)
700   DO I=1,ISKY
      DO J=1,JSKY
      HA(J)=(LST*15)-RA(J)
C     Hour angle and Declination are transformed to Azimuth and altitude
      A1=HA(J)
      B1=DEC(I)
      A0=0
      B0=56.7
      AP=0
      BP=-33.3
      SB0=0.8358
      CB0=0.5490
      SBP=-0.5490
      CBP=0.8358
      SB1=SIND(B1)
      CB1=COSD(B1)
      CALL COORD(A2,B2)
      IF(B2.LE.ILAA)GO TO 2700
      IF(SNAIL.EQ.'C')THEN
      A0=A2+90
      B0=0
      AP=A2
      BP=B2
      A1=AZ
      B1=ALT
      SB0=SIND(B0)
      CB0=COSD(B0)
      SBP=SIND(BP)
      CBP=COSD(BP)
      SB1=SIND(B1)
      CB1=COSD(B1)
      CALL COORD(A2,B2)
```



```
      IF(B2.LE.SPECP.AND.B2.GE.-SPECP)IQK(J,I)=IQK(J,I)+1
      ELSE
C     Formula for the angular separation between the radiant and the
C     echo direction:
      ERAD=AZ-A2
      CSEP=SIND(ALT)*SIND(B2)+COSD(ALT)*COSD(B2)*COSD(ERAD)
      SEP=ACOSD(CSEP)
C     Specularity check:
      IF(SEP.GE.ZLIM.AND.SEP.LE.ALIM)IQK(J,I)=IQK(J,I)+1
      END IF
2700  END DO
      END DO
      END DO
C-----------------------------------------------------------------------
C     MODULE E: Radiant weightings are corrected to take account of
C     ========  the anisotropic beam.
C
C     For each radiant point we now have: (a) Sigma P over the 180
C     degree echo line over the whole day; and (b) Sigma Y, the total
C     number of echo registrations assigned to a radiant. For each
C     radiant we compute Sigma Y/Sigma P.
C
5555  DO I=1,ISKY
      DO J=1,JSKY
      IF(ROUX(J,I).NE.0)THEN
      DECRA(J,I)=IQK(J,I)/ROUX(J,I)
      ELSE
      DECRA(I,J)=0
      END IF
      IF(DECRA(J,I).GT.MAX)MAX=DECRA(J,I)
      IF(IQK(J,I).GT.ZAIRE)ZAIRE=IQK(J,I)
      END DO
      END DO
      WRITE(6,'(X,A,F10.4)')'MAX=',MAX
      WRITE(6,'(X,A,F10.4)')'ZAIRE=',ZAIRE
      DO I=1,ISKY
      DO J=1,JSKY
      IDECRA(J,I)=(DECRA(J,I)*1000)/MAX
      IQK(J,I)=(IQK(J,I)*1000)/ZAIRE
      END DO
      END DO
6000  WRITE(4,'(6(X,I4))')NPTSX,NPTSY,IRA1,IDEC1,IDX,IDY
      WRITE(3,'(6(X,I4))')NPTSX,NPTSY,IRA1,IDEC1,IDX,IDY
      DO I=1,ISKY
      DO J=1,JSKY
      WRITE(4,'(X,I4)')IDECRA(J,I)
      WRITE(3,'(X,I4)')IQK(J,I)
      END DO
      END DO
      STOP
      END
```

A46 (a)

```
      PROGRAM AMPBIN
C     ==============
C
C     Does amplitude distribution in all alt (5 degrees) and az (15 degrees)
C     bins. Plots to the EPSON. Written by David Roux. Modified 2 April 87.
C
      DIMENSION SECLINE(14),KTH(104),C(104,18,24),MIDAZ(24),MIDALT(18)
      CHARACTER*2 GEN,PS,FFILE,LFILE,DISCNO,GENF,GENL,F23
      CHARACTER F24*3,DISC*3,FLNM(16001)*7,FILETD*27,JUNK*5
      REAL X(106),Y(106),CC(106)
      LOGICAL DAVID
C-----------------------------------------------------------------------
      CALL START_PLOT(DAVID)
      CALL FILENAME(FLNM,ILF)
C-----------------------------------------------------------------------
      IHR0=-1
      DO J=1,18
      MIDALT(J)=(5*(J-1))+2.5
      END DO
      DO I=1,24
        IF(I.LE.12)THEN
        MIDAZ(I)=(15*(I-1))+7.5
        ELSE
        MIDAZ(I)=(15*(13-I))-7.5
        END IF
      END DO
      DO I=25,128
      K=I-24
      KTH(K)=I
      X(K)=ALOG(FLOAT(I))/2.30259
      END DO
      DO I=1,24
      DO J=1,18
      DO K=1,104
      C(K,J,I)=0
      END DO
      END DO
      END DO
C-----------------------------------------------------------------
      DO IFL=1,16001
      IF (FLNM(IFL).EQ.'Z')GO TO 3000
      OPEN(UNIT=1,FILE='DUA1:[USER.GRAHAM]'//FLNM(IFL),
     *READONLY,FORM='FORMATTED',STATUS='OLD',IOSTAT=IOS1,ERR=99)
      READ(1,'(X,A)') FILETD
      READ(1,*)(SECLINE(I),I=1,14)
      GEN=FLNM(IFL)(6:7)
15    FRA=0
      READ(1,*,END=98)IAD,IDAY,HRS,NS,FRA,
     *IAMP,FAVE,RAVE,DMIN1,WV,ALT,AZ
C     ALGORITHM FOR FAULTY CH4
      IF(GEN.EQ.'03'.OR.GEN.EQ.'02')THEN
      F23=FLNM(IFL)(2:3)
      F24=FLNM(IFL)(2:4)
        IF(GEN.EQ.'03')THEN
        IF(F23.EQ.'11'.OR.F23.EQ.'12'.OR.F24.EQ.'09B'.
     *  OR.F24.EQ.'10B'.OR.F24.EQ.'13A'.OR.F24.EQ.'14A')DMIN1=0.1
        END IF
        IF(GEN.EQ.'02')THEN
        IF(F23.EQ.'09'.OR.F23.EQ.'10'.OR.F23.EQ.'11'.
     *  OR.F23.EQ.'12'.OR.F24.EQ.'07B'.OR.F24.EQ.'08B')DMIN1=0.1
```

A46 (b)

```
        END IF
      END IF
C-----------------------------------------------------------------
      IF(FRA.EQ.0.OR.ABS(DMIN1).GE.0.05)GO TO 15
      IHR=INT(HRS)
      IF(IHR0.EQ.-1)GOTO 45
      HRS1=HRS0+((76.8+NS0)/230400)
      DHRS=HRS-HRS1
45    IF(DHRS.GT..0005.OR.IHR0.EQ.-1)THEN
        J=INT(0.2*ALT)+1
        IF(AZ.GT.0)I=INT(AZ/15)+1
        IF(AZ.LT.0)I=INT(ABS(AZ/15))+13
        DO K=1,104
        IF(IAMP.GE.KTH(K))C(K,J,I)=C(K,J,I)+1
        END DO
      ELSE
        WRITE(6,'(X,A,X,I5)')'ADDRESS',IAD0
      END IF
50    HRS0=HRS
      NS0=NS
      IHR0=INT(HRS0)
      IAD0=IAD
      GO TO 15
C-----------------------------------------------------------------
1000  END DO
99    IF(IOS1.EQ.29)THEN
      WRITE(6,'(X,A,A)')FLNM(IFL), 'NOT FOUND,'
      ELSE
      WRITE(6,'(X,A,I2)')'ERR NO ',IOS1
      END IF
      GO TO 1000
98    CLOSE(UNIT=1)
      GO TO 1000
C     START PLOTTING ROUTINE
3000  DO I=1,24
      DO J=1,18
      IK=INT(0.1*I)
      JK=INT(0.1*J)
      IT=I-(10*IK)
      JT=J-(JK*10)
      JUNK='X'//CHAR(IK+48)//CHAR(IT+48)//CHAR(JK+48)//CHAR(JT+48)
      DO K=1,104
      IF(C(K,J,I).GT.0)THEN
      Y(K)=ALOG(C(K,J,I))/2.30259
      ELSE
      Y(K)=0
      END IF
      WRITE(3,*)JUNK,X(K),Y(K)
      END DO
      CALL FACTOR(0.6)
      CALL PLOT(1.0,1.0,-3)
      X(105)=1.39
      X(106)=0.03
      Y(105)=0.00
      Y(106)=0.15
      CALL AXIS(0.0,0.0,'LOG A',-5,36.0,0.0,1.39,0.03)
      CALL AXIS(0.0,0.0,'LOG N',5,40.0,90.0,0.0,0.15)
      CALL LINE(X,Y,104,1,-1,1)
      CALL PLOT(-1.0,-1.0,3)
      CALL PLOT(-1.0,41.0,2)
```

```
CALL PLOT(37.0,41.0,2)
CALL PLOT(37.0,-1.0,2)
CALL PLOT(-1.0,-1.0,2)
CALL END_PLOT
END DO
END DO
STOP
END
```

A46 (c)

Appendix 2 is an exposition of the statistics of calculating the most efficient estimator of N (defined in section 6-2). This section was written by Prof. P. van der Watt of the Department of Mathematical Statistics, Rhodes University.

1. Introduction and Summary

The objective of an experiment is to estimate the numbers of meteors that enter the atmosphere along particular radiant vectors or bins surrounding those vectors with a view to obtaining a contour map of the intensity of meteor incidence. A meteor entering the atmosphere causes a stream of ionised particles which can be detected as a radio echo on the upper edge of an annulus by a receiving device. The annulus is a semicircular slice whose plane is perpendicular to the vector along which the meteor enters. The echo is generated by a transmitting device which sends out electromagnetic waves ; the transmitter is geared to a receiving device which picks up any reflections of the transmitted waves and also records the direction from which the reflections come. Each entering meteor will be the cause of one reflection and the point from which the reflection will come will be like from a point chosen at random on the arc of the edge of the annulus. The receiving device is not equally sensitive to reflections from different points on this arc ; it requires the received reflection to have an amplitude in excess of a certain threshold, and the received amplitude will depend, amongst other things on the orientation of the transmitter and the receiver with respect to the point on the arc from which the reflection comes. The distribution of received amplitudes under fixed near-ideal conditions is known and from this and the known properties of the transmitter and the receiver, the probability of detecting an echo caused by an arbitrary meteor from any point on an annulus can be calculated. We will assume these probabilities to be known and expressible as a function $p(y)$: $0 \leqslant p(y) \leqslant 1$; $0 \leqslant y \leqslant 1$ where, for a point on the arc of an annulus, y is the proportion of the arc length the point is distant from a specific end of the arc.

If, for a smallsection of arc of an annulus centered at y_i the probability of detecting a reflection caused by an arbitrary meteor is $p_i = p(y_i)$, then one reflection will, on average, mean an incidence of $1/p_i$ meteors and hence if $Y_1, Y_2, - - -, Y_k$ reflections are detected from k small sections of arc of an annulus, a naive estimator of the total incidence of meteors, N, for the region associated with this annulus would be $\tilde{N} = \sum_{i=1}^{k} Y_i/p_i$.

This estimator is an unbiased estimator of the total number of incident meteors, N, but it suffers from the disadvantage that it does not take into account the correlatedness of the Y_i. The existence of very small p_i's in practice appears to be the cause of high ridges on the contour map of intensity of meteor incidence as evidenced by the fact that in many cases

a high percentage of the value of $\tilde{N} = \sum_{i=1}^{k} Y_i/p_i$ comes from a single term with a small value of p_i.

In order to overcome these difficulties a regression estimator of N based on a multinomial model was derived.

This estimator of N, viz. $\hat{N} = k \sum_{i=1}^{k} Y_i / \sum_{i=1}^{k} p(y_i) \approx \sum Y_i / \int_0^1 p(y)dy$ does not suffer from the disadvantages of the naive estimator $\tilde{N}$, and its relative efficiency with respect to $\tilde{N}$ is :

$$\left(\sum_{i=1}^{k}(1/p_i)-1\right)\left(\sum_{i=1}^{k} p_i\right)/k^2\left(1-\sum_{i=1}^{k} p_i/k\right) \approx \left(\left(\int_0^1 dy/p(y)\right)-1\right)\left(\int_0^1 p(y)dy\right)/\left(1-\int_0^1 p(y)dy\right) \geq 1$$

The distribution of $\hat{N}$ is easily obtained and can be used in the usual way to obtain interval estimates of N.

2. The Regression Estimator of N.

Consider the arc of the annulus associated with a small region on the celestial sphere. Suppose N meteors enter this region giving rise to reflections from N points chosen at random on the arc of the annulus. Divide the arc of the annulus into k contiguous segments of equal length and let N_i, i = 1, 2, - - -, k be the number of reflections coming from the ith segment. Let Y_i and Y_j be the number of reflections detected from the ith and jth segments centred at relative distances y_i and y_j respectively from a specified end of the arc. Let $p_i = p(y_i)$; then $N_1, N_2, - - -, N_k$ are jointly multinomially distributed each with parameter 1/k and the conditional distribution of Y_i and Y_j conditional on $N_i = x$ and $N_j = y$ is :

$$P(Y_i=r,\ Y_j=s \mid N_i=x,\ N_j=y) = \binom{x}{r} p_i^{\,r}(1-p_i)^{x-r}\binom{y}{s} p_j^{\,s}(1-p_j)^{y-s}$$

for r = 0, 1, 2, - - -, x ; s = 0, 1, 2, - - -, y and $0 \leq x+y \leq N$.

It follows easily that the unconditional distribution of Y_i and Y_j is :

$$P(Y_i=r,\ Y_j=s) = \frac{N!}{r!s!(N-r-s)!}\left(\frac{p_i}{k}\right)^r\left(\frac{p_j}{k}\right)^s\left(1-\frac{p_i}{k}-\frac{p_j}{k}\right)^{N-r-s}$$ for

r = 0,1,2, - - -,N; s = 0,1,2, - - -,N and $0 \leq r+s \leq N$. Let $\alpha_i = k/p_i$ it follows that $E(Y_i) = N/\alpha_i$, $Var(Y_i) = (N/\alpha_i)(1-1/\alpha_i)$ and $Covar(Y_i,Y_j) = -N/\alpha_i\alpha_j$. An unbiased estimator of N is $\alpha_i Y_i$ for each i, i = 1, 2, - - -, k where $Var(\alpha_i Y_i) = N(\alpha_i-1)$ and $Covar(\alpha_i Y_i, \alpha_j Y_j) = -N$.

Now since we can write, identically :

$$\alpha_i Y_i = N + (\alpha_i Y_i - N) = N + \varepsilon_i \text{ for } i = 1,2, - - -, k$$

we have, on putting $Y' = (\alpha_1 Y_1, \alpha_2 Y_2 - - - \alpha_k Y_k)$ and $1' = (1\ 1 - - - 1)$:

$$Y = 1N + \varepsilon \text{ where } E(\varepsilon) = 0 \text{ and } E(\varepsilon\varepsilon') = V \text{ where}$$

$$V = \begin{bmatrix} N(\alpha_1-1) & -N & -N & - - - & -N \\ -N & N(\alpha_2-1) & -N & - - - & -N \\ - & - & - & - & - \\ -N & -N & -N & & N(\alpha_k-1) \end{bmatrix} = NV_1$$

This is a regression model with one constant regressor, one unknown parameter, heteroscedasticity and unstabilised variance. A possible method of estimating N is by means of an iterative procedure in which N is approximated by N_1 in order to render V known. Generalised least squares can then be used to estimate N and this new estimate of N used as N_1 to obtain an improved estimate of N and the process repeated until convergence is obtained.

Suppose then that N_1 is our initial estimate for N. Then the generalised least squares estimator for N is :

$$\hat{N} = [1'(N,V_1)^{-1}1]^{-1} \quad 1'(N,V_1)^{-1}Y$$

and from this we see that the value of the GLS estimator of N does not depend on N_1 nor on N ; i.e.

$$\hat{N} = [1'V_1^{-1}1]^{-1}1'V_1^{-1}Y$$

It can be proved that $|V_1| = \Delta = \alpha_1\alpha_2 - - - \alpha_k - \sum_{r=1}^{k} \alpha_1\alpha_2 - - - \alpha_k/\alpha_r$

and that the (i,j)th element of V_1^{-1} is a_{ij}/Δ where

$$a_{ij} = \begin{cases} \alpha_1\alpha_2 - - - \alpha_k/\alpha_j - \sum_{r\neq j} \alpha_1\alpha_2 - - - \alpha_k/(\alpha_j\alpha_r) & \text{for } i = j \\ \alpha_1\alpha_2 - - - \alpha_k/(\alpha_i\alpha_j) & \text{for } i \neq j \end{cases}$$

It follows that : $(1'V_1^{-1}1)\Delta = \sum_{j=1}^{k} \alpha_1\alpha_2 - - - \alpha_k/\alpha_j$ whilst the co-efficient of Y_j/Δ in $1'V_1^{-1}Y$ is :

$\alpha_j\{\alpha_1\alpha_2 - - - \alpha_k/\alpha_j - \sum_{r\neq j} \alpha_1\alpha_2 - - - \alpha_k/(\alpha_j\alpha_r) + \sum_{i\neq j} \alpha_1\alpha_2 - - - \alpha_k/(\alpha_i\alpha_j)\}$

$= \alpha_1\alpha_2 - - - \alpha_k$ and hence :

$$\hat{N} = \sum_{i=1}^{k} (\alpha_1\alpha_2 - - - \alpha_k)Y_i / \sum_{j=1}^{k} \alpha_1\alpha_2 - - - \alpha_k/\alpha_j = \sum_{i=1}^{k} Y_i / \sum_{j=1}^{k} 1/\alpha_j$$

$= k \sum_{j=1}^{k} Y_i / (\sum_{i=1}^{k} p_i)$ is the best linear unbiased estimator for N.

3. The Distribution of $\hat{N}$ and its efficiency relative to $\tilde{N}$.

Since the Y_i have a joint multinomial distribution it follows that $\sum_{i=1}^{k} Y_i$ is binomially distributed with parameters N and $p = \sum_{i=1}^{k} p_i/k \approx \int_0^1 p(y)dy$,

and confidence intervals for N can be found from either the Normal distribution or the Binomial distribution in the usual way depending on the estimated magnitude of Np.

The efficiency of $\hat{N}$ relative to $\tilde{N}$ is the ratio of the variance of $\tilde{N}$ to the variance of $\hat{N}$. It is easy to show that

$$\mathrm{Var}\,(\sum_{i=1}^{k} Y_i/p_i) = N(\sum_{i=1}^{k} 1/p_i k - 1) \approx N((\int_0^1 dy/p(y)) - 1) \quad \text{and that}$$

$$\mathrm{Var}((\sum_{i=1}^{k} y_i)/\sum_{i=1}^{k} p_i/k) = N(1 - \sum_{i=1}^{k} p_i/k)/\sum_{i=1}^{k} p_i/k) \approx N(1-\int_0^1 p(y)dy)/\int_0^1 p(y)dy$$

For very large k the relative efficiency of $\hat{N}$ relative to $\tilde{N}$ is therefore

$((\int_0^1 dy/p(y))-1)/((\int_0^1 p(y)dy)^{-1} - 1) \geq 1.$

Literature cited

Baggaley, W.J. (1970) Mon. Not. Roy. Astr. Soc., 147, 231.

Baggaley, W.J. & Cummack, C.H. (1974) J. Atmos. Terr. Phys., 36, 1759.

Baldwin, J.P. & Kaiser, T.R. (1964) Mon. Not. Roy. Astr. Soc., 129, 85.

Beech, M. (1984) Mon. Not. Roy. Astr. Soc., 211, 617.

Brahic, A. (1985) Adv. Space Res., 5, 97.

Burns, J.A. (1985) "The motion of interplanetary dust", a paper presented at the Enrico Fermi International School of Physics, Varenna, Italy, August 1985.

Chapman, C.R. (1985) "Physics, chemistry and collisional evolution of the asteroids", a paper presented at the Enrico Fermi International School of Physics, Varenna, Italy, August 1985.

Clegg, J.A. (1948) Phil. Mag., 39, 577.

Clegg, J.A., Hughes, V.A. & Lovell, A.C.B. (1947) Mon. Not. Roy. Astr. Soc., 57, 369.

Davies, J.G. & Ellyett, C.D. (1949) Phil. Mag., 40, 614.

Davies, J.G. & Gill, J.C. (1960) Mon. Not. Roy. Astr. Soc., 121, 437.

Ellyett, C.D. & Kennewell, J.A. (1980) Nature, 287, 251.

Ellyett, C.D. & Roth, K.W. (1955) Aust. J. Phys., 8, 390.

Fox, K., Williams, I.P. & Hughes, D.W. (1982) Mon. Not. Roy. Astr. Soc., 199, 313.

Fox, K., Williams, I.P. & Hughes, D.W. (1983) Mon. Not. Roy. Astr. Soc., 205, 1155.

Hapgood, M., Rothwell, P. & Royrvik, O. (1982) Mon. Not. Roy. Astr. Soc., 201, 569.

Hawkes, R.L. & Jones, J. (1975) Mon. Not. Roy. Astr. Soc., 173, 339.

Hawkes, R.L. & Jones, J. (1978) Mon. Not. Roy. Astr. Soc., 185, 727.

Helin, E. (1985) "Near-earth asteroids", a paper presented at the Enrico Fermi International School of Physics, Varenna, Italy, August 1985.

Herlofson, N. (1948) Rept. Prog. Phys., 11, 444.

Hill, A. (ed.) (1977) "The Cambridge Encyclopedia of Astronomy", Jonathan Cape Ltd., London.

Huxley, L.G.H. (1952) Austr. J. Sci. Res., 5, 10.

Jacchia, L.G. (1955) Astrophys. J., 121, 521.

Jones, J. (1975) Mon. Not. Roy. Astr. Soc., 173, 637.

Jones, J. (1977) Bull. Astron. Inst. Czech., 28, 272.

Jones, J. & Hawkes, R.L. (1975) Mon. Not. Roy. Astr. Soc., 171, 159.

Jones, J. & Kaiser, T.R. (1966) Mon. Not. Roy. Astr. Soc., 133, 411.

Jones, J. & Morton, J.D. (1977) Bull. Astron. Inst. Czech., 28, 267.

Jones, J. & Morton, J.D. (1982) Mon. Not. Roy. Astr. Soc., 200, 281.

Kaiser, T.R. (1953) Phil. Mag. Suppl., 2, 495.
Kaiser, T.R. (1960) Mon. Not. Roy. Astr. Soc., 121, 284.
Kaiser, T.R. (1961) Mon. Not. Roy. Astr. Soc., 123, 265.
Kaiser, T.R. & Closs, R.L. (1952) Phil. Mag., 43, 1.
Kaiser, T.R., Pickering, W.M. & Watkins, C.D. (1969) Planet. Space. Sci., 17, 519.
Keay, C.S.L. (1963) Mon. Not. Roy. Astr. Soc., 126, 165.
Keay, C.S.L. & Ellyett, C.D. (1969) Mem. Roy. Astr. Soc., 72, 185.
Kresak, L. (1985a) "The systems of interplanetary objects".
(1985b) "Ageing of comets and their evolution into asteroids"; papers presented at the Enrico Fermi International School of Physics, Varenna, Italy, August 1985.

Lindblad, B.A. (1976) Nature, 259, 99.
Lindblad, B.A. (1987) Astron. Astrophys., 187, 931.

Manning, L.A. (1958) J. Geophys. Res., 63, 181.
McCrosky, R.E. (1955) Astron. J., 60, 170.
McIntosh, B.A. (1975) Bull. Astron. Inst. Czech, 25, 362.
McIntosh, B.A. & Hajduk, A. (1977) Bull. Astron. Inst, Czech., 28, 280.
McIntosh, B.A. & Hajduk, A. (1983) Mon. Not. Roy. Astr. Soc., 205, 931.
McIntosh, B.A. & Millman, P.M. (1970) Meteorics, 5, 1.
McIntosh, B.A. & Simek, M. (1975) Bull. Astron. Inst. Czech., 25, 305.
McIntosh, B.A. & Simek, M. (1980) Bull. Astron. Inst. Czech., 31, 39.
McKinley, D.W.R. (1961) "Meteor sceince and engineering", McGraw-Hill, New York.
Millman, P.M. & McKinley, D.W.R. (1956) Canad. J. Phys., 54, 50.
Morton, J.D. & Jones, J. (1982) Mon. Not. Roy. Astr. Soc., 198, 737.

Olsson-Steel, D. (1987) Mon. Not. Roy. Astr. Soc., 228, 23p.
Olsson-Steel, D. & Elford, W.G. (1987) J. Atmos. Terr. Phys., 49, 243.
Opik, E.J. (1955) "The masses and structure of meteors." Meteors, Pergamon Press Ltd., London.

Pickering, W.M. (1973) Planet. Space Sci., 21, 1671.
Poole, L.M.G. (1965) Phd. thesis.
Poole, L.M.G. (1967) Smithsonian Contrib. Astrophys., 11, 157.
Poole, L.M.G. (1973) Mon. Not. Roy. Astr. Soc., 163, 129.
Poole, L.M.G. (1988) "The Grahamstown all-sky meteor radar". In publication.
Poole, L.M.G. & Kaiser T.R. (1972) Mon. Not. Roy. Astr. Soc., 156, 283.
Poole, L.M.G. & Nocholson, T.F. (1975) Planet. Space Sci., 23, 1261.

Safronov, V.S. (1969) NASA TTF, 667, 1972.
Safronov, V.S. (1985) "On the origin of comets", a paper presented at the Enrico Fermi International School of Physics, Varenna, Italy, August 1985.
Simek, M. (1976) Bull. Astron. Inst. Czech., 27, 168.

Thomas, R.M., Whitnam, P.S. & Elford, W.G. (1986) Proc. ASA, 6, 303.

Verniani, F. (1969) Space Sci. Rev., 10, 230.

Webster, A.R., Kaiser, T.R. & Poole, L.M.G. (1966) Mon. Not. Roy. Astr. Soc., 133, 309.

Weiss, A.A. (1955) Austr. J. Phys., 8, 148.
Weiss, A.A. (1957) Austr. J. Phys., 10, 299.
Weiss, A.A. (1959) Austr. J. Phys., 12, 54.
Weiss, A.A. (1960) Austr, J. Phys., 13, 532.
Whipple, F.L. (1950) Astrophys. J., 111, 464.